Evaluation of Endometer ES-2 accuracy through control measurements of extracted teeth

Stare, Zoran; Galić, Nada; Šutalo, Jozo; Šegović, Sanja; Prskalo, Katica

CROMBES & KoREMA

Proceedings

10th International Symposium on Biomedical Engineering '94

10th ISBE '94 ZAGREB CROATIA

CROMBES & KoREMA Proceedings (1994)

Zagreb, Croatia, November 24 - 26, 1994.

VOL 28 № 01

Organizers

CROMBES

Croatian Medical and Biological Engineering Society
The Member of the International Federation for Medical & Biological Engineering IFMBE
The Member of the European Federation of Organisation for Medical Physics EFOMP
Office: Unska 3, Zagreb, Croatia
Phone: (+385 41) 62 99 38; 62 99 11; fax: (+385 41) 62 95 52

&

KoREMA

Croatian Society for Communications, Computing, Electronics, Measurement & Control
The Member of the International Measurement Confederation IMEKO
The Member of the International Federation of Automatic Control IFAC
Office: Avenija Vukovar 39, P.O.Box 473, Zagreb, Croatia
Phone: (+385 41) 62 98 93; 62 98 69; fax: (+385 41) 62 98 70

Sponsored by

Ministry of Science and Technology of the Republic of Croatia
Belupo, d.o.o.
Pliva, d.d.
Sonomed, d.o.o.

Under high patronage of

Ministry of Health of the Republic of Croatia

University of Zagreb:

Faculty of Electrical Engineering
School of Medicine
School of Dentistry

Publishers

CROMBES & KoREMA

Design

Neda Štambuk-Boršić
Ratko Magjarević

Print

Europrint

Issue

100

ISBN 953-6037-06-8

On the occasion of the 75th Anniversary of the Technical Faculty in Zagreb

Nacionalna i sveučilišna biblioteka, Zagreb
CIP - Katalogizacija u publikaciji

61(063)(082)

INTERNATIONAL Symposium on Biomedical Engineering (10 ; 1994 ; Zagreb)
Proceedings / 10th International Symposium on Biomedical Engineering '94, Zagreb, November 24-26, 1994. - Zagreb : CROMBES : KoREMA, 1994. - 194 str. : ilustr. ; 30 cm

Bibliografija uz svaki rad. - Summaries.

ISBN 953-6037-06-8 (KoREMA)

941104140

The Proceedings was published by the support of the Ministry of Science and Technology of the Republic of Croatia.

Additional copies may be ordered from the publishers.

WELCOME TO 10th ISBE FROM THE PRESIDENT

The 10th Symposium on Biomedical Engineering is a jubilatory Symposium and it is now the time to look back on its evolution and progress through almost 20 years. The first Symposium on Biomedical Engineering was held in 1977 in organization of JUREMA (the predecessor of KoREMA) and Zagreb Fair. The name of the Symposium was "Medicine and Engineering", the same as is the name of specialized exibition of the Zagreb Fair. At that time the number of presented papers was usually below 30. However, in the latest ten years the number of presented papers is in a steady growth. On this jubilatory Symposium we have accepted 48 papers for presentation. In the years 1985 and 1986 biennial sequence was interrupted and the Symposium was held in to two subsequent years. In 1992 the name of the Symposium was changed as is called now what is more appropriate, and the organizer Zagreb Fair is changed as well because the term of the Symposium was moved from May to November. The Symposium organization was in 1992 entrusted to CROMBES (Croatian Medical and Biological Engineering Society) and KoREMA as well.

On the Symposium participated besides electrical engineers physicists and in a great number physicians and dentists what is a good feature of this Symposium. Most of the physicians participants are orthopaedists, some are doing functional rehabilitation, mainly dealing with biomechanics. A group of dentists is doing research on myography and sonography on jaw muscles or other research in dentistry connected with technology. These are of course not all activities this Symposium is dealing with. These are just a few examples among the broad current research activities, which are presented through the topics of eight sessions:

1. Biomedical Instrumentation
2. Biomedical Signal Measurements and Processing
3. Biomechanics
4. Medical Imaging
5. Medical Informatics
6. Bioelectrical Measurements
7. Bioengineering in Dentistry
8. Modelling and Simulation

All submitted papers were reviewed by international reviewers group and 48 of them has been accepted for presentation on the Symposium. Also, to the first time we have more papers from abroad than ever before particulary from Germany, England, Austria, Italy, Slovenia and some other foreign countries. We hope that with the more stabilized situation in Croatia the number of foreign participants will grow.

On behalf of the Organizing Committee

A. Šantić

Prof.dr.sc. Ante Šantić

Content

Biomedical Signal Measurement and Processing

Biomedical Instrumentation

Biomechanics

Medical Imaging

Medical Informatics

Bioelectrical Measuremnts

Bioengineering in Dentistry

Modeling and Simulation

AUTHORS INDEX

SINGLE-TRIAL EEG CLASSIFICATION BASED ON COHERENCE VALUES[+)]

Colin Andrew, Doris Flotzinger, Joachim Kalcher and Gert Pfurtscheller
Dept. of Medical Informatics, Institute of Biomedical Eng., Graz University of Technology and Ludwig Boltzmann-Institute of Medical Informatics and Neuroinformatics, Brockmanngasse 41, A-8010 Graz, Austria

Summary

A critical step in the development of a Brain-Computer Interface (BCI) is that of feature extraction, that is, what parameters are extracted from multi-channel EEG data to be used for distinguishing different spatio-temporal EEG patterns. This paper investigates the feasibility of using coherence measures between different scalp regions as possible features for the BCI. In particular, coherence values calculated between the supplementary motor area and the sensorimotor hand areas of left and right hemispheres are used as features for a learning vector quantization (LVQ) classifier to distinguish between side of hand movements. Classification accuracy's of up to 83% were achieved in classification between left and right finger movements based on single-trial, band-averaged coherence values.

1. INTRODUCTION

A Brain-Computer Interface (BCI) is a system which records bioelectrical signals from the intact scalp (EEG) and uses the classification of these signals to control devices, e.g. movement of a cursor on a monitor [1]. Such a system relies on the ability to successfully classify, in real-time, different spatio-temporal EEG patterns related to mental thought processes (e.g. prepare left or right hand movement). A critical step in the development of a BCI is that of feature extraction, i.e. the choice of what parameters to extract from the raw EEG data for use as features for the classification stage.

As a prerequisite for the development of such a system, planning of left and right finger movements were studied. From the work of Jasper and Penfield [2] and Chatrian et al. [3] it is known that the EEG displays characteristic changes prior to movement. The mu rhythm of the contralateral central region is desynchronised or blocked about 1-2 seconds before movement-onset. This event-related desynchronisation (ERD) can be quantified and displayed either for one electrode in the form of a time course, or for one moment in time and multiple electrodes in the form of a topographical map, and gives spatio-temporal information about activation of sensorimotor areas during planning of movement. The different spatial patterns of cortical activation for planning of left and right movement are shown in Figure 1 and show that different types of mental activity without any sensory input or motor output result in characteristic ERD maps.

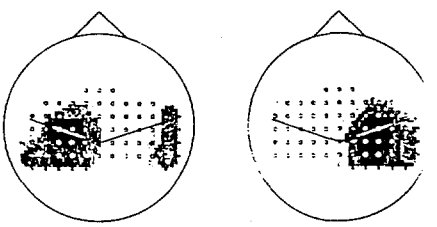

Figure 1: Different cortical activation patterns for left and right finger movements. 'Black' marks cortical regions with large ERD and large cortical activation.

[+)] Supported by the "Fonds zur Förderung der wissenschaftlichen Forschung" in Austria, project P10 000, the Austrian Nationalbank, project 4534 and the South African Foundation for Research and Development.

Pfurtscheller et al. [4] have shown further, that ERD quantified in the alpha band in single-trial EEG data recorded prior to movement, can be used for prediction of the side of hand movements. Thus, using band-averaged EEG amplitudes or power values as features, a BCI was developed for control of cursor movement on a monitor ('left' or 'right'), and with this system classification accuracy's of 85% were achieved [1].

During planning of movement, not only the sensorimotor hand areas, but also the supplementary motor area (SMA) [5] is involved. The functional relationships or couplings between these areas can be measured using coherence analysis, and provides additional information to the ERD. This paper studies short-lasting changes in coherence between the SMA and the contralateral sensorimotor hand area, and between the SMA and the ipsilateral sensorimotor hand area during planning of finger movements using averaging over trials. We then investigate the use of single-trial coherence values between these cortical regions as features for a neural network classifier to distinguish between planning of left and right finger movements.

2. FEATURE EXTRACTION AND CLASSIFICATION

2.1 Data Acquisition and Pre-processing

Data were recorded from a grid of electrodes (2.5 cm interelectrode distances) overlying the left sensorimotor hand area, the right sensorimotor hand area and the SMA, during a stimulus-cued right or left finger movement paradigm. All EEG channels were recorded with a common nose reference electrode. Six seconds of data prior to movement and two seconds of data after movement were recorded and digitised at a sampling frequency of 128 Hz. Approximately 120 trials of artefact-free data were available for each type of movement. Local average reference (LAR) derivations were calculated to obtain reference-independent data for calculation of coherence values [6].

2.2 Event-related Coherences (ERCoh)

For calculation of coherence values, each trial was divided up into short 125 msec segments. Each short segment was then augmented with zeros, and auto (Pxx, Pyy) and cross (Pxy) spectra calculated for the zero-padded data. Auto and cross spectra were then averaged across all trials thus reducing the variance of the estimates, and a band-averaged value of coherence calculated from the trial-averaged spectra according to the squared coherence function shown in Equation 1. By repeating this for each short-time segment, a time course of coherence is obtained which is termed event-related coherence (ERCoh) [7].

$$\overline{Coh(f_1 - f_2)} = \frac{\left|\overline{Pxy(f_1 - f_2)}\right|^2}{\overline{P_{xx}(f_1 - f_2)}.\overline{P_{yy}(f_1 - f_2)}} \quad (1)$$

ERCoh's were calculated between different combinations of electrodes overlying the SMA and the left sensorimotor hand areas (left hemisphere), and between the SMA and the right sensorimotor area (right hemisphere) as shown in Figure 2, for both left and right finger movements. Coherences were calculated for both the alpha (10-12 Hz) and gamma (38-40 Hz) frequency bands for LAR data.

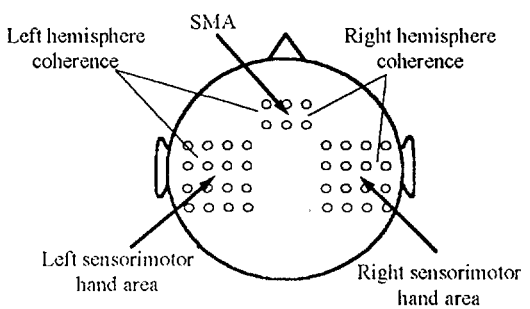

Figure 2 : Regions for coherence calculation.

The results for the alpha ERCoh showed that this frequency band provided no information for discrimination between left and right movements as there were no significant differences between the ERCoh of contralateral and ipsilateral hemispheres. SMA-sensorimotor hand area coherences were high during rest, and decreased during planning of movement for both hemispheres. However, in the gamma band, differences were seen between the contra- and ipsilateral hemisphere as shown in Figure 3. A transient increase of coherence was found between the SMA and the contralateral sensorimotor hand area, this increase occurring 1 to 1.5 seconds before movement-onset. On the ipsilateral side, no increase in coherence was found and coherence remained low throughout the trial.

Thus, from these trial-averaged coherence results, it appeared that gamma band coherences might provide discriminative information to predict the side of hand movement. However, for

classification, coherences could not be calculated as an average over trials, and single-trial coherence values needed to be calculated.

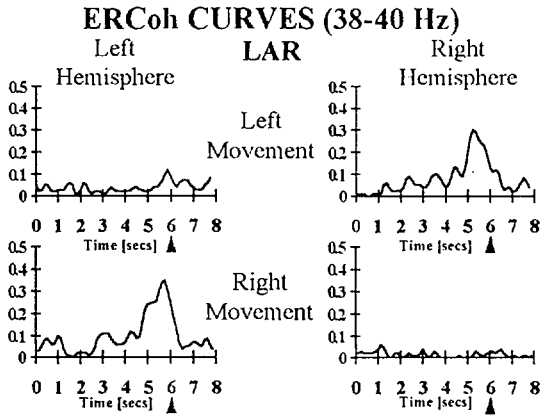

Figure 3 : ERCoh curves in the gamma band for left and right hemispheres. Upper ERCoh curves are for left finger movement and lower curves for right finger movement. The arrow marks the time of movement-onset.

2.3 Single-Trial Coherences

Band-averaged coherence values were calculated according to Equation 1, from single-trial auto and cross spectra computed for a 1 (1.5) second segment of data directly preceding movement-onset. Since the averaging was performed across only a few frequency samples and not across all trials, coherence estimates with high variance were obtained.

As features for the LVQ classifier, band-averaged coherence values were calculated for 6 electrode combinations between SMA and left sensorimotor hand area, and 6 combinations between SMA and right sensorimotor hand area, thus providing 12 input features to the classifier (12-dimensional feature space). Classifications were performed for 3 different frequency bands (36-38 Hz, 38-40 Hz and 36-40 Hz) and for 2 different pre-movement intervals (5.0-6.0 secs and 4.5-6.0 secs) and results compared. For the 1 second interval (5.0-6.0), the classification result for the 10-12 Hz band is also given. A total of 244 examples (120 for left movement, 124 for right movement) were available for classification using the LVQ-algorithm.

2.4 LVQ Classification

The LVQ-algorithm divides the multi-dimensional feature space into a predefined number of regions. Each region is represented by a reference vector and assigned a class label. Since several reference vectors can represent one category, arbitrarily complex decision borders (piecewise linear) can be created. During classification, a new example is assigned the class label of the region into which it falls. This region is determined by looking for the reference vector to which the example is closest according to the Euclidean distance measure.

Effective values for the reference vectors to minimise the number of misclassifications are found using an iterative algorithm which basically works as follows: examples are drawn randomly from a labelled training set and classified. If the classification attempt is wrong then the closest reference vector is pushed slightly away from the current example. If the classification attempt is correct then the closest reference vector is pulled closer to the current example. These adjustments are repeated for a predetermined number of iterations.

The classification results given in Table 1 were achieved using 20-fold cross-validation. For cross-validation the set of 244 examples was divided into 20 disjoint sets and 20 LVQ classifiers were built using 19 of these sets leaving the remaining set as a testing set. Table 1 contains the average results on these testing sets. Each LVQ classifier consisted of 6 reference vectors (3 for 'left' and 3 for 'right finger movement') and was trained for 5000 iterations using the LVQ3 algorithm [8].

	10-12 Hz	36-38 Hz	38-40 Hz	36-40 Hz
5.0-6.0 secs	53.65	75.90	67.56	81.09
4.5-6.0 secs	-	71.19	70.93	83.27

Table 1 : Percentage correct classification results for different frequency bands and pre-movement data segments.

The best classification result of 83.27% was achieved for the 36-40 Hz band from 1.5 seconds of data (4.5-6.0 secs) recorded before movement. Coherences in the lower gamma band (36-38 Hz) contained more discriminative information than the upper gamma band (38-40 Hz), but the best results were achieved with values calculated over the combination of these two bands (36-40 Hz). Also, coherences calculated from a longer pre-movement data segment (4.5-6.0 secs) gave better results than the 1 second segment (5.0-6.0 secs).

Coherences in the alpha band (10-12 Hz) gave a classification result of only 53.65%.

3. CONCLUSIONS

The ERCoh results demonstrate, that during the final programming of the motor act, there is a functional coupling in the gamma band between the SMA and the contralateral sensorimotor hand area. This coupling is found between the SMA and the contralateral sensorimotor area only, and no change in coherences on the ipsilateral side are seen.

A LVQ classifier was able to classify between planning of left and right finger movements from single-trial coherence patterns of left and right hemispheres, with a classification accuracy of up to 83%. The classifier gave the best results for a wider frequency band. The reason for this can be explained by the fact that coherence estimates calculated over a wider band have a lower variance due to the increase of averaging over more frequency samples, and the LVQ classifier thus performs better in this case where the features are less noisy. The better performance due to a larger pre-movement data segment can also be explained by a decrease in variance of the estimates due to increased averaging. An increase in the pre-movement segment length results in an increase of frequency resolution in the spectrum and therefore an increase in the number of frequency samples in the band of averaging.

4. REFERENCES

[1] G. Pfurtscheller, D. Flotzinger and J. Kalcher. Brain-Computer Interface - A new communication device for handicapped persons. Journal of Microcomputer Applications, 16, 293-299, 1993.

[2] H.H. Jasper and W. Penfield. Electrocorticograms in man: effect of the voluntary movement upon electrical activity of the precentral gyrus. Archives Psychiat. Z. Neurol., 183, 163-174, 1949.

[3] G.E. Chatrian, M.C. Petersen and J.A. Lazarte. The blocking of the rolandic rhythm and some central changes related to movement. Electroenceph. clin. Neurophysiol., 11, 497-510, 1959.

[4] G. Pfurtscheller, D. Flotzinger, W. Mohl and M. Peltoranta. Prediction of the side of hand movement from single-trial multi-channel EEG data using neural networks. Electroenceph. clin. Neurophysiol., 82, 313-315, 1992.

[5] P.E. Roland. Organization of motor control by the normal human brain. Human Neurobiol., 2, 205-216, 1984.

[6] G. Pfurtscheller, C. Neuper and J. Berger. Source localisation using event-related desynchronization (ERD) within the alpha band. Brain Topography, 6, 269-275, 1994.

[7] P. Rappelsberger, G. Pfurtscheller and O. Filtz. Calculation of event-related coherence - A new method to study short-lasting coupling between brain areas. Brain Topography, in press, 1994.

[8] T. Kohonen. The Self-Organizing Map. Proceedings of the IEEE, 78, 1464-1480, 1990.

EEG Coherence and Bicoherence Measurements during Finger Movement [+)]

Günter Edlinger, Colin Andrew, Gert Pfurtscheller

Dept. of Medical Informatics, Institute of Biomedical Eng., Graz University of Technology and Ludwig Boltzmann-Institute of Medical Informatics and Neuroinformatics, Brockmanngasse 41, A-8010 Graz, Austria

Summary

Relations between cortical areas were analysed using bioelectrical signals measured from different electrode positions on the scalp. Linear and non-linear phase relationships between EEG signals recorded during preparation and execution of finger movements were investigated. Interrelations between left and right primary hand areas and between left hand area and supplementary motor area were computed. For linear analysis coherence and for non-linear interrelations crossbicoherence was used. Intrasignal relations were analysed with the bicoherence.

1. INTRODUCTION

For the investigation of functional brain topography in human subjects it is important to analyse bioelectrical signals from different electrode locations. One important aspect is the relationship of harmonic components in one signal (e.g. between alpha and beta rhythm in EEG), another is the linear and non-linear interrelation between signals from different electrodes. One mathematical tool available to compute linear relations between two signals is the coherence and for non-linear is the crossbicoherence. For detecting non-linear phase relationships within one signal the bicoherence can be used (Dummermuth et al. 1971, Kim and Powers 1979).

Preparation and execution of voluntary finger movement involves different cortical and subcortical structures. Among these are: primary motor and somatosensory areas, supplementary motor area (SMA) and premotor area. Primary sensorimotor area have intrinsic rhythms known as mu and central beta rhythms (Jasper and Penfield 1949, Chatrian et al. 1959, Pfurtscheller and Neuper 1994). These rhythms are desynchronized when the corresponding area is activated during motor action.

The goal of this paper was to analyse the coherence and crossbicoherence and therefore the linear and non-linear phase relationships between left and right primary hand area and left hand area and SMA. The phase relation between the mu rhythm and the central beta rhythm was tested using the bicoherence.

2.COHERENCE AND BICOHERENCE

2.1 Method

Movement-related EEG trials (6s before and 2s after movement onset) were recorded from electrodes overlaying the primary hand areas (electrode position C3 and C4 according to the international 10/20 system) and the SMA. The sampling frequency was 128 Hz and 73 trials were recorded and stored. To overcome the reference problem the local average reference (LAR, Pfurtscheller et al. 1994) was calculated for all 3 electrode locations. For linear analysis the coherence which measures the linear correlation between two signals at frequency f was calculated (for details see e.g. Jenkins and Watts 1968). Spectral analysis based on higher order statistics

[+)] Supported by the "Fonds zur Förderung der wissenschaftlichen Forschung", in Austria, project P10000, the Austrian Nationalbank, project 4534 and the South African Foundation for Research and Development

detects non-linear interrelations between frequency components. QPC (quadratic phase coupling) is detected by bispectral analysis for one signal. For quadratic relations between two signals the crossbispectral analysis is used.

Assuming that signals $x(t)$ and $y(t)$ are sampled with a sampling frequency f_a (Nyquist frequency $f_s = f_a/2$) which gives $x(l) = x(l\Delta t)$ and $y(l) = y(l\Delta t)$ and the record length is $T = N/f_a$ sec., bispectral and crossbispectral analyses were applied according to the "direct method" based on the FFT technique [Kim and Powers 1979, Ning and Bronzino 1993].

For estimating the bispectrum ,the bicoherence, the crossbispectrum and the crossbicoherence following steps are required:

1) Form K sets of data records of length N of sampled signal $x(t)$ and $y(t)$ (K ... number of trials, N ... number of data points used for FFT) which gives

$$x^{(i)}(l), y^{(i)}(l), i = 1, \cdots, K \text{ and } l = 0, \cdots, N-1$$

and a frequency resolution of $\Delta f = 1/\Delta t = f_a/N$.

2) Subtract the mean value from each trial and apply the FFT to K sets of data by

$$X_k^{(i)} = \frac{1}{N}\sum_{l=0}^{N-1} x^{(i)}(l) e^{-i2\pi kl/N}$$
$$Y_k^{(i)} = \frac{1}{N}\sum_{l=0}^{N-1} y^{(i)}(l) e^{-i2\pi kl/N} \quad (1)$$
$$k = 0, \cdots, N/2 \text{ and } i = 1, \cdots, K.$$

3) Estimate the bispectrum and the crossbispectrum by averaging over K trials and compute the squared bicoherence and crossbicoherence values.

bicoherence:

$$\hat{b}(k,l)^2 = \frac{\left|\frac{1}{K}\sum_{i=1}^{K} X_k^{(i)} X_l^{(i)} X^{*(i)}_{k+l}\right|^2}{\left[\frac{1}{K}\sum_{i=1}^{K}\left|X_k^{(i)} X_l^{(i)}\right|^2\right]\left[\frac{1}{K}\sum_{i=1}^{K}\left|X^{(i)}_{k+l}\right|^2\right]} \quad (2)$$

crossbicoherence:

$$\hat{bc}(k,l)^2 = \frac{\left|\frac{1}{K}\sum_{i=1}^{K} X_k^{(i)} Y_l^{(i)} X^{*(i)}_{k+l}\right|^2}{\left[\frac{1}{K}\sum_{i=1}^{K}\left|X_k^{(i)} Y_l^{(i)}\right|^2\right]\left[\frac{1}{K}\sum_{i=1}^{K}\left|X^{(i)}_{k+l}\right|^2\right]} \quad (3)$$

$$0 \le l \le k, l + k \le f_S$$

'*' denotes the complex conjugate

4) Estimate the 95% significance level of non zero bicoherence and crossbicoherence values. For a KN-point data record and with K sets of data records (trials) each with length N, the degrees of freedom are $2K$ (dof) and the 95% significance level for the non zero squared bicoherence and crossbicoherence is $6/dof$ [Elgar and Guza 1988].

2.2 Results

The squared coherence between C3 and C4 in the alpha band was low during rest and movement, indicating that the mu rhythms on both hemispheres are independant (see (1)). During rest the squared coherence between SMA and primary hand area (C3) which was 0.55, indicated a linear coupling between the signals recorded at C3 and the electrode overlaying the SMA in the alpha band. During movement this coherence value in the alpha band was near zero.

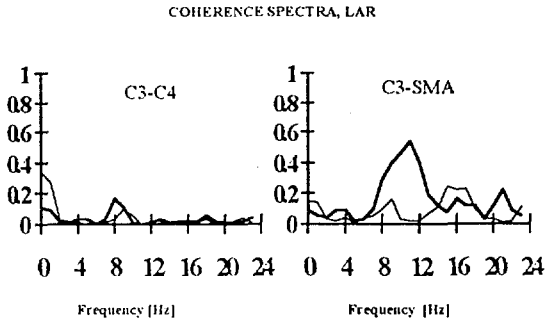

Figure 1: Left panel shows the squared coherence between C3 and C4 during rest (thick line) and movement; the right panel shows the squared coherence between C3 and SMA during rest (thick line) and movement.

Non-linear analysis showed that the squared bicoherence value which was 0.5 at the frequency pair 11 and 11 Hz was significant (the 95% level of significance was for 73 trials 0.041) indicating that the beta rhythm at 22 Hz was phase coupled with the mu rhythm during rest (see (2)).

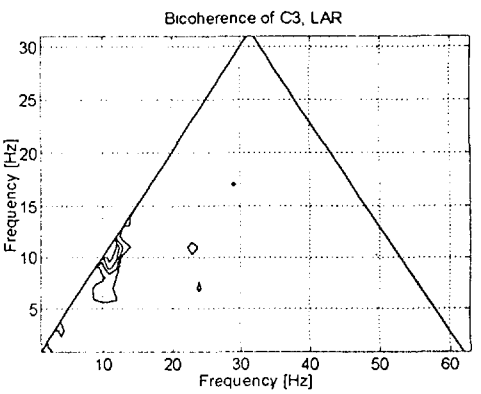

Figure 2: Contour plot of the squared bicoherence of signal recorded at C3 during rest.

Non-linear analysis between the SMA and C3 (see (3)) with a significant squared crossbicoherence value of 0.35 at the frequency pair of 11 and 11 Hz indicated a non-linear phase coupling between SMA and C3 during rest, whereas the bicrosscoherence value computed between C3 and the SMA was not significant.

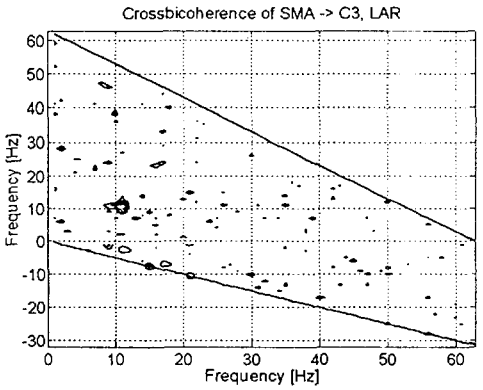

Figure 3: Contour plot of the squared crossbicoherence indicating a non-linear coupling between SMA and C3 during rest.

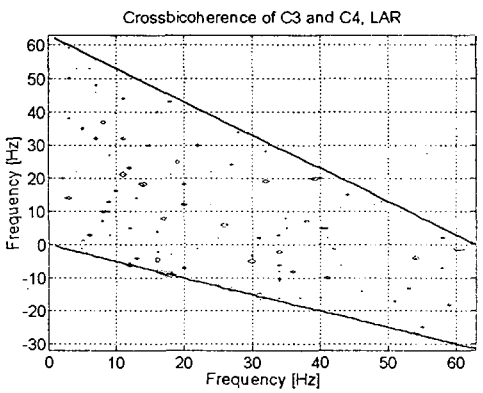

Figure 4: Squared crossbicoherene between signals recorded at C3 and C4.

The squared crossbioherence value which was not significant at the frequency pair 11 and 11 Hz indicates that during rest there was no quadratic phase coupling between C3 and C4 in the alpha band (see (4)).

3. CONCLUSION

Coherence and crossbicoherence values close to zero were found between both central areas (electrode C3 and C4). This confirms the work of Storm van Leeuwen et al. 1972 that in both hemispheres relative independant mu generator systems exist. However, a significant coherence was found in the alpha band between signals from primary hand area and SMA. This can be interpreted in a way that both areas are linearly coupled. Furthermore a crossbicoherence value was found between these areas indicating that the SMA has a non-linear influence on beta rhythms in the hand area. The SMA plays an important role during planning of preparation of movement (Goldberg 1985) and it is therefore not surprising that linear and non-linear couplings exist between the SMA and the primary hand area.

4. REFERENCES

[1] G. Dummermuth, P. J. Huber, B. Kleiner, Th. Gasser, Analysis of the interrelations between frequency bands of the EEG by means of the bi-spectrum. A preliminary study. Electroenc. Clin. Neurophysiol., 31, 137-148, 1971.

[2] Y.C. Kim, E. J. Powers, Digital bispectral analysis and ist application to nonlinear wave interactions. IEEE Trans. Plasma Sci., vol PS-7, 120-131. 1979.

[3] H. H. Jasper, W.Penfield, Electrocorti-cograms in man. effect of the voluntary movement upon the electrical activity of the precentral gyrus. Arch. Psychiat. Z. Neurol., 183, 163-174, 1949.

[4] G.E. Chatrian, M.C. Petersen, J.A. Lazarete, The blocking of the rolandic wicket rhythm and some central changes related to movement., Electroenceph. clin. Neurophysiol., 11, 497-510, 1959.

[5] G. Pfurtscheller, C. Neuper, Event-related synchronization of mu rhythm in the EEG over the cortical hand area in man. Neurosci. Lett., 162, 179-182, 1994.

[6] G. Pfurtscheller, C. Neuper, J. Berger, Source localization using event-related desynchro-nization (ERD) within the alpha band. Brain Topography, 6 , 269-275, 1994.

[7] G. Jenkins, D. Watts, Spectral analysis and ist applications. Holden Day, San Fransisco, 1968.

[8] T. Ning, J. D. Bronzino, Nonlinear analysis of the hippocampal subfields of CA1 and the dentate gyrus. IEEE Trans Biomed. Eng., 40, 870-876, 1993

[9] S. Elgar, R. T. Guza, Statistics of bicoherence. IEEE Transaction on Acoustics, Speech and Signal Processing, 36, 1667-1668, 1988.

[10] W. Storm van Leeuwen, G. Wieneke, P. Spoelstra, H. Versteeg, Lack of bilateral coherence of mu rhythm., Electroenceph. clin. Neurophysiol., 44, 140-146, 1978.

[11] G. Goldberg, Supplementary motor area structur and function: Review and hypotheses. Behav. Brain Sci., 8, 567-616, 1985.

BRAIN COMPUTER INTERFACE: AN EEG-BASED COMMUNICATION DEVICE*

Kalcher J., Flotzinger D., Gölly S., Neuper Ch., Pfurtscheller G.
Department of Medical Informatics, Institute of Biomedical Engineering, Graz University of Technology, and Ludwig-Boltzmann Institute of Medical Informatics and Neuroinformatics, Brockmanngasse 41, A-8010 Graz, Austria

Summary

This paper describes the new setup of the Graz Brain-Computer Interface (BCI) system II, which is based on on-line classification of EEG patterns to determine which of three kinds of movement are planned by a subject. This classification can be exploited for on-line control which may constitute a great help for handicapped persons in the future.

1. INTRODUCTION

Theoretically, specific mental activities of a person should be reflected in the person's brainwaves and therefore be measurable by electrodes on the person's scalp. In practice, several groups have shown that such 'thoughts' can be discriminated based on the recorded EEG with surprising accuracy, e.g. such 'thoughts' as mentally answering 'yes' and 'no' [1], intention to move a joystick [2] or planning of hand movement [3, 4]. These findings have led to the idea to exploit EEG for control in cases where other means of control are either impossible, e.g. in cases of handicapped persons, or infeasible, e.g. if both hands are occupied.

A system which uses EEG to build a communication line between the brain and an electrical appliance has become known as a Brain-Computer Interface (BCI).). The basic idea of such a BCI is to record the EEG during specific mental activity and to classify the EEG on-line. The classification result can be used to control any electronic devices or can be used as an input to a computer. Several teams all over the world are currently working at such systems [5, 6]; this paper describes the work done in Graz. The Graz BCI is a system which is mainly based on the discrimination of various types of spatiotemporal EEG patterns during movement planning [7, 8].

2. METHOD

The basic idea of the Graz BCI system has already been outlined in previous papers[7]. The Graz BCI 1 was a one-dimensional cursor control system which could discriminate between left and right hand movement planning whereby in the initial session the subject had to press a microswitch with either the left or right index finger. The cortical areas involved in these two kinds of movement planning are primarily the left and right sensorimotor hand areas; the corresponding electrode positions overlying these areas are C_3 and C_4 (international 10-20 system) [3].

To increase the dimensions of control, additional EEG patterns have to be found which are discernable from left and right hand movement. Studies of foot and tongue movement showed that these two kinds of movement can indeed be discriminated from left and right hand movement, especially in the movement planning phase [8] (see Fig. 1). Therefore, the additional movement type 'foot flexion' was built into the Graz BCI which, due to several changes in the recording scheme and experimental paradigm, is now called Graz BCI II.

The experimental paradigm of the Graz BCI II is shown in Fig. 2. The subject is seated in a comfortable chair looking at a fixation cross on a monitor 1 meter in front of the subject's eyes. One second after an acoustic warning stimulus ('beep') a cue in the form of an arrow, pointing either left, right or down, appears and indicates to the subject

* Supported by the 'Fonds zur Foerderung der wissenschaftlichen Forschung', in Austria, project P9043 and the 'Forschungsförderungsfonds für die gewerbliche Wirtschaft' project 2/312.

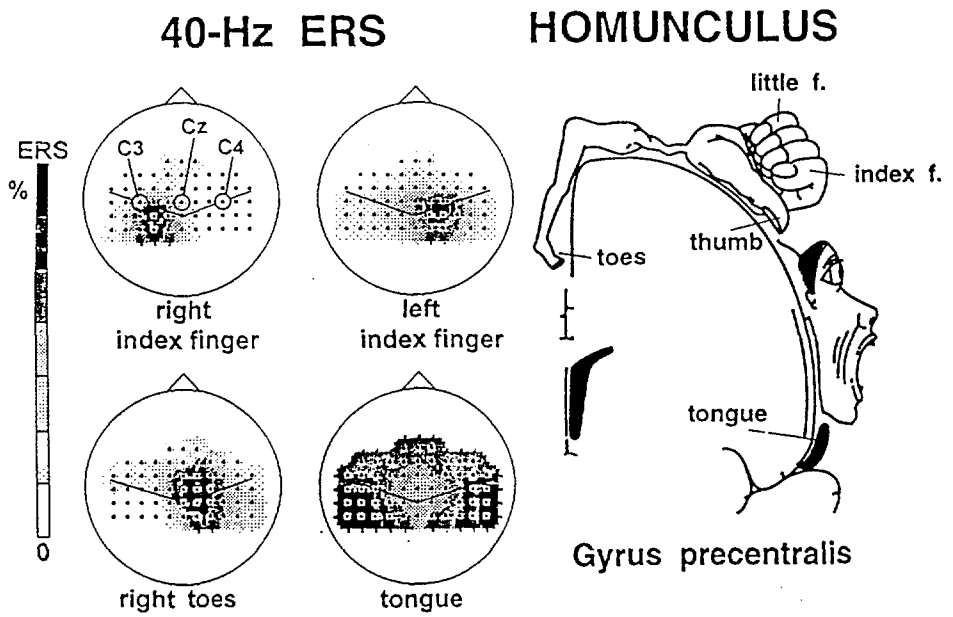

Fig. 1. Topographic maps display beta power changes during planning of hand, foot and tongue movement. "Black" indicates cortical areas with largest power increase. The electrode positions and the approximate location of the central sulcus are indicated.

that as soon as the arrow vanishes (after 1250 msec) he should either press a microswitch with his left index finger, his right index finger or move the toes of his right foot upwards (dorsal flexion), respectively. A 1-second period starting 250 msec after presentation of the cue is classified into one of the three movement tasks and the corresponding classification of the system is fed back to the subject either as correctly identified ('+'), undecided ('0') or wrong classification ('–').

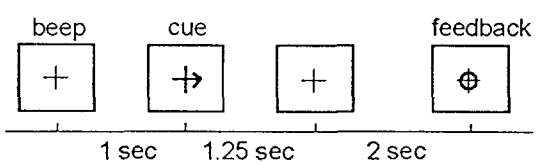

Fig. 2. Experimental paradigm of the Graz BCI II

A PC486 with a DSP-board records and classifies the EEG and provides the feedback to the subject. Three bipolar EEG channels are used for on-line classification: C_3-C'_3, C_z-C'_z and C_4-C'_4 (see Fig. 2). The signals are sampled at 64 Hz, whereby the features extracted from the 1-second period of EEG and presented to the classifier are comprised of four power estimates, each representing 250 msec, per EEG channel. These power estimates are calculated by squaring each sample and then averaging over 16 samples. The 12 features (3 EEG channels times 4 power estimates) are offered to a classifier which calculates both a classification and a measure describing the certainty with which the classification was obtained. Depending on this quality measure and the correctness of the classification, the system provides a feedback to the subject in the form of a small or large '+' if the classification is correct and the quality measure is in medium or large range, respectively, a small or large '–' if the classification is incorrect, and '0' if the quality measure is very small.

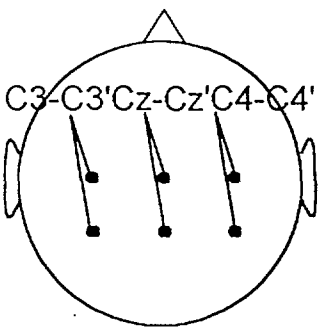

Fig. 3. Positions of the electrodes on the scalp

Four subjects (1 female and 3 male students aged between 23 and 27 years) participated in four experimental sessions on different days within 2 weeks. Each session lasted about 1.5 h and comprised four blocks of 60 trials each with 5 min breaks between blocks. In the first session, data were collected for the creation of the classifier and therefore no feedback was provided. In the following sessions 2 and 3, the classifier was used to discriminate the 3 kinds of movement out of the movement planning phase and to give feedback to the subject as described above. In session 4 no

motorl behavior took place: using the same stimulation procedure as in the first sessions. the subject was asked to concentrate on left hand. right hand or foot movement. In this session the classifier was applied to EEG data recorded during mental activity and provided feedback about discriminability of three different mental states.

3. EEG CLASSIFICATION

The classifier built into the Graz BCI II system is a Learning Vector Quantizer (LVQ) [9. 10]. Its classification speed and ease of use in the Graz BCI I system have suggested its further use in on-line EEG classification of more than two categories.

Basically, a LVQ is a nearest-neighbour classifier whereby a labelled codebook is generated such that for each training example the nearest codebook vector is of the same category as the given example. Thereby, LVQ tries to optimize the representation of the training examples by the codebook vectors (also known as Vector Quantization) and at the same time to minimize the classification error. The labelled codebook is generated using an iterative learning procedure where in each iteration a randomly selected training example of known classification is compared to the codebook and the two closest codebook vectors are found. Depending on the class labels of the given example and of the two codebook vectors the latter two are updated by either pushing them towards the example (if the class labels are identical to the known classification of the example, correct classification) or pushing them away from the example (for a detailed description of the algorithm see [9, 10]). The overall aim of this learning algorithm is to increase the probability of correct classification the next time the given example is presented.

Extensive off-line analyses have shown that only a very small number of codebook vectors is needed to provide satisfactory performance, usually 3-4 codebook vectors per category suffice. Searching twelve (4 codebook vectors times 3 categories) 12-dimensional vectors for the nearest codebook vector is an extremely simple and fast form of classification.

The quality measure of the classification can be obtained by not only searching for the nearest codebook vector but also for the nearest codebook vector of a second category. By comparing the distances of these two codebook vectors it can be determined whether the given example lies near a class boundary, in which case the distances to the two codebook vectors d_1 and d_2 will be very similar, or whether the given example clearly belongs to the category of the closest codebook vector, in which case distance d_1 will be much smaller than d_2. Therefore, the quality measure can be computed as

$$qu(d_1, d_2) = 1 - \frac{d_1}{d_2}.$$

It is obvious that this formula will provide values close to zero if the distances d_1 and d_2 are about the same and values close to one if distance d_1 is much smaller than d_2.

Using two pre-defined threshold the quality measure is turned into a feedback of big or small '+', '-' or 'o' corresponding to correct, incorrect or no classification, respectively.

'A6'	big +	+	o	-	big -
Session 2	21,7%	37,5%	21,7%	16,7%	2,5%
Session 3	25,0%	34,6%	23,8%	13,3%	3,3%
Session 4	20,8%	24,2%	24,2%	24,6%	6,3%

'B9'	big +	+	o	-	big -
Session 2	20,0%	21,7%	15,4%	30,4%	12,5%
Session 3	18,8%	23,3%	15,8%	28,8%	13,3%
Session 4	12,9%	20,8%	22,5%	28,8%	15,0%

'A1'	big +	+	o	-	big -
Session 2	22,9%	27,5%	18,8%	23,3%	7,5%
Session 3	20,0%	21,3%	20,8%	26,7%	11,3%
Session 4	19,6%	24,2%	20,4%	21,3%	14,6%

'B8'	big +	+	o	-	big -
Session 2	10,4%	27,9%	21,7%	33,3%	6,7%
Session 3	21,7%	25,0%	13,8%	29,6%	10,0%
Session 4	14,2%	26,3%	24,6%	26,3%	8,8%

Table 1. On-line performance (%) of four subjects in three sessions.

4. ONLINE RESULTS

The on-line performance for the last three sessions (the first was used for training the classifier) of each subject are given in Table 1. All subjects showed more than random on-line performance of up to 60% (random performance in 3 categories would be 33.33% correct).

From Table 1 can be seen:

(i) There are always more trials classified correct (+) compared with incorrect (-).

(ii) About 20% of the trials are not classified into any of the 3 classes (o). This number depends on the threshold used and is a potential for further improvement.

(iii) In the first "mental" session (session 4) the majority of trials were correctly classified for three subjects.

These results are far from optimal but they show for the first time that after only 4 sessions a discrimination between 3 different EEG patterns is possible. It has to be kept in mind, that the systems of Clark and Tizard [1], Hiraiwa et al. [2] and Wolpaw et al. [5] were all designed for a 2-class discrimination problem and none of these systems were applied to 3 classes.

There are different possibilities for further improvement:

(i) Selection of the optimal frequency band with the largest EEG reactivity. For the parameter estimation not only the alpha but also the beta band can be used.

(ii) Selection of the optimal electrode positions. It was shown recently, that classification results depend on the location of the electrodes [11] whereby the optimal positions are not the same for each subject. Such electrode positions should be selected in a pre-experiment, where the EEG is recorded from a large number of electrodes.

(iii) Increase the number of sessions.

5. CONCLUSION

The Graz BCI is based on mental preparation of different kinds of movement. It was shown, that 3 "movement planning patterns" can be differentiated in an on-line experiment within one second. It is planned to extend the Graz BCI to more than 3 classes, e.g. by incorporating other movement planning patterns, concentration on parts of the body (mental movement) or visual imagination.

There are, however, still a number of problems to be solved in relation to optimize the performance of the system. Among these are the improvements in the experimental paradigm including a more effective feedback, the estimation of more specific EEG parameters, improvements in the classifier and in the features presented to the classifier, such as selection of the optimal electrode positions.

6. REFERENCES

[1] Clark C.R., Tizard J.: Single-trial analysis of scalp electrical fields using artificial neural networks. Proceedings of 3rd Int. Congress on BET Amsterdam, 1992.

[2] Hiraiwa A., Shimohara K., Tokunaga Y.: EEG topography recognition by Neural Networks. Engineering in Medicine and Biology, pp. 39-42, 1990.

[3] Pfurtscheller G., Berghold A.: Patterns of cortical activation during planning of voluntary movement. Electroenceph. and clin. Neurophysiol., Vol. 72, pp. 250-258, 1989.

[4] Pfurtscheller G., Flotzinger D., Mohl W., Peltoranta M.: Prediction of the side of hand movements from single-trial multi-channel EEG data using neural networks, Electroenceph. and clin. Neurophysiol., Vol. 82, pp. 313-315, 1992.

[5] Wolpaw J. R., McFarland D., Neat G. W., Forneris C. A.: An EEG-based brain-computer interface for cursor control, Electroenceph. and clin. Neurophysiol., Vol. 78, pp. 252-259, 1991.

[6] McFarland D. J., Neat G. W., Read R. F., Wolpaw J. R.: An EEG-based method for graded cursor control, Psychobiology, Vol. 21, No. 1, pp. 77-81, 1993.

[7] Pfurtscheller G., Flotzinger D., Kalcher J.: Brain-Computer Interface - a new communication device for handicapped persons. Journal of Microcomputer Appl., Vol. 16, pp. 293-299, 1993.

[8] Pfurtscheller G., Flotzinger D., Neuper Ch.: Differentiation between finger, toe and tongue movement in man based on 40-Hz EEG, Electroenceph. and clin. Neurophysiol., Vol. 90, pp. 456-460, 1994.

[9] Kohonen T.: The Self-Organizing Map, Proceedings of the IEEE, Vol. 78, No. 9, pp. 1464-1480, 1990.

[10] Flotzinger D., Kalcher J., Pfurtscheller G.: EEG Classification by Learning Vector Quantization, Biomedizinische Technik, Vol. 37, No. 12, pp. 303-309, 1992.

[11] Flotzinger, D., Pregenzer, M., Pfurtscheller, G.: Feature Selection with Distinction Sensitive Learning Vector Quantisation and Genetic Algorithm Proceedings of IEEE conference on Neural Networks (ICNN 94), pp. 3448 -3451, 1994.

SOMATOSENSORY EVOKED POTENTIALS IN WISTAR RATS: A COMPARATIVE ANALYSIS IN RELATION TO AGE

Milica Bjegović[1], Velimir Išgum[2] and Milivoj Slijepčević[3]
[1]Laboratory for Molecular Neuropharmacology, Rugjer Bošković Institute, [2]Department of Neurology, Clinical Medical Center, [3]Laboratory for Experimental Diabetes and Immunology, Rugjer Bošković Institute, Zagreb, Croatia

Summary

Short latency somatosensory evoked potentials (SEPs) as the response to subcutaneous electrical stimulation of peripheral nerves were investigated in healthy male Wistar rats of different age. Averaged SEPs evoked in aging rats (12 months old) were compared to those of 16 and 18 months. SEPs consistetd of early negative components (N1,N2,N3), part of far-field potential proceeding to NPN wave complex. In transiently anaesthetized rats they occurred 2.40 to 25 ms from the stimulus onset. Significant differences of SEPs in the examined age groups as measured in terms of latencies and the amplitudes of the registered waves were found in both early and later part of the SEP. Statistically significant prolongation (48.7%) of N1 potential accompanied by the amplitude decrease (53.0 %) obtained in our experiments on the 18 months old rats might lead us to the assumption of the prolonged peripheral conduction time correlated to aging. On the other hand the latency prolongation of the later N peaks, as well as the increased duration of NPN wave in aged rats were accompanied by the statistically significant increase of the amplitudes (523%). The presented data obtained in our study on aging rats are consistent with the reports in human studies.

Key words: somatosensory evoked potentials, aged rats

Introduction

Short-latency somatosensory evoked potentials (SEPs) elicited by electrical pulses are generated in the afferent pathways and somatosensory cortex. Recorded electrically from the surface electrodes, they represent the summed neural activity as a complex waveform with several well defined peaks and valleys. Early-latency peaks of SEPs reflect the initial stages of the sensory information processing. Any damage or dysfunction of the nerve cells, connections and white matter to various degrees leads to the abnormality in the waveforms of the SEPs (1). It has been reported that aging is one of the conditions which influences some components of the evoked potentials. The neural basis of visual deficits as normal (non-pathological) age-related changes has widely been explored (2). Visual evoked potentials (VEPs) studies point to significant prolongation of the characteristic latencies of VEPs components (3). Significant lengthening in brainstem and auditory evoked potential latencies after noise exposure was observed in the older subjects; men were markedly more sensitive. Furthermore, in mid-life the SEPs remain stable, in aged subjects the late SEPs component become larger and latencies are slightly prolonged (4). Since no studies of SEPs in aged nonhuman species were found, we thought it would be of interest to learn whether there are any wave changes in advancing age in a manner that parallels the changes in human components of the SEPs. In addition such data would enable us the more reliable investigations of SEPs in development of certain pathophysiological conditions (as experimental diabetes) already investigated in our laboratory (5).

Material and methods

Twelve male Wistar rats aged 12, 16 and 18 months bred in "R. Bošković" Institute, Zagreb, Croatia were used in our experiments. In animals weighed and anaesthetized by iv. injection (tail vein) of alpha-chloralose (72-80 mg/kg) and thereafter monitored the respiration frequency and constant body temperature (37+/-1^{0}C) SEPs were evoked by electrical stimulation of the contralateral forepaw subcutaneously and recorded from the scalp, above the underlying somatosensory cortex with the reference needle electrode placed medially to the neck. Peripheral stimulation consisted of singular rectangular pulses of 0.5 ms duration and 0.25 Hz frequency; the stimulus strength was

adjusted supramaximally. More detailed description of the computorized program with adapted structure of hardware and software to satisfy the specific demands necessary for recording of SEPs in small animals, as well as storage and analysis of averaged SEPs was reported elsewhere (5). SEPs were measured repeatedly in the appropriate age (i.e. 12,16 and 18 months) of each animal thanking to the transient anaesthesia and noninvasive recording method (5). Statistical evaluation of the results were performed using one-way analysis of variance (ANOVA) followed by Newman-Keuls test, or by Student's t-test, where appropriate. Significance was accepted when p values were less than 0.05.

Results

When recording SEPs in healthy 12 months old male Wistar rats we found six characteristic peaks typical and reproducible also through the advancing age of animals. Three of them belongs to short tiny evoked potentials (N1, N2 and N3) in the early phase of the SEPs appearance, and in later phase there were another three peaks of longer latencies and much higher amplitudes constituting the later wave complex (N19, P22 and N25). Early wave components, part of the complex waveform of recorded SEPs, are characterized by three negative wave deflections (N1, N2 and N3) of short latencies and low amplitudes (Figs 1 and 2, Table 1). N1 and N2 waves do not exceed 4.8 - 7/uV in the peak-to-peak (p-t-p) amplitude, while N3 p-t-p amplitude is larger (in average 25 - 29/uV). Aging induced a marked influence on the small short latency potentials. N1 peak is mostly affected. Statistically significant prolongation (48.7%) of N1 potential (Table 1; ANOVA, $F(3.32)=5.38$ $*P<0.05$, i.e, Newman-Keuls test $**P<0.01$ versus 12 months old rats) and N3 peak in much less extent, accompanied by the amplitude decrease (53%) (Table 1; ANOVA, $F(3.32)=26.58$ $**P<0.01$) develops in elderly animals (18 months) as compared to the "mid-life" ones (aged 12 months). Although the second tiny wave of the SEPs (N2) exhibits the slight amplitude enhancement, its latency is slightly prolonged (20.6%; ANOVA $F(3.59)=4.91$ $*P<0.05$) in the 16th month of age. In general, we might say that the early components of SEPs in elderly rats studied in our experiments are definitively characterized by further prolonged latency and markedly decreased amplitude (53% for N1 and 47 % for N3) in the aging process (Table 1). Interpeak latency of N1-N2 wave is usually increased more then the equivalent prolongation of N1-N3 waves.

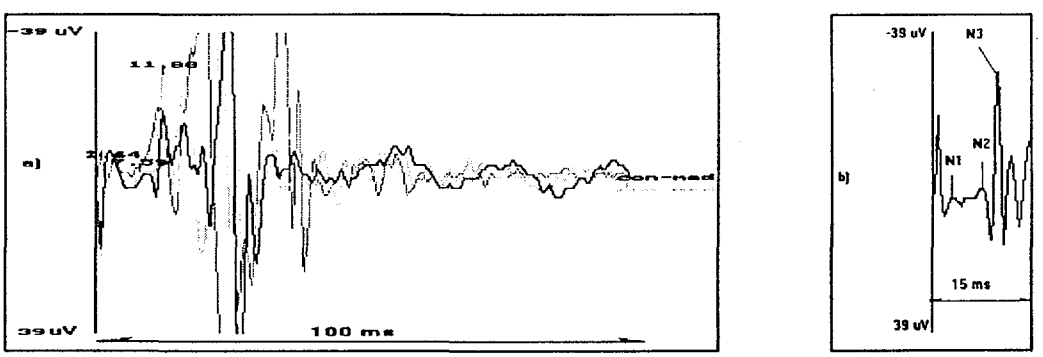

Fig 1. Somatosensory evoked potentials (SEPs) recorded from the scalp of chloralose anaesthetized healthy 12 months old male Wistar rat a) represents the course of the experiment in one animal (SEPs were recorded every 15 min in three time intervals. Each curve is the average of 64 SEPs elicited by the contralateral electrical forepaw stimulation). b) represents three early short latency negative peaks of the SEPs (N1, N2, N3) occurred within first 12 ms.

Latencies (ms)

Age (months)	N1	N2	N3
12	2.40 +/- 0.094 (7)	7.43 +/- 0.480 (6)	11.02 +/- 0.270 (6)
16	2.97 +/- 0.247 (14)	8.95 +/- 0.097 (8) **	10.32 +/- 0.224 (8)
18	3.57 +/- 0.214 (12) **	8.03 +/- 0.479 (6)	11.83 +/- 0.287 (6) *

Amplitudes (uV)

Age (months)	N1	N2	N3
12	-28.24 +/- 0.494 (7)	-29.29 +/- 1.092 (6)	-51.02 +/- 5.554 (10)
16	-31.47 +/- 1.620 (14)	-38.85 +/- 2.326 (8)	-41.05 +/- 3.483 (7)
18	-13.30 +/- 2.546 (12)**	-29.90 +/- 9.709 (6)	-27.04 +/- 8.670 (14)*

Values are means +/- S.E.M.

Table 1. Early components (N1, N2, N3) of the somatosensory evoked potentials in the aged healthy (untreated) male Wistar rats

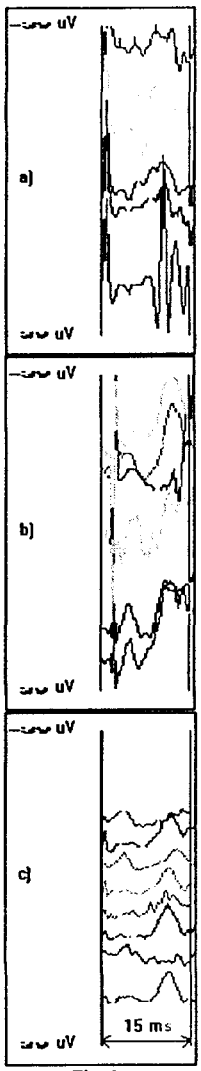

Fig. 2.

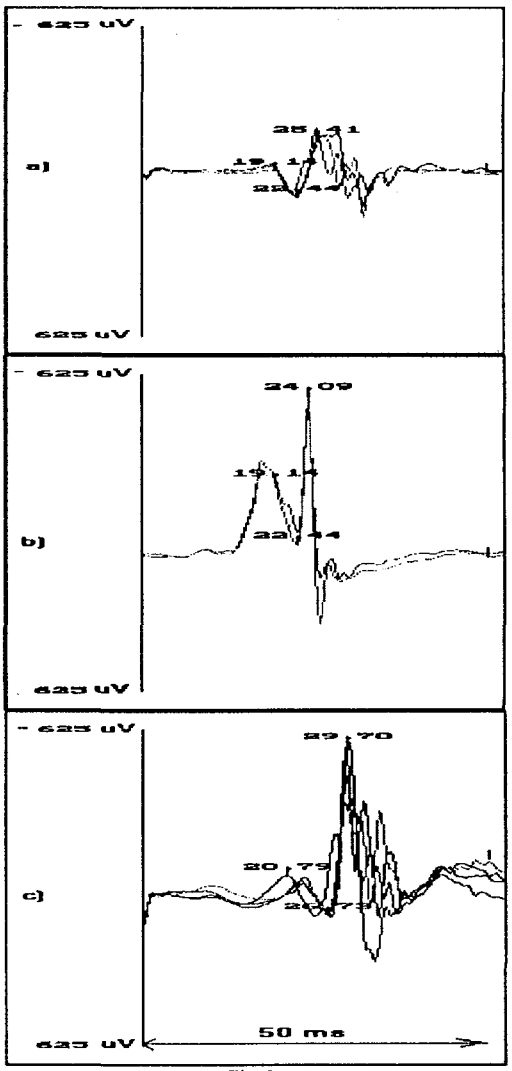

Fig. 3.

Fig 2. Early negative peaks (N1, N2, N3) of the averaged SEPs in the male Wistar rats of different age (a - 12 months, b - 16 months, c - 18 months). Each picture represents SEPs recorded from the two different animals. Note the latency prolongation (b-,c-) and amplitude decay (c-).

Fig 3. Later waves (N19-P22-N25) of the somatosensory evoked potentials in aging male rats. (age: a - 12 months, b - 16 months, c - 18 months) Each single curve recorded in 15 min intervals represent the average of 64 responses to the peripheral stimulation. Note the amplitude increase and latency prolongation with advancement of age.

Latencies (ms)

Age (months)	N19	P22	N25
12	19.17 +/- 0.567 (11)	22.43 +/- 0.391 (11)	25.02 +/- 0.310 (11)
16	19.95 +/- 0.693 (11)	22.60 +/- 0.576 (11)	24.72 +/- 0.745 (11)
18	20.07 +/- 0.664 (11)	25.69 +/- 0.529 (11)**	27.93 +/- 0.342 (11)**

Amplitudes (uV)

Age (months)	N19	P22	N25
12	- 49.49 +/- 9.950 (11)	50.82 +/- 8.601(11)	- 45.050 +/- 7.068 (11)
16	-308.47+/-68.009 (11)**	-96.53 +/- 38.751(11)**	-378.506+/-136.338 (11)
18	- 79.14 +/- 23.114 (11)	47.02 +/- 27.683(11)	-328.450+/-148.636 (11)

Values are means +/- S.E.M.

Table 2. Later components (N19-P22-N25 wave complex) of the somatosensory evoked potentials in the aged male healthy Wistar rats.

According to our results late wave components (N19, P22, N25) as a typical and reproducible part of SEPs in the aging male rats used in our experiments are extremely sensitive to the aging process. Progressive tendencies to the amplitude enhancement of both negative peaks (N19, N25) have been seen (Fig 3, Table 2 and 3). Highly significant increase of N19 (523.3%; ANOVA, $F(3.32)=11.45$ $P<0.01$ followed by Newman-Keuls test) is opposed to the significant reduction of P22 component (189,9% (changing polarity); ANOVA $F(3.32=9.94$ $P<0.01$) in 16 months old rats. Diminishing tendency of P22 amplitude continuous in higher age group (18 months), as shown in

Tables 2 and 3. Latency changes of the late wave complex are expressed in developed age (18 months), and are of modest quantity as compared to early waves; P22 component (14.2%) and N25 (11.4%), both significant (P<0.01) according to ANOVA and Newman-Keuls test. N19 latency remained unchanged throughout the experiment. However, the interpeak latency differences are significantly longer (P<0,01) in the group of old animals (18 months), as it is the p-t-p amplitude in 16 months old rats (Table 3).

-A- delta (ms)

Age (months)	N19-P22	P22-N25
12	3.26 +/- 0.366 (11)	2.59 +/- 0.170 (11)
16	2.65 +/- 0.394 (11)	2.12 +/- 0.433 (11)
18	4.89 +/- 0.390 (11)**	2.34 +/- 0.370 (11)

-B- delta (uV)

Age (months)	N19-P22	P22-N25
12	100.31 +/- 16.136(11)	- 95.87 +/- 11.752(11)
16	211.94 +/- 48.149(11)*	-281.98 +/- 105.538(11)
18	126.17 +/- 46.457(11)	-375.48 +/- 169.681(11)

Values are means +/- S.E.M.

Table 3. Interpeak latency differences (delta ms) -A- and corresponding peak-to-peak amplitudes (delta uV) -B- for the characteristic later wave deflections (N19-P22-N25) on the somatosensory evoked potentials recorded in the aged healthy (untreated) male Wistar rats

Conclusion

Using the previously developed experimental model (5) which offers the possibility of long term detection of physiological state of aging, because of the noninvasive method of recording SEPs and their good reproducibility in transient anaesthesia in rats, the presented results suggest that the aging process affects the SEPs in male Wistar rats in a way similar to humans (6) Increased latency and decreased amplitude of small short-latency ("far-field") potentials (N1, N2, N3) as well as near-field SEPs (P22) in our experiments point to dysfunction of subcortical somatosensory pathway and augmentation of the amplitudes (N19, N22) in aging according to numerous reports (6) might be a result of cortical dysfunction and/or diffuse distant damage. Namely, 50% reduction of neuronal activity from age 20 to age 80 has been reported for the visual cortex including also the changes in neurotransmitter function and increased synaptic delay in the neurons of visual cortex. Since the VEPs in elderly are characterized by latency prolongation and the amplitude changes it is believed that this changes should be ascribed to dysfunction of visual pathways developed in aging process (2,3,4). Similar observations were reported for SEPs (1,6). The interference between aging process and transmitter involvement has been confirmed recently, when age related changes in presynaptic modulation of transmitter release during aging in Wistar rats of both sexes (4. 12 and 24 months) were detected in striatal and hypocampal slices (7). We believe, therefore, that age induced changes of SEPs presented in this paper are the result of developing cortical dysfunction and/or diffuse distant damage of somatosensory pathways developing in aging process.

References

1. J.I.Mattson, W.K.Boyes, J.F.Ross, Neurotoxicology, eds. H.Tilson and C.Mittchell, Raven Press,Ltd., New York, 1992.

2. P.D.Spear: Neural basis of visual deficits during aging Vision Research 33:18:25.89-2609 December 1993

3. M.Kutas, V.Iragui, S.A.Hillyard: Effects of aging on event-related brain potentials (ERPs) in a visual detection task, Electroencephalography and Clinical Neurophysiology 92:2:126-129, March 1994

4. R.Emmersonhanover, D.E.Shearer, D.J.Creel, R.E.Dustman: Pattern reversal evoked potentials-gender differences and age-related changes in amplitude and latency, Electroenceohalography and Clinical Neurophysiology 92:2:93-101, March 1994

5. M.Bjegović, V.Išgum, M.Slijepčević, I.Blažinović : Somatosensory evoked potentials in normal and alloxan treated rats, Periodicum biologorum 95:1:113-116 June 1993

6. H.E.Lowndes, Electrophysiology in neurotoxicology, ed. H.E.Lowndes, CRC Press Inc., Boca Paton, Florida 1987

7. G.Zsilla, T.Zelles, A.Mike, A.Kekesszabo, E.Milusheva, E.S.Vizi: Differential changes in presynaptic modulation of transmitter release during aging, International Journal of Developmental Neuroscience 12:2:107-115, April 1994

NON INVASIVE TECHNICAL APPROACH OF ABDOMINAL EXPLORATION

by Joseph THOUVENOT
and Marie-Christine LEMAIRE
Physiology
Faculté de Médecine de TOURS
FRANCE

Summary :

Electrical visceral activity derivated by the surface electrodes used in the gastric or colic situation will be associated with mechanical signals abdominal compliance.
The sounds and echographic dynamic recordings improve the comprehension of process where abdomen is sometimes in tensive or extensive situation with the consequences for the breathing interactions.

1. INTRODUCTION

In the course of abdominal situations, the electrophysiological signals (electrosplanchnography) are compared with other ones of biomechanical nature such as deformations, pressure, vibrations, hydraulic sounds.

Such a comparison is possible from identification of areas of activity thanks to echographia, such as cardia, stomach, antrum, pylorus, duodenum and transverve colon considered here.

The abdominal field retains many interactions : pulse, breathing, internal and parietal motility.

In fact, the electrophysiological signals in front of mechanical ones arise the problem of so called artefacts. Also two meanings for this word : signal of foreign sources (cable or 50 Hz), signal of physiological process but not considered in the exploration - or difficult to put in relation in a very energetic situation with perturbation of stationnarity condition (pain reaction f. i.).

2. TECHNICS

Electrosphanchnography (1-2)

Ag-Cl electrodes, are placed according to orthogonal bipolar derivations : epigastric oblic for electrogastrography and in square (14-14 cm) for colonic activity. Amplitude of signals is ranging from 0,05 to 10 mV in DC recording, and smaller for a time constant amplification as great as 2-5 s.
Impedance (4-20 KΩ) for square waves 50 Hz. Visceral frequencies in cycles per minute : 1-2 (colon), 3 (stomach), 8-14 (intestine), 8-25 (breathing).

Mechanical pressure recording :

The best mean to record movements of abdominal wall, after trials of strain gauge, was pneumatic amplifying levers according to compliance (1,2 mm.KPa^{-1} for contact area 1,8. $10^{-6}m^2$).

Sounds (3)

Sounds are recorded from contact "electret" microphone, then filtered (1-40 Hz for pulse, 60-600 Hz for elastic or turbulence noises) and registered by pen writer.

Echography (4)

The sequencies of echography (Akola device 3,5-5 MgHz) are recorded on a magnetic tape, then analysed photometrically. A pen record of grey levels is obtained according to a previous technic (4).

3. RESULTS

Many time relations are observed between mechanical signals and sounds (Fig. 1).

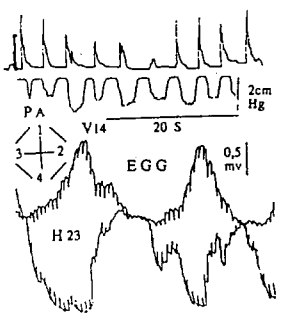

Fig. 1
Women, 40 old.
Trace 1 : Sound, scale 1 dB, Filters 60-600 Hz.
Trace 2 : Abdominal pressure PA, scale 2 cm Hg.
Trace 3 et 4 : ESG, scale 0,5 mV, time 20 s.
Vertical (1-4) and horizontal (3-2) bipolar components of EGG. Electrodes d = 12 cm.

The mechanical signals, sounds and echography records show two states of abdomen :

- tensive state with quick thoracical breathing up to 20-25 c.min^{-1} (Fig. 2).

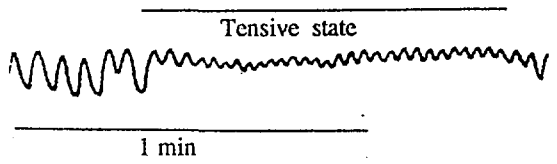

Fig. 2
Abdominal surface mechanogram : tensive state.
Man 60 old. Mechanical pressure record from epigastric area.

- extensive state with deformations specially in hepatic region, with an ample breathing of 1-2,5 cm in abdominal protursions in gastric sequencies (Fig. 3).

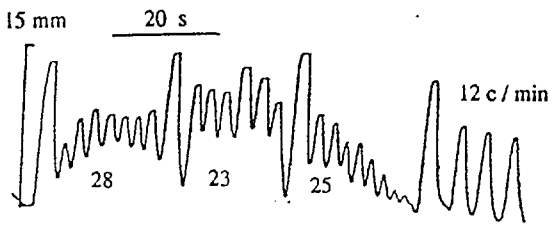

Fig. 3
Abdominal surface mechanogram : extensive state
Lever with pneumatic amplification : abdominal distension with three gastric periods 28,2 and 25 s respectively followed with breath at 12 c.min-1.

The sounds appear in extensive phase of contractility with hydraulic displacements shown by echography (Fig. 4).

Fig. 4
Grey levels integration. Diameter of cross section of antrum scan : 5 cm.
Typical gastric rhythm.

During recording periods, care may be made to avoid intempestive observation of the trace by the patient, leading to feed-back situation.

These interactions may be observed with pulse and breathing always present then weak postural change and internal movements such visceral flows.

The confrontation is helped by echographic observations and its graphic restitution according to a method previously described (4)

4. CONCLUSION

Also each type of signal brings complementarities for the state informations.

The use of mechanical signals previously applied in deglutition (4) with a good accessibility, a weak cost and possibilities of magnetic records, may be used in physiological alimentary situation, and other pathological cases, pain state, and in dysphagia, sleep apnea, drug and post-surgical monitoring.

5. REFERENCES

(1) J. THOUVENOT, S. TONKOVIC, J. PENAUD : Electrosplanchnography.. Acta Med. Jug : 227-247,27, 1973.

2) I. GIORGIO, N. ABBATTISTA, M.C. LEMAIRE, F. PEZZOLA, J. THOUVENOT : La composante spectrale de l'électrograstrogramme (EGG) : ses facteurs de variation chez le sujet normal, cancéreux et ulcéreux.. Path. Biol.: 712-719, 37(6), 1989.

(3) D. LEBEL, C. PAREL, J. THOUVENOT : Exploration de la déglutition à partir de son signal sonore.. Arch. Int. Physiol. Biochim.: 75-86, 98, 1990.

(4) J. THOUVENOT, J. DECAUD-LAROCHE, L. POURCELOT : Possibilité d'une nouvelle exploration dynamique de la contractilité des viscères abdominaux à partir d'images échographiques.. Path. Biol. : 945-951, 32, 1984.

TIME SERIES ANALYSIS OF ELECTROENCEPHALOGRAM DURING GENERAL ANAESTHESIA IN NEUROSURGERY

Sekulić Ante M.D.
University department of neurosurgery, Division of neuroanaesthesia
University Hospital Zagreb, Kišpatićeva 12, Croatia

Summary

Intraoperative electroencephalography was continuously monitored in fourteen neurosurgical patients operated on because of lumbar spine pathology. Sampling was done by ABM2 DATEX monitor connected to an IBM PC. Using zero - crossing frequency algorithm average frequencies and amplitudes were recorded each 30 seconds. Statistical analysis of these comma delimited ASCII files was performed with the aid of STATGRAPHICS 3.0. The values of the EEG frequencies of the dominant cerebral hemisphere were taken for analysis. Visual inspection of plotted data,autocorrelation and autocorrelation after differencing were done. According to this simple analysis it can be considered that the values of the frequencies of intraoperative EEG, during administration of anesthetics, are stationary time series.

Introduction

The electrical activity of the brain, discovered by Caton in 1875. (1), reflects changes in cerebral physiology. As general anaesthesia profoundly affects cerebral physiology it seems reasonable to measure and analyze electroencephalogram (EEG) during the administration of anaesthetics.

Several methods are used for monitoring, recording and analyses of intraoperative EEG. At present, the most popular one is spectral analysis in according with the fast Fourier transformation algorithm (FFT)(2). Another technique is the counting of zero - crossing frequency (ZXF)(3,4).

Recently was shown by using spectral analysis and autoregressive models (AR), that EEG during general anaesthesia seems to be the realization of a Gaussian stochastic process (5). One presumption for AR models is stationarity of time series. Because of that, the aim of this study is to investigate the stationarity of EEG time series after sampling by ZXF instead of FFT.

Methods

Fourteen patients ASA 1/2 (6) operated on due to of lumbar spine pathology received total intravenous anaesthesia with alfentanyl and propofol. EEG was recorded by ABM2 monitor DATEX connected to an IBM compatible PC. Averaged zero - crossing frequency and amplitude were recorded every 30 seconds as comma delimited ASCII file. Statistical analysis was performed by using STATGRAPHICS 3.0. Left

hemisphere frequencies data were used for all patients.

Results

One patient dropped out of analysis because of temporarily disconnected EEG electrodes and missing values of EEG. In all other patients visual inspection of plotted time series EEG data, autocorrelation function of original series and autocorrelation after differencing of the series was done. According to this simple analysis, it can be considered that EEG data (after the ZXF sampling) are stationary time series. Original data, autocorrelation function and autocorrelation after differencing time serie can be seen on Fig.1, Fig.2 and Fig.3.

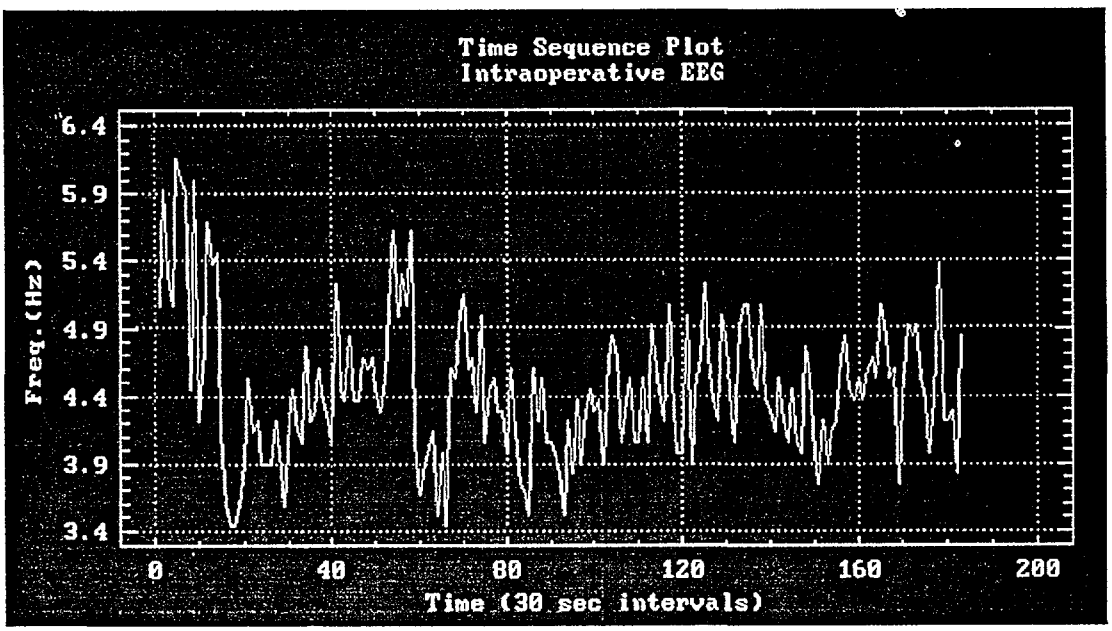

Fig. 1. Original time serie of intraoperative EEG.

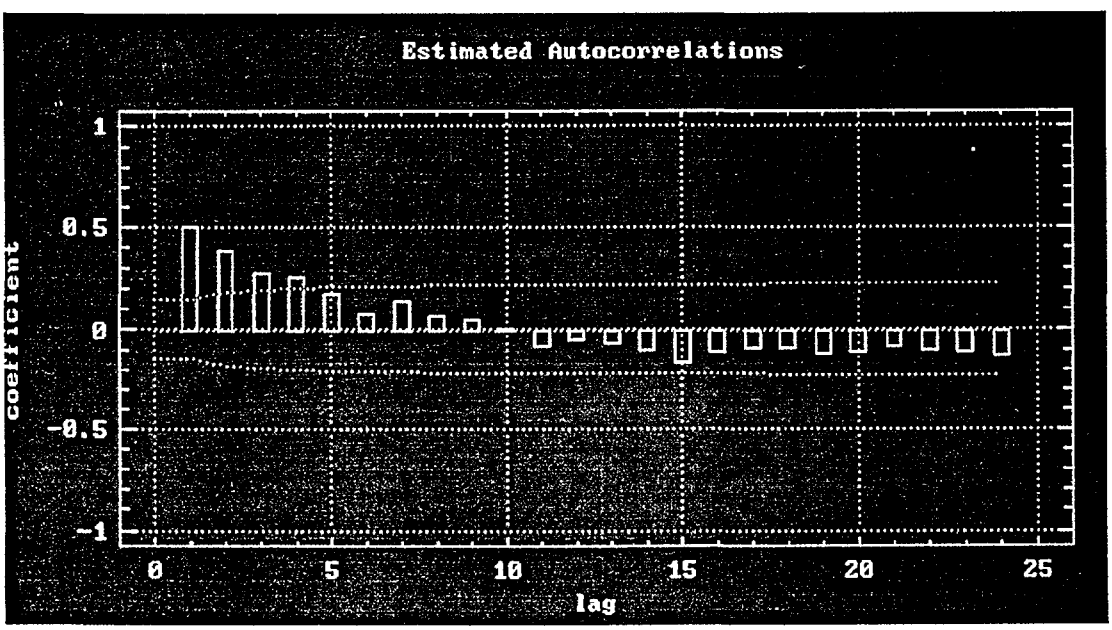

Fig. 2. Autocorrelogram of original time serie of intraoperative EEG

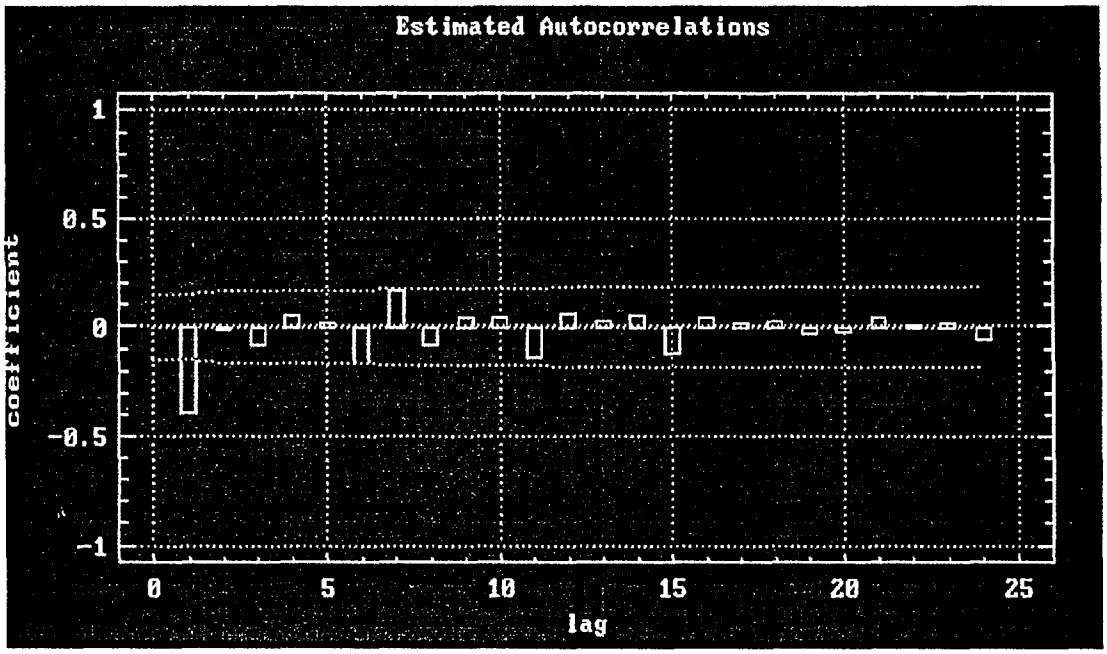

Fig. 3. Autocorrelogram after differencing the original time serie for lag 1.

Discussion

ZXF is an old technique, not very popular today, because it lacks specificity (4). Mathematical appropriateness of ZXF is limited to narrow bandwidth signals with Gaussian frequency spectrum (4). This was verified in drug-free, awaked and relaxed human subjects (7). It is also well known that bandwidths and spectra may vary widely in other states, such as anaesthesia, sleep and coma (8). Intraoperative EEG during neurosurgical anaesthesia is made on ABM2 monitor DATEX in our department. Based on ZXF sampling of EEG, it is a relatively simple and robust machine with an open architecture for connections with other monitoring devices. Despite limitations ZXF seems to be useful in the detection of depression of cerebral function (4,8).It was also shown that the mean EEG frequency is the clinically most useful and statistically most accurate descriptor of frequency changes associated with cerebral ischemia (9).

Due to controversies in the field of intraoperative EEG analysis (4) time series analysis tends no more than to be a contribution to solving the problems. As neurosurgical procedures are long lasting, there is a good chance for large data samples of intraoperative EEG. A low sample size is one of the problems in testing the normality of human EEG (5).

Autoregressive models found a great popularity in EEG analysis (5). The results of this study open the possibility for application of these models even after the ZXF sampling of intraoperative EEG. More detailed analysis of stationarity of time series of EEG should include removing of systemic components (trend, cyclic), analysis of residuals, their possible autocorrelation (Durbin-Watson test) and changes of variance of error terms (heteroscedasticity) (10,11).

References:

1. Caton R.The electric currents of the brain. Br Med J 1875;2:228.

2. Cooley JW,Tukey JW. An algorithm for the machine computation of complex Fourier series. Mathematics of Computation 1965;19:297-301.

3. Klein FF. A waveform analyzer applied to the human EEG.IEEE Trans Biomed Eng 1976;23:246-252.

4. Levy WJ, Shapiro HM, Maruchak G, Meathe E. Automated EEG processing for intraoperative monitoring: a comparison of techniques. Anesthesiology 1980; 53:223-236.

5. Bender R, Scultz B, Schultz A, Pichlmayr I. Testing the Gaussianity of the human EEG during anesthesia.Meth Inform Med 1992;31:56-59.

6. American Society of Anaesthesiologists: New classification of physical status. Anesthesiology 1963;24:111.

7. Sulg IA, Sotaniemi KA, Tolonen U, Hokkanen E. Dependence between cerebral metabolism and blood flow as reflected in the quantitative EEG. Adv Biol Psychiat 1981; 6:102-108.

8. Edmonds HL. Paloheimo M. Computerized monitoring of the EMG and EEG during anesthesia. Int J Clin Monit Comp 1985; 1:201-210.

9. Sotaniemi KA, Sulg IA, Hokkanen TE. Quantitative EEG as a measure of cerebral dysfunction before and after open-heart surgery. Electroenceph Clin Neurophsiol 1980; 50:81-95.

10. Neter J, Wasserman W, Whitmore GA. Applied statistics. 4 th ed.Boston: Allyn and Bacon,1993.

11. Dougherty C.Introduction to Econometrics. New York:Oxford University Press, 1992.

TEMPERATURE AND PULSE OXIMETER WAVEFORMS IN ANESTHESIA

Katarina Šakić, Dubravko Orlić, Šime Šakić

Department of Orthopaedic Surgery, School of Medicine, University of Zagreb, Croatia

Key Words: temperature, pulse oximeter, regional, general anesthesia

ABSTRACT

To determine whether regional-epidural anesthesia affects temperature and pulse oximeter signals in upper and lower extremity, 21 war injured patients were studied and compared with 20 patients with scoliosis, surgically treated in general anesthesia. Methods. Temperature and pulse oximeter probes were placed on the finger and toe. Results. After lumbar epidural injection of Anekain 0,5%, the temperature on the toe increased average 9,2^{o}C and decreased average 5,11^{o}C in general anesthesia. Conclusion. The increase in temperature and pulse amplitude from the toe may aid in the early detection of succesful epidural block and good regional tissue perfusion and oxygenation. Hypothermia occured during general anesthesia must be prevented in the operating room with careful attention to preventing heat loss and monitoring of vital functions.

INTRODUCTION

Heat loss occurs in the operating room because anesthesia obtunds thermoregulatory mechanisms.(1) Sympathetic nervous system (SNS) activation leads to peripheral vasoconstriction with cold induced vasodilatation (CIVD) possibly due to a decrease in norepinephrine release from peripheral nerves of SND (2). General anesthesia renders a patient unconscious, but transmission of stress impulses from the surgical site to the brain is not inhibited, but regional anesthesia blocks the transmission of afferent stress impulses (3). Hypothermia with shivering markedly increased oxygen demands (4-6). A study was undertaken to determine the alterations in skin temperature during general and regional anesthesia.

PATIENTS AND METHODS

Measurements were carried out on patients who had undergone elective surgery. Disposable skin temperature probes (SIEMENS - SIRECUST 403 P) were placed over the palmar aspect of the distal phalank of the right thumb and plantar aspect of the great toe of the nonoperative limb in twenty one injured patients, ages 20-45 years, who were scheduled to undergo reconstructive surgery of lower extremities in epidural anesthesia with Anekain 0,5%. Disposable pulse oximeter probes (OHMEDA-ABIOX 3700) were applied across the second digit of the right hand and second toe of the nonoperative foot. Finger temperature and pulse oximeter probes were continously measured in twenty patients, ages 14 (13-16) years, 19 females and one male with surgically treated thoracic scoliosis in general anesthesia. Ten patients underwent spondylodesis posterior and another ten patients had spondylodesis anterior with transthoracic approach. In all cases, Midazolam (Dormicum) was used to induce anesthesia, nondepolarising relaxants (Pancuronium bromid), Fentanyl, $N_20/0_2$ and reversal was achieved with neostigmine and atropine. Laboratory gas analysis were performed after surgical procedure one hour later.

RESULTS

Skin temperature of the thumb decreased in 5 minutes from 28,6 to 27,0°C and continued to decrease slowly to 26,0°C over the 30 minutes observation period. By contrast, surface temperature of the toe was not significantly increased until 10 minutes after epidural injection, rising from 25,4 to 27,0°C by 30 minutes, the temperature had increased to 34,6°C (Fig. 1). Temperature gradient of average 9,2°C (range 4,3-11,6) on the toe increased and amplitudes of the pulse oximeter waveform on the toe increased, but declined in the finger. The increase in amplitude of pulse oximeter waveform in the foot preceded the temperature rise. Finger temperature during general anesthesia is shown in Figure 2 and Figure 3. Skin temperature in general anesthesia continued to decrease slowly from 34,6 to 23,7°C over the observation surgically period. Temperature gradient of average 5,6° (2,9-7,8) was observed during operating time of average 270 minutes (range 240-330). Average shivering time (minutes) after general anesthesia was 36,0 minutes (28-49) measured in 93% patients. One hour after general anesthesia, $PaCO_2$ were average 6,49 (range 5,2-7,7) kPa. In spite of decreased temperature and reduction in pulse amplitude in the finger, recordings of the pulse rate and oxygen saturation remained the same, both in the finger and the toe oximeter in all patients.

DISCUSSION

Blood flow through the fingers and toes is under adrenergic control as part of thermoregulatory process (2). Epidural anesthesia blocks sympathetic efferent outflow, resulting in opening of the arteriovenous anastomoses in feet and toes. This accounts for the marked rise in pulse waveform amplitude and the significant increase in temperature after sympathetic blockade. General anesthesia obtunds thermoregulatory mechanisms and operating rooms are usually too cold for patients to maintain their body temperature while breathing dry gases or while body cavities are open. Shivering in response to hypothermia during emergence from anesthesia makes prediction of oxygen demand difficult (1). In one study (6) ixygen demand was increased 135-486%. Increase in oxygen demand of this magnitude, coming at a time when the patients may still be severely haemodiluted are undesirable and potentially dangerous. For example, a doubling of the oxygen demand in the face of a 50% reduction in oxygen-carrying capacity will necesitate a fourfold increase in cardiac output to maintain some haemodynamic condition. Under these circumstances, the lung will be presented with blood that is grossly desatureted and that has a very short mean transit time. Both of these factors may operate to inhibit arteralisation of the venous blood, thus contributing to hypoxemia. At the same time the vasoconstriction that occurs as part of the reflex reflex response to hypothermia enhances the vasoconstriction caused by sympathetic responses to pain. Bradycardial dysrhythmias, myocardial depression, coma, can occur when $T<28^{o}C$. Cardiac arrest due to ventricular fibrilation or asystole can be refractory to drugs, defibrilation, pacing until patients are warmed.

CONCLUSION

However the most appropriate approach is prevention of hypothermia (T decreased $5,6^{o}C$) during general anesthesia and choice of regional anesthesia if it is possible. Prevention of hypothermia begins in the operating room with careful attention to preventing heat loss and use of warming technique and monitoring of vital functions - PO_2, PCO_2 and temperature. In recovery room, supplemental oxygen is required, warm blankets are used and drugs are effentive in holting shivering.

REFERENCES

1. H. Rosenberg, R. Clofine, O. Bialik. Neurologic changes during awekening from anesthesia. Anestesiology, 54: 125-130, 1981.

2. D.I. Sessler. Temperature monitoring. In.R.D.Miller, Ed. Anesthesia. Churchil Livingstone, New York, 1990: 1227-1242.

3. J.O. Arndt, A. Hoeck, M.S. Hicks, K.D. Stuehmeier. Peridural anesthesia and distribution of blood in supine humans. Anestesiology, 63: 616-623, 1985.

4. T.H. Benzinter. Heat regulation. Physiol. Rev. 49: 671-754, 1969.

5. D.G. Brown. The effect of high altitute hypoxia and noise on peripheral responses to cold. Coll. Antropol. 18,1: 35-43, 1994.

6. J. Bay, J.F.Nunn, C. Prys-Koberts. Factors influencing arterial PO_2 during recovery from anesthesia. Br. J. Anesth. 40: 398-407, 1968.

FIG 1. CHANGES IN TEMPERATURE IN THE TOE AND THUMB OVER TIME AFTER EPIDURAL INJECTION

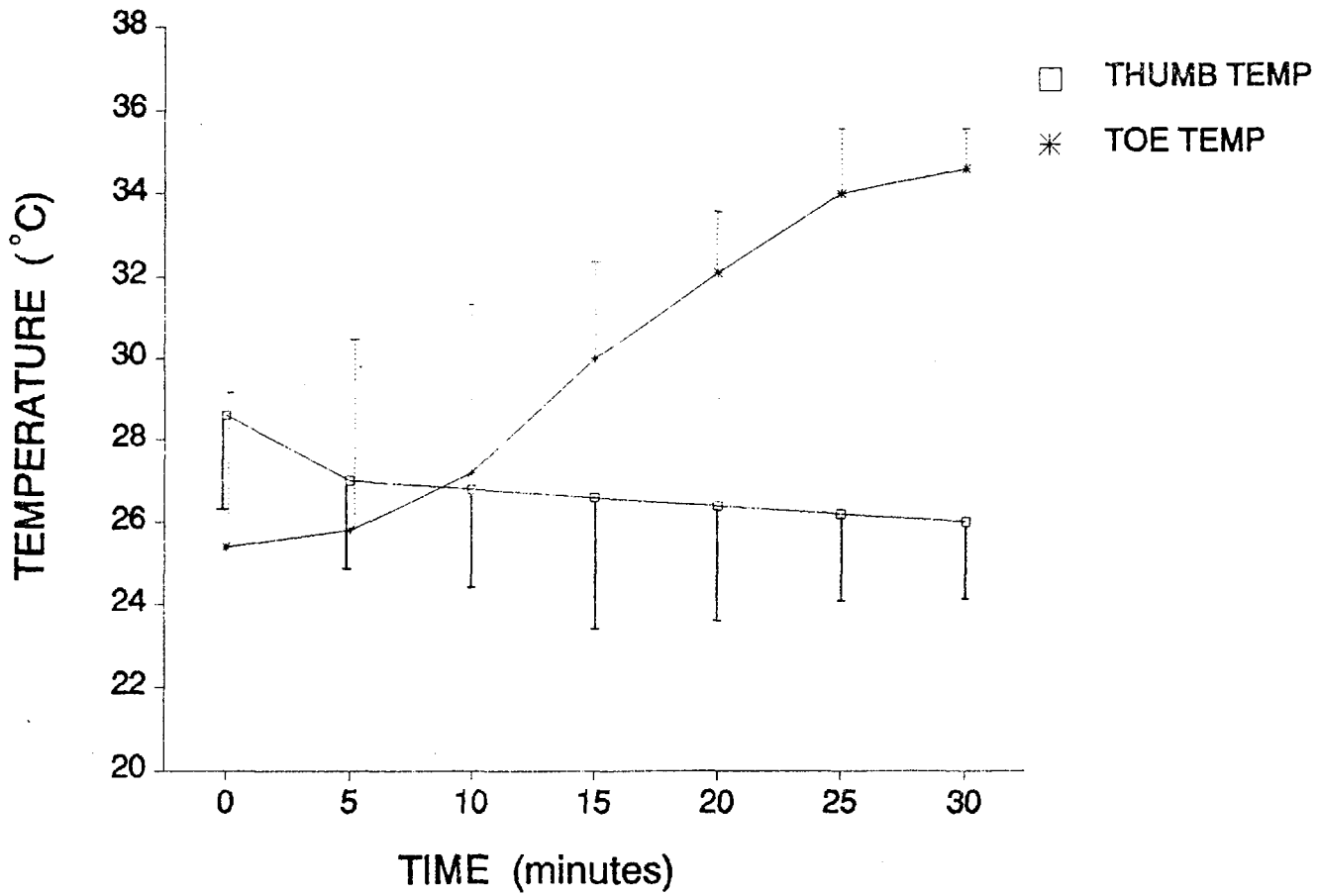

FIG 2. FINGER TEMPERATURE DURING GENERAL ANAESTHESIA FOR TEN PATIENTS WITH THORACOTOMIA - VENTRAL DEROTATIVE SPONDYLODESIS (VDS)

MEAN AND STANDARD DEVIATION PARAMETERS.

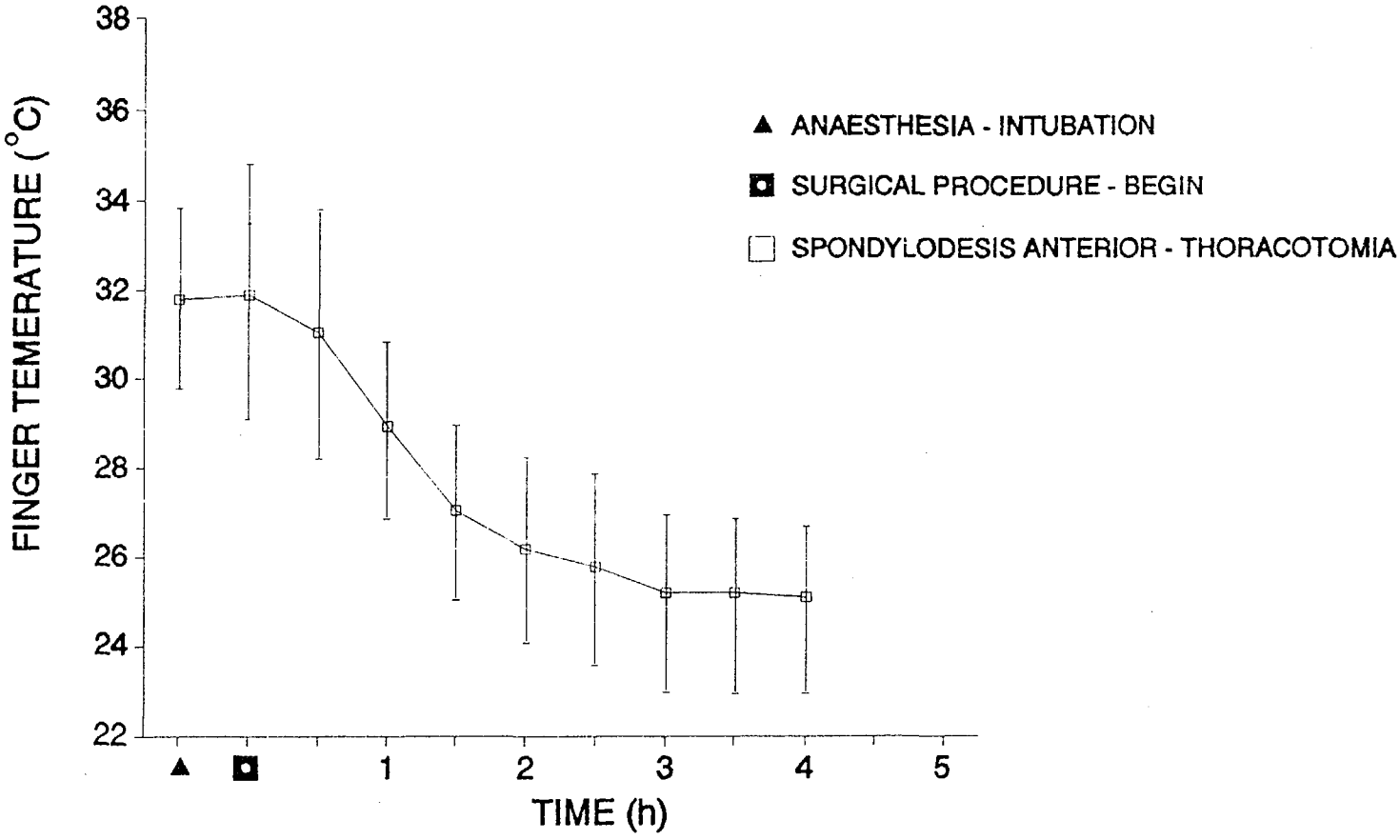

FIG 3. FINGER TEMPERATURE DURING GENERAL ANAESTHESIA FOR TEN PATIENT WITH SPONDYLODESIS POSTERIOR (S.HARRINGTON - LUQUE)

MEAN AND STANDARD DEVIATION PARAMETERS.

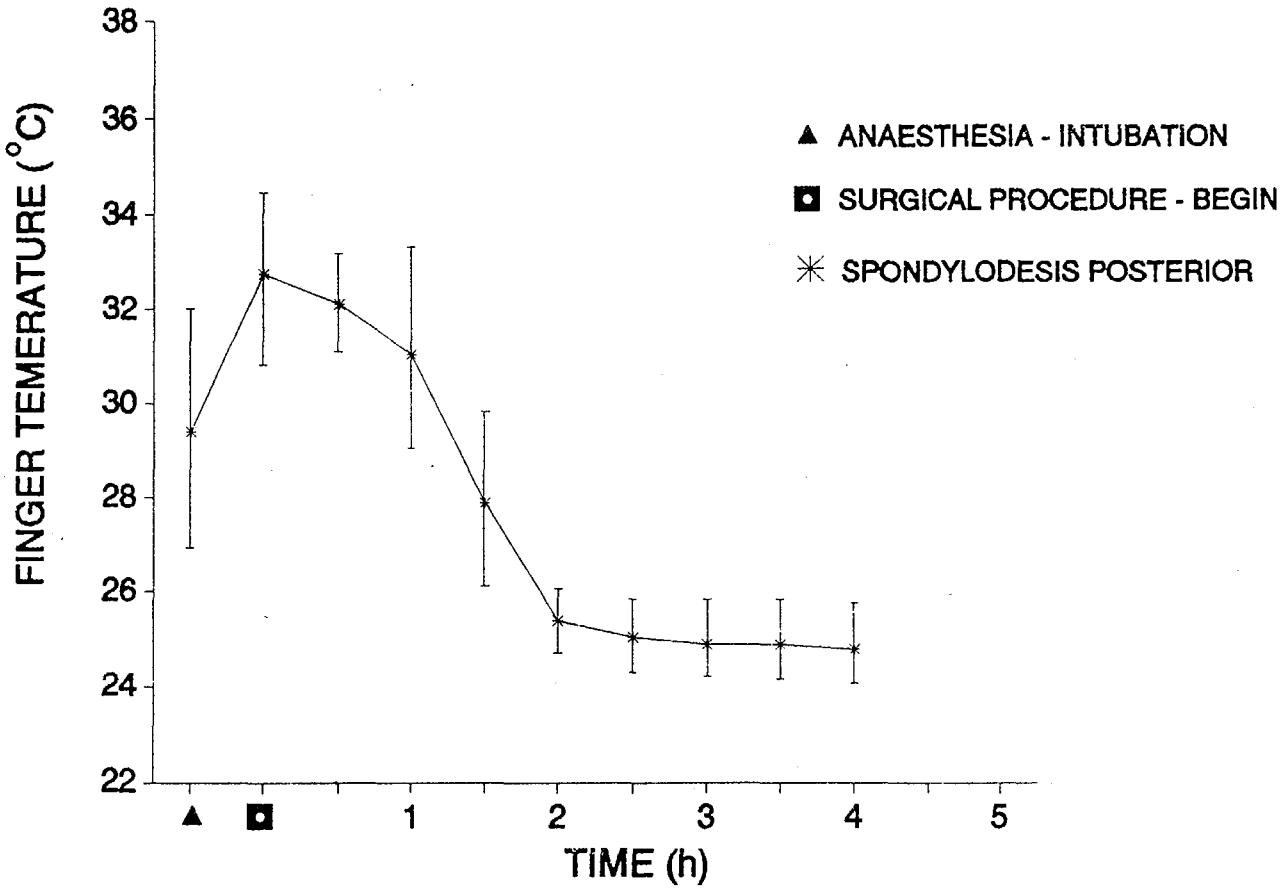

A MULTICHANNEL TELEMETRY SYSTEM FOR FORCE MEASUREMENT IN THE LEGS AND CRUTCHES

Ante Šantić, Miroslav Šaban, Vedran Bilas
Elektrotehnički fakultet, Zagreb, Unska 3

Abstract.

A six channel telemetry system is realized. Four channels are measuring forces in feet, and two in the crutches, or one in the cane. A special transducer based on measurement reflections of infrared radiation is realized. The relationship between force and the output voltage is linear. The flat capacitive transducer is applied for measurement of the force in the feet. For determination of the force in the leg at least to locations on the foot are used: the metatarsal part of the foot and the heel. The capacitive transducer, first converts, the force into pulse frequency and after it, the frequency into voltage. For this telemetry system a pulse-position modulation is applied. The infrared transmission is provided for the confined space but for the open space a RF-transmission should be applied. In this paper the principles of this six channel telemetry system are given with measuring diagrams of the force in the legs, feet and cane during the walk.

VIŠEKANALNI TELEMETRIJSKI SUSTAV ZA MJERENJE SILE U NOGAMA I ŠTAKAMA

Sažetak.

Izveden je šestero-kanalni sustav koji mjeri s četiri kanala sile u stopalima, s dva sile u štakama, odnosno jednim silu u štapu. Za mjerenje sile u štakama odnosno štapu izveden je poseban pretvornik na načelu refleksije infracrvenog zračenja. Odnos između sile i napona je linearan. Plosnati kapacitivni pretvornik upotrebljen je za mjerenje sile u stopalima. Da bi se odredila sila u nozi, potrebno je odrediti silu u stopalima najmanje na dva mjesta i to: u metatarzalnom dijelu stopala i u peti. Kod kapacitivnog pretvornika najprije se vrši pretvorba sile u frekvenciju impulsa, a zatim frekvencije u napon. Za prijenos šest kanala, koristi se vremenski multipleks i pulsno-položajna modulacija. Prijenos impulsa ostvaren je infracrvenom telemetrijom, ali se može u slučaju mjerenja u otvorenom prostoru upotrijebiti prijenos radio valovima. U radu je prikazano načelo rada cijelog telemetrijskog višekanalnog sustava, kao i prikaz mjernih krivulja za vrijeme hoda u nogama, stopalima i štapu.

1. INTRODUCTION

To analyze the different joint disease and lower extremity injuries, and also the progress surveillance during the rehabilitation period, the measurement of the forces in the legs and assistance devices like cane or crutches is very helpful in diagnoses establishment. In this regard the most significant is the force-time diagram which can be obtained as well in the legs also in cane or cruches. In realization of this aim six channel measuring system is realized. For determination of the force in a leg at least to parts of the foot must have force sensors i.e. to measure the force anytime the foot is in contact with the floor. To realize this a force transducer in the heel as well in the frontal i.e. metatarsal part of the foot must be placed. Sometimes a separate observation of the force in the metatarsal part and heel may help in diagnosis determination particulary for joint

diseases. According to this, force-time diagram is measured in the metatarsal part and in the heel of both legs what requires four channel. Also the sum of these two forces in the foot is important to be known the total force in the leg as well. For the measurement of forces in crutches another two channels are required. This means that at list six channels are required but this system can be easily extended in an eight channels system.

For the force measurement in the legs two flat capacitive transducers for each foot i.e. for the heel and metatarsal part of the foot must be placed on the outer side of sole of the shoe. For the force measurement in the cane or two crutches a new type of optical transducer based on infrared radiation is developed. The capacitive tranducer is depicted in Ref.[1] and improved optical transducer with now linear characteristic is described in Ref.[2]. The capacitive tranducers have, a nonlinear characteristic with saturation towards higher forces. For this reason a linearization must be provided what deteriorate the measurement accuracy for about 3%.

2. MULTICHANNEL TELEMETRY SYSTEM

2.1 TRANSMITTER

For the wireless data transmission an infrared pulse transmitter is applied. The infrared transmission is based on the reflections of the walls which fill up whole the room with the infrared radiation where the patient is moving. This type of transmission enables a clean noiseless transmission without any interference. However if the patient has to walk up-stairs or down-stairs or in an open space a classic way of RF (radio frequency) transmission is unavoidable.

The four flat capacitive transducers for measurement of forces in the legs are built in monostable multivibrators to change their time constant T and the pulse duration T_p which is proportional to the capacitance C i.e. $T_p = RC$. The transducer relative capacitance change $\Delta C/C_0$ is small. To make it bigger and $\Delta T_p/T_{po}$ as well ($T_p = T_{po} + \Delta T_p$) unchanged part of T_p

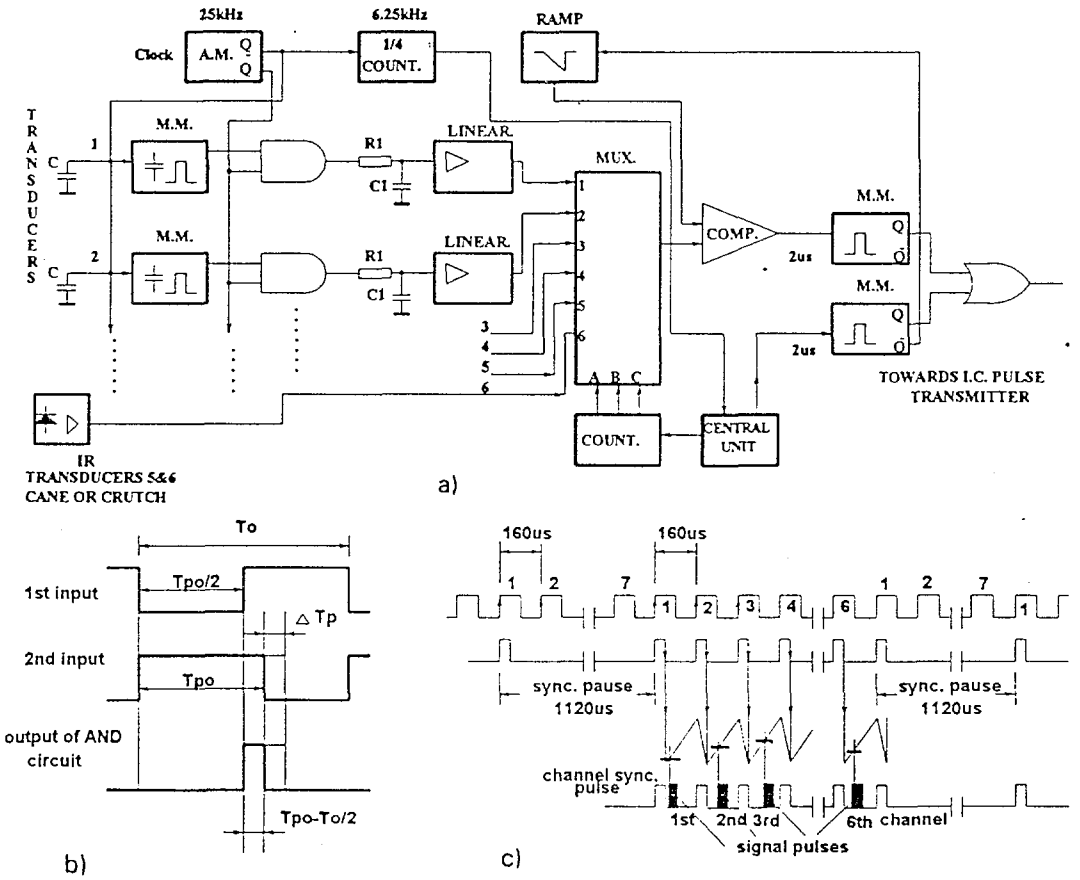

Fig.1. a) Transmitter circuit diagram b) Improvement of modulation depth
c) Transmitter time diagram

can be made smaller by subtraction $T_0/2$ from T_{po} by an AND circuit so that is afterwards $\Delta T_p/(T_{po} - T_0/2)$ with bigger relative changes. To obtain the analog signal the DC component from pulsed signal must be extracted. This is done by a simple RC low pass filter. This is possible to realize because is a very high ratio between pulse frequency f_0 = 25 kHz and the highest signal frequency f_{sg} = 20 Hz. The pulse amplitude is U_0 and the pulse frequency is $f_0 = 1/T_0$ so that the DC component $U_=$ is

$$U_= = U_0 f_0 [(RC - T_0/2) + \Delta CR] \qquad (1)$$

At the output of the infrared transducer the analog signal is already present so that it can be directly led to the multiplexer inputs as 5th and 6th channel. The 1st to the 4th channel are brought to the input of the multiplexer after a stage of linearization.

comparator changes his state, the monostable multivibrator is triggered and a signal pulse is created in duration of 2 μs. The channel sync pulses which come from Control Unit, start also the ramp voltage in the same moment. The Control Unit also takes care that after six channel time-intervals (160 μs) stops to control the multiplexer (MUX) and transmission of channel sync. pulses. During this time of seven channel time intervals (160 μs) without channel sync. pulses a sync. pause is created which marks the beginning of the next cycle. The time diagram is presented on the Fig. 1.c.

2.2 RECEIVER

The optical receiver converts the infrared-pulses in electrical pulses of the same duration as they use to be transmitted. After a Control Unit on the input of receiver side the

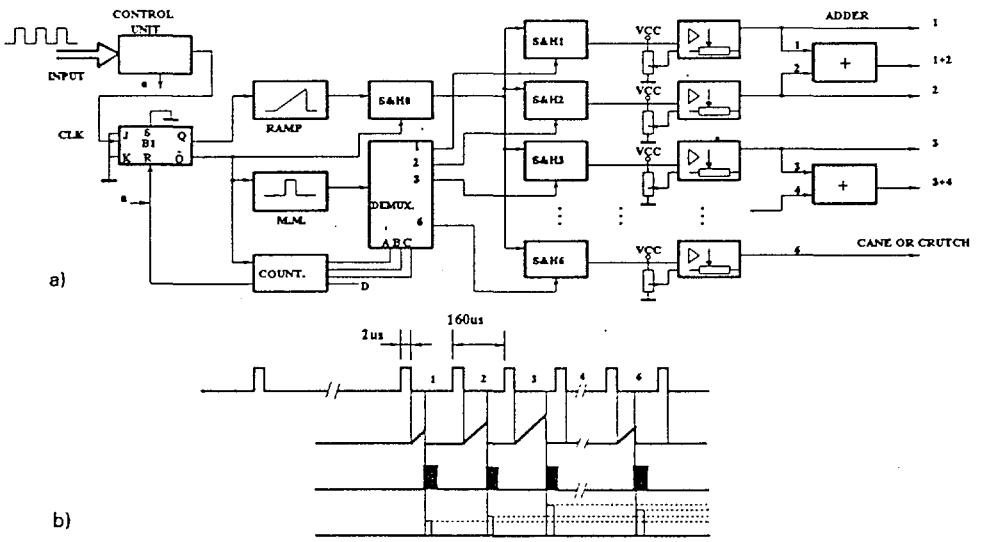

Fig.2. a) Receiver circuit diagram b) Receiver timing diagram

In the multiplexer the channels are arranged one after another. Analog signal voltage u_S of each channel is compared with a ramp voltage u_p in the comparator (comp.) and when the coincidence occurs signal voltage u_S is converted in time t_S according to the relationship $t_S = k\ u_S$ producing a signal pulse. In this way each signal pulse is located on the position t_S in regard to the channel sync pulse proportional to the signal voltage u_S at this moment. So each sample is taken in the time interval of 160 μs what corresponds to the sampling frequency of 6.25 kHz. The moment of coincidence, when the ramp voltage u_p becomes equal to the signal voltage u_S and sync. pulses for each channel are extracted after each sync pause. The channel sync. pulses trigger after are distributed by a demultiplexer (Demux), the sample & hold (S&H 1,2.....6) circuits of each channel. The sample value of each channel is kept to the arrival of the next pulse of the same channel what is the time of one cycle or frame. The cycle duration is composed by sync. pause and six channel time-interval of 160 μs what is all together 2080 μs. Each channel sync. pulse starts the ramp voltage of the ramp generator which is increasing until the signal pulse comes and takes the sample u_S of the ramp voltage by the sample & hold circuit (S&H0). The taken sample by S&H 0 circuit last until

next sample will be taken. The voltage taken by the each of the six sample & hold circuits is than led to six differential amplifiers which serve for signal amplitude calibration and "zero level" (voltage offset) adjustment. Two additive circuits are provided to add up each two channels belonging to same foot i.e. its metatarsal part and the heel.

The output signals are than led to a six channel direct writing recorder. However it can be used also storage oscilloscopes with possibilities to plot the force-time diagrams afterwards. It is also possible to use a PC-computer and to present data simultaneously on the monitor and to plot them afterwards the data are previously stored in a computer memory. In the case that a computer is applied the receiver part presented on the Fig. 2 should be replaced by a much simple receiver which requires only restoration of the received pulses. Counting the pulses from a separate clock in the time interval t_S the A/D conversion is realized.

3. EXPERIMENTAL RESULTS

Fig. 3. shows the measurement results obtained by an eight-channel storage oscilloscope with a pen recorder. In the figure is presented 7-channel force-time diagram during the walk. There are shown with six channels force-time diagrams of the metatarsal part of the foot, the heel and their sum for the right and left leg, and the force in cane on the seventh channel. In Fig.4. the forces in the metetarsal part, the heel and their sum, are shown on the same line of abscissa what enables examination of the larger size diagrams, which are easier to compare, but still with good distinction possibility. In the Fig.4. is shown a healthy person walking, and in the Fig.5. a person with injured joint using a cane during the walk.

The accuracy of the measuring voltage obtained by the optical transducers is about 3%, but these obtained by capacitive flat tranducers because of linearization requirements are in the range of ± 5.5%.

The multichannel transmitting system is carried by the patient on his belt and the infrared transmitter is carried on the shoulder. The transmitter power supply is 9 V battery. The size of the transmitter is 90x130x40 mm and his weight is 180 g.

4. CONCLUSION

A six channel telemetry system is realized for force measurement in the legs, cane or crutches during the walk. The complete force-time diagram in the leg is composed by the force developed in the heel and in the front part of the foot so called metatarsal part. For diagnostic purposes it might be interesting to see the force in metatarsal part and heel separately as well their sum. With the six channel system all this requirements are fulfilled. However in the case that is required to be shown simultaneously metatarsal force and the force in the heel in both legs, their sum and the forces in the crutches, an eight channel system will be required. The multichannel system here described is very easy to extend to an eight-

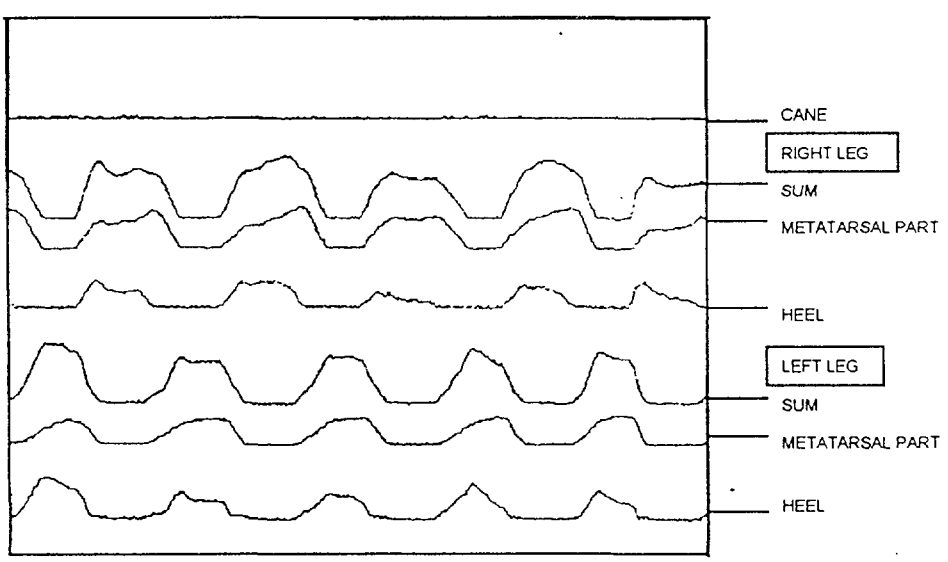

Fig.3. Seven channel force-time diagram obtained on the legs without cane

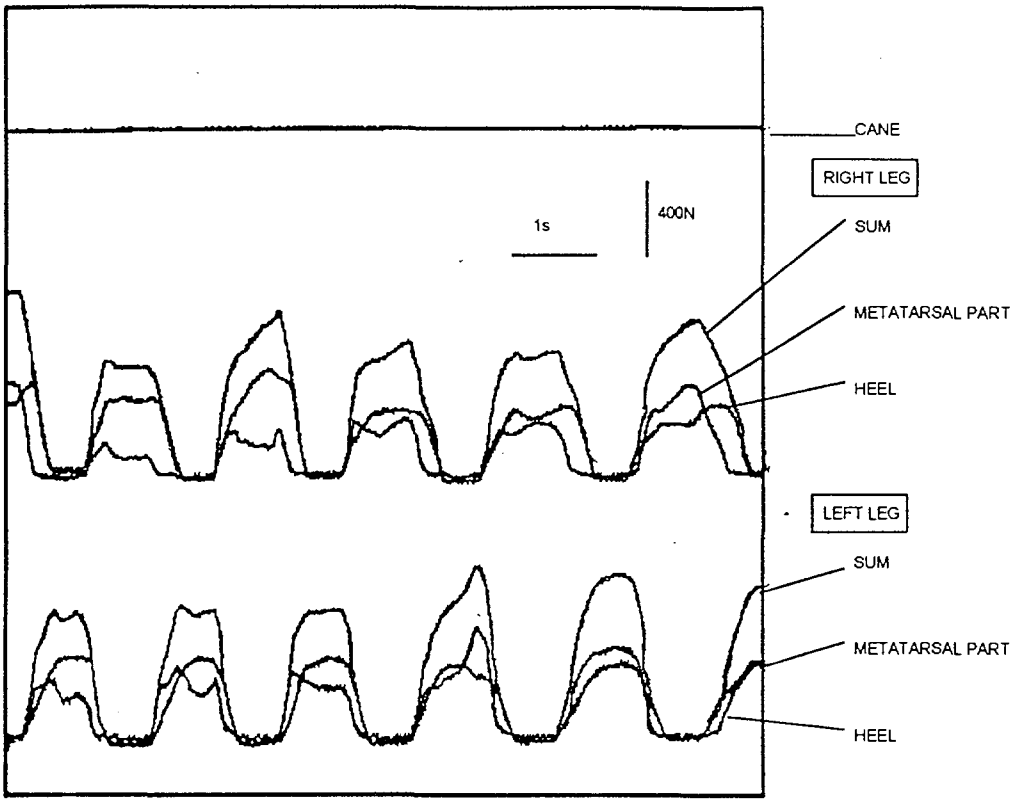

Fig.4. Force-time diagram of the metatarsal part of the foot and heel and their sum for both legs, without cane

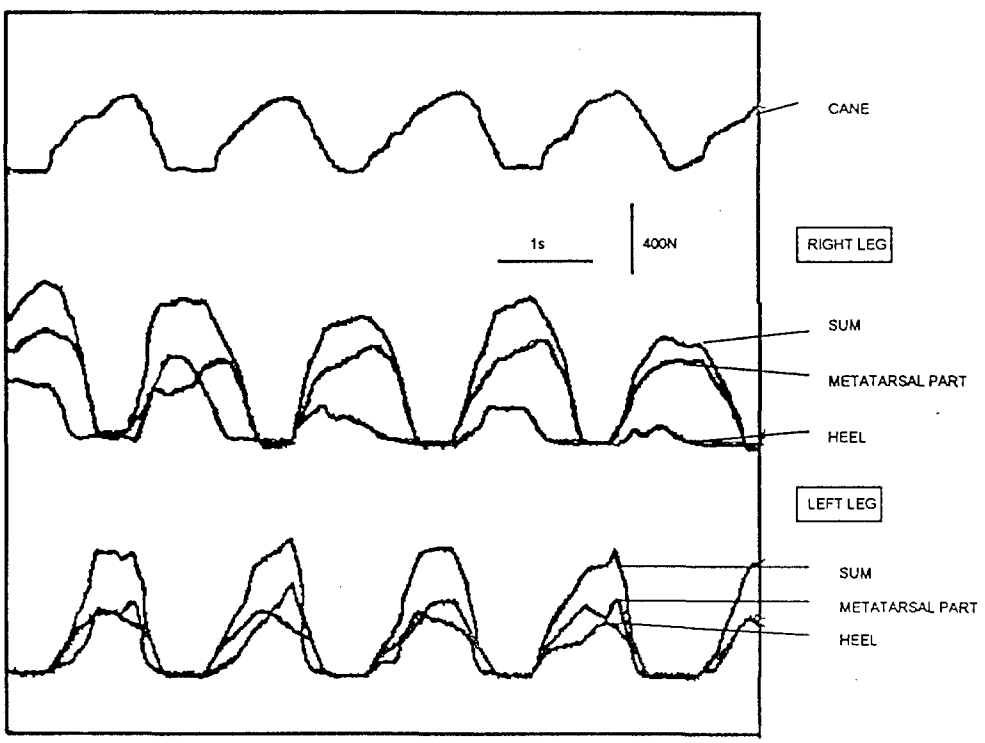

Fig.5. Force-time diagram, the same as in Fig.4., but with the cane.

channel system with only changing a few connections in the Control Unit because multiplexers and demultiplexers are already done with eight inputs.

Acknowledgment. We gratefully acknowledge financial support of this work by the Ministry of Science and Technology, of the Republic of Croatia with the grant No. 2-07-259.

REFERENCES:

[1] A. Šantić, M. Šaban: Transducers for the force analysis in lower extremities and cane during the walk. Periodicum Biologorum. Vol. 95. No.1 63-66, 1993.

[2] A. Šantić, M. Šaban: An Optical Transducer for Force Measurement. KoREMA Proceedings 39 (1994). Part 1.

[3] M. Kljajić, J. Krajnik: The use of Ground Reaction Measuring Shoes in Gait Evaluation. Clin. Phys. Physiol. Meas., 1987, Vol. 8, 133-142.

[4] S. Miyazaki, H. Iwakura: Foot-Force Measuring Device for Clinical Assessment of Pathological Gait. Med. & Biol. Eng. & Comput., 1978, 16, 429-436.

A SIX CHANNEL EMG ACTIVITY MEASURING TELEMETRY SYSTEM

Igor Kršić*, Ratko Magjarević*, Melita Valentić-Peruzović, Goranka Prpić-Mehičić**, Asja Čelebić**, Mladen Zobundžija***, Antun Brkić***, Zlatko Matolek*****

***Faculty of Electrical Engineering, Dept. for Electronic Meas. and Syst., Unska 3**

****School of Dentistry, Gundulićeva 5**

*****School of Veterinary Medicine, Heinzlova 55**

University of Zagreb, Croatia

Abstract

A portable, six channel telemetry system has been developed to enable EMG activity measurements in animal experiments, sports medicine and rehabilitation. Each channel has its own bandpass filter with high common mode rejection ratio as well as a precise rectifier. The rectified and smoothed EMG signals are transmitted in RF band. The receiver is connected to a personal computer and digitally decoded data is stored on a PC hard disk for further processing running under WINDOWS software tool MS Excel. The system was evaluated in masticatory muscle activity measurements on dogs and on some simple exercise performances in sports medicine.

ŠESTEROKANALNI MJERNI TELEMETRIJSKI SUSTAV EMG AKTIVNOSTI

Sažetak

Razvijen je šesterokanalni prenosni telemetrijski sustav za mjerenje mioelektričkih potencijala prilikom pokusa na životinjama, u sportskoj medicini i rehabilitaciji. Svaki mjerni kanal ima pojačalo s visokim stupnjem potiskivanja zajedničkog signala, pojasno propusnim filtrom i preciznim ispravljačem. Ispravljeni i usrednjeni EMG signali su kodirani i prenose se u radiofrekvencijskom području. Prijemnik je povezan s osobnim računalom u kojem se digitalno dekodirani podaci spremaju na tvrdom disku. Daljnja obrada podataka odvija se u WINDOWS okruženju uz programsku podršku MS Excel. Sustav je vrednovan mjerenjima mioelektrične aktivnosti mastikatornih mišića pasa te na nekoliko jednostavnijih sportskih vježbi.

1. INTRODUCTION

In movement research, several signals have to be transmitted from freely moving subjects. Because of the cables, that interfere with movement, the subject can hardly move more than a few meters. Telemetry enables transmission of signals on larger distances and usually does not reduce movement since the devices are small and can be attached on a suitable part of the body. In sports medicine and rehabilitation there is often a need to measure some parameters of movement like myoelectric signals, kinematic data, foot switch signals etc. Because of its wide bandwidth (typically from 20 Hz to 1 kHz), special problems arise when unprocessed myoeletric signals have to be transmitted. A suitable solution is to rectify and smooth them before modulation and transmission.

This results in low frequency signals which can be transmitted in a much more simple way and can give enough information about the process under investigation.

2. DESIGN CONSIDERATIONS

In this paper, a six channel telemetry system is described. This system consists of four units: input unit with an amplifier, rectifier and filter for each channel and encoder/ transmitter unit, both on the moving subject, a receiver/decoder unit and finally a analog to digital converter card which is plugged into a PC (Fig. 1).

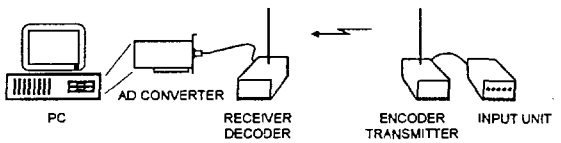

Fig. 1. The entire telemetry system.

Analog, myoelectric signals are preprocessed and conditioned to be compatible with the input of a standard radio control encoder/transmitter (LM 1871 by National Semiconductor). In this way six signals in time multiplexed pulse width modulation and a synchronization pulse are transmitted at 47 MHz carrier frequency. Special consideration was taken about the practical aspect of the portable part of the system, i.e. small dimensions (two cases of 110 mm x 60 mm x 30 mm) and a construction suitable for being attached to the moving subject during the measurements. The modulated signals are reconstructed with the compatible receiver/decoder (LM 1872 by National Semiconductors). Though this receiver allows analog reconstruction of two channels, the obtained PWM pulses were led to the A/D card in the PC and used as gate signals for a CMOS programmable interval timer (82C54 by AMD). The timer was connected to a personal computer enabling storage of the measured data for further processing.

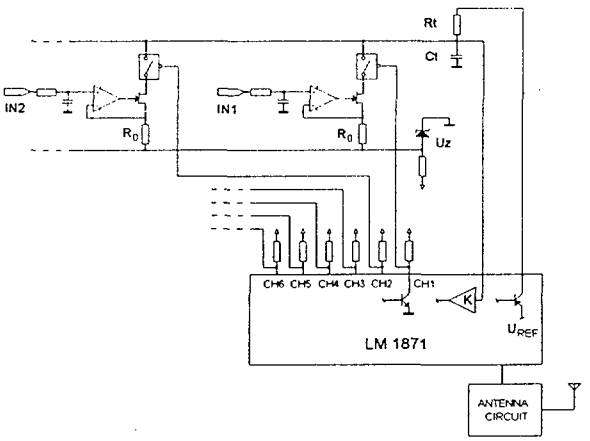

Fig. 2. The encoder / transmitter.

2.1. Analog processing

Each channel of the system has a EMG preamplifiers designed with quad operational amplifiers (TL 074 by Texas Instruments). Three amplifiers were connected into a instrumentation amplifier with low cut off frequency 7.3 Hz and the fourth amplifier was used for the realization of an active rectifier. The amplification of the preamplifiers could be selected in four steps between 200 and 2000.

2.2. Encoding and Transmission

After additional amplification, the rectified signals were used for driving a current sink of the corresponding PWM input of the encoder/transmitter (Fig. 2). In this way, pulses of duration t_{pi} are created as a result of discharging the timing capacitance C_t with constant current (Fig. 3a, 3b). In standard applications of the this encoder/transmitter, variable resistors (potentiometers) are used for creating the information. The pulse width t_{pi} is not a linear function of the input voltage U_{INi} but

$$t_{pi} = \frac{R_0 \cdot C_t}{3} \cdot \frac{U_{REF}}{A \cdot U_{INi} + U_Z}$$

where R_0 is the resistance of the resistor in the sink, C_t capacitance of the timing capacitor, U_{REF} internal referent voltage of the transmitter, U_Z the voltage of external reference and A the gain of the

preamplifier, the active rectifier and the filter. For the maximal span of the input voltage (from -4 V to 0 V), pulse widths of 5.06 ms to 1.01 ms are obtained, respectively.

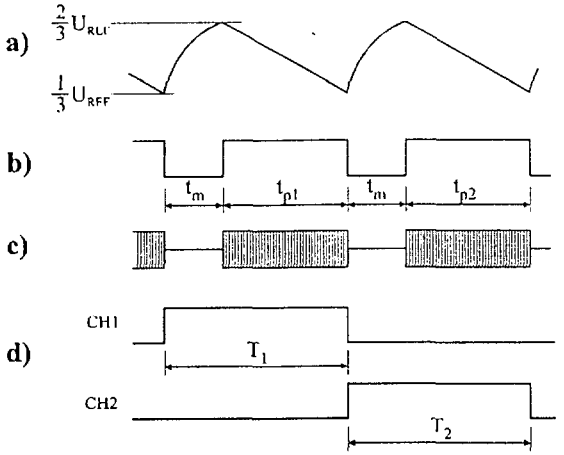

Fig. 3. The timing Diagram.

These pulses (t_{pi}) modulate the crystal oscillator carrier frequency 47.693 MHz and are transmitted to the receiver (Fig. 3c). The transmission and receiver antennas are 64 cm long flexible wires. Flexible antenna has a lot of advantages fixation to the moving object. The difference in antenna position and the resulting changes in effective length of the dipole does not affect transmission / receiving quality so long it is kept approximately straight - for example, fixed around the human torso. A working range of approximately 250 m is available in this configuration.

The RF carrier is interrupted for short fixed intervals (t_m in Fig. 3b) with each internal followed by variable width pulses (t_{pi}). Synchronization is accomplished by allowing one of the transmitted variable pulse widths to exceed the duration of the receiver-based timer, thus allowing the receiver to recognize this pulse for synchronization purposes.

2.3. Decoding

The receiver design allows decoding of the demodulated RF waveform from the transmitter by negative edge triggering of a cascade of binary dividers. In this way, six variable pulses T_i (Fig. 3d) are obtained

$$T_i = t_m + t_{pi}.$$

Since the data are to be sent to a PC, the A/D conversion is done by measuring the duration of the pulses T_i with a 16 bit counter (Fig. 4). In this way the duration of the pulses T_i is proportional to the number n_i of counted pulses of frequency f_{ADC},

$$n_i = T_i \cdot f_{ADC}.$$

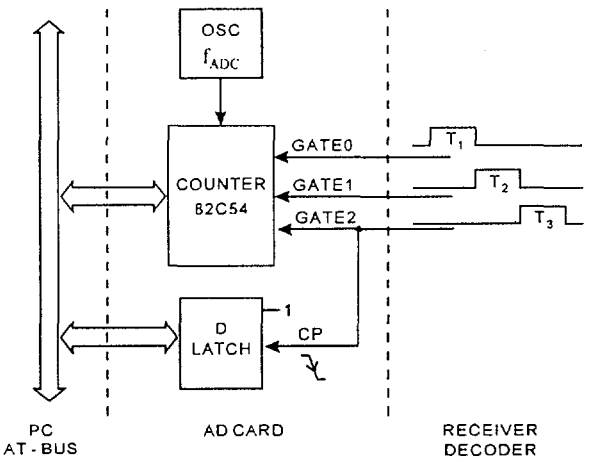

Fig. 4. The analog to digital converter block diagram.

2.4. Data Processing

The data containing information about the pulse width are stored in a file for further processing. This file is imported into MS Excel and the input voltage U_{INi} of each channel is calculated from the measured time data according to

$$U_{INi} = \frac{1}{A}\left(\frac{1}{3}\cdot\frac{R_0 C_t f_{ADC}}{n_i - t_m f_{ADC}}\cdot U_{REF} - U_Z\right).$$

In Fig. 5 a sequence of processed EMG data obtained from both, left and right masseter muscle of a dog during chewing hard food (bones) is shown. The myoelectric activity was recorded with needle electrodes fixed 20 mm apart. The experimental animal was caring the amplifier and encoder / transmitter cases on the back and the antenna was attached to the protective collar with self adhesive tape. When smashing hard food, dogs use one side of their jaws dominantly, resulting in increased myoelectrical activity on that side (Ch. 2 in Fig. 5).

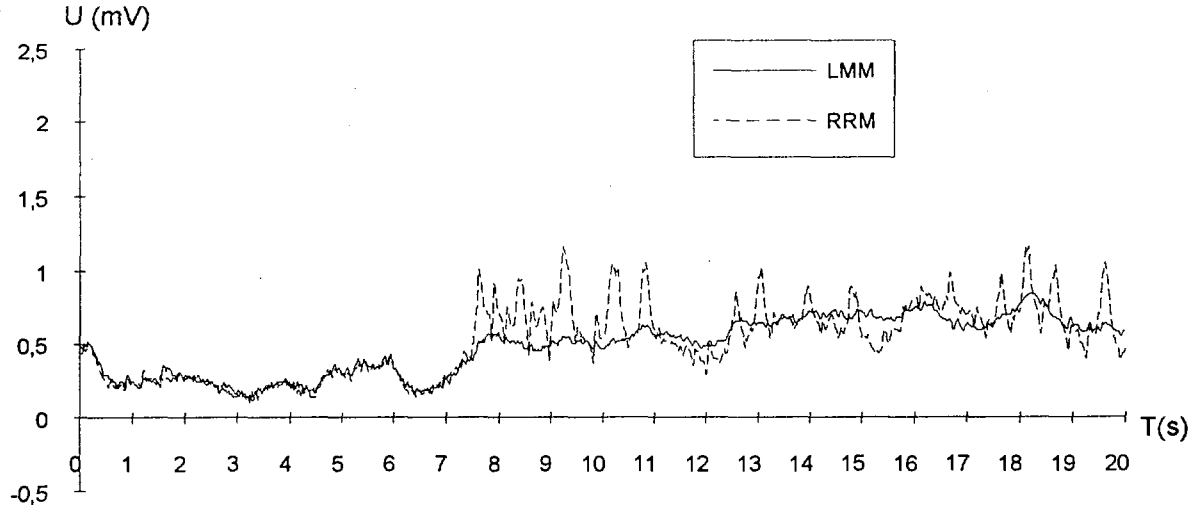

Fig. 5. The processed signals from left (LLM) and right (RMM) masseter muscle of an experimental animal.

3. CONCLUSION

The advantage of the presented system is the simplicity of it's hardware, small dimensions and power consumption as well as the possibility to process the obtained data with users friendly software running under windows. The information one can get with this system is signal strength in time but because of filtering and smoothing, frequency domain information is lost. Preliminary measurement have shown that this telemetry system gives useful information about myoelectric activity from six different muscles. The estimated overall error of the system due to subject movement, crosstalk and power supply instability is ±3% of the full range. With small changes, it can be adopted for transmission of any other low frequency bioelectrical signal. Further evaluation of the system in sports medicine is in progress.

4. LITERATURE

[1] S. Gogaert, M. Styaer, T. Van Nuland, W. Sansen, A Low Power, Eight Channel EMG Measuring System with Bidirectional Telemetry Link, Biotelemetry XII, 367-374, Ancona, Sept. 1992.

[2] A. L. Hof, G. J. J. Bonga, F. G. J. Swarte, L. de Pater, Modular PPM Telemetry System with Radio, Infra-red and Inductive Loop Transmission, Med. & Biol. Eng. & Comput., 32, 107-112, Jan. 1994.

[3] N. E. Evans, Baseband Transmit and Receive Processor for Two-channel PWM Telemetry, Med. & Biol. Eng. & Comput., 27, 215-220, March. 1989.

Tricuspid Flow Controlled Cardiac Pacing System

BOŽIDAR FEREK-PETRIĆ, BRANKO BREYER AND VOJTJEH BRIDA

University Hospital Rebro, Kišpatićeva 12, 41000 Zagreb, Croatia

SUMMARY. *- Installing a blood flow velocity device on the cardiac pacing lead enables the blood flow measurement arround the pacing lead axis by means of the special electronic circuits connected to the said device. If the blood flow through the tricuspid valve is measured, the waveform consists of the early diastolic filling wave and the atrial filling wave. Pacemaker is able to detect the appearance of the atrial filling wave and to stimulate the ventricle after determined atrioventricular delay synchronously with detected atrial filling wave. Pacemaker is able to detect disappearance of the atrial filling wave caused by the atrial fibrillation as well as disappearance of the early diastolic filling wave caused by either ventricular arrhythmia or loss of capture. The time interval from the pacing spike to the uprise of the diastolic filling wave, diastolic filling wave duration, the diastolic filling acceleration, the peak velocities of the filling waves, and the rapid diastolic filling fraction are the sensors for the rate adaptation in the rate responsive pacing mode. Peak velocities ratio as well as the filling waves integrals ratio enable the rate induced ischemia and therefore the determinetion of the maximal tracking rate.*

Key words: *VDD pacing, rate responsive pacing, tachycardia detection*

INTRODUCTION

Physiologic cardiac pacing is very important on temporary as well on permanent basis. Temporary pacing is usually applied either after cardiac surgery or during myocardial infarction because of the transient conduction disturbance or arrhythmia. Patients in rest have significantly improved cardiac output when ventricular contraction is synchronous with atrial filling of ventricles. There are two basic modes of physiologic cardiac pacing: sequential and synchronous. The sequential atrio-ventricular pacing is used to restore normal atrio-ventricular relationships. In this mode an atrium and a ventricle are paced by twin stimuli separated by an appropriate physiologic interval. However the heart rate is controlled by the pacemaker programme and does not vary according to the physiological needs. The synchronous cardiac pacing approximates most closely to the normal cardiac rhythm. The spontaneous atrial electrogram (P-wave) is sensed by an electrode usually in contact with the atrial endocardium and this is used to trigger the ventricle after an appropriate preset delay. Because the atrial rhythm is paced by our natural pacemaker sinus-atrial node, the frequency varies naturally according to the body workload. There is a significant drawback of physiologic pacing systems which complicates the surgical procedure in comparison with non-physiologic pacing. The physiologic pacing requires the implantation of two leads: one atrial and one ventricular. If the patient has a normal function of the sinus node and atria, the atrial lead is only used to sense the atrial activity and the ventricular lead is used to sense the ventricular activity and to pace the ventricles. Because the sensing of atrial activity may be done by an electrode floating within the right atrial cavity, a lot of effort has been done to design a single pass lead for P-wave synchronous ventricular pacing comprising the atrial and ventricular electrode on the same lead.[1] The purpose of this study was to investigate the feasibility to use the blood flow through the tricuspid valve instead the sensing of the P-wave in order to synchronize and control the ventricular pacing.[2,3]

MATERIALS AND METHODS

Figure 1 illustrates the basic principle of the proposed system comprising the flow measurement pacing lead shown within the anatomic structures of the human heart. The heart is disclosed in the four chamber cross-section and the myocardial cross-section is visible of the left-ventricular wall 10, the right-ventricular wall 11, the interventricular septum 12, the left-atrial wall 13 and the right-atrial wall 14. Two chambers of the left heart, left ventricle 15 and left atrium 16 are

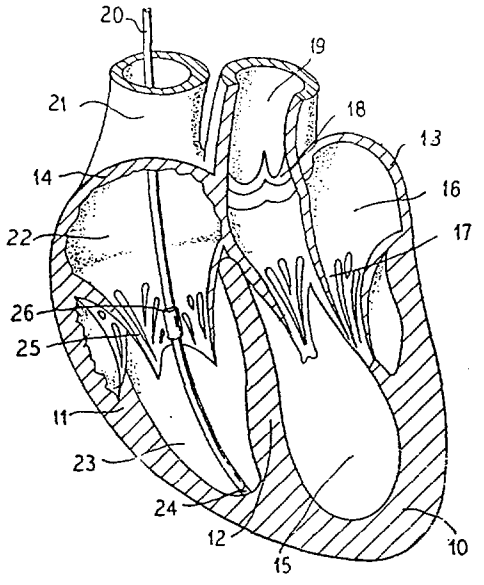

Figure 1

separated by the mitral valve 17. The left ventricular outflow tract consists of the aortic valve 18 and aorta 19. A cardiac pacing lead 20 is implanted through the vena cava superior 21 and the right atrium 22 in the right ventricle 23, with its pacing electrode 24 located in the apex of the right ventricle. In the low right-atrial region, in the proximity of the tricuspid valve 25, the lead 20 comprises a flow velocity measurement assembly 26. The physiologic principle of the system is disclosed in figure 2 with an an example of the electrocardiogram and corresponding tricuspid flow waveform. P waves, QRS complexes and T waves are designated illustrating a normal ECG. The flow velocity waveform through the tricuspid valve is disclosed under the ECG in time correlation to the ECG. Important timing intervals are designated like measurement refractory period (MRP), flow velocity measurement interval (FMI) and atrioventricular interval. Every sensed or paced ventricular event initiates the flow velocity measurement refractory period which is followed by the flow velocity measurement interval. These intervals are inversely proportional to the heart frequency. After the repolarization of the heart which caused the T wave (30), the relaxation of the heart muscle causes the early diastolic filling wave (31) having the peak blood velocity E. The following atrial depolarization causes the P wave (32) and corresponding atrial muscle contraction which pumps additional blood quantity producing the blood flow wave (33) having peak velocity A. The ratio of peak velocities E/A is a hemodynamic parameter showing the cardiac muscle performance. The similar waveform is obtained when measuring the mitral valve flow where peak velocities are having greater values (in order of 1 m/s) in comparison with tricuspid valve velocities being half slower. Another hemodynamic parameter being used in clinical practice is the ratio of the time integrated wave E and the time integrated wave A. The example is given for the healthy human heart, but pathologic conditions may disturb this relations. This is used in this invention for diagnostic purposes. First of all, synchronized pacing is obtained in this invention by means of sensing the flow velocity

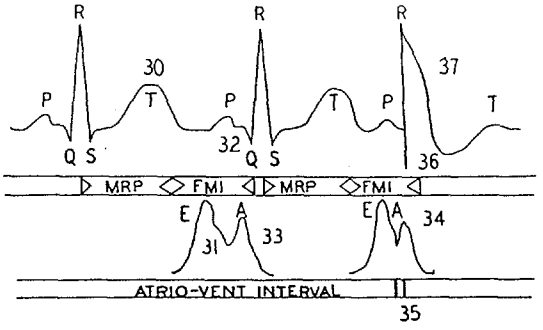

Figure 2

A wave and synchronizing the ventricular pacing with it, and not with the endocardial P wave as it is done in conventional VDD pacing systems. This is illustrated in the last complex of disclosed ECG strip where the subsequent A-wave (34) is sensed and the atrio-ventricular interval (35) is initiated (shown as a black bar). At the end of the A-V interval the pacing impulse (36) is generated producing the paced R-wave (37). It is obvious that A-V intervals in this system are much shorter than in systems which sense the atrial electrogram. In the case of severe ventricular arrhythmia like ventricular fibrillation, E waves disappear because the missing ventricular contraction causes missing ventricular relaxation. Ventricular tachycardia will produce irregular peak velocity of E waves having significantly lower magnitude of that in normal ventricular contraction. Decrease of peak velocity magnitude is dependent of the tachycardia frequency. This is used for reliable life threatening arrhythmias detection. Any ischemic episode like pacing induced high rate ischaemia will change the ratio of peak velocities as well as the ratio of time integrals. This is used for physiologic maximum tracking rate response to prevent angina pectoris. The

E/A ratio is significantly decreased in the case of ventricular premature contraction without the compensatory pause, which enables the exact detection and counting of the premature beats. 34 patients were selected for this study. All of them have been programmed into the VVT mode. In order to enable the chest wall overdrive stimulation, two percutaneous adhesive chest electrodes were applied: one above the active electrode in RV and another one above the pacemaker case, both for the purpose of external electric field production. Implanted pacemaker ventricular contractions. The simulation of the tricuspid flow controlled pacemaker was done by an external sophisticated measurement system in connection with standard implanted pacemaker. 34 patients having normal sinus node function,

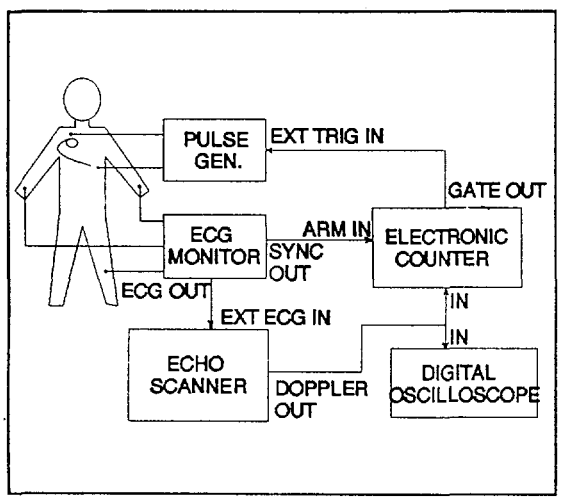

Figure 3

total atrio-ventricular block and implanted unipolar VVIM pacemakers, were selected. The pacemaker was programmed to the low basic rate 50. Figure 3 illustrates the measurement assembly used in this study. The output of a Doppler quadrature detector of an echocardiographic scanner was connected to an input of a digital oscilloscope for monitoring the envelope of the pulsed Doppler signal, as well as to the electronic counter for accurate trigger adjustment and for atrioventricular delay generation. Blood flow waveform through the tricuspid valve was obtained by adjusting the pulsed Doppler cursor close to the tip of the tricuspid valve in 2-D image. The electronic trigger was adjusted to detect the atrial filling wave and to trigger an external pulse generator with adjustable delay responsive to the trigger signal. Output of the pulse generator was connected to the two chest electrodes. Patients were examined by the echocardiographic scanner. Patients were connected to the ECG monitor. The ECG lead II was monitored and the monitor synchronization circuit was used to generate the ventricular refractory period 380 ms long. The defibrillator synchronization signal was connected to an external arming input of the electronic counter. ECG waveform of the monitor was led to the external input of the echocardiographic scanner in order to display tricuspid flow waveform together with corresponding ECG waveform.

RESULTS

In all patients, the implanted pacemaker was successfully overdriven and the A-wave synchronized ventricular pacing was obtained. Normal physiologic A-V interval was established and the ECG waveform revealed the VAT mode of pacing. Figure 4 is an example of the VDD pacing. 2-D image discloses the Doppler cursor (bright spot on the dashed line) adjusted onto the tip of the tricuspid valve. Doppler waveform exhibits the normal pattern comprising E and A waves. Pacing spikes are synchronous with the A-wave, producing the evoked QRS complex and a consequent E-wave.

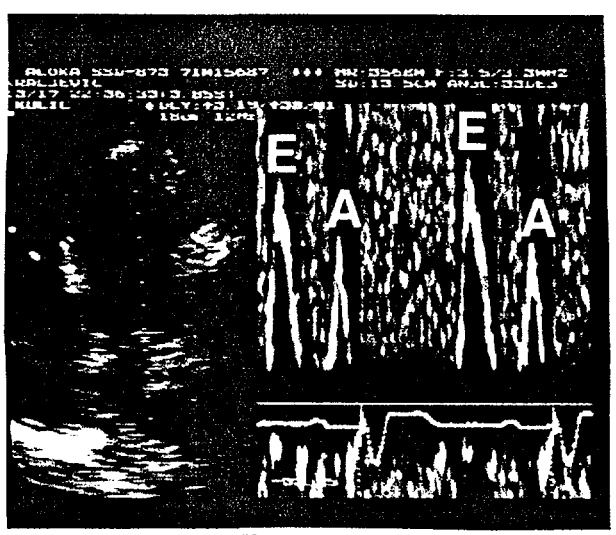

Figure 4

DISCUSSION

Disclosed system provides a pacemaker which, in normal atrial rhythm, acts in a synchronous mode and maintain atrio-ventricular synchronism, yet with the need for implantation of a single lead. It is obvious that A-V intervals in this system are much shorter

than in systems which sense the atrial electrogram. In the case of severe ventricular arrhythmia like ventricular fibrillation, E waves disappear because the missing ventricular contraction causes missing ventricular relaxation. Ventricular tachycardia will produce irregular peak velocity of E waves having significantly lower magnitude of that in normal ventricular contraction. Decrease of peak velocity magnitude is dependent of the tachycardia frequency. This is used for reliable life threatening arrhythmias detection. Any ischemic episode like pacing induced high rate ischaemia will change the ratio of peak velocities as well as the ratio of time integrals. This is used for physiologic maximum tracking rate response to prevent angina pectoris. The E/A ratio is significantly decreased in the case of ventricular premature contraction without the compensatory pause, which enables the exact detection and counting of the premature ventricular contractions. It can also provide a pacemaker comprising sensors for rate responsive ventricular pacing: spike to E interval, E-wave acceleration, E-wave deceleration, A-wave acceleration, etc. It also provides a pacemaker comprising a reliable means for atrial fibrillation detection and which will maintain the rate responsive pacing while the atrial fibrillation is sustained. Such a pacemaker will monitor the right ventricular filling dynamics in order to estimate the ventricular muscle performance, and will automatically reprogram the maximum tracking rate in such a way as to prevent the angina pectoris and high-rate induced myocardial ischemia. The system will be capable to detect premature ventricular contractions without as well as with compensatory pause. It will be also capable to confirm the ventricular capture, as well as to discriminate the sinus tachycardia from the pathologic tachycardia. The sensor used for blood flow measurement has to accurately measure the flow but without significant battery drain increase. Doppler measurement transducer[4,5] mounted on the lead significantly increases the complexity of an implantable device as well as the battery drain. Therefore it is feasible for use in implantable cardioverter defibrillator wherein accuracy of tachycardia detection system is a major goal. However, low power system[6,7] has been developed using the pressure transducers, which is feasible for implementation in the single lead VDD pacemaker. Even the closed loop regulation of the AV interval will be possible.[8]

CONCLUSION

According to this results and to numerous studies of diastolic function of the heart in medical literature, tricuspid flow would be ideal sensor for cardiac pacing control.

REFERENCES

1. ANTONIOLI G E, ANSANI L, AUDOGLIO R ET AL. 1994. Single lead VDD pacing: an update. In: Cardiac pacing and electrophysiology (Eds: A.E.Aubert & R.Strobandt), Kluwer Academic Publishers Dordrecht.

2. FEREK-PETRIĆ B, BREYER B. 18.3.1992. Cardiac Electrotherapy System. European Patent Application No. 91104561.5, Publication No.0474958, München.

3. FEREK-PETRIĆ B, BREYER B. 14.9.1993. Tricuspid Flow Synchronized Cardiac Electrotherapy System with Doppler Blood Flow Measurement Transducer and Controlled Pacing Signal Based on Blood Flow Measurement. U.S. Patent No. 5,243,976., Washington D.C.

4. FEREK-PETRIĆ B, BREYER B. 18.3.1992. Ultrasonic Doppler Synchronized Cardiac Electrotherapy Device. European Patent Application No. 91104555.7., Publication No.0474957, München.

5. FEREK-PETRIĆ B, BREYER B. 31.5.1994. Cardiac Measurement System for Measuring Blood Flow Velocity by Use of a Sensor Implanted Inside the Heart. U.S. Patent No. 5,316,001., Washington D.C.

6. BREYER B, FEREK-PETRIĆ B. 30.9.1992. Hydrodynamic System for Blood Flow Measurement. European Patent Application No. 92105160.3, Publication No.0506030, München.

7. BREYER B, FEREK-PETRIĆ B. 21.12.1993. Hydrodynamic System for Blood Flow Measurement. U.S. Patent No. 5,271,408., Washington D.C.

8. FEREK-PETRIĆ B, BREYER B. 7.6.1994. Pacing Method and System for Blood Flow Velocity Measurement and Regulation of Heart Stimulating Signals Based on Blood Flow Velocity. U.S. Patent No. 5,318,595., Washington D.C.

THE SIGNIFICANCE OF INTERELECTRODE SPACING AND CURRENT PULSE PARAMETERS ON TRANSESOPHAGEAL PACING

R. Magjarević*, B. Ferek-Petrić, D. Kraš*****
*** Faculty of Electrical Engineering, Univ. of Zagreb, Zagreb, Croatia**
**** Surgery Clinic, KBC Rebro, Zagreb, Croatia**
***** Artronic d.o.o., Zagreb, Croatia**

Abstract: The analysis of the electric field of esophageal bipolar leads showed the significance of interelectrode spacing for successful pacing. Variation of interelectrode spacing enables changes in lateral penetration of the electric field and achieving optimal stimulation of the heart. Optimal stimulation parameters are those which ensure minimal energy for pacing. In case of the application of optimal stimulating parameters, the selectivity of heart stimulation is increased, minimizing the unpleasant manifestations for the patient.

1. INTRODUCTION

Transesophageal cardiac pacing is a method of preference in emergency cases where immediate implantation of transvenous temporary lead is not possible as well as in prophylactic pacing during general anaesthesia. Studies of optimal spacing between electrodes on different bipolar esophageal leads were performed on a number of patients and volunteers [1,2]. As a result of these studies, atrial pacing was used more often than ventricular and predominantly as a diagnostic procedure. Relatively high pacing threshold in comparison to the endocardial lead as well as unreliable capture in some cases have limited esophageal pacing to be extensively used for ventricular pacing. Optimal positioning of esophageal electrodes relatively to the heart was defined as procedure [3,4] and special aids were developed in order to simplify the procedure [4]. On the basis of the analysis of the electric field of the transesophageal lead [5], significant parameters for esophageal pacing were pointed out and their importance was evaluated in a number of experiments.

2. ESOPHAGEAL LEAD ANALYSIS

The aim of this study was to compare the results of the analysis of the electric field of bipolar esophageal leads with experimental data and to evaluate them. Esophageal electrodes placed within the esophagus produce an electric field during the presence of the stimulus. The volume within the strength of the electric field is equal or higher than the myocardial threshold is defined as stimulus volume. The excitative volume is a geometrical cross-section between the stimulus volume and the excitable cardiac muscle. The shape of the stimulus volume varies as the electrode bipolar spacing and the output current of the stimulator are changed. As the stimulator output current increases, the stimulus volume is augmented as well, penetrating laterally from the esophagus. When the stimulator current is sufficient to produce electric field grater than the threshold within the myocardium, excitative volume is formed and the heart will be paced. The current flowing through the lead at the moment of excitative volume development is the esophageal pacing threshold.

If the distance of the heart from the esophagus is greater, the esophageal stimulation threshold will be higher because the lateral penetration of the electric field must be radially deeper. The basic problem of the esophageal heart stimulation is to achieve effective increase of stimulus volume. Assuming that the optimal position of the lead has been acquired [4,5] i.e. that the midplane of the bipolar lead is comprising the myocardial mass closest to the esophagus, the mathematical analysis was fulfilled with approximation that the media is homogenous and the heart is a sphere. The esophageal lead was presented as a point current source and a point current drain. The most significant penetration of

the electric field occurs at the bipolar lead midplane which is the zero equipotential surface of the lead field [6]. The equation (1) shows the current density J in that plane as a function of radial distance from the esophagus r, interelectrode spacing d and pacemaker output current I.

$$J = \frac{I}{4\pi} \cdot d \left(r^2 + \frac{d^2}{4} \right)^{-1.5} \qquad (1)$$

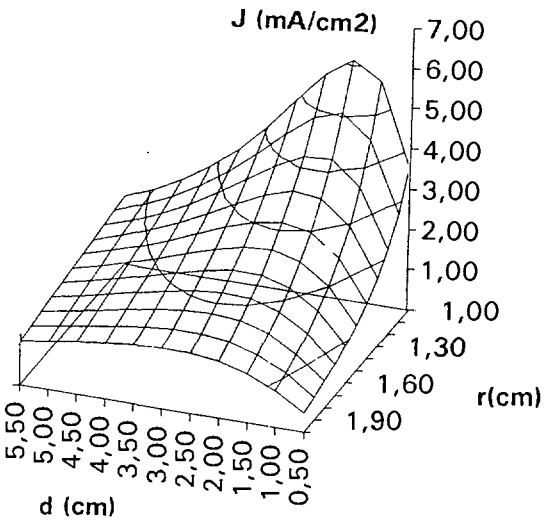

Fig. 1 Current density **J** in the bipolar lead midplane as a function of radial distance from the esophagus **r** and interelectrode spacing **d**.

There is an optimal relationship $d = r\sqrt{2}$ between the bipolar spacing d and the distance from the electrode to the cardiac muscle r in order to obtain the maximal current density (Fig. 1). To reach the esophageal pacing threshold, it is possible to increase either the magnitude of the current pulse or the interelectrode distance. The increase of current pulse magnitude is more effective for cases in which the myocardial mass is closer to the esophagus. For larger distances between myocardial mass and the esophagus, increasing (switching the stimulator output to electrodes with larger interelectrode distance) is more suitable. For each multipolar lead, the distance rs from the esophagus at which the current density curves cross can be calculated from

$$r_s = \frac{1}{2} \sqrt[3]{d_1 d_2} \sqrt{\sqrt[3]{d_1^2} + \sqrt[3]{d_2^2}} \qquad (2)$$

where d_1 and d_2 are two different interelectrode spacings on a multipolar lead. Assuming that d_1 is smaller than d_2, the meaning of equation (2) is that the current density obtained with smaller interelectrode distance is higher than the current density obtained with bigger interelectrode spacing at points closer to the esophagus than r_s and vice versa.

3. MATERIALS AND METHOD

The sensitivity of different types of tissue to electrical stimulation is usually tested through measurement of their strength-duration (SD) curves. Due to the analysis of the electric field of esophageal leads, SD curves obtained from the same examinee with different interelectrode spacing should be different.

The SD curves were measured on ten medium sized dogs (14 - 26 kg). All of them were taken under anaesthesia with intramuscular application of Combelen (0,1 - 0,2 mL/kg), Atropini sulf.(0,5 - 2 mL 1‰ / 20 kg) and Heptenon (15 mg/10 kg). After implantation of the hexapolar esophageal lead (Vygon, type 1182.06) into the optimal position for either atrial or ventricular pacing according to [4], SD curves were recorded for small (23 mm), medium (66 mm) and great (110 mm) interelectrode distance. The magnitude of the current pulses was measured with a DC current probe (AM 502, Tektronix) connected to a digital storage oscilloscope (2221A, Tektronix). Both, the magnitude and the duration of the pulses were measured with cursors. Cardiac capture was confirmed by monitoring the surface ECG and plethysmograph on a ECG monitor (HP 78324A, Hawlett Packard). In this way, 10 groups of three SD curves for ventricular and 8 groups of three SD curves for atrial pacing were obtained.

4. RESULTS

From the obtained SD curves for a particular cardiac chamber of a particular dog, we considered as optimal (for the Vygon lead) those curves which were lying closest to the duration (time) and strength (magnitude of current pulse) axes. We counted the number of in that way defined optimal SD curves. For the same group of dogs. The results are shown in Fig. 2. From the graph it can be seen that optimal stimulation of atria was obtained with small or medium interelectrode

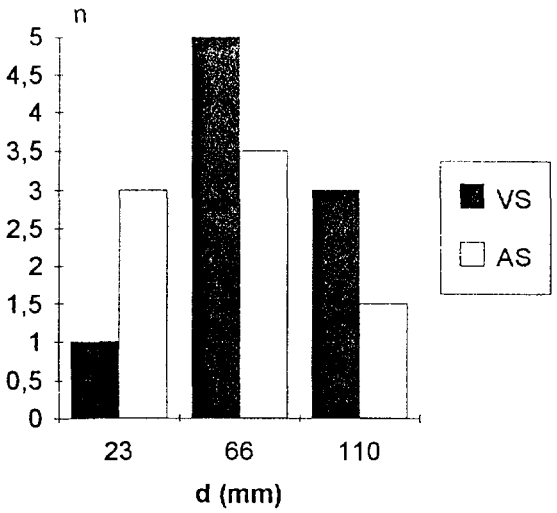

Fig. 2 The number **n** of minimum energy SD curves for ventricular (VS) and atrial (AS) stimulation obtained with interelectrode spacing **d** on Vygon hexapolar lead.

distance and for the ventricle with medium or big interelectrode distance.

SD curves are described through either hyperbolic (empirical or Lapicque) or exponential (theoretical or Blair) model [7]. On the basis of the measured points of SD curves, curve fitting was performed using the least squares regression algorithm (Fig. 3). The shape of the SD curves remained the same, but the rheobase was different from case to case. The average values of chronaxie and time constant for atrial and ventricular pacing of this group of dogs is shown in Table 1.

Table 1 Average time constant (τ) and chronaxie (k) for atrial (AS) and ventricular (VS) heart stimulation.

	τ (ms)	k (ms)
AS	1.35	1.14
VS	1.28	1.04

These results confirm that in the same group of experimentees it has to be expected a higher number of atrial captures with small and medium interelectrode spacing as well as higher number of ventricular captures with medium and big interelectrode spacing.

5. DISCUSSION

The measurements confirmed the results of the lead field analysis, i.e. the importance of proper choice of interelectrode distance for different anatomic relations that occur in human thorax. The values of time constant and chronaxie of the obtained dogs SD curves match with literature [7,8]. The same as in [7], the curves do not fit ideally either of the models. Compared to the values of time constant cited in [8], our values match better with those obtained from direct cardiac pacing studies.

6. CONCLUSION

The main problem of transesophageal pacing is a successful penetration of electric field from the esophagus to the cardiac muscle. The required interelectrode spacing is a function of the distance between the lead axis and the stimulated tissue. Accordingly, the pacing threshold is a function of the interelectrode spacing. Strength - duration curves for esophageal pacing, obtained with different interelectrode spacings, do not differentiate from intracardiac in shape but in higher rheobase values. Time dependent variables of esophageal pacing SD curve are well matching with intracardiac values.

7. LITERATURE

[1] D.W. Benson at al.: Transesophageal Atrial Pacing Threshold: Role of Interelectrode Spacing, Pulse Width and Catheter Insertion Depth, Am. J. Cardiol., 1984, **53**, 63-67

[2] H.R. Andersen, P.Pless: Transesophageal Pacing, PACE, 1983, **6**, 674-679

[3] R. Magjarević at al.: Optimal use of Multipolar Esophageal Stimulation Leads, Proc. IV Int. Symp. Biomed. Eng., Peniscola, Spain, 1991, 195-196

[4] R. Magjarević: Optimisation of Trans-esophageal Heart Stimulation, Ph. D. Thesis, Univ. of Zagreb, Zagreb, Croatia, 1994.

[5] R. Magjarević, B. Ferek-Petrić, D. Kraš: Analysis of the Electric Field of Multipolar Leads in Transesophageal Pacing, Proc. V Int. Symp. Biomed. Eng., Santiago de Compostela, Spain, 1994, 190-191

[7] G.A. Mouchawar, at al.: Ability of the Lapicque and Blair Strength-Duration Curves to Fit Experimentally Obtained Data from the Dog Heart, IEEE Trans. Biomed. Eng., 1989, **36**, 971-974

[8] L.A. Geddes, J.D. Bourland: Tissue stimulation: theoretical considerations and practical applications, Med. & Biol. Eng. & Comp., 1985, **23**, 131-137

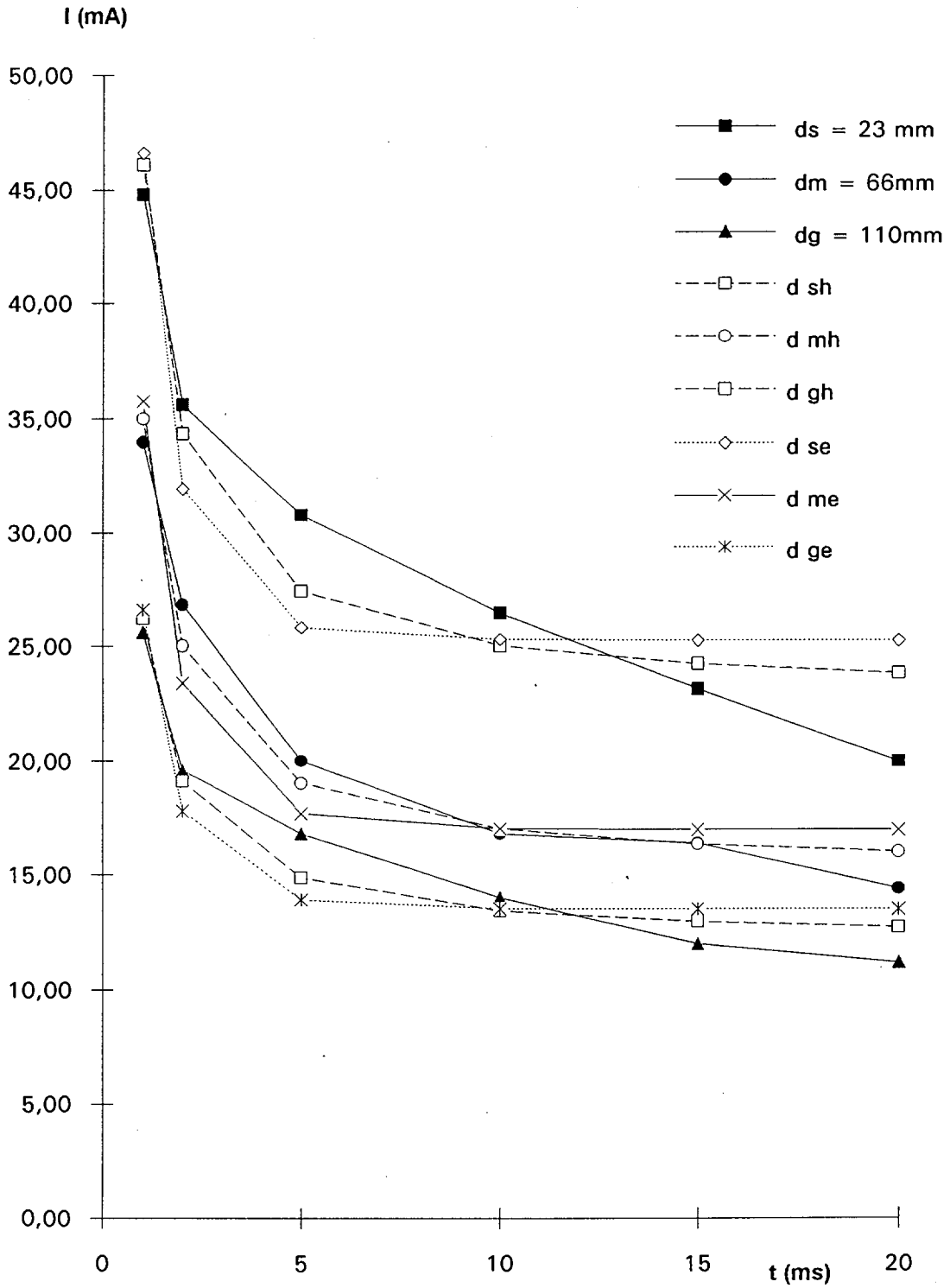

Figure 3. Strength-duration (SD) curves for atrial pacing of the dog Nr. 10 measured with small (ds), medium (dm) and great (dg) interelectrode spacing on the Vygon esophageal lead and their approximations according to hyperbolic (d ih, i indicating approximations for s - small, m - medium, g- great interelectrode spacing) and exponential (d ie) model of SD curve.

IMPLANTABLE STIMULATOR FOR SELECTIVE STIMULATION OF THE COMMON PERONEAL NERVE

Janez Rozman, [1]Igor Tekavčič, [2]Srečko Maček, [3]Stanislav Žerovnik, and E. Pretnar, *student*

ITIS d. o. o. Ljubljana, Centre for Implantable Technology and Sensors, Bičevje 2, 61000 Ljubljana, [1]University Medical Centre, University Clinic of Neurology, Zaloška 7, 61000 Ljubljana, [2]Jožef Stefan Institute, Department of Ceramics, Jamova 39, 61111 Ljubljana, [3]S & H d. o. o. Ljubljana, Mlinska pot 19, 61000 Ljubljana, Republic of Slovenia

Abstract - In this paper we present the modelling and design of an implantable system with a monopolar half-cuff electrode for selective stimulation of superficial regions of the human common peroneal nerve thus making a selective activation of muscles contributing to strong dorsal flexion and moderate eversion of the hemiplegic foot. The development of the electrode was based partly on the data obtained by a histological examination of human common peroneal nerves and on models of excitation of myelinated nerve fibres. The modelling objectives were to determine the electric field that would be generated within the deep peroneal branch of the nerve by the half-cuff electrode. Moreover, the extent of initial excitation of the fibres within the superficial region of the deep peroneal branch was predicted.

1. INTRODUCTION

In upper motor neuron disease such as stroke, electrical stimulation can restore function in paralyzed muscles. Moreover, Funtional Electrical Stimulation (FES) of the common peroneal nerve in patients with upper motoneuron lesion has been shown to be a potentially useful means for the restoration of functional movement in the lower extremities of hemiplegic individuals (1). Several groups of investigators have developed implantable devices for stimulation of the common peroneal nerve (1,2,3,4) but in most cases their use has been abandoned due to different problems and mostly due to unsatisfactory elicited functional movement. The stimulation is applied during the swing phase of the affected leg dorsiflexing the foot and preventing its equinovarus position. Raising the leg, the patient releases the heel switch that turns the external unit in function. Close the switch at the beginning of the stance phase stimulation is turned off. Stimuli are therefore synchronized with the swing phase by a heel switch which is worn inside the shoe. According to the aforementioned facts and the aim of obtaining satisfactory movement for a long period, the main goal in the work was to develop an implantable system with a cuff electrode for selective stimulation of the superficial region within the common peroneal nerve innervating mostly the tibialis anterior muscle, peroneus brevis muscle and to a lesser degree the triceps surae muscle. The development of the cuff system which selectively stimulates a certain group of nerve fibres without excitation of other nerve fibres was required. Peripheral nerves are organized into individual fascicles near their terminal branching points (5). It was demonstrated that electrodes placed proximal to the branching point provide the ability to stimulate a single fascicle and thus activate selectively an individual muscle (6). In this study we predicted the efficacy of a monopolar half-cuff electrode in activating an individual fascicle in a multifascicular human common peroneal nerve just above its bifurcation in superficialial and deep peroneal branches. Acute human testing of a single electrode half-cuff for selective activation of a nerve was performed on the common peroneal nerve in two hemiplegic patients (4). The semi-cuff was 18mm long and was

constructed in a range of diameters to fit different size nerve trunks. The goal was to develop a simple implantable gait stimulation system which is needed to ensure that this technology will be made available to paralyzed individuals.

2. BODY OF THE PAPER

2.1. Methods

Modelling of the common peroneal nerve and half-cuff electrode was based on histological examinations and the data obtained in literature (5,6). At the level above its bifurcation in the superficial and deep peroneal division, tibial fibres lie mostly within the superficial region of the deep peroneal division. The dimensions of the half-cuff was determined according to the request that the surface of the nerve covered by the cuff should be as small as possible to prevent damage associated with the blood supply system. Moreover, any rotation of the system should be excluded because it could induce a mechanical force resulting in nerve damage. It was assumed that leads to the stimulating half-cuff would play a minimal role in the infliction of neural damage, if care is taken at implantation. Accordingly, it was concluded that the optimal length of the semi-cuff was 18mm. It was shown (10) that the activating function for myelinated axons is given by the second differential quotient of the external potential at the Ranvier nodes, which is the component of an electric field that lies parallel to the myelinated axons within a nerve trunk. Thus, sharp transitions in the current generated by the extracellular stimulating electrodes that flows longitudinally outside of the nerve fibres within a nerve elicits changes in axonal excitability (10,12). The nerve model used in this study consists of a number of compartments with different conductivities (13). Intrafascicular conductivity was considered to be anisotropic while all other compartments were assumed to be isotropic. The extrafascicular connective tissue was divided into the perineurium enfolding the fascicles, and the epineural tissue comprises fascicles. In the model, conductivity of the half-cuff was supposed to be zero. It was recently shown that the insulating layer has the desirable effect of restricting current flow near the nerve trunk surface into a longitudinal component only (7). Moreover, a monopolar small electrode configuration was expected to focus current well near the electrode. Besides, in the model for evaluating the electric field (11) generated in the nerve the virtual neutral electrode was supposed to be situated at the proximal edge of the half-cuff as presented in Fig. 1.

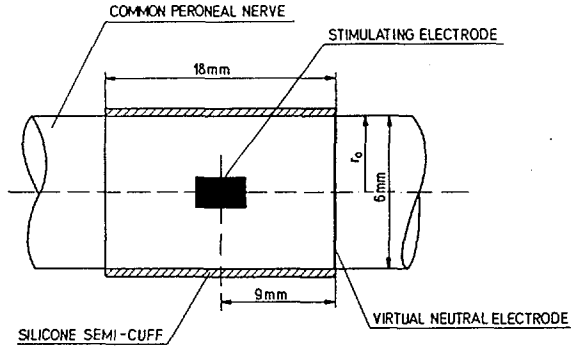

Fig. 1. Schematic diagram of single-electrode half-cuff for selective stimulation of the superficial region of the human common peroneal nerve and position virtual neutral electrode.

In the vicinity of the stimulating cathode, we anticipated a current flow composed of a vertical and longitudinal component, while elsewhere, only a longitudinal current flow in the nerve trunk between the virtual anode and stimulating cathode was presumed to exist. A current from the common anode entering the nerve during stimulation is supposed to have a low density and, consequently, poor ability to block elicited propagating action potentials (8,14). Besides, an occurrence of the active virtual cathode during reversed polarity of the stimulating pulse is not expected. For the purpose of evaluation, the numerical solution of potential distribution due to an externally applied source was based on the method of finite elements approximation of Laplace's differential equation (11).

2.2. Results

Fig. 2a. shows equipotential lines in the common peroneal nerve generated by the electrode according to a dissection through the longitudinal axis and stimulating electrode. In order to determine the position of an axon within the region of the deep peroneal nerve which could be activated by the electrode, the activating function given by the second differential quotient of the external potential generated by the electrode was calculated. Moreover, we saught to determine the region within the deep peroneal nerve stimulated by the electrode where activation of nerve fibres

could be expected. This was done by calculating the activating function for nerve fibres situated in six vertical levels within the

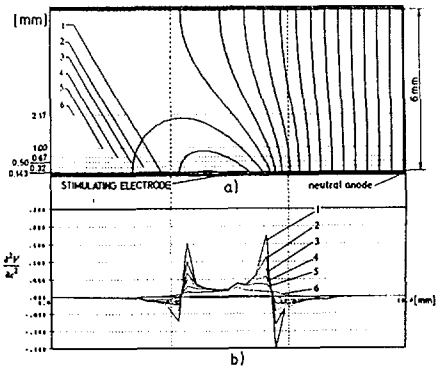

Fig. 2. (a) Equipotential lines in the human common peroneal nerve, in a plane through the stimulating eletrode situated close to the deep peroneal branch and longitudinal axis of the semi-cuff generated by the electrode. Horizontal dotted lines indicate six positions where activating functions are calculated. (b) Evaluated activating functions corresponding to the six positions.

deep peroneal nerve as presented in Fig. 2b. The half-cuff was manufactured by bonding two silicone sheets together (7). A rectangular electrode made of platinum ribbon connected to the insulated lead wires was mounted in the centre on the third reinforced sheet. This composition was then bonded on the inner side of the mechanically opened spiral cuff. The completed half-cuff with an inner diameter of 3.5mm was then trimmed to a length of 18mm. The completed half-cuff is presented in Fig. 3a. A difficulty encountered with direct nerve stimulation through an electrode within the cuff is that the difference in current level between threshold excitation and maximal recruitment is not large. Moreover thick nerve fibres are recruited before thin ones as they have lower excitation threshold. Acordingly, appropriate type of stimulus versus functional response (recruitment of motor units) characteristic is desirable in proposed system as some gradation of the dorsiflexion is desired. A more gradual recruitment of nerve fibres during stimulation can be obtained if it is possible to increase the difference in threshold between different diameter nerve fibres. According to Gorman (1983) (14) a decrease in pulse width shifts the stimulus amplitude versus force curve towards greater stimulus amplitudes and it also decreases the slope. Accordingly we suppose to use relatively short cathodic or stimulating pulse with higher amplitudes. It was previously found (14) that the presence of secondary anodic phase of the biphasic pulse coud be used to abolish excitation initiated by the primary cathodic pulse. Namely, during cathodic part of the stimulus all fibres close to the electrode are activated. However, because of the relatively short stimulating pulse action potentials of thin slow conducting fibres are not able to leave activated region before reversed polarity occurs. Therefore, they are expected to be blocked there while action potentials of thick, fast conducting fibres leaved aforementioned region. Thus, relatively rapid, low gradation dorsilexion could be expected. It was supposed that introduction of short delay beteween stimulating, cathodic and anodic part could prevent aforementoned situation. However, an introduction of the delay produces a slightly steeper recruitment curve but it could be minimized by limiting of the delay to low value (14). The stimulus employed in this work were current, charge balanced, and biphasic pulses with a rectangular cathodic component, and delayed exponential decay anodic component (8,9). The delay between the cathodic and anodic pulses could be set between 0 to 0.1ms. The output current of the stimulating cathodic component to the stimulating cathode was adjustable up to 10mA using the trimmer potentiometer situated within the external unit. The complete IGC (Implantable Gait Corrector) system is an electronic device, part of which is worn externally and part implanted. It consists of three main units: (1) a external stimulator and antenna; (2) a heel switch; and (3) a surgically implanted unit as passive receiver is a disc-like body as presented in Fig. 3b. Packaging the hybrid electronic circuitry and connection to thestimulating electrode involved the utilization of the unique properties of several biomedical materials. The use of these materials was necessitated by the constraints imposed by the stimulator electronics including: non-metallic encapsulation due to RF coupling and long service life after implantation. An indifferent electrode made of platinum ribbon was situated on one side of the body to be form part of the surface of the implant body as also presented in Fig. 3b.

3. CONCLUSION

The orthosis implanted in Ljubljana over a period of 10 years (4) enabled the patient to

extend walking radius, increase gait velocity and improve overall gait pattern. Better transfer of the weight and more appropriate symmetry were also observed. However, in its development, the use of the system for gait assistance has encountered a number of problems.To overcome them the main goal of the work was to develop stimulating system with reliable, selective, and reproducible force recruitment characteristics (4), primarily of the

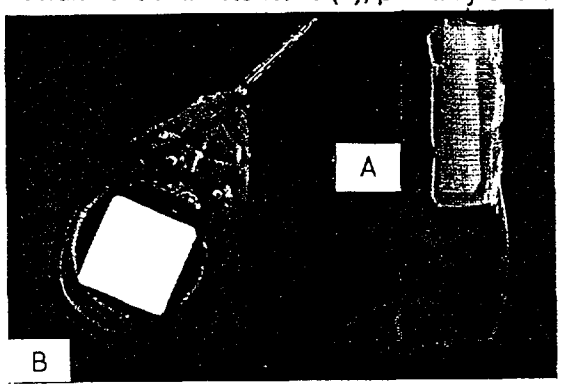

Fig. 3. (a) Single electrode half-cuff for selective stimulation of superficial region in peripheral motor nerve. (b) Implantable stimulator.

tibialis anterior muscle of hemiplegic patients which can be implanted chronically. Also important behind the application of selective stimulation of the common peroneal nerve is the concept that electrical stimulation by means of implanted half-cuff electrodes can be applied to other peripheral nerves innervating paralyzed muscles. One important aspect of selective stimulation not yet taken into account by this work is selectivity dependent upon nerve fibre size. Namely, a half-cuff enables the incorporation of an array with a large number of electrodes arranged within the cuff in a way that enables both selective stimulation of different superficial regions in the nerve and selective stimulation of nerve fibres of different sizes.

4. REFERENCES

1) Liberson, W. T., Holmquest, H. J., Scot, D. and Dow, M.: Functional electrotherapy: stimulation of the peroneal nerve synchronized with the swing phase of the gait of hemiplegic patients. Arch. Phys. Med., 42: 101-105, 1961.

2) Strojnik, P., Aćimović, R., Vavken, E., Simič, V. and Stanič, U.: Treatment of drop foot using an implantable peroneal underknee stimulator. Scand. J. Rehab. Med., 19: 37-43, 1987.

3) Waters, R. L., McNeal, D. R., Faloon, W. and Clifford, B.: Functional electrical stimulation of the peroneal nerve for hemiplegia. J. Bone and Joint Surg., 67: 792-793, 1985.

4) Rozman, J., Aćimović-Janežič, R., Tekavčič, I., Kljajić, M. and Trlep, M.: Implantable stimulator for selective stimulation of the common peroneal nerve: a preliminary report. J. of Med. Eng. & Techn., 18: 47-53, 1994.

5) Sunderland, S.: Nerves and nerve injuries. E.& S., Livingstone Ltd., Edinburgh and London, 1968.

6) McNeal, D. R. and Bowman, B. R.: Selective activation of muscles using peripheral nerve electrodes. Med. & Biol. Eng. & Comput., 23: 249-253, 1985.

7) Sweeney, J. D., Ksiensky, D. A. and Mortimer, J. T.: A nerve cuff technique for selective excitation of peripheral nerve trunk regions. IEEE Trans., BME-37: 706-715, 1990.

8) Bonner, M., Mortimer, J. T. and Daroux, M.: Effect of pulse width and delay on stimulating electrode charge injection in-vitro. Proceedings, 12th Ann. Conf. IEEE Eng. in Med. & Biol. Soc., Philadelphia, 1-4 Nov., pp. 1482-1483, 1990.

9) Roblee, L. S., Rose, T. L.: The electrochemistry of electrical stimulation. Proceedings, 12th Ann. Conf. IEEE Eng. in Med. & Biol. Soc., Philadelphia, 1-4 Nov., pp. 1479-1480, 1990.

10) Rattay, F.: Ways to approximate current-distance relations for electrically stimulated fibres. J. Theor. Biol., 125: 339-349, 1987.

11) Coburn, B. and Sin, W. K.: A theoretical study of epidural electrical stimulation of the spinal cord - Part I: Finite element analysis of stimulus field. IEEE Trans., BME-32: 971-977, 1985.

12) McNeal, D. R.: Analysis of a model for excitation of myelinated nerve. IEEE Trans., BME-23: 329-337, 1976.

13) Geddes, L. A. and Baker, L. E.: The specific resistance of biological material - A compendium of data for the biomedical engineer and physiologist. Med. & Biol. Eng., 5: 271-293, 1967.

14) Gorman, P. H. and Mortimer, J. T.: The effect of stimulus parameters on the recruitment characteristics of direct nerve stimulation. IEEE Trans., BME-30: 407-414, 1983.

THE INFLUENCE OF MAGNETIC STIMULATION ON DENERVATED SKELETAL MUSCLES

Dragica Bobinac , Tea Schnurrer , Igor Grubješić , Danijela Malnar - Dragojević
Zavod za anatomiju , Medicinski fakultet Sveučilišta u Rijeci , Hrvatska

Abstract

Male, rats, y - line, were treated 10 days by time-varying, pulse, low frequency, magnetic field. We wanted to fortify the influence of magnetic field density 10 mT, with frequency of 10 Hz, 10 minutes daily, through 10 days continuously, on denervated skeletal muscles. Denervation was performed by compression of sciatic nerve and after that rats were stimulated. On transverse sections of soleus and tibialis anterior muscles we were represented the types of muscle fibre and capillaries by histochemical methods.

The biggest change in stimulated muscles was increasing the number of capillaries. That number is greater in healthy or denervated muscles which were stimulated, than in healthy or denervated controls. Measuring the muscle mass we noticed decreasing the percentage of atrophy in stimulated muscles after 18 days of denervation.

UTJECAJ MAGNETSKE STIMULACIJE NA DENERVIRANE SKELETNE MIŠIĆE

Sažetak

Promjenljivim pulsirajućim magnetskim poljem tretirani su štakori y-soja, kroz deset dana. Željeli smo utvrditi utjecaj magnetskog polja jakosti 10 mT, frekvencije 10 Hz, u trajanju od 10 minuta dnevno na denervirani skeletni mišić. Nakon denervacije kompresijom n. ischiadicusa, životinje su stimulirane. Na poprečnim presjecima m. tibialis anteriora i m. soleusa, histokemijskim metodama prikazivali smo tipove mišićnih vlakana i kapilare.

Najjača promjena u mišićima stimuliranih životinja je povećanje broja kapilara. Broj kapilara je veći u zdravim i denerviranim mišićima koji su stimulirani, nego u zdravoj i denerviranoj kontroli. Mjerenja mišićne mase pokazuju smanjenje atrofije uz stimulaciju nakon 18 dana od denervacije.

1. INTRODUCTION

The influence of low frequency magnetic field is currently used in therapy of many diseases, especially in therapy of skeletal and nervous systems. Magnetic stimulation is generally used in experimental works, because electrical impulse which is performed by magnetic stimulation of central motor pathways (motor neurones of brain cortex and spinal cord) provokes muscle contraction[1]. Besides, it provokes depolarisation in tissue, exactly at the cell membrane [2]. Consequently contraction is appeared in the muscle beside the normal conducting of nerve by magnetic stimulation When the nerve is broken by cutting or crushing, conducting of impulse is interrupted. Muscle reaction on it is atrophy and loss of elementary function because the muscle cells lost the connection with nervous system.

The purpose of our experimental work is to examine the influence of low frequency magnetic field with specific characteristics to the denervated muscle. Especially we were interested at the fibrous component of muscle and number of capillaries, because we supposed that the existence of the muscle depends on local conditions and intensity of the blood flow.

2. CENTRAL PART OF ARTICLE

2. 1. Description of methods

In experimental work we used male rats, y-line, 6 months of age, with mean body weight of 350 g. The sciatic nerve was denervated by crushing, 5 mm proximal of its main bifurcation.

For stimulation we used pulsing magnetic apparatus "FLORA 02 "(Acoustic engineering of Rijeka, Rijeka, Croatia), with round coil, inner diameter 9 cm and outer diameter 16 cm. The stimulator delivers time - varying, pulse, low frequency magnetic field. We chose magnetic field density of 10 mT, with frequency 10 Hz, 10 minutes daily, through 10 days continuously.

In experiment we used 32 rats divided into 4 groups: 8 rats as a healthy control; 8 healthy stimulated rats; 8 denervated rats, sacrificed on the 18th day since the day of denervation; 8 denervated rats, with the beginning of stimulation on the 6th day since the day of denervation, sacrificed on the 18th day, too.

The rats were sacrificed with cervical dislocation and soleus and tibialis muscles were taken out. After weighing, we calculated, on the basis of muscle mass the percentages of atrophy of treated muscles in relation to healthy control.The muscles were quickly frozen with liquid nitrogen at - 80 ° C . After that 7 μm thick serial transverse sections were cut in cryocut at - 20 ° C. Transverse sections were stained by histochemical method for demonstrating myosin's ATP-ase activity at pH 9,4 and pH 4,3. Distribution of muscle fibre types I and II was performed by this method. Myosin's ATP-ase method at pH 9,4 was done on the same sections together with Verhoef Van Gieson staining for demonstrating capillaries and fibrous tissue.

2. 2. Experimental results

In the group of healthy stimulated rats, muscle mass of soleus is increased, but the mass of tibialis is even decreased. As we expected, the muscle mass of denervated muscles is decreased. But, in the group of denervated and stimulated rats percentage of atrophy of muscle mass is less than in the group were the muscles are only denervated (Tbl.1, Fig.1).We searched for the number of capillaries at the transverse sections on both muscles in every searching group, because the number of capillaries around single fibres depends on metabolism characteristic[3]. The results showed that such magnetic stimulation increased the number of capillaries (Tbl.2). In healthy control mean number of capillaries around single fibres is 3 to 4. That number increased in healthy stimulated muscles to 6 or 7. There is no difference in the number of capillaries concerning fibre types, between healthy and healthy stimulated soleus and tibialis anterior muscles (Fig.2,Fig.4.). The results given by Plyley indicate that the major number of muscle fibres in healthy muscle has 4 capillaries and there is no difference between both muscles, too [4]. Only denervated muscles have a lack in a number of capillaries. The more significant results we received in denervated and stimulated muscles were the numbers of capillaries remained equal as in healthy control ones (Fig.3,Fig.5). The number of fibres which are surrounded by 3 to 4 capillaries has even increased. Therefore we point out significant influence of such magnetic stimulation at vascularity of muscles and respectively the blood flow.

3. CONCLUSION

Lots of articles talk about the magnetic field's effective impact to the peripheral nerves functional recovery.But there are no particulars on the influence to a muscle which is to react on an impulse coming through nerve fibre. We consider that the upkeeping of metabolism of the muscle in the condition of peripheral innervation interruption is as important as the returning of nerve to a previous function. Therefore our results demonstrate that the muscles in such conditions are to be stimulated as the maintaining of the normal circulation is one of the prerequisites to normal muscle recovery.

4. REFERENCES

[1] N.M.F. Murray, Electrodiagnosis in Clinical Neurology,M.J.Aminoff, New York,Churchill Livingstone,1986.

[2] A. Murro, A model for focal magnetic brain stimulation,Int.J.Biomed.Comput.,31,37-43,1992.

[3] D.Pette,Neural control of phenotypic expression in mammalian muscle fibers, Muscle&Nerve,676:689, October 1985.

[4] M.J.Plyley,Geometrical distribution of capillaries in mammalian striated muscle,Am.J. of Physiology, Vol.228,No5,1376-1383,May1975.

Table 1: Muscle mass and percentage of atrophy in soleus and tibialis ant. muscle

	Soleus muscle				Tibialis ant. muscle			
Group of animals	X	Sd	p	% of atrophy	X	Sd	p	% of atrophy
H M	132,6	24,7			813,07	120,1		
H M + S	136,3	16,05	< 0,05	2,7	765,3	100,5	< 0,05	- 5,8
D M	69,5	4,96	< 0,05	- 47,6	318,6	33,4	< 0,05	- 60,8
D M + S	75,3	13,4	< 0,05	- 43,2	367,3	138,6	< 0,05	- 54,8

H M - healthy muscle
H M + S -healthy muscle + stimulation
D M - denervated muscle
D M + S - denervated muscle + stimulation

Fig.1

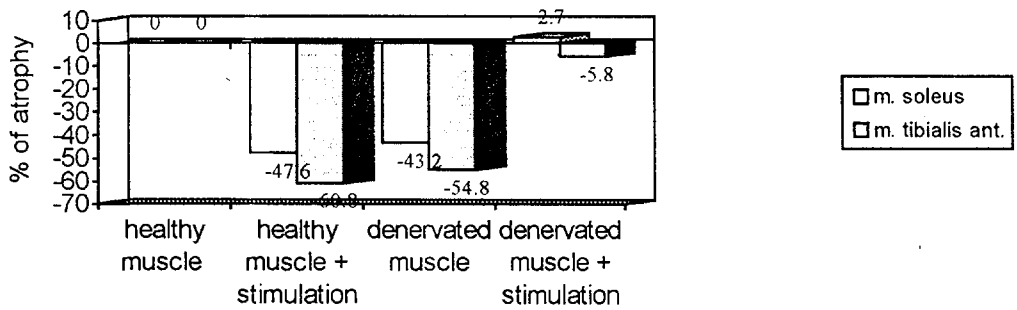

Fig 1: Percentage of atrophy in soleus and tibialis ant. muscle

Fig.2

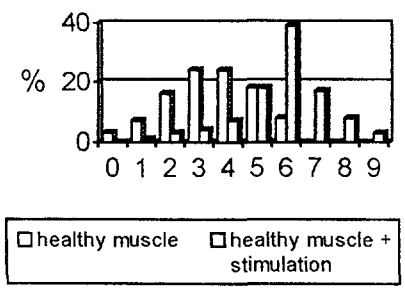

Fig.2: Percentage of fibres surrounded by capillaries from 0 - 9 in healthy and healthy stimulated tibialis ant. muscle

Fig.3

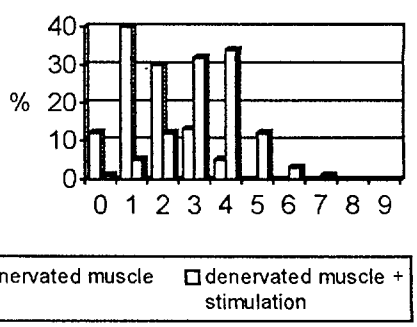

Fig.3: Percentage of fibres surrounded by capillaries from 0 - 9 in denervated and denervated + stimulated tibialis ant.muscle

Fig.4

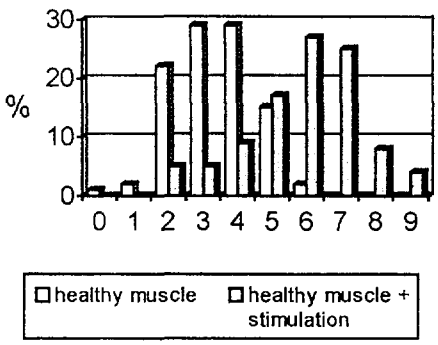

Fig.4: Percentage of fibres surrounded by capillaries from 0 - 9 in healthy and healthy stimulated soleus muscle

Fig.5

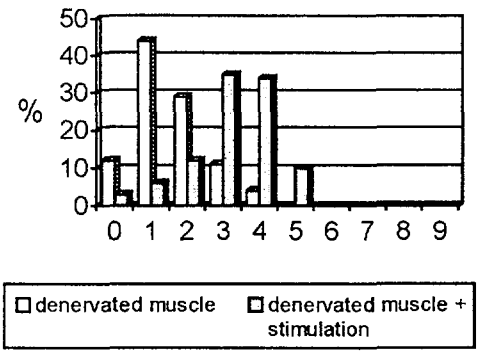

Fig.5: Percentage of fibres surrounded by capillaries from 0 - 9 in denervated and denervated + stimulated soleus muscle

Table 2: Numbers of capillaries around muscle fibres

		Percentage of fibres surrounded by 0 - 9 capillaries									
Group of animals	Muscle	0	1	2	3	4	5	6	7	8	9
H M	m.tibialis ant.(n=75)	3	7	16	24	24	18	8	0	0	0
„	m.soleus (n=65)	1	2	22	29	29	15	2	0	0	0
H M + S	m.tibialis ant.(n=65)	0	1	3	4	7	18	39	17	8	3
„	m.soleus (n=65)	0	0	5	5	9	17	27	25	8	4
D M	m.tibialis ant.(n=75)	12	40	30	13	5	0	0	0	0	0
„	m.soleus (n=75)	12	44	29	11	4	0	0	0	0	0
D M + S	m.tibialis ant.(n=75)	1	5	12	32	34	12	3	1	0	0
„	m.soleus (n=75)	3	6	12	35	34	10	0	0	0	0

H M - healthy muscle
H M + S - healthy muscle + stimulation
n= No. of fibres
D M - denervated muscle
D M + S - denervated muscle + stimulation

THE IMPORTANCE OF MUSCLE ELECTROSTIMULATION IN THE SURGICAL TREATMENT OF HIGH IMPERFORATE ANUS

Božidar Župančić, Ivan Bradić, Stipe Batinica, Marija Frković, Božidar Ferek, Eva Jendriš-Škrljak, Dražen Belina, Ljiljana Popović, Tomislav Luetić, Anko Antabak.
Department of Pediatric Surgery, Scool of Medicine, Clinical Hospital Center Rebro, Kišpatićeva 12, Zagreb, Croatia.

Abstract

Posterior sagittal anorectoplasty (PSARP) is a technique for the repair of high anorectal malformations. It is based on complete exposure of the anorectal region by means of a median sagittal incision that runs from the sacrum to the anal dimple, cutting through all muscle structures behind the rectum. This procedure showed that the external sphincter is a functionally useful prominent structure. No puborectalis sling, as recognise a muscle continuity from the skin to the sacral insertion of the levator ani. Since it is impossible to pull the generally ectatic rectum through without destroying the muscle structures present, the rectum must be tapered to allow suturing the muscle behind it. In all these anomalies the rectum and urethra (or vagina) are very closely joined, sharing a common wall, and their separation calls for extensive exposure. The employment of PSARP without use of a muscle stimulator is contraindicated. By using muscle electrostimulation during the operation complete visualization and reconstruction of the muscle sphincter responsible for the fecal continence is made possible. The authors present their experience with nine children treated with this surgical procedure during the last five years. The preliminary results of the examination of fecal continence indicate that a great number of our children will become continent.

VAŽNOST ELEKTROSTIMULACIJE MIŠIĆA KOD KIRURŠKOG LIJEČENJA VISOKIH ANOREKTALNIH ANOMALIJA

Sažetak

Posteriorna sagitalna anoplastika (PSARP) je kirurška metoda u liječenju visokih anorektalnih anomalija. Kroz stražnju medijalnu sagitalnu inciziju kompletno se prikazuje anorektalna regija i pripadajuća muskulatura.

Primjena posteriorne sagitalne anorektoplastike bez elektrostimulacije mišića je kontraindicirana. Elektrostimulacija mišića omogućava u tijeku operativnog zahvata potpunu vizualizaciju, a kasnije i rekonstrukciju mišićnog sfinkternog kompleksa odgovornog za kasniju kontinenciju.

Autori prikazuju svoje iskustvo na devetoro djece liječene ovom kirurškom metodom u zadnjih pet godina.

Prvi rezultati ispitivanja analne kontinencije ukazuju da će velik broj naše djece postati kontinentan.

1. INTRODUCTION

Anorectal anomalies present a medical problem of considerable practical significance as a result of their rather high incidence (1/3000-5000 delivery) (1, 2). Such anomalies have been known to physicians since ancient times and some of the currently used surgical approaches, such as anoplasty low and two-stage operations for high lesions, were first introduced in the 19th century.

The malformations result from arrests or abnormalities in the embryonic development of the anus, lover rectum and urogenital tract. The main goal after the surgical treatment of children with high inperforate anus is to achieve fecal and urinary continence. The degree of success of currently used procedures varies (3,4,5,6,7), but the overall results are still far from ideal.

Probably the most significant contribution to this field was made by Stephens and Smith (8). Their work based on anatomical studies as well as on a large clinical experience provided the first rational approach to imperforate anus. Stephens proposed that the puborectalis portion of the levator musculature constituted the only potANKOential sphincter for continence. He desingned a sacral approach to create a space within the puborectalis sling and behind the posterior urethra through which the bowel could be inserted for the creation of an anorectum. The external sphincter was considered as rudimentary and not useful. Many surgeons introduced technical variants of Stephens' approach, but all procedures preserved the puborectal sling. Stephens' sacral approach was very limited. Ligation of the fistula was sometimes difficult, in particular when it was connected to the bulbar urethra. Furthermore, separation of the rectal pouch from the urinary tract or vagina was not always easy. This experience stimulated Pena and de Vries, (9) to explore these patients throught a posterior sagittal incision extending all the way from the midsacrum to the anal dimple. Division of all the striated muscle structures in the midline provided easy access to the rectum and urethra or vagina. Important steps in the operation included the use of a muscle stimulator in order to stay precisely in the midline, thus minimizing damage to muscles and their nerve supply.

A totally diverting transversal or sigmoid colostomy to avoid overflow of feces from proximal to distal bowel is performed as a primary procedure in all patients. Some redudancy of colon distal to the stoma is left to facilitate mobilization of the rectum for the pull through procedure. Most patients underwent the definitive operation after one year of age or were at least 9 kg in weight. Recently, however, several younger infants underwent the definitive procedure, provided good weight gain was established and no other major malformations exsisted.

2. PATIENTS AND METHODS

Our expirience with PSARP as described by Pena-de Vries, witch has been used in this institution since 1989, is based on nine operated cases, including eight boys and one girl (Table 1).

	MALE	FEMALE	TOTAL
RECTOURTHRAL FISTULAS	5	-	5
RECTOVAGINAL FISTULAS	-	1	1
HIGH MALFORMATION WITHOUT FISTULAS	3	-	3
TOTAL	8	1	9

TABLE1. Clinical expirience with 9 patients whom the PSARP was used

In addition to anal atresia, 5 boys had a rectourethral fistula, and the girl a rectovaginal fistula. Urinary tract abnormalites were common (6 cases), while other anomalies, such as trisomy or musculoskeletal defects occurred less frequently. The diagnosis of high anal atresia was based on clinical examination, x-ray studies according to Wangeesten-Rice and ultrasonography. Computed tomography was not employed. Following diagnosis, a totally diverting transversal or sigmoid colostomy was performed as a primary procedure in the operative management. Upon complete pediatric treatment, definitive operative correction of the defect was undertaken according to the previously mentioned recommendations (up to one year of age, approximately 9 kg in weight). In addition to detailed laboratory studies, ECG, and chest x-ray a through urinary tract examination (intravenous urography, voiding cystography) was performed in all patients prior to surgery in order to detect possible intestinal communication. Irrigography through colostoma to distal bowel was performed preoperatively to define accurately the level of atresia and delineate any rectourethral or rectovaginal juncture.

3. RESULTS

The only early complication observed during PSARP was distal rectal retraction and stenosis, which was effectively managed by bougienage. No late complications were recorded. Bougienage of the newly created anorectum was commenced rather early in the postoperative course, i.e. already on the fourth day after surgery, and after the child had been discharged from hozpital it was continued at the home by the mother. The average duration of hospitalisation after definitive surgical correction was 12 days. The colostoma was usually closed 3 months after satisfactory definitive correction of the defect had been obtained. Early findings of electromyographic and manometric studies of the anal sphincter in PSARP-treated patients are rather optimistic, suggesting satisfactory late results (Table 2).

RESULTS	No. casess
Excellent	3
Good	5
Bad	1
TOTAL	9

TABLE 2. Results of Treatment

4. DISCUSSION

The surgical procedure employed in our patients was described in detail elsewhere (9,10). The application of PSARP without the use of a muscle stimulator is contraindicated. The muscle stimulator utilized, was custom designed constant current pulse generator (11). The main objective of the operation, which is performed with the aid of a muscle stimulator, is to stay in midline, expose the muscle-sphincter complex, open it like a book, mobilize the atretic rectum - occasionally by means of laparotomy - and eventually exactly reconstruct, with the aid of the muscle stimulator, the sphincter complex throught the mobilized rectum, which is then sutured to the skin in the previously defined anal dimple.

The adventage of transversal colostoma was observed in two cases in which laparotomy had to be emlpoyed for mobilization of the rectum due to excessively high rectal atresia. The most delicate step of definitive surgical correction of anal atresia is exposure of the fistula extending from the bowel to the urethra or the vagina. The atretic rectum is always dilated and it must be modelled so as to fit Hegar's dilator No. 15. Hoffman suggested that the sphincter mechanism should be reinforced with intestinal smooth muscle, and this technique was employed in our patients on two occasions (12).

However, the preliminary results obtained with PSARP in the surgical management of this severe congenital anomaly are encouraging, suggesting that future employment is warranted. It appears that with PSARP an increasing number of our little patients stand a fairly good chance of eventually achieving good fecal continence.

The PSARP technique does not seem to be the final answer for anorectal malformations since results have not been universally perfect. The procedure does not cure severe congenital innervation deficits associated with sacral anomalies or the socalled "flat bottom" cases which have poor musculature. The approach does not seem to be helpful in patients with a narrow pelvis resembling a form of caudal regression in which, regardless of the magnitude of the tapering, there is very little space left and the surgeon is unable to achieve the goal of surrounding the bowel by striated muscle along its entire intrapelvic path.

5. REFERENCES

1. Bradham RR (1958) Imperforate anus: Report of 130 cases. Surgery 44:578.
2. Kiesewetter WB, Turner CR and Sieber WK (1964): Imperforate anus: Review of sixteen years experience with 146 patients. Am J Surg 107.412.
3. Taylor I, Duthie HL and Zachary RB (1973): Anal continence following surgery for imperforate anus. J Pediatr Surg 8:497.
4. Cywes S, Cremin BJ and Louw JH (1971): Assesment of continence after treatment for anorectal agenesis: A clinical and radiological correlation. J Pediatr Surg 6:132.
5. Iwai N, Ogita S, Kida M et all (1979): A clinical and manometric correlation for assesment of post-operative continence in perforate anus. J Pediatr Surg 14:538.
6. Smith EI, Tunnell WP and Williams GR (1977): A clinical evaluation of the surgical treatment of anorectal malformations (imperforate anus). Ann Surg 187:583.
7. Karkowski J, Pollock WF, Landon CL (1973): Imperforate anus. Eighteen to

thirty year follow up study. Am J Surg 126:141.
8. Stephens FD, Smith ED (1971): Operative management of rectal deformities. In: Anorectal Malformations in Children. Chicago, Year Book Publishers 212-257.
9. De Vries PA and Pena A (1982): Posterior sagittal anorectoplasty. J Pediatr Surg 17:638.
10. Pena A and de Vries PA (1987): Posterior sagittal anorectoplasty: Important technical considerations and new applications. J Pediatr Surg 17:796.
11. Radumilo S, (1994): " Elektrostimulator analnog sfinktera." Elektrotehnički fakultet, Zagreb., Diplomski rad.
12. Hoffmann V, Kap-herr S, Koltai I (1981): Neue Wegw zur Behandlung der anorectalen Incontinenz. Kinderchir 32:258.

A WHOLE BODY COUNTER FOR *IN VIVO* MEASUREMENTS OF RADIOACTIVITY

M. Medvedec, S. Popović, B. Kasal, Grošev D.
Clinical Department of Nuclear Medicine and Radiation Protection,
University Hospital Rebro, Kišpatićeva 12, Zagreb, Croatia

Abstract

A special parallel slit collimator for 10.2×10.2×40.6 cm NaI(Tl) detector for the Model 2260 Canberra Accuscan shadow shield whole body counter was designed to enable better determination of radioactivity distribution in the subject and measurement of higher diagnostic activities.
Characteristics of the whole body counter (spatial resolution, counting efficiency, background, geometric uniformity) with and without collimator were studied by measuring gamma reference sources in air and in phantoms and by performing in vivo studies.
The use of the collimator greatly improves spatial resolution and enables measurement of much higher activities without losses. Whole body counting has therefore been established as one of the comparative methods for different clinical purposes.

BROJAČ CIJELOG TIJELA ZA *IN VIVO* MJERENJA RADIOAKTIVNOSTI

M. Medvedec, S. Popović, B. Kasal, Grošev D.
Klinički zavod za nuklearnu medicinu i zaštitu od zračenja,
Klinički bolnički centar Rebro, Kišpatićeva 12, Zagreb, Hrvatska

Sažetak

Specijalni kolimator s pravokutnim otvorom konstruiran je za 10.2×10.2×40.6 cm NaJ(Tl) detektor brojača cijelog tijela Canberra Accuscan Model 2260 kako bi bila moguća bolja lokalizacija radioaktivnosti u tijelu i mjerenje viših dijagnostičkih aktivnosti.
Svojstva brojača cijelog tijela (prostorna razlučivost, efikasnost, osnovno zračenje, geometrijska uniformnost) s i bez kolimatora analizirana su mjerenjem referentnih izvora gama zračenja u zraku i fantomima, te in vivo studijama.
Upotreba kolimatora bitno poboljšava prostornu razlučivost i omogućava mjerenje mnogo viših aktivnost bez gubitaka. Brojanje cijelog tijela utemeljeno je tako kao jedna od usporednih metoda s različitim kliničkim primjenama.

1. INTRODUCTION

Whole body counting is a direct *in vivo* technique for the measurement of radioactivity in the entire body. Whole body counters are mainly used for monitoring professionals having contact with radioactive materials or people after radiation accidents, but there are also many medical applications [1, 7]. In this paper the particular whole body counter is discussed as a clinical and

research tool, especially due to its possible use in nuclear medicine.

2. METHODS AND MATERIAL

The Canberra Accuscan Horizontal Bed Whole Body Counter Model 2260 system for *in vivo* dose measurement consists of:
- one 10.2×10.2×40.6 cm NaI(Tl) and one 47.2×50 mm high purity closed ended coaxial Ge detector with relative efficiency of 20%, both placed above the subject,
- 10 cm thick pre-1945 naval laminar steel shadow shielding in all straight directions from the detectors,
- nuclear instrument modules (NIMs): high voltage power supplies, preamplifiers, amplifiers, discriminator, AD converters and multichannel scaling unit (MSC),
- multichannel analyzer (MCA) (4×2048),
- step motor with a motor controller and scanning speed from 0.13 to 51 mm/s and
- DEC micro PDP 11/73 computer.

Monitoring room is placed in the sub-basement of the building, 147 m above the sea level and it has 20–60 cm thick concrete walls. There is a heating/cooling system and no special air filtration in the room.

For the construction of the collimator low level background plates were used, the plates which were delivered as an optional part of the original configuration. Standard lead bricks were also used and additional lead plates were especially made. Design and all parts of the collimator were chosen and made according to the existing geometric relationships of detectors and shielding, weight, size, technology, costs and supposed clinical application.

In our studies we used gamma reference point and I-131 sources measured in air and in the Canberra/RMC Transfer Phantom or Bottle Manikin Absorption (BOMAB) Phantom.

A quantitative approach to spatial resolution evaluation with and without collimator was through the point spread function (PSF) [4]. The counting-rate profiles were fitted to a bell shaped function(s) by the method of least mean squares [2, 3, 4]. Linear interpolation was applied for Full Width at Half Maximum (FWHM) determination.

The counting efficiency was determined by means of a set of point sources measured on the bed in air, or in the thyroid, lung or gastrointestinal cavity of the Canberra/RMC Transfer phantom. The photo peak efficiency indices (counts per emitted photon) were calculated taking into account known activities of the measured sources and photo peak counts in MCA channels. The number of MCA channels was chosen to comprise approximately 1.6 FWHM centered on the peak [5].

The background index as good measure of a whole body counter ability was determined by

$$N_{0,index} = \int_{0.1}^{2.0MeV} f(E)dE \qquad (1)$$

where f(E) is a density function

$$f(E): \frac{counts/\min}{(cm^3)crystalvolume \cdot energy}$$

[1]. The minimum detectable activity (MDA) was defined as the activity A yielding a net counting rate N_N during time t_N in the amount of 3-fold standard deviation of the background N_0 with the counting time t_0,

$$N_N = kA, \qquad MDA = \frac{3}{k}\sqrt{\frac{N_0}{t_0}} \qquad (2)$$

[1]. The geometric uniformity of the whole body counter was evaluated by measuring I-131 source in the upper, middle and lower position in each compartment of the BOMAB phantom. *In vivo* studies of patients after oral administration of approximately 370 kBq of I-131 were also performed to verify some results of the phantom studies [8]. All measurements were done with the collimator opening varied from 1 to 10 cm, or without the collimator.

3. RESULTS

3.1. Collimator

The parallel slit collimator (Figure 1) consists of four 3×13×59 cm horizontal low background steel plates weighing 18.2 kg each (heavy dots-marked), two 2×10×45(59) cm vertical lead plates weighing 11.1 kg each (light dots-marked) and eight 3×10×10 cm vertical lead bricks weighing 3.4 kg each (bricks-marked). Figure 1 shows cross section through the upper central part of the whole body counter illustrating of basic shielding (hatch-marked) and additional shielding with the collimator in relation to the arrangement of the detectors. The detector cavity of the standard shield can accommodate up to 3 large NaI(Tl) detectors, 1 or 2 Ge detectors, or 2 NaI(Tl) and 2 Ge detectors, all placed above the subject. Therefore,

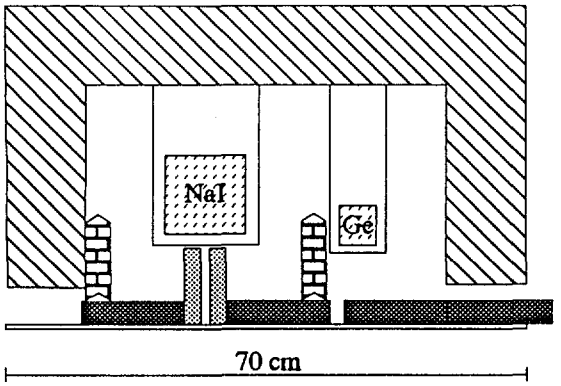

Figure 1 Cross section through the upper central part of the whole body counter with the parallel slit collimator.

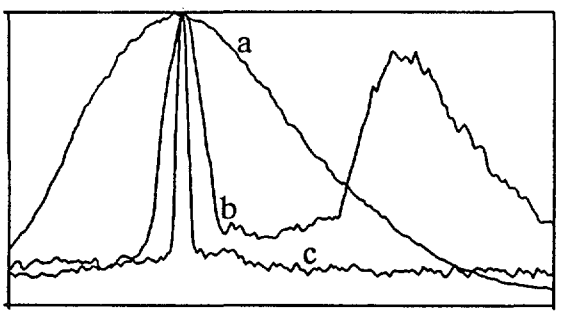

Figure 2 Normalized point spread functions of Ba-133 measured on the bed in air in case without the collimator (a), with four original collimator plates (b) and with the parallel slit collimator (c).

inside the basic shielding the existing NaI(Tl) detector is exposed to radiation from its three sides, what is not an usual case. In addition, Ge detector is mounted on axis at an approximately 15 cm offset. According to these facts, the response of whole body counter without the collimator (Figure 2, curve a) or with the original collimator plates (one of the characteristic PSF is shown in Figure 2, curve b) did not ensure acceptable response in MSC mode and simultaneous measurement with both detectors, as it does the final design of the collimator (Figure 1, Figure 2, curve c). Normalized point spread functions in Figure 2 qualitatively illustrate improvement of spatial resolution.

3.2. Spatial resolution

The point spread function is according to the measurements generally best described by

$$PSF(x)=\sum_i a_i e^{-\frac{1}{2}\frac{(x-b_i)^2}{c_i^2}}+\sum_j d_j\frac{e_j}{(x-f_j)^2+e_j^2}+gx+h \quad (3)$$

where i=1, 2 or 3 and j=0, 1 or 2. Except for high energies (for example Co-60), one Gaussian and one Lorentzian or another Gaussian function give very good fit. Some values of FWHM are shown in Table 1.

collimator opening (cm)	BED		LUNG	
	Ba-133	Cs-137	Ba-133	Cs-137
1	4.8	6.4	3.7	5.1
2	8.3	10.8	7.1	8.8
4	16.2	19.2	13.2	14.8
6	22.0	23.3	17.7	18.2
8	24.6	25.2	19.8	20.2
10	27.7	29.0	22.6	23.0
without col.	89.5	88.2	62.1	65.4

Table 1 FWHM of the PSF for two different radionuclides measured on the bed in air and in the Canberra/RMC Transfer phantom.

3.3. Background

The background index varies with the collimator opening and is 0.45 for 1 cm collimator opening, 0.56 for 10 cm collimator opening and 0.93 without collimator. The lowest MDA of the whole body counter is 14 Bq (Co-60, E=1.32 MeV). For typical counting time of 445 s MDA for Ba-133 (356 keV) measured in the thyroid cavity is 140 Bq without the collimator, and 9990 Bq with the 1 cm collimator opening.

3.4. Counting efficiency

The efficiency index of about 1.3 to 3.2‰ without the collimator and 0.007 to 0.15‰ with the 1 cm collimator opening was obtained for energies between 0.06 and 1.32 MeV. An explanation for strictly positive slope of efficiency curves in the case of smaller collimator openings is mainly more significant penetration of radiation through collimator plates with increasing energies.

3.5. Geometric uniformity

If the middle of the BOMAB abdomen compartment is considered as reference position with relative response 1.00, then characteristic responses (*-without collimator, **-collimator opening 1 cm) among thirty positions in phantom are:

- maximum:
  - 1.34* and 1.55** (Compton)
  - 2.22* and 1.97** (Peak)
  - 1.60* and 1.60** (Full)
- minimum:
  - 0.47* and 0.53** (Compton)
  - 0.31* and 0.40** (Peak)
  - 0.42* and 0.50** (Full)
- average:
  - 0.84 ± 0.23* and 1.05 ± 0.28** (Compton)
  - 1.10 ± 0.54* and 1.15 ± 0.47** (Peak)
  - 0.92 ± 0.32* and 1.08 ± 0.33** (Full).

Great differences in the response [3, 5], due to unilateral detectors, show necessity of measurements in a scatter window [8], or in a anterior-posterior and posterior-anterior position and calculating a geometric mean of those two measurements. Namely, the geometric mean largely compensate variations of sensitivity with depth, as it is described by others [3].

4. CONCLUSION

This work has determined main characteristics of the particular whole body counter, mostly unknown so far. The use of specially designed slit collimator and description of point spread function improves to a large extent originally very limited capabilities of the radioactivity localization. The use of the collimator improves spatial resolution up to 20 times, decreases counting efficiency up to 200 times and background index up to 2 times. Total range of activities which can be measured with and without collimator is approximately from 37 Bq to 37 MBq. The sum of line, Gaussian and Lorentzian distribution(s) gives the best fit of point spread function. No significant changes of geometric uniformity were indicated and different energy windows were discussed. Simultaneous measurement with both detectors is available regardless of additional shielding. On that basis whole body counter is expected to contribute not only to dosimetry problems of internal contamination with low level activities, but also to quantitative profile scanning in different clinical problems. At the moment the focus is on the optimization of therapeutical doses of patients having I-131 treatment after surgical thyroidectomy.

5. REFERENCES

1. P Mariß, E. Jahns, O. Schober. A Whole Body Counter with an Invariant Response for Whole Body Analysis. Eur. J. of Nucl Med. 3, 129-135, 1978
2. O. Schober, E. Jahns, P Mariß. Evaluation of Linear Profile Scans; Mathematical Treatment of Line-Spread Function. Eur. J. of Nucl Med. 3, 137-143,1978
3. P. Tothill, J. M. Galt. Quantitative Profile scanning for the Measurement of Organ Activity. Phys. Med. Biol. Vol.16, No.4, 625-634, 1971
4. J. A. Sorenson, M. E. Phelps. Physics in Nuclear Medicine. W. B. Saunders Company., Philadelphia, 1987
5. R. A. Dudley, A. ben Haim. Comparison of Techinques for Whole-Body Counting of γ-Ray Emitting Nuclides with NaI(Tl) Detector I: Point Sources in Phantoms. Phys. Med. Biol. Vol.13, No.2, 181-193, 1968
6. R. A. Dudley, A. ben Haim. Comparison of Techniques for Whole-Body Counting of γ-Ray Emitting Nuclides with NaI(Tl) Detector II: Distributed Sources in Phantoms and Humans. Phys. Med. Biol. Vol.13, No.2, 181-193, 1968
7. R. Toohey et al. Current Status of Whole Body Counting as a Means to Detect and Quantify Previous Exposures to Radioactive Materials. Health Physics. Vol. 60, Sup. 1, 7-42, 1991
8. W. D. Gibbs, H. D. Hogges, M. Bailey, C. C. Lushbaugh. Accurate Whole-Body Quantitation of I-131 Retention by Counting a Scatter Window. J. Nucl. Med., Vol. 11, No. 8, 487-490, 1970

STRUCTURE AND STRENGTH OF THE DISTAL FOREARM: EXPERIMENTAL COLLES FRACTURES AND MATHEMATICAL MODELLING BY FINITE ELEMENTS METHOD

Vasilije Nikolić [1], Draško Pavlović [2], Zvonimir Žagar [3], Tanja Nikolić [1], Mladen Hudec [4], Janko Hančević [5], Miljenko Hajman [3].
[1] Zavod za anatomiju "Drago Perović", Medicinski fakultet Zagreb, [2] Opća bolnica "Sveti Duh", Zagreb, [3] Građevinski fakultet, Zagreb, [4] Rudarsko geološki naftni fakultet, Zagreb, [5] Kirurška klinika KBC Rebro, Zagreb.

Abstract

The experimental Colles' fractures were carried out on 20 anatomical specimens of the hand by means of an impactor constructed in our laboratory. Bone mineral content and bone mineral density were determined in distal portion of radius. The site of the fracture varies within the zone from the radiocarpal joint to as far as slightly more than 4 cm proximally of the joint, i.e. within the area of the bone mineral measurement by single photon absorptiometry (SPA). From serial CT scans as well from serial SPA scans of the distal forearm we obtained data for finte elements meshwork. Features of the exeprimental Colles' fractures on anatomical specimens were compared with the results of modelling by finite elements method.

INTRODUCTION

Bone carrying capacity is defined by quality, structure and geometry of bone cross section.(1) Bone loss in postmenopausal women, in elderly subjects, metabolic diseases, decreased bone mineral density (BMD), is well known to be related to increased risk of bone fractures. BMD and bone mineral content (BMC), could be measured with adequate precision by quantitative computorized tomography (QCT) or simpliest, by single (SPA) or by dual (DPA) photon absorptiometry.(2,3) Mechanical properities of bones as organs are better related to the data of cross-

sectional structural geometry, such as moments of inertia.(1) These parameters include both, the geometric data and material distribution within the bone cross section.

The aim of these investigation is to show that the data of the cross sectional structural geometry could be obtained from the measurements of the forearm BMD and BMC by SPA and QCT as well that the same data could be used for matehmatical modelling by finte elements method (FEM).(4)

MATERIALS AND METHODS

Awbery's method (5) were used in measuring distal and ultradistal BMC and BMD in 170 normal adult subjects of both sexes aged between 30 and 87 years.

The second group consists of 20 anatomic specimens of the forearm bones. Twenty embalmed anatomic specimens of distal part of the forearm was experimentally fractured in a "Hudec' pendulum" impactor hammer to obtain Colles' fractures.(2)

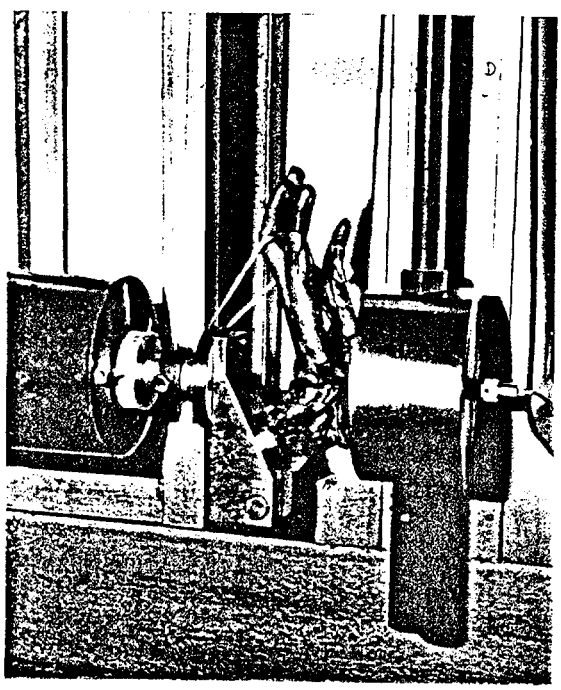

Figure 1. Anatomical specimens of the hand and distal forearm in a pendulum impactor according Hudec.

Mathematical model for finite elements analysis has been obtained from CT and SPA data. The finite elements model of the forearm was developed by use of the FEA COSMOS'S (SRAC) graphic modelar GEOSTAR. For the bones SOLID SD FE, and for the interosseal membrane GAP-frictionless FE and PLANE2D were used. (Figure 2a & 2b)..

RESULTS

The pure kinetic energy of the fracture of the distal radius is between 7 Nm and 30 Nm. (Figure 1). The energy absorbed in the soft tissues of the palma manus exceeds greatly the energy necessary for the fracture of the radius in the typical area.

The absorbed energy in the specimens on wich all soft tissues, including skin were preserved ranged from 32 to 75 Nm. There was a significant positive correlation between BMD and impact energy, $r=0.57$ ($p<0.01$), as well between absorbed energy and AP moments of inertia, $r=0.49$ ($p<0.01$). Shape and position of the fracture gap has been shown radiographically.

The FE model was held by the use of boundary conditions as it was done in the laboratory experiments. The applied forces as pressures were applied on facies articularis carpea as supposed to be by a fall on outstretched arm. The principal stresses P1, P2, P3, the component stresses SX, SY, TXY. TYZ, TXZ and the Von Mises stresses for all elements were obtained. Stress concentration in FEM appear at the same site of the radius as in real anatomical specimens and in the area of typical Colles' fractures.

CONCLUSION

Fractures of the distal end of the radius, i.e. Colles' fractures are most frequently seen between six and ten years of age and between sixty and seventy years (6).

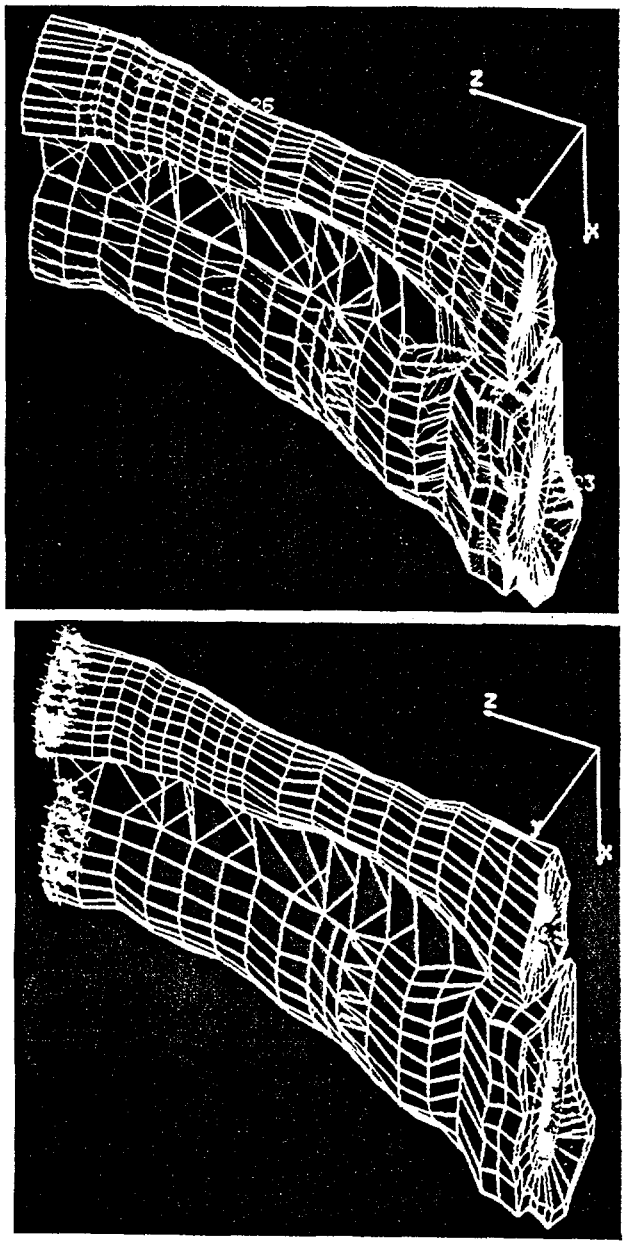

Figures 2 a & b Three-dimensional finite-element mesh of the distal part of radius and ulna.

In a later group it is often the first indication of a severe osteopenic condition. Earely diagnosis of ostepenia is difficult, BMC and BMD measurements are helpful in screening patients at risk, bu they are insufficient to define mechanical properties of bones.

We developed a method using data obtained by SPA and QCT scans to define mehanical properiteis of the bone and compared them with the results of finite elements method. Such a model requires further clinical evaluation.

REFERENCES

1: V. Nikolić, M. Hudec. Principi i elementi biomehanike. Školska knjiga, Zagreb, 1988.

2. V. Nikolić, J. Hančević, M. Hudec, B. Banović. Absorption of the impact energy in the palmar soft tissues. Anat Embryol 148:215-221, 1975.

3. I. Fogelman, P. Ryan. Measurement of bone mass. Bone 13:S23-S28, 1992.

4. E.M. Alhava. Bone density measurements. Calcif Tissue Int 49:S21-S23, 1991.

5. J. Mizrahi, J.Silva, T.M. Keaveny, T. Edwards, W.C. Hayes. Finite-element stress analysis of the normal and osteoporotic lumbar vertebral body. Spine 18:2088-2096, 1993.

6. B.J. Awbery, P.C. Jacobson, S.A. Grubb, W.H. McCartney, L.M. Vincent, R.V. Talmage. Bone density in women: a modified procedure for measurement of distal radial density. J Orthopaed Res 2:314-321, 1984.

7. J.B. Jupiter. Fractures of the distal end of the radius. J Bone and Joint Surg 73-A:461-469, 1991.

A SUPLEMENTARY STUDY OF THE ANATOMY OF LUMBAR PEDICULAR SEGMENT

Štimac D., Nikolić V., Jouni H.

Department of Anatomy "Drago Perović", School of Medicine,
University of Zagreb, Šalata 11, Zagreb

ABSTRACT:

A study of pedicular morphology and dimensions is of great importance for modern spinal surgery which applies transpedicular screw or pin fixation for stabilization of an unstable spine. Precise measurements of pedicular dimensions on lumbar spine CT-scans and on macerated anatomical specimens were made. Authors came to the conclusions that there were significant statistical differences in dimensions of the left pedicle as compared with dimensions of the right one. In average, the left pedicle is 3% lower and 5% shorter but 9% wider than the right pedicle. The product of these values shows that the volumes of both pedicles are more or less the same. The cause of the asymmetry should undergo further investigation.

PRILOG POZNAVANJU ANATOMIJE PEDIKULARNOG SEGMENTA LUMBALNIH KRALJEŠAKA

SAŽETAK:

Poznavanje morfologije i dimenzija pedikla kralješaka od velike je važnosti za današnju spinalnu kirurgiju u kojoj se stabilizacija nestabilne kralješnice bazira na transpedikularnoj fiksaciji šrafima ili pinovima. Autori su preciznim mjerenjima istih pokušali baciti malo više svjetla na te nepoznanice. Preciznim mjerenjem dimenzija pedikla na CT-snimkama lumbalne kralješnice i mjerenjima izvršenim na maceriranim anatomskim preparatima došli su do zaključka da postoje znatne razlike u dimenzijama desnog i lijevog pedikla istog kralješka. Lijevi pedikl je u prosjeku 3% niži i 5% kraći od desnog, ali je za 9% širi od desnog. Umnožak tih vrijednosti pokazuje da su volumeni lijevog i desnog pedikla približno isti. Razotkrivanje uzroka te asimetrije lijevo-desno biti će predmet daljnjeg našeg istraživanja.

INTRODUCTION:

A pedicular segment is a relatively small part of a vertebra of great importance for modern spinal surgery. Although much has already been written about pedicles, there are still many unknowns as regards the morphology of this vertebral part. Modern fixation of an unstable spine (fracture) is based on transpedicular fixation - either with screws or with pins. Such fixation is limited by the anatomy of the pedicle; its height, width, thickness of the cortex, quality of spongiosis, angle that the pedicle makes with the vertebral body. Our intention has been to contribute a little to the study of pedicular shapes and dimensions particularly dealing with the asymmetry of left and right pedicles.

Pedicular morphology: Vertebral pedicles are tube-shaped bony structures which, on their surface, are made of firm, compact bone and of poor spongiosis in the middle. They are backward and slightly outward bound (seen from A-P direction). The pedicular edge reaches the back side of the vertebral body and in the upper 2/3 of a vertebra it is in close contact with the vertebral edge. The posterior pedicular edge is connected to the upper half of the outer

edge of the lamina. The superior pedicular edge is thick and concavely bent upward while its inferior edge, thinner than the superior one, is also concave and bent downward (1).

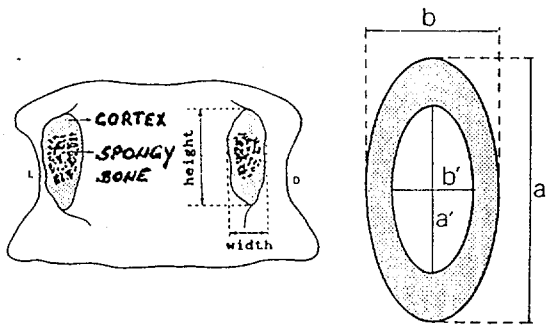

Figure 1. A) Pedicular cross-section through the frontal plane at the level of the corpo-pedicular junction (seen from the back side); B) vertical and transversal diametres (external and internal).

Such rough and general description lacks many a detail which would enable better comprehension of the segment in daily performed surgery of the spine. The connection point of the pedicle and the superior articular extension is laterally reinforced in the shape of an ossified extension. Looking from L1 to L5, this extension becomes bigger and bigger.

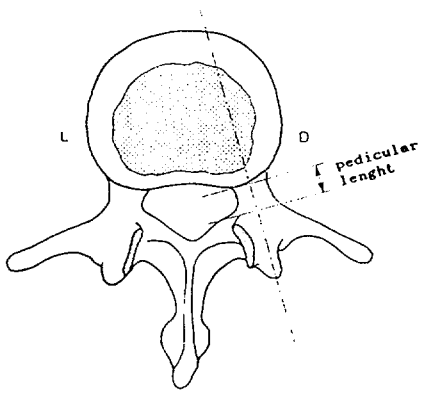

Figure 2. "In the narrow sense of the word", pedicular length is the crucial part of "effective pedicular length". In this sense, pedicular length = "effective pedicular lenhth" + length of the articular and mammillary extension.

The inferior part of bone mass includes: 1) inferior edge of the superior articular extension, then thickened, therefore well observable mammillary extension, 2) accessory extension occupying the median part of the back side of the costiform extension base.
The sagittal axis of the pedicle goes through a depression confined with 1) posterior edge of the superior articular extension immediately above, 2) accessory extension 3-4 mm laterally and 3) through the bone shaft medially.
The identification of the posterior pedicular edge is of particular significance whereas a screw of pin is placed exactly there. This particular point presents the posterior end of the pedicle.
Pedicular dimensions are also of great importance whereas the dimension of screws to be applied in osteosynthesis.

MATERIAL AND METHODS:

The research study consists of two parts. On a sample of 31 lumbar vertebrae, in the first part of the study, the authors measured vertical and transversal diametres of the pedicle (Figure 2). The measurements were carried out on a caliper. As regards their axis, pedicles are further vertically cut in three different heights: 1) at the transition point of the vertebral body into pedicle, 2) in the middle of the pedicle, 3) in the laminar (=back) side of the pedicle, namely at the transition point of the pedicle into the anterior part of the superior articular extension base. Following the descriptive analysis of the above and applying a movable measuring device, external vertical and transitional diametres of the pedicle (its height and width) were measured at all three levels, then thickness of the cortex af all four walls (at all three levels) and dimensions of the pedicular canal itself.
In the second part of the study, the authors analysed 30 CT-scans of the spine of healthy controls who underwent the diagnostic procedure for diseases not connected with the spine.
After statistical processing, measurement results obtained in both groups were then compared. Special attention was paid to comparative values obtained in the left or right pedicle.

RESULTS:

Pedicular structure: The results of the study confirm that a pedicular segment is the most compact part of a vertebra.Cross-section of the pedicle is most fre-

quently shaped an irregular ellipsis that can be laterally protruded. The shape of cross-section depends on the section point in respect to the pedicular length. The pedicle is a short tube filled with spongy bone, while its cortex is of uneven thickness. The thickness of the cortex varies even within the same cross-section. The cortex is most thickened in the inferior and superior edge where it sometimes reaches 4 mm. Both, the two superior and two inferior areas represent half of the pedicular length and region of the principal pedicular junction with the vertebral body. In all cross-sections, the pedicle is clearly marked from the median part, namely towards the spinal canal, while its thinnest part is seen in the lateral region.

Pedicular dimensions: Table 1 shows the results obtained by measuring of pedicular dimensions on anatomical vartebral preparations. The measurement was performed on 31, previously macerated and unlubricated lumbar vertebrae.
Another part of the research study is engaged in measuring the pedicles on available CT-scans of the lumbar spine of patients who were scanned for diseases not related to the lumbar spine. Therefore, the CT-scans may be considered as scans of healthy controls.

		$\bar{X}$		MIN.		MAX.	
		D	L	D	L	D	L
a	External vertical diameter	15.7	15.2	12.1	11.5	18.0	18.0
b	External transversal diameter	8.9	9.6	5.0	5.0	13.0	14.0
I_P	Pedicular index	0.59	0.65	0.28	0.31	1.07	1.22
I_{LR}	Index of L-R asymmetry	Sagitt 0.97	Transv 1.09	Sagitt 0.85	Trans 0.87	Sagit 1.15	Tran 1.61
L	Pedicular lenght	6.5	6.2	5.0	4.1	8.8	7.5

TABLE 1. Mean, maximal and minimal values of the pedicles of the lumbar veretebre.

As a rule almost, osteoporosis invades the lateral and dorsolateral wall, whereas median and inferior walls remain compact. The fact is significant concerning the introduction of a screw or pin at osteosynthesis, where the thickness of the cortex that separates the pedicular cavity from the spinal canal is firm enough to protect the spinal canal and direct the screw or pin toward the pedicular axis. The inferior compact cortex enables firm enough hypomochlion over which the screw or pin fixation can produce the extension or reposition of a broken vertebra. Spongiosis within the pedicle makes an irregular net with trabecules. The trabecules that encircle spherical or elliptical regions go off at a tangent and are more dense in peripheral pedicular parts. On the other hand, in the median part and inferolateral regions in particular, spongiosis is less frequent, trabecules are thinner and interspace less dense. This enables the screw or pin go smoothly through the median pedicular part. Bony traverses present within spongiosis, their structure and direction have already been described by Gallois and Japoit (2).

The results thus obtained were compared to the values got at measuring of native anatomical preparations. The comparison proved that dimensions of the pedicles measured in both groups does not significantly differ.
Our most valuable observation concerns the statistically significant asymmetry found in dimensions of the right pedicles as compared with the left one.

DISCUSSION:

The research study focused on the height, width and length of the pedicle.
Pedicular height (= vertical diametre): Studies of Saillant (3), Berry (4), Zindrick (5), Moran (6) and Olsewski (7) show generally comparable values of the pedicular height that vary within 15 mm.
Olsewski (7) observes significant differences in dimensions of female patients as compared with male. For Zindrick (5), the pedicular height decreases proportionally from L1 to L5. For Berry (4) and Moran (6), the decrease of diametrical values is most obvious at L5 level, whereas Saillant (3) points

at a reverse phenomenon - the pedicle is the highest at L4 level. Olsewski (7) alone demonstrates a distinct height increase at L5 level.

Pedicular width (=transversal diametre): The pedicular width is in fact its smallest dimensions. It also represents the most important dimensions which determines the diametre of a screw to be applied in osteosynthesis. The measure should therefore be taken accurately , vertically to the pedicular axis. Generally speaking, the diametre increases from L1 to L5, but the values obtained by various authors differ a lot. According to Berry (4) and Moran (6), who obtained an almost identical curve, the pedicular width increases alowly and irregularly from L1 to L5. On the other hand, Krag (8), Zindrick (5), Olsewski (7) and Saillant (3) observe that the increase is well marked only from L3 segment and towards L5.

YEAR	AUTHOR	pedicular height (mm)		pedicular width (mm)	
1959.	Berry	L1 = 15.6 L2 = 15.3 L3 = 14.7 L4 = 13.1 L5 = 13.8	$\overline{X}$ = 14.5	L1 = 7.0 L2 = 7.5 L3 = 9.3 L4 = 10.2 L5 = 11.0	$\overline{X}$ = 9.0
1979.	Saillant	L1 = 15.6 L2 = 15.1 L3 = 15.1 L4 = 15.3 L5 = 14.6	$\overline{X}$ = 15.1	L1 = 8.0 L2 = 8.5 L3 = 9.1 L4 = 12.1 L5 = 16.4	$\overline{X}$ = 10.8
1986.	Krag			L1 = 7.2 L2 = 8.8 L3 = 9.5 L4 = 11.0 L5 = 15.1	$\overline{X}$ = 10.3
1987.	Zindrick	L1 = 15.0 L2 = 14.5 L3 = 14.6 L4 = 14.6 L5 = 14.0	$\overline{X}$ = 14.5	L1 = 9.0 L2 = 9.0 L3 = 10.0 L4 = 12.9 L5 = 17.9	$\overline{X}$ = 11.8
1989.	Moran	L1 = 15.7 L2 = 14.9 L3 = 14.4 L4 = 12.8 L5 = 14.4	$\overline{X}$ = 14.4	L1 = 7.0 L2 = 7.1 L3 = 9.2 L4 = 9.8 L5 = 10.1	$\overline{X}$ = 8.6
1990.	Olsewski	L1 = 16.3 L2 = 15.8 L3 = 15.6 L4 = 15.8 L5 = 16.8	$\overline{X}$ = 16.6	L1 = 8.4 L2 = 8.8 L3 = 10.8 L4 = 13.7 L5 = 19.9	$\overline{X}$ = 12.3

TABLE 2. Average dimensions of the pedicle of the lumbar vertebre according different authors.

According to these authors, the pedicular width is twice multiplied from L1 toward L5. These authors measured up the smallest pedicular width on L1 segment. From author to author, the maximum diametre measured at L5 level differs from even 10 mm (Moran (6), Olsewski (7)), whereas the diametre measured at L1 level varies for only 2 mm.

Pediculo-corporal length: The pediculo-corporal length marks the distance from the vertebral corpus (body) to the posterior edge of the pedicle, measured along the vertical axis. The lenght, which also includes the superior articular extension, presents "the effective pedicular length". According to Krag (8), the pedicular length decreases from L1 to L5. Saillant (3) measured the length in the plane parallel to the median one. Conforming to him, the pedicle of L3 vertebra is the shortest. Results obtained by Berry (4) and Krag (8) are approximately the same, whereas the values Saillant (3) got are significantly lower. Berry (4) showed that the maximum pedicular length in the lumbar segment of the spine differs 5 mm from the minimum one (table 2). Our descriptive and morphometric analysis of the pedicle led to the following conclusion: 1) pedicle vary in dimensions; 2) ratio of the pedicular height and width of the left and right side is not the same; 3) the medullary canal is very narrow; 4) thickness of the cortex of both pedicles is not the same; 5) cortex is the thickest in the inferior part of the pedicle, the superior part follows, then the medianw hereas the cortex is the thinnest in the lateral end; 6) osteoporosis, spongization of the cortex occurs beginning from the medullary canal towards the superior pedicular edge and towards the external cortex. Further on, 1)vertical diameters are more regular than transversal (from L1 to L5 they change less), 2) from author to author, transversal diametre median values differ much more than vertical ones; 3) our pedicular height values are closest to those obtained by Saillant (3), while the values we got for the external trasversal diametre almost match those got by Moran (6); 4) the greatest contribution of ours is that we have recognized the necessity of measuring

each side of the pedicle separately which we did not find described in literature available to us; 5) our findings on the asymmmetry lead to the conclusion that the vertical diametre of the left pedicle is about 3% smaller then of the right one. On the other hand, the transversal diametre of the left pedicle is about 9% larger than that of the right pedicle.

CONCLUSION:

The morphologic, morphometric and structural analysis of lumbar spine pedicles shows possibilities of macroscopic and descriptive anatomy when based a practical problem of a surgeon or radiologist. It also stands open towards their future cooperation. From the functional point of view, the research study demonstrates an important role of pedicle situated in the region where they are pressed with the vertebral body in front, and by the articular extension in the back side. Their privileged location drives the attention of spinal surgeons (neurosurgeons and orthopaedics) to these structures who will thus learn more about their morphology.

REFERENCES

1. C Maillot, R Wolfram-Gabel. Pedicles of lumbar vertebrae. Surg. Radiol. Anat. 15: 295-300, 1993.
2. Gallois, Japoit. Arhitecture interieure des vertebres. Rev. Chir. 63: 688-708, 1925.
3. G Saillant. Etude anatomique des pedicules vertebraux. Rev. Chir. Orthop. 62: 151-160, 1976.
4. JL Berry, JM Moran, WS Berg, AD Steffee. A morphometric study of human lumbar and selected thoracic vertebrae. Spine 12: 362-367, 1959.
5. MR Zindrick, LL Wiltse, A Doornik, EH Widell, GW Knight, AG Patwardhan, JC Thomas, SL Rothman, BT Fields: Analysis of the Morphometric Characteristics of the Thoracic and Lumbar Pedicles. Spine 12(2): 160-166, 1987.
6. JM mOran, WS Berg, JL Berry, JM Greiger, AD Steffee. Transpedicular screw fixation. J. Orthop. Res. 7: 107-114, 1989.
7. M Olsewski, EH Simmons, FC Kallen, FC Mendel, CM Severin, DL Berrens. Morphometry of the lumbar spine: anatomical perspectives related to transpedicular fixation. J. Bone Joint Surg. (Am) 72: 541-549, 1990.
8. MH Krag, BD Beynnon, MH Pope, JW Frymoyer, LD Haugh, DL Weaver. An Internal Fixator for Posterior Aplication to Short Segment of the Thoracic, Lumbar, or Lumbosacral Spine. Clin. Orthop. 203: 75-98, 1986.
9. JN Weinstwin, BJ Rydevik, W Rauschning. Anatomic and Technical Considerations of Pedicle Screw Fixation. Clin. Orthop. 284: 34-46, 1992.
10. E Sim. Location of Transpedicular Screw for Fixation of the Lower Thoracic and Lumbar Spine. Acta Orthop. Scand. 64(1): 28-32, 1993.
11. TS Whitecloud, TC Skalley, SD Cook, EL Morgan. Roentgenographic Measurement of Pedicle Screw Penetration. Clin. Orthop. 245: 57-68, 1989.
12. MH Krag, DL Weaver, BD Beynnon, LD Haugh. Morphometry of the Thoracic and Lumbar Spine Related to Transpedicular Screw Placement for Surgical Spinal Fixation. Spine 13(1): 27-32, 1988.
13. GR Misenhimer, RD Peek, LL Wiltse, SLG Rothman, EH Widell. Anatomic Analysis of Pedicle Cortical and Cancellous Diametar as Related to Screw Size. Spine 14(4): 367-372, 1989.
14. SD Gertzbein, SE Robbins. Accuracy of Pedicular Screw Placement in vivo. Spine 15(1): 11-14, 1990.
15. MH Krag, BD Beynnon, MH Pope, TA DeCoster. Depth of Insertion of Transpedicular Vertebral Screws into Human Vertebrae: Effect upon Screw-Vertebra Interface Strenght. J. Spinal Disord. 1(4): 287-294, 1989.
16. R Roy-Camille, G Saillant, C Mazel. Internal Fixation of the Lumbar Spine with Pedicle Screw Plating. Clin. Orthop. 203: 7-17, 1986.
17. JN Weinstein, KF Spratt, D Spengler, C Brick, S Reid. Spinal Pedicle Fixation: Repiability and Validity of Roentgenogram-Based Assessment and Surgical Factors on Successful Screw Placement. Spine 13(9): 1012-1018, 1988.
18. MR Zindrick, LL Wiltse, EH Widell, JC Thomas, WR Holland, T Field, CW Spencer. Clin. Orthop. 203: 99-111, 1986.

CORTICAL AREA OF THE SHAFT OF FEMUR IN EVALUATION OF THE FUNCTIONAL ADAPTABILITY OF THE BONE

Savo Jovanović, Igor Jovanović
Department of Orthopaedics, Clinical Hospital Osijek,
Faculty of Electrical Engineering, University of Zagreb

The study dealt with cortical area of the upper part of the shaft of femur in patients with coxarthrosis. Radiogrametric measurements of 454 X-ray pictures of the hip joint and the proximal part of the shaft of femur produced in a-p projection were performed by means of specially designed scheme. Values of the subperiostal diameter and the lateromedial diameter of the medullar canal were inserted into formulae for calculation of the cortical area. After processing the data, we obtained values of the cortical area of the shaft of femur on sixteen measurement levels in relation to age, sex, magnitude of the colodiaphysial angle and the longitude of limping in the hip. In patients with coxarthrosis, owing to intensified strains, which was the result of the change of direction of the resulting force of loading, a functional adaptability of the bone emerges, manifested by an enlargement of the cortical area on some measurement places.

INTRODUCTION

The functional adaptation of the bone caused by mechanical stimuli appears as a morphological and structural adaptation [16].

The problems of functional adaptation of the skeleton have not been solved yet even in some basic elements, and scientific research is carried out in the most suitable way, i. e. analysis of mechanical causes of adaptation and its structural consequences [17].

In the study of the functional adaptation of locomotory system to the mechanical load various methods have been applied. The radiogrametric method of studying the functional adaptation of the skeleton can be treated as one of the more precise.

In 1951 Astanin [2] studies the functional adaptation of the locomotory system in athletes using the osteometric method, while Barnett and Nordin in 1960 introduce the cortical parameters in the study of functional adaptation of the skeleton [4].

In later studies many authors study biomechanical characteristics and the carrying capacity of the bone [1-8, 16, 18-21].

The cortical parameters of the bone can be represented as absolute or relative values. Relative values are represented as cortical indexes.

One of the better or possibly the best parameter, which shows the carrying area of the bone, is the cortical area. It thoroughly follows the tendency of the change of cortical thickness.

EXAMINEES AND METHODS

The study of cortical area of the proximal part of femur in patients with coxarthrosis and sideways limping in the hip was performed on 454 a-p X-ray pictures of the hip joint and proximal part of femur. 260 cases were female, while 194 cases were male patients. The ratio of women to men is 1.34:1. The average age of the patients was 51.54 years. On the a-p X-ray pictures we determined the colodiaphysar angle (CCD) and the subperiostal diameter of the shaft of femur and the lateromedial diameter of the medullar canal on sixteen levels, starting with the place of osteotomy, performed during aloarthroplastical operations on the hip. The distance between consecutive levels of measurement was 1 cm.

The data was inserted into formulae for calculation of the cortical area, and processed by a computer.

RESULTS

We present the results of our study of the cortical area of the shaft of femur in the patients with coxarthrosis and foreseen total replacement of

the hip joint in relation to sex, age, length of sideways limping and CCD angle.

The cortical area of the shaft of femur, observed from the levels 0 to 15, was between 10.074 cm^2 and 6.842 cm^2. The older female patients have greater values of the cortical area (Fig. 1).

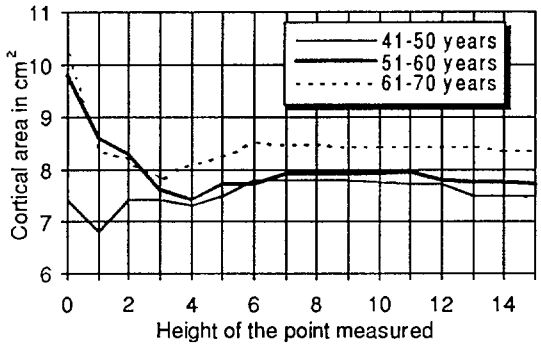

Fig 1. Cortical area of the shaft of the femur in female patients depending on age

The averages of the cortical area of femur of the male patients with coxarthrosis are between 10.689 cm^2 and 7.450 cm^2, corresponding to levels 0-15. The cortical area is the least between 31 and 40 years of age. In the region of proximal levels of measurement, the value of the cortical area of femur is greater in older male patients. On the distal levels of measurement, a definite relationship between those two variables does not exist (Fig. 2).

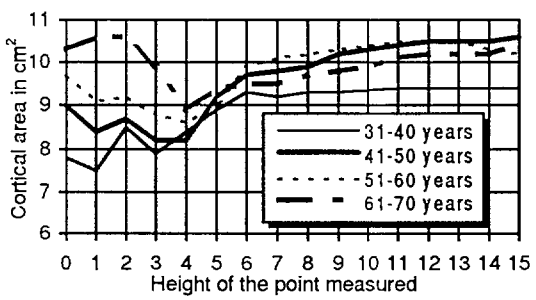

Fig 2. Cortical area of the shaft of the femur in male patients depending on age

Between the levels 0 and 6, the value of the cortical area of femur is greater in the female patients with longer sideways limping (Fig. 3).

Male patients with longer sideways limping in the hip have greater values of the cortical area of femur, between levels 0 and 5 (Fig. 4).

Female and male patients with coxa vara have greater value of the cortical area of femur than female and male patients with normal CCD angle and coxa valga (Fig. 5 and 6).

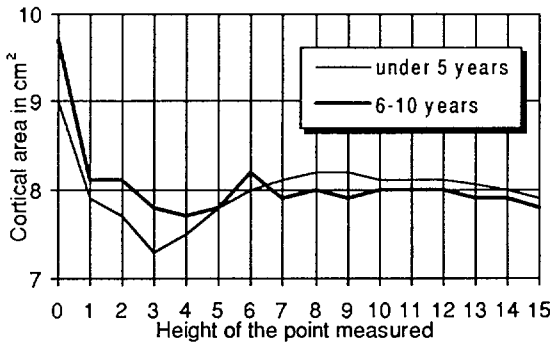

Fig 3. Cortical area of the shaft of the femur in female patients depending on sideways limping in the hip

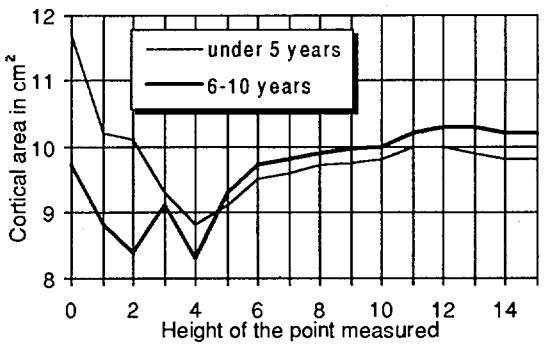

Fig 4. Cortical area of the shaft of the femur in male patients depending on sideways limping in the hip

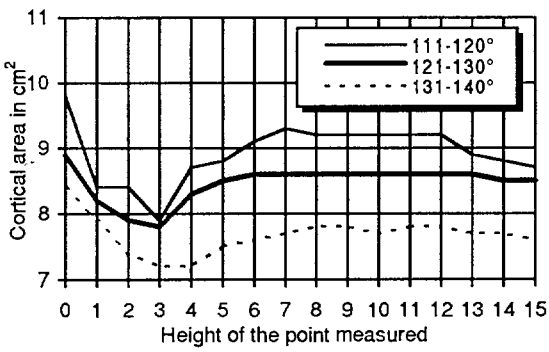

Fig 5. Cortical area of the shaft of the femur in female patients depending on size of CCD angle

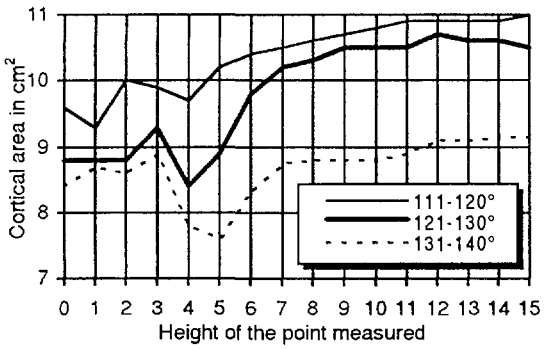

Fig 6. Cortical area of the shaft of the femur in male patients depending on size of CCD angle

DISCUSSION

The study of the cortical area of femur as a possible factor for estimating the functional adaptation of the bone suggests that the older female patients have greater value of this cortical parameter. In male patients, only in the region of proximal levels of measurement, the value of the cortical area increases with age. The studies of other authors show that in female and male examinees with normal load of the hip joint, the cortical area reaches maximum between 20 and 30 years of age, while it shoes a tendency of decrease as the age increases [19, 20]. Vrdoljak [21] observes that the cortical area of femur, measured 1 cm and 3 cm under the massive of trochanter minor, is the greatest in the period of stabilization of the skeleton, while it gradually decreases in the involutive age.

The female and male patients with longer sideways limping in hip have greater values of the cortical area of femur in the region of proximal levels of measurement. In the literature accessible to us we have not found studies of the relationship between the cortical area of femur and the length of sideways limping in hip.

Our study suggests that with the increase of the CCD angle, the value of the cortical area of femur decreases on separate levels of measurement, which is in accordance with the studies of Vrdoljak [21].

CONCLUSION

The studies of numerous authors [5-7, 11, 16, 19-21] undoubtedly suggest that the functional adaptation of the bone can be investigated using the method of morphometry, as well as many other methods [11, 12].

By the analysis of our own studies, we concluded that in the patients with coxarthrosis and sideways limping in hip, due to verticalization of the resulting force of load and increasing tensions, a functional adaptation of the proximal part of femur takes place, emerging as the increase of the value of cortical area on distinct levels of measurement.

Our studies are unquestionably in agreement with the studies up to the present and elementary foundations about the functional adaptation of the bone [9-12, 13-17].

Concluding our paper, we can add that cortical area can be used as one of the better, if not the best, parameters in studying the functional adaptation of the bone by a morphometrical method.

REFERENCES

[1] H. G. Amstutz. Total Hip Replacement. In: Surgery of the Hip Joint, R. G. Tronzo, ed. Lea and Febinger, Philadelphia, 1973.

[2] L. P. Astanin. O stroenii kisti gimnastov. Izv A P N RSFSR, 133-142, 1951.

[3] P. J. Atkinson, C. Woodhead. The Development of Osteoporosis, Clin Orthop, 217-228, 1973.

[4] E. Barnett, B. E. C. Nordin. The Radiological Diagnosis of Osteoporosis: a New Approach, Clin Radiol, 166-174, 1960.

[5] S. Jovanović. Morphological Changes of the Body of Femur in Patients with Changeable Conditions of Loading of the Hip Joint. Dissertation, Zagreb, 1986.

[6] S. Jovanović. An Influence of Verticalization of the Resulting Force of Weight-Bearing of the Hip Joint "R" on the Morphological Characteristics of the Medullar Canal of the Shaft of Femur in Patients with Coxarthrosis, Reumatizam, 2:7-11, 1992 .

[7] S. Jovanović, R. Nedeljković. "Standard Values" of Surfaces of Transversal Sections of the Medullar Canal of the Proximal Portion of the Shaft of Femur, Acta orthop Iugosl, 1:8-11, 1989.

[8] R. B. Martin, P. J. Atkinson. Age and Sex-Related Changes in Structure and Strength of the Human Femoral Shaft, J Biomech, 10:223-231, 1977.

[9] O. Muftić. About the Relationship Among the Rules of the Theory of Border Construction and the Structure of Biological Materials, Dissertation, Zagreb, 1972.

[10] V. Nikolić, V. Nutrizio, J. Hančević, B. Gjurić, H. Cerovec, D. Buković. The Possibility of Denzitometry of the Layer Pictures of Skeleton, Acta med iug, 26:107-120, 1972.

[11] V. Nikolić, B. Banović, J. Hančević, O. Muftić. Spectral Vibration Analysis of Certain Structures of the Proximal Portion of the Thigh Bone, JAZU, 336:123-136, 1973.

[12] V. Nikolić. The Possibility of Control of the Functional Adjustment of Skeleton to the Result of the Mechanical Forces in vivo, Folia anat iugosl, 3:113-124, 1974.
[13] D. Orlić. Etipatogenical Analysis of the Bone Apposition on the Medial Part of the Femur in Coxarthrosis, Dissertation, Zagreb, 1978.
[14] D. Orlić, I. Ruszkowsky. The Radiological Appearance of Appositional New Bone on the Medial Part of the Femur in Coxarthrosis, International Orthopaedics (SICOT), 16:7-11, 1983.
[15] F. Pauwels. The Meaning and Causal Explanation of Spongiaous Architecture in New Interpretation, Arztl Wschr, 3:379, 1948.
[16] M. Pećina. Fibula in Clinical and Experimental Check of the Theory of Functional Adjustment of the Bone, Habilitational Work, Zagreb, 1976.
[17] I. Ruszkowsky, et al. Biomechanical Investigation of the Functional Adaptation of the Skeleton in Normal and Changed Conditions, Final report of a scientific project, Zagreb, 1975.
[18] A. Stanström, L. I. Hansson, K. G. Thorngren. Cortical Bone Remodelling in Normal Rat, Calcif Tiss Res, 2323:161, 1977.
[19] D. P. Van Gerven. Thickness and Area Measurements as Parameters of Skeletal Involution of the Humerus, Femur and Tibia, J Geront, 28:40-45, 1973.
[20] P. Virtama, T. Helela. Radiographic Measurements of Cortical Bone, Acta Radiol Suppl, 293, 1969.
[21] J. Vrdoljak. Functional Adaptation of the Cortical Bone of the Proximal Part of Femur to the Special Load with Variations of the CCD angle, Master's thesis, Zagreb, 1979.

POSSIBILITY OF COMPUTERISED MEASUREMENTS AND GRAPHIC PRESENTATION OF GAIT PARAMETERS

Vladimir Hohnjec[1] , Dubravko Orlić[2] , Amir Dubravić[3] , Karol Skala[3] and Miroslav Gluhinić[1]
1. General Hospital "Holly Ghost", Zagreb
2. Departement of Orthopaedic Surgery School of Medicine Univeristy of Zagreb
3. Institut "Ruđer Bošković", Zagreb

Abstract

Our aim is to present the original method of computerised measurement and graphic presentation of number of parameters that are typical for normal walking and antalgic limping in the hip joint. The method was tested on 20 healthy persons, and 20 patients with one painful hip. The original graphs are presented.

MOGUĆNOST KOMPJUTERSKOG MJERENJA I GRAFIČKOG PRIKAZIVANJA NEKIH PARAMETARA HODA

Sažetak

U radu je opisana originalna metoda kompjuterskog mjerenja i grafičkog prikazivanja nekih parametara hoda koji su tipični za normalan hod i antalgično šepanje u kuku. Metoda je testirana na 20 zdravih ispitanika i na 20 bolesnika koji su se tužili na bol u jednom kuku. Prikazani su originalni grafički prikazi normalnog hoda i antalgičnog šepanja u kuku.

1. INTRODUCTION

Dynamic analysis of objective phenomena are being increasingly used in clinical practice, especially for objective assessment of patient with locomotor disorder (1,2,3). How to objectify the patients walking patterns is an issue of specific interest. The discussions may be found about the analysis of time parameters of walking, the load on the leg during walking, etc. They proved highly useful for the evaluation of medical or surgical therapy effects (4,5,6). Our method of computerised measurements and graphic presentations of number of gait parameters is easy for use. We choosed for the registratration the upper body tilting in the frontal plane during gait and support - swing time of the leg because these manifestations are typical and obvious in normal and pathological gait. Other external body expressions of gait are not included in the measurements. The measurements may be performed on hospital departments and do not need special kynesiologic laboratory. The gait graph we obtained is reproducible, reliable and suitable for analysis.

2.1. Patients And Method

A number of electronic devices linked to the central computer were used for data acquisition on upper trunk deflection from vertical body axis into frontal plane, and for registration of the support and swing phases of legs during walking. We have

designed a specific programme for acquisition, measurement, processing and graphic presentation of results in real time in the form of plotted graph of the gait. The data obtained on this basis are as follows: angles of bilateral trunk deflection expressed in degrees and the duration of the left and right foot support phase during walking, expressed in seconds. The method was tested on 20 healthy persons and on 20 patients with painful hip.

2.2. Measurement of trunk deflection

A dynamic electronic protractor-sensor which is situated in the rectangular box with output potential proportionate to the angle of trunk deflection was used for the measurement of trunk deflection angle in relation to the vertical body axis. The output voltage of the sensor is determined by following equation: $U(t) = \alpha(t) \times A$, where $U(t)$ is output voltage of the sensor, $\alpha(t)$ is sensor deflection angle, A is proportionality constant, t is time. Through channel selector the sensor is linked to the analog-digital converter (A/D converter) and to the computer. During the measurement the sensor is put on the patient's back and fastened by belts to the upper part of thoracic spine in the inter scapular space. It must remain steady in that position to avoid any significant shift during measurements.

2.3. Measurement of leg support duration

The duration of support phase of legs was measured by micro-switches implanted in the rubber soles of the shoes worn by the patient during measurements. Micro-switches (Polycontact, USA), are implanted in the heel and toe region for registering the heel and toe contact with the ground during walking. The moment of support of the foot is defined by the presence of the electrical potential in the switches. The voltage appears when the switches are in contact with the ground, while the voltage is absent when the foot is off the ground. These changes in voltage are registered by the computer and are plotted as hind foot and forefoot support curve in real time.

2.4. Data acquisition and processing software

The software starts the A/D converter with 12-bit resolution and selects the inputs in sequence through the channel selector. The data is stored in the PC-RAM. The result of data processing is the trunk deflection curve and curves showing the support of the foot, presented simultaneously in real time. The ordinate of the graph represents the trunk deflection angles in degrees, and the abscissa represents the time axis. The programme defines duration of the measurement up to 120 seconds, allowing for maximal deflection to be 45° to both sides. During the measurement, the patient walks on a flat floor and after the measurement time is off, programme plots the curves which may be saved on disk. The trunk deflection curve is sinusoid like. The curve of micro-switches has to levels: "0" and "1". Level "1" shows the presence of voltage in the micro-switches when the switch is in contact with the ground. Figure 1 represents the block diagram of the equipment.

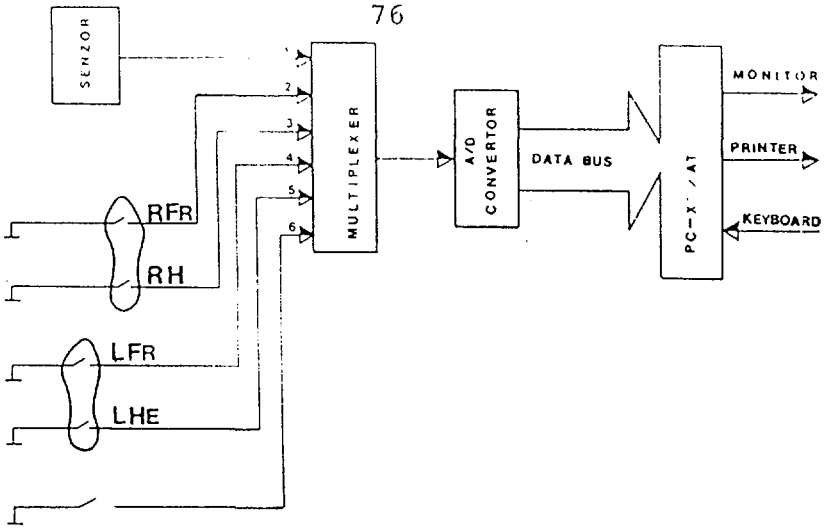

Fig.1. 1. Sensor-electrodynamic protractor connected to computer via multiplexer and A/D converter. 2. Microswitch-right forefoot (RFR). 3. Microswitch-right hind foot (RH). 4. Microswitch left forefoot (LFR). 5. Microswitch left hind foot (LHE).

Figure 2 represents the typical "gait curve" recorded during gait of healthy person.

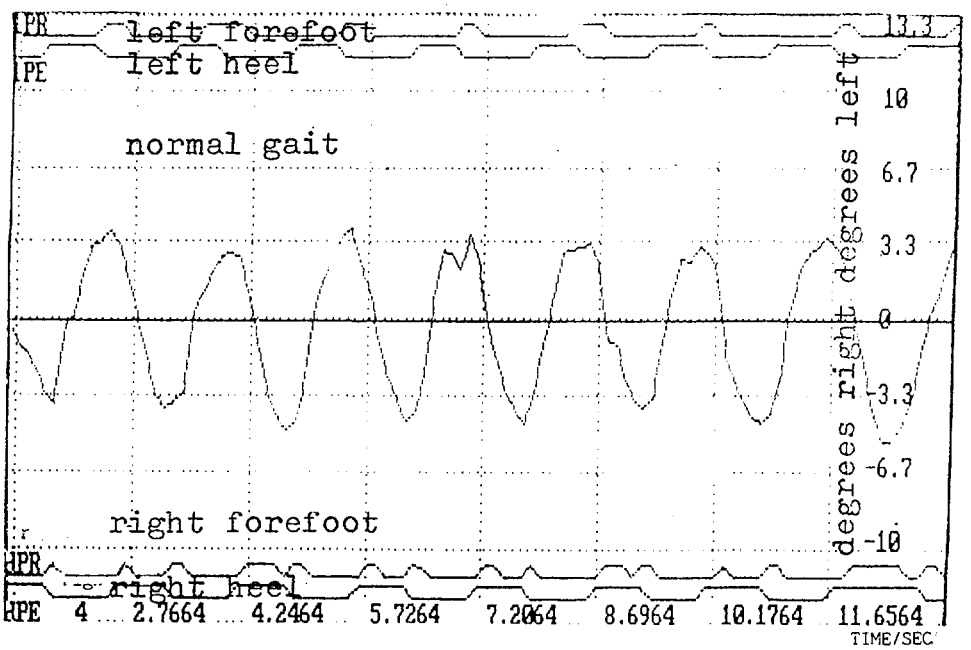

Fig. 2. Figure 2 represents the graph recorded during gait of healthy person. The trunk deflection curve is sinusoid like and is in mid portion of the graph. Declination to the left is above the abscissa, declination to the right is below the abscissa. The measurement scale in degrees is located on the ordinate of the graph. The left foot support (LFS) curves are settled on the top of the graph. Upper curve represents the left forefoot micro-switch action (LPR). The bottom curve represents the left hind foot microswitch action (LPE). The right foot support curve (RFS) curves are settled on the bottom of the graph. The upper curve represents right forefoot micro-switch action (DPR). The bottom curve represents the right heel micro-switch action (DPE). The time axis is the abscissa. Analysis of this graph shows the left foot support (LFS) of 0.86 s, and the right foot support (RFS) of 0.88s. The trunk declination from vertical body axis to the left was 3.6°, and to the right side 4.2°. T statistics of obtained data shows no significant differences between the body tilting to the left and the right side, and between the support time of the left and right foot.

Figure 3 represents the typical "antalgic gait" curve recorded during the gait of the patient with painful hip (fig.3).

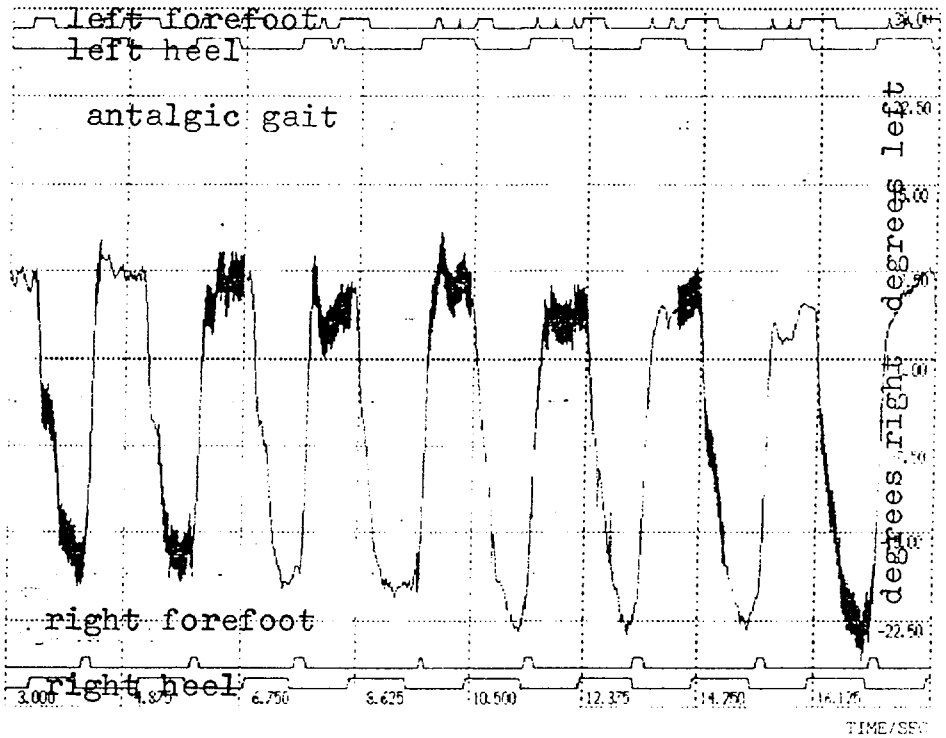

Fig. 3. A typical antalgic gait curve recorded in the patient with severe pain in the right hip. The left foot support (LFS) is 1.21 s, and right foot support (RFS) is 1.12 s. Deflection of upper trunk to the left (DUTL) is 7°, and to the right side from vertical body axis (DUTR) is 22°. The right foot support (RFS) is obviously shorter, and deflection of upper trunk (DUTR) to the right is increased regarding to the left side. These differences are statistically significant ($P < 0.001$).

3. CONCLUSION

The presented method enable us the acquisition, measurement, processing and graphic presentation of some gait parameters which are of interest in medical specialities concerning with locomotion system. The obtained graphs are reproducible, reliable and suitable for further analysis. The obtained data are in accordance with the results of the other authors (1,2,3), butour results are obtained from the "gait graph" which is not presented in this form until now.

4. REFERENCE

[1] Murray M.P., Gore D.R., Clarkson B.H.: Walking patterns of patients with unilateral hip pain due to osteo arthritis and a vascular necrosis. J. Bone Joint Surg, 53-A(2):259-74, 1975.

[2] Murray M.P., Gore D.R., Sepic S.B. et al.: Antalgic manoeuvres during walking in man with unilateral knee disability. Clin Orthop, 199:192-200, 1985.

[3] Murray M.P., Drought A.B., Kory R.C.: Walking pattern of normal men. J Bone Joint Surg, 46-A(2):335-60, 1964.

[4] Demottaz J.D., Mazur J.M., Thomas W.H. et al.: Clinical study of total ankle replacement with gait analysis. J Bone Joint Surg, A(7):976-88, 1979.

[5] Berman A.T., Zarro V.J., Bosacco S.J.: Quantitative gait analysis after unilateral or bilateral total knee re-

placement. J Bone Joint Surg, 69-A(9):1340 -45, 1987.

[6] Simon S.R., Trieshmann H.W., Burdett R.G. et al. Quantitative Gait Analysis after total knee Arthroplasty for Monarticular Degenerative Arthritis. J Bone Joint Surg, 65-A(5): 605-13,

[7] Hohnjec V. Biomechanical Analysis of antalgic limping in the hip joint as possibilities of impartial evaluation of pain in the hip joint. Master Thesis. Medical Faculty,University of Zagreb, 1989.

THE RUNNING SHOE AS A SHOCK ABSORBER

Ante Agic
Faculty of Chemical Engineering and Technology
41000 Zagreb, CROATIA

Abstract

Many injures in running are related to insufficient shock-absorption properties of the shoes. A critical test for shoes is how well they absorb the shock and transmit the force through the body. Recently , improved sole design in running shoes have considerably reduced shock, through the use of modern foam materials with air-pump system developed to act ás shock absorbers. It was found that the damping characteristics of the foot- ground interaction play the key role in reduction of the incoming shock waves . The quality of a shock isolation in the shoe is usually described by a dimensionless parameters curve as efficiency of energy return , shock spectra and transmissibility matrix properties. In this paper, a mathematical model for running is presented with biomechanical experiment validation. Dynamic analyses of normal walking are performed by measuring foot pressure distributions. This method of analysis provides a powerful tool for the future design of footwear.

Introduction

In the design of sports shoes and their components in general, and particularly in the design of running and walking shoes, it is necessary to consider biomechanical criteria for the protection of the runner against injury while at same time improving his or her performance. A series of experimental results are given from many investigators [1], in order to predict important phenomena in the mechanics of running without rigorous theoretical explanations. Furthermore, today technology allows footwear designers to chose materials that offer not only the right combinations of energy return, permeability and durability for demanding physical protection applications, bat also the necessary comfort and elegance.
The aim of this study was to develop a mathematical tool which could explain the shock isolation phenomena in athletic shoes.

The model

Hundreds of times a day, with every step we take, we crash down upon our heel with a force that often reaches several times our total weight. The shoe sustains these impacts and reduces potential injury to the body by deforming upon striking the ground. Modern running shoe incorporate a cushioned midsole to protect the foot from potentially injurious impact with the ground. The main function of the cushioning system is to attenuate the shock of impact and reduce magnitude of localised pressure peaks by distributing forces over a larger plantar surface. The study of the ground reaction forces and foot pressure distributions during running is important beyond providing insight into the basic mechanism of running [1]. The dynamic pressure distribution measurements under the human foot provide valuable information for the treatment of foot deformities and for the construction of shoes. The pressure distribution levels are usually translated into colore values (Figure 1).
The plantar pressure distribution recorded using an EMED system. The system incorporates a 64x32 matrix of piezo-capacitive pressure transducers mounted on mat a with a sensor density of 2 cm^2. The output of each transducer element is single force-time curve.

The example curve presented by Figure 2. is characterised an initial peak (first contact) followed by a large peak (flexing motion). This clearly demonstrates that the criteria applicable to the shoe structure in the region of the heel are not valid for the ball of the foot.

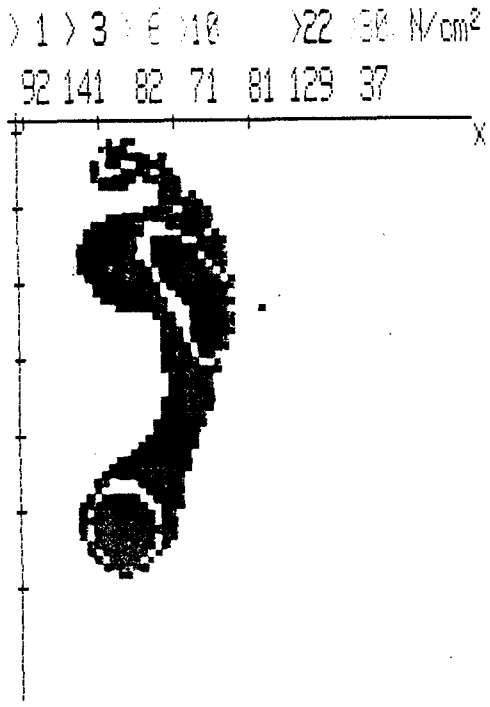

Figure 1. The contact human foot-ground pressure distribution levels

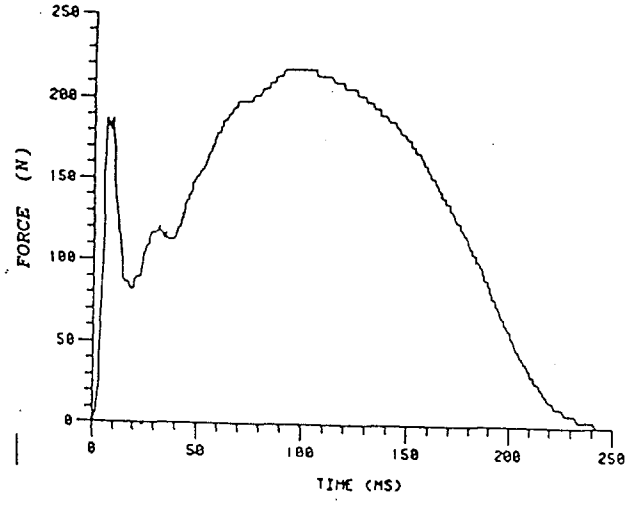

Figure 2. Typical force-time distribution

The idealized shock isolation system is considered to be comprised of a rigid mass (human body) supported on a rigid foundation by a single isolator (athletic shoe) undergoing unidirectional dynamic motion (Figure 3). Shock excitation is defined in terms of the sudden variation of the displacement imposed upon a foundation. Linear stiffness element in parallel with a pneumatic damping element is used to characterize the isolator.

The differential equation of motion of the mass is

$$m\overset{oc}{x} + cx = cx_p + (p_2 - p_1)A$$

where $\overset{o}{()} = d/dt$

m - mass of mounted body

c - stiffness of isolator

p_1 and p_2 are air pressures on either side of the piston

A - the piston area

The additional equations are equations of state and conservation of masses in the piston, respectively

$$m_i R \vartheta_i = p_i V_i$$

$$\sum \frac{dm_i}{dt} = 0 \qquad (2)$$

The subscript i = 1,2 refers to the two sides of the piston which is model for air bag system with transmission channel. In equation (2) m_i is mass, V_i is volume , ϑ_i is temperature, p_i is pressure of the air and R is gas constant. The operation of the pneumatic damper is analyzed by assuming an adiabatic process (n = 1.4). The mass flow rate through an orifice is given by

$$\frac{dm}{dt} = C_o\, p\, \sqrt{\vartheta} \qquad (3)$$

where C_o is constant.

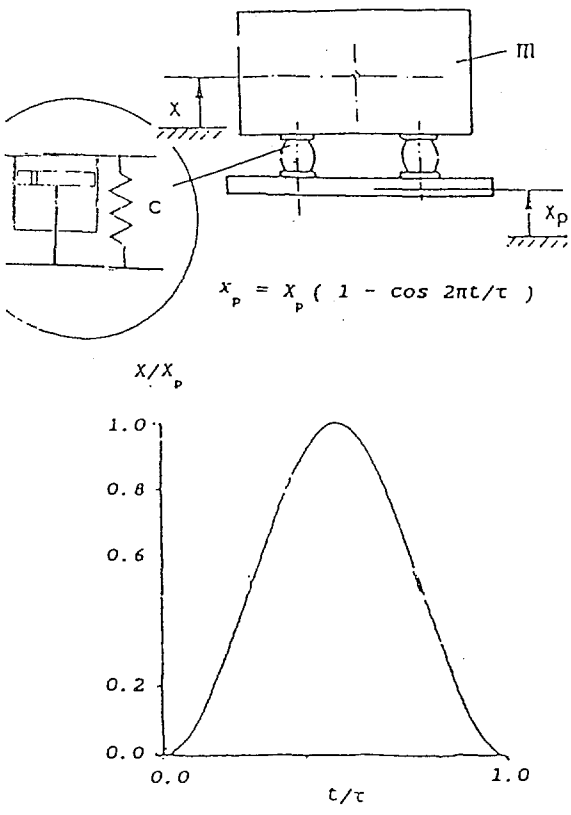

Figure 3. The shock isolation system

The equations have been integrated by using the 4-th order Runge-Kutta scheme. The solution of the equation gives the motion of the mounted body x= x(t) . The performance characteristic of shock isolation systems are described by two dimensionless response matrix , the shock transmissibility T and shock amplification matrix H as described in literature [2]. The residual shock amplification curves for displacements and accelerations for isolation system in terms of the relative values of the shock pulse time duration τ and the isolation system natural period T is presented on Figures 4 and 5 respectively. For the purpose of this investigation the ground displacement is given in cosine pulse form.

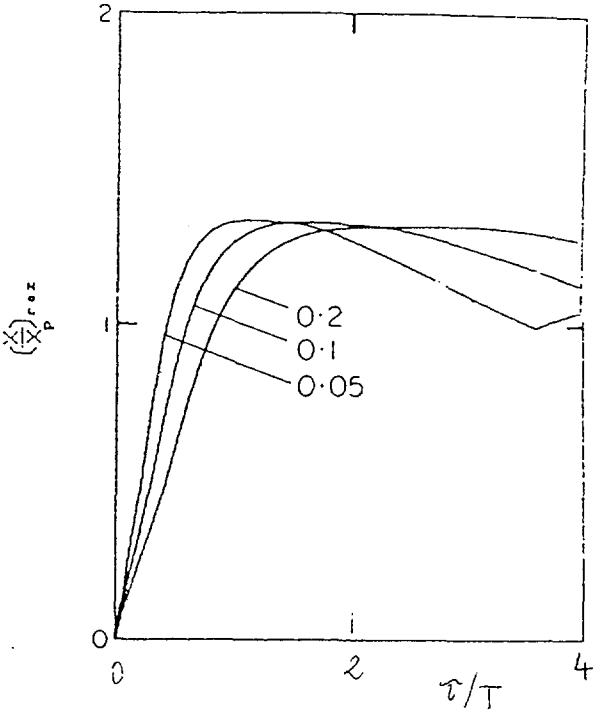

Figure 4. Residual shock displacement curve

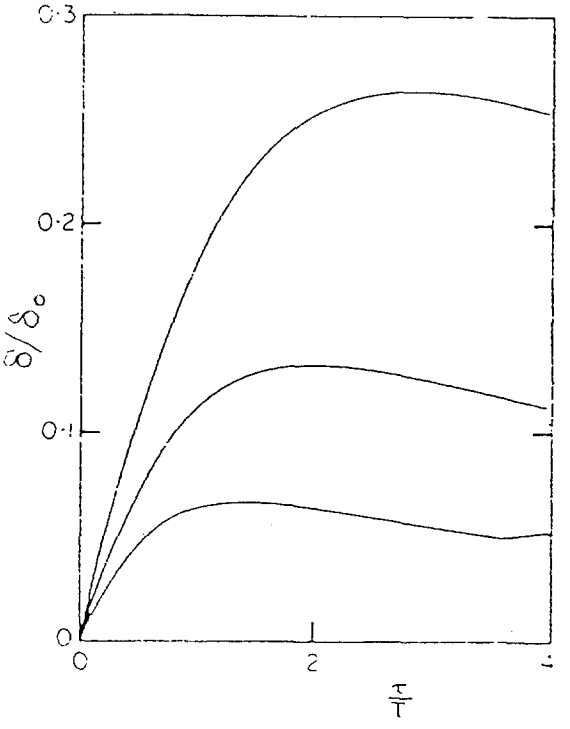

Figure 5. Residual shock relative displacement curve

Conclusions

A mathematical model for shock-absorption phenomena in athletic shoes is presented. To validate the results of the paper in general, the model is formulated in terms of dimensionless variables. This renders the results obtained to be more general than would otherwise be the case.The theoretical study correct many inadequate generalizations based upon the results of the experiments and statistical analysis.

References

1. Shorten, M.R.: The Energetics of Running and Running Shoes, J. Biomechanics, 26: Suppl. 1, 41-51, 1993
2. Harris, C.M., Crede, C.E.,(eds.): The Shock and Vibration Handbook, McGraw-Hill, New York, 1961.
3. Hundal, M.S.: Passive Pneumatic Shock Isolator: Analysis and Design, J. of Sound and Vibration. 84:1-9,1982

3-D Brain Image Registration using Optimal Morphological Processing

Sven Lončarić and Atam P. Dhawan†

Faculty of Electrical Engineering
University of Zagreb, 41000 Zagreb, Croatia

†Department of Electrical and Computer Engineering
University of Cincinnati, Cincinnati, OH 45221-0030, USA

Abstract

The three-dimensional (3-D) registration of Magnetic Resonance (MR) and Positron Emission Tomographic (PET) images of the brain is important for analysis of the human brain and its diseases. A procedure for optimization of (3-D) morphological structuring elements, based on a genetic algorithm, is presented in the paper. The registration of the MR and PET brain images is done by means of a registration procedure in two major phases. In the first phase, the Iterative Principal Axis Transform (IPAR) is used for initial registration. In the second phase, the optimal shape description method based on the Morphological Signature Transform (MST) is used for final registration. The morphological processing is used to improve the accuracy of the basic IPAR method. The brain ventricle is used as a landmark for MST registration. A near-optimal structuring element obtained by means of a genetic algorithm is used in MST to describe the shape of the ventricle. The method has been tested on a set of brain images demonstrating the feasibility of approach.

1 INTRODUCTION

The multi-modality medical imaging has become important tool for analysis of various human organs. In the case of human brain imaging, a combination of MR and PET modalities provides a powerful diagnostic tool. MR imaging modality provides information about the anatomical structure of the brain while PET imaging modality detects the metabolic activity of the brain. In order to utilize both sources of information it is necessary to correlate independently acquired MR and PET brain images. Several approaches for registration of MR and PET have been investigated and presented in literature such as techniques based on the use of stereotactic frames or external markers [1], anatomic landmarks [2], and surface or volume matching [3]. An accurate and practical volume-based registration method has been developed by Arata et al. [4]. It is called Iterative Principal Axis Registration (IPAR). In this method a principal axis transform of MR and PET binary volumes is used to align the volumes. An improvement to the IPAR method has been developed by Lončarić and Dhawan [5]. It uses 3-D morphological processing of brain ventricles for an improved registration. The ventricle shape is described by means of the Morphological Signature Transform (MST) based method for shape description [6, 7].

In this paper, we present a solution to the problem of selection of 3-D structuring element for MST shape description. The procedure is based on a method for optimization of 2-D structuring elements [8, 9, 10]. The optimization method employs a genetic algorithm to select a shape of a near-optimal 3-D structuring element (SE) for MST-based morphological processing.

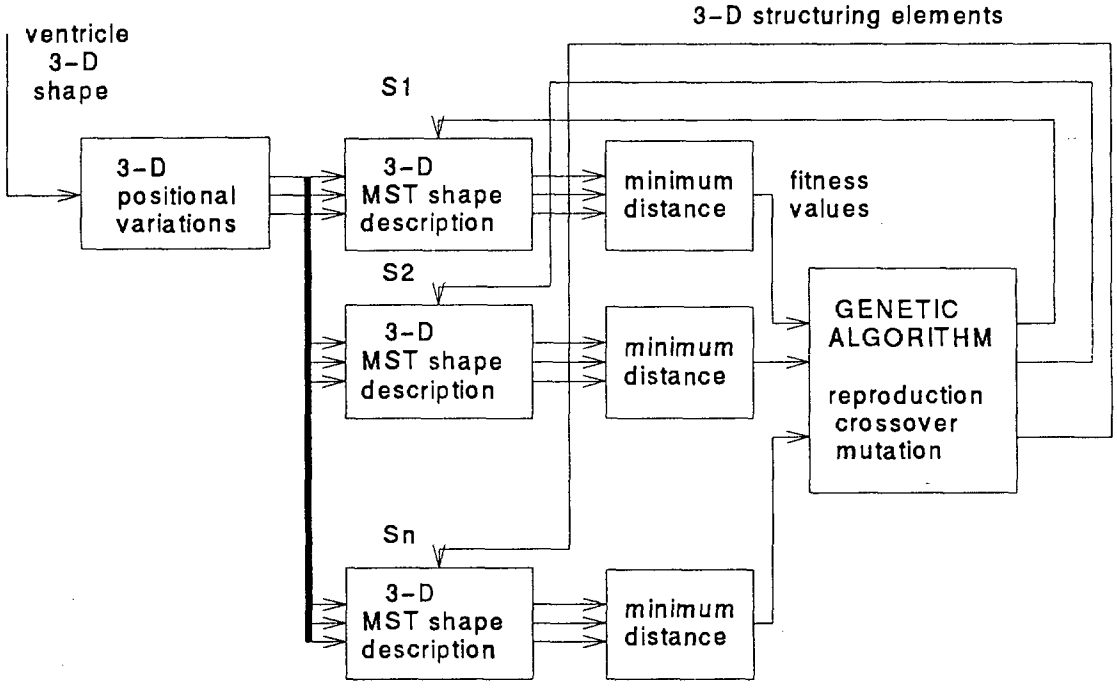

Figure 1: Block-diagram representation of the 3-D GA optimization procedure.

2 METHODS

2.1 Preprocessing and Segmentation

Due to a varying brightness of the brain scan films it is necessary to do a preprocessing of images so that variability is eliminated. Subsequent image processing algorithms are then confronted with an easier task. A preprocessing of the MR and PET images consists of several steps. The first step is a normalization of the image brightness which is based on the K-means clustering algorithm [11]. This step brings image background, brain skull, and brain tissue brightness into a pre-defined range so that all analyzed images have the same characteristics. The MR and PET images are interpolated in the second step to provide cubic voxels which are necessary for subsequent steps in image analysis.

A segmentation of the preprocessed gray-scale MR and PET images is performed for two purposes. First, the segmentation of the brain volume is performed for the needs of the volume-based IPAR method. Second, the segmentation of the brain ventricle is performed to provide the additional reference volume for the MST-based registration. The brain and the ventricle are segmented automatically by means of thresholding and 2-D and 3-D morphological postprocessing. The segmentation result is corrected manually, if necessary, by an expert neuroradiologist.

2.2 A Genetic Algorithm for Optimal MST Registration

The MST-based shape description method can be applied to both two and three-dimensional shapes. In this paper, MST method is applied to three-dimensional shapes. The MST method is based on successive morphological processing of a binary shape by a binary SE. Volumes of successively processed shapes are used to form a shape descriptor vector. The problem associated with many morphological methods is the problem of the selection of the SE which provides the optimal processing. Here, we propose the use of genetic algorithm (GA) for optimization of the 3-D SE shape. Every GA must include a criteria for elimination of non-efficient (non-optimal) candidates for the optimal solution. In this work, the GA optimization criteria

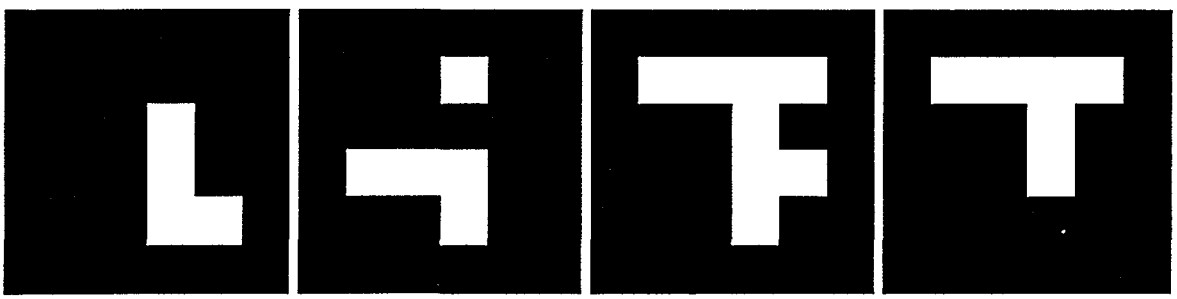

Figure 2: The four planes of a near-optimal 3-D binary structuring element obtained by means of GA. The SE size is $4 \times 4 \times 4$.

is designed to enable the best discrimination between fine 3-D positional variations of the ventricle shape. This discrimination is required by MST method for registration. The conventional reproduction, crossover, and mutation GA procedures are here extended to 3-D optimization space. A variable crossover rate controlled by the population entropy and 3-D chromosomes are used in the GA. The block-diagram of the 3-D genetic algorithm optimization procedure is represented in Figure 1. The input ventricle shapes in Figure 1 are produced from a single ventricle by means of fine 3-D rotations of the original 3-D shape. This is required because the 3-D SE which best discriminates between fine positional variations of the single (original) 3-D shape has to be determined. The resulting SE is called the *optimal* SE. It actually is just a near-optimal solution because of the nature of genetic algorithms which cannot guarantee that the optimal solution is reached. However, in practise it is often satisfactory to know a near-optimal solution to the problem.

3 EXPERIMENTAL RESULTS

3.1 Genetic Algorithm

In SE optimization experiment, the structuring element size is set to $4 \times 4 \times 4$. The optimization procedure is conducted using the GA-based procedure shown in Figure 1. The four planes of a near-optimal 3-D SE, obtained by means of GA, are shown in Figure 2. The resulting SE is near-optimal in the sense that fine positional variations of the brain ventricle are best discriminated when this particular SE is used in MST shape description procedure. This provides precise registration of the MR and PET brain volumes.

3.2 Brain Registration

A set of IPAR and optimal MST matched images is shown in Figure 3. For a better graphical presentation to a user, a pseudocolored image is produced for each pair of registered MR and PET slices. The produced color images have the brightness determined by the intensity of MR gray images and the color determined by the brightness of PET gray images. Such a pseudocolored image is a convenient way of combining the anatomical information provided by MR imaging modality and metabolical information provided by PET imaging modality.

4 CONCLUSION

Brain ventricles are used as an additional reference for brain registration. This registration method uses a combined IPAR-MST approach. A genetic algorithm for selection of a near-optimal 3-D structuring element is presented in the paper. A near-optimal structuring element provides better discrimination of the ventricle shape using the MST shape description method. The discrimination property is critical for description of fine positional variations of the brain ventricle. Experimental results demonstrate feasibility of the genetic algorithm based method for structuring element optimization and its successful application to the registration of medical images.

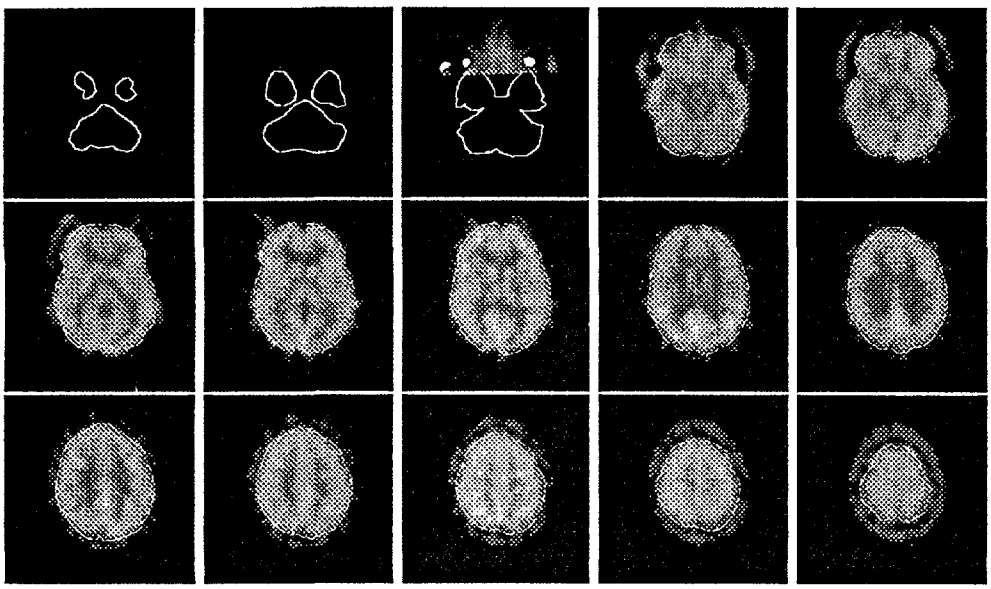

Figure 3: IPAR/MST registered PET images. MR brain contours are superimposed on PET brain image.

References

[1] M.Bergstrom and et al. Head fixation device for reproducible position alignment in transmission ct and positron emmision tomography. *Journal of Computer Assisted Tomography*, 5:136–141, 1981.

[2] A.C.Evans and et al. Mri-pet correlation in three dimensions using a volume-of-interest (voi) atlas. *Journal of Cerebral Blood Flow and Metabolism*, 11:A69–A78, 1991.

[3] C.A.Pelizzari and et al. Accurate three-dimensional registration of ct, pet, and/or mr images of the brain. *Journal of Computer Assisted Tomography*, 13:20–26, 1989.

[4] L.K.Arata and A.P.Dhawan. Iterative principal axes registration: A new algorithm for retrospective correlation of mr-pet brain images. In *Proceedings of IEEE EMBS Conference*, 1992.

[5] S. Loncaric and A. Dhawan. 3-d brain image registration using morphological processing and iterative principal axis transform. In *Proceedings of the 15th Annual International Conference of IEEE Engineering in Medicine and Biology Society*, 1993.

[6] S. Loncaric and A. Dhawan. A morphological signature transform for shape description. *Pattern Recognition*, 26:1029–1037, 1993.

[7] S. Loncaric and A. Dhawan. A morphological residue approach to shape representation. In *SPIE Proceedings 1658: Nonlinear Image Processing III*, 1992.

[8] S.Loncaric and A.P.Dhawan. Optimal mst-based shape description using genetic algorithm. *Pattern Recognition*, accepted for publication, 1994.

[9] S. Loncaric. *Morphological Signature Transform for Shape Representation and Matching.* PhD thesis, University of Cincinnati, 1994.

[10] S. Loncaric and A. Dhawan. Optimal shape description using morphological signature transform v ia genetic algorithm. In *SPIE Proceedings 2030: Image Algebra and Morphological Image Pr ocessing IV*, 1993.

[11] S.Loncaric and A.P.Dhawan. 3-d image analysis of intracerebral brain hemorrhage. *Computer Methods and Programs in Biomedicine*, submitted for publication, 1994.

DIGITAL 3D MOIRÉ - TOPOGRAPHY

Gerhard Windischbauer and Hermann Neugebauer
Institut f. Med. Physik, Vet.Med. Universität Wien, 1030 Linke Bahngasse 11, Austria

Summary

In the last decade moiré-techniques were proved to be efficient means for the detection of back shape deformities of the human trunk. Methodical improvements include a PC-based digital real time measuring system for data-application and image-processing.

A new developed frame-grabber is used for digitizing the video-signals sent by a video-camera. Two memory-banks are used for storing the images and for combining them in real time. Image-processing algorithms can be applied on the individual and on the combined image-functions. Pattern classification will be supported by neural networks. An electronic pin-board is used for cutting the images and for extracting essential details. A dBase-compatible image-database is used for entering and storing patient data together with compressed images. Thus up to 30 moiré-topograms can be exported to a single floppy disk for subsequent analysis by an orthopedic specialist.

1. MOIRÉ SCREENING STUDIES

In 1985 the authors performed a pilot study in Vienna screening 3256 school children aged between 9 and 16 years on scoliosis [1]. The first check was done by moiré photography, the second by physical examination and the third by low-dose X-raying but only for a preselected group with "very suspect" findings. 38,1% of the children had normal back shapes, 13,4% showed distinct humpbacks, 5,6% had flatbacks and 7% of them had a scoliosis with a Cobb angle of 5° or more. Only 5,3% of the moiré-findings were "false positive" thus agreeing very well with the results of other international studies.

The Viennese study was based on a screening program on scoliosis which was started by the Chiba University Medical School in Japan in 1979 using moiré topography, low dose X-raying and a final X-ray examination. Till 1986 the number of children was 1.246.789. The incidence of scoliosis of more than 15° increased linearily with age from the fifth grade primary school (0,07% boys, 0,44% girls) to the second grade high school students (0,25 % male, 1,77% female). The female predominance of scoliosis cases with curvatures more than 20° detected during the total period was10:1 and it was the same for primary school children und junior high school students.

The incidence of scoliosis of more than 20° decreased significantly every year among junior high school student, because they were screened periodically in school. This study shows that screening for scoliosis is cost-effective with a low risk of radiation hazard [2].

2. COST-EFFECTIVENESS

In 1990 Stig Willner presented a survey on diagnosis and treatment of structural scoliosis. In spite of the fact that much of genesis and development remains unknown today, there are available current methods of an effective treatment. But an imperative demand would be a diagnosis as early as possible, because the development of scoliosis can be prevented chiefly by an easy to use treatment like bracing during the growth period. Surgery should be indicated only in complicated cases [3]. Three different screening methods were analysed with respect to their cost-effectiveness: no specific screening, the conventional clinical screening and the combined clinical moiré screening [4]. Data from retrospective studies in Malmo were used. The costs for health care and production loss were calculated and applied to the time profiles of the

three screening alternatives. Health care costs as well as costs in loss of production increased with the introduction of the conventional clinical screening program. However, when the clinical screening was combined with the moire technique, the costs were markedly reduced. Thus, the combined clinical moire screening would be the cost-effective way of using resources to prevent scoliosis from developing into a more severe deformity.

In 1992 Austrian orthopedists tried to catch the attention of the politicians once more by pointing out, that an increasing number of Austrian people is suffering from disturbances of the spine, a process, which is lasting for years and is steadily summing up little defects to continual complaints. Children at the age of six years are forced to sit still for some hours every day. Watching TV as the prevalent leisure time organization is prolonging these periods without exercise. School sport cannot compensate anymore. More than 15 % of the children attending the first school year are showing signs of posture weakness [5]. Thus the early diagnosis of posture defects is gaining great importance. Considering the national health care expenses caused by early disability of persons suffering from changes in the shape of the spine, the economial importance of an effective posture screening can be recognized without difficulty. At least twice the journal of the Austrian medical association tried to catch the attention by placing a coloured moiré topogram on the cover page [6,7].

3. DIGITAL SCREENING SYSTEM

The planning of a large scale check-up like a school screening for posture weakness and defects ordered by government and assisted by instruments has to consider not only the qualities of the method (non-invasive and no exposition to ionizing radiation, sensitivity and effectiveness), but also to etimate the accumulating expenditures. Substantial factors are the mobility of the screening device, the examination time per child and the training level of the staff as well as the expenditures for material and the ease of documentation exchange.

After having used moiré-topographical devices in scoliosis screening for many years, the authors tried to install a new technological basis once more. For an introduction to moiré-topographical methods see [8]. The intention was to develop a system for acquisition and processing three-dimensional structures. Methodical improvements include realtime measuring, which can be used for conventional moiré-topographical work as well as for projection methods for stationary, time varying or moving objects.

3.1 PC-basis

The new system is based on an IBM-compatible personal computer (PC 486/33MHz) equipped with a specially designed framegrabber (HW-Elektronik, Wien). A standard video-camera (480.000 pixels) or a still-camera is used as image source. The framegrabber digitizes the RGB video-signal in realtime and stores it in one of two 2Mbyte memory-banks. During operation it is possible to superpose the image-content of one memory-bank onto the digitized image and to store it in the second one. The superposition is done by a 3x3 matrix calculating device in real time. Images can be added, subtracted or multiplied on a pixel by pixel basis.

3.2 Modi of operation

Thus the system offers three modi of operation. In modus one it acts as a conventional image-digitizing device, transferring the incoming videosignal to the harddisk of the computer and reading stored images into the videobuffer for RGB video-output. This modus is used for grating-shadow moiré-topography, for slide to memory conversions and subsequent image-processing.

In modus two the content of the second image-memory is superposed continuously onto the incoming image. If the object carries any kind of structured illumination, and if the image of the undisturbed structure is superposed as reference image, the video screen will show moiré-figures on the objetc's surface, which are moving with its movements. In modus two projection-type moiré-topography is realized in real-time. In modus three the object is illuminated with conventional light without any structure. The objects view at a given moment is stored as refence and is continously digitally subtracted from the incoming signal. Modus three produces a difference image of the present state of the three-dimensional structure and its stored past. Thus a difference pattern due to the breathing movement of a thorax may be observed on the video-diplay.

3.3 Software-features

The software is menu-driven. All the subroutines are written in computer language C++. Having started an application the program checks the status of all peripheral devices and clears all image memories. The operator watches the digitized image on a multisync-monitor in video-mode, while the menu of operations is displayed on the second computer monitor. He can freeze the video-image, cut a region of interest by a "rubber-band" and stick it on an electronic

pinboard on the video-screen. The patient data are listed at the right side of the pinboard. The operator can enlarge parts of the image or stick a second one on it. Having prepared all pictorial information the image with a size of 800 kbytes is transferred to the harddisk of the computer. Parallel to the the multisync video-display a RGB video-printer is connected for hardcopies of the images and patient data.

The patient data are stored in a dBase-compatible database together with all pointers for assigning the stored images. For exporting the patient data and the digitized images a JPEG compression algorithm is used. The compressed images have a size of 30 to 40 kbytes, thus up to 30 images can be stored on a single 3,5" high density disk. To study the images of a disk every computer graphicprogram, preparing only the standard JPEG decompression algorithm, can be used. Therefore the exchange of documentation is very simple. Read the patient data out with a simple dBase-programm and decompress the stored images with a standard program on a standard PC.

4. OUTLOOK

At present the digital moiré system is used for screening purpose. Image-processing algorithms are being developed for filtering the structured illumination and for enhancing contrast and sharpeness of the fringes. The thinned and binarized contourlines are fed to a neural network simulator. First experiments showed, that simple networks will be able to process moiré-patterns. Thus the development, which started in 1980, when for the first time orthopedists and scientists were discussing the interpretation of moiré figures of the human back , may come to an end.

5. REFERENCES

[1] H. Neugebauer, G. Windischbauer, School screening: a new pilot study in Vienna. In: I.A.F. Stokes, J.R. Pekelsky, M.S. Moreland (Ed.), Surface Topography and Spinal Deformity. pp. 177-186. ISBN 3-437-11180-9. G. Fischer Verlag, Stuttgart, 1987.

[2] Y. Ohtsuka, M. Yamagata, S. Arai, H. Kitahara and S. Minami, School screening for scoliosis by the Chiba University Medical School screening program. Results of 1,24 million students over an 8-year period. Spine , pp.1251-1257 Nov. 13 (11) 1983.

[3] S. Willner, Skoliosis - en oversikt. (Scoliosis - A Review). Nord.Med., pp.82-85, 105 (3) 1990.

[4] F. Montgomery, U. Person, G. Benoni, S. Willner and B. Lindgren, Screening for Scoliosis. A Cost - Effectiveness Analysis. Spine, pp.67-70, Feb. 15 (2) 1990.

[5] Eva Egger, Schulärzte sind besorgt: Haltungsschäden bei Kindern. Österreichische Ärztezeitung, pp. 30 - 32, 19 1992.

[6] H. Neugebauer, G. Keck und G. Windischbauer, Die Moiré-topographische Dokumentation der Wirbelsäule und des Rückens. Österreichische Ärztezeitung front cover and p.1, (12) 1978.

[7] Editorial, Marterpfahl Wirbelsäule. Österreichische Ärztezeitung front cover, (11) 1991.

[8] H. Neugebauer, G.Windischbauer (Ed.), Surface Topography and Body Deformity. ISBN 3-437-11242-2. G- Fischer Verlag, Stuttgart (1990).

MULTICHANNEL BIOMAGNETIC SYSTEM FOR THE USE IN CLINICAL ENVIRONMENT

Dietmar Drung[1], Gert Lindner[1], Hans-Juergen Scheer[1], Allard Schnabel[1], Detlef Stollfuss[1] and Zvonko Trontelj[2,1]
[1]Physikalisch-Technische Bundesanstalt, Institut Berlin, Abbestr 2-12, D-10587 Berlin, Germany
[2]Physics Department and Institute of Mathematics, Physics and Mechanics,University of Ljubljana, Jadranska 19, 61000 Ljubljana, Slovenia

Summary

The present generation of biomagnetic measuring systems are of multisensor configurationm with the ability od fast data acqusition and analysis. The system which will be described here has sensors distributed in 3 parallel planes and allows a realization of an electronic first or second order gradiometric configuration. 83 dc-SQUIDs are included in the multisensor multichannel system and provide the information on the vertical (B_z) and horizontal (B_x and B_y) biomagnetic field components. The system is installed within the standard magnetically shielded room at the University hospital "Benjamin Franklin" der FU Berlin in Steglitz. This system is modularly constructed (11 dc-SQUIDs within each module) and it achieves 2.5 $fT/\sqrt{Hz}$ average white noise in the first order gradiometric configuration. Incorporated in the measuring system is also a visualising system, based on the transputer technology, providing continously all necessary data on the measurements, status of vital parts of the system and necessary warnings. Results of first clinical test measurements confirm our expectations.

1 INTRODUCTION

The biomagnetic measuring systems are entering after about 20 years of research work the clinical environment and are almost ready for the routine diagnostic work with stationary patients. The present, i.e. the youngest generation of biomagnetic measuring systems are of multisensor configuration and are able to collect all necessary data and analyse them in clinically accepteble time. Two types of sensor distributions in the dewar vessel (SQUID sensors have to be at 4K - immersed in liquid helium) are common: a) spherical distribution within the whole head dewar, intended for the brain studies, developed and made by the BTI - San Diego, Neuromag - Helsinki, CTF - Vancouver and b) the distribution within the horizontal plane in a flat bottom dewar, developed and made by Siemens - Erlangen and PTB - Berlin.

At the PTB, Institute Berlin the magnetocardiography - MCG and the study of peripheral nerve system have a longer tradition and therefore a flat bottom dewars with sensors positioned in a plane have been primarily used. The first PTB multichannel system [1] consists of 37 channels and has been completed in 1990. This system is installed within the Berlin magnetically shielded room (BMSR) [2] and is still in use. However, at the institute one cannot study stationary patients and since it is clear that the biomagnetic measuring and diagnostic technique will expand only if and when it will find a way to university hospitals, the PTB has organized a laboratory within the university hospital "Klinikum Benjamin Franklin der FU Berlin" in Steglitz. This laboratory will provide a place for the biomagnetic measuring facility at the clinical level, as well as a place where one could introduce new measuring and diagnostic instruments which appear very rapidly in the

field of medicine.

2 METHOD

The biomagnetic measuring system for the PTB clinical laboratory is an improved version of the 37 channel system [1]. Briefly, the improvements include:

a) The modular design and construction of sensor arrangement

The whole system consists of seven modules. Within each module are 11 selected dc-SQUID magnetometers (Fig.1) of highest quality, reaching in the first order gradiometer configuration 2.5 fT/$\sqrt{Hz}$ average white noise [3]. It should be pointed out that each dc-SQUID magnetometer reaches average white noise at 1 kHz equal to 1.4 fT/$\sqrt{Hz}$ measured separately with the SQUID in the lead shield. The best-one is characterized with the white noise 1 fT/$\sqrt{Hz}$ and the worse-one with 3.0 fT/$\sqrt{Hz}$.

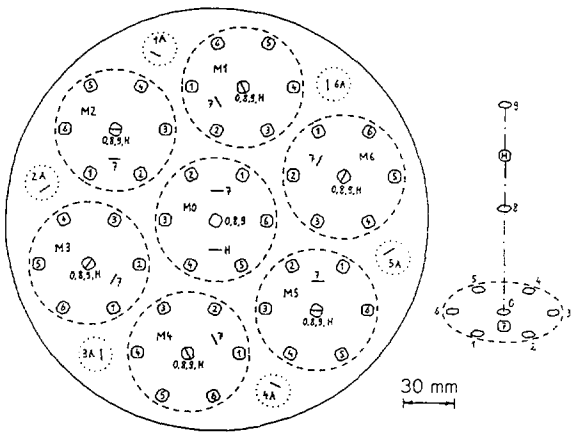

Figure 1: The distribution of dc-SQUID magnetometers in the PTB clinical multichannel system.

Magnetometers in each module are positioned in three planes (Fig.1) separated by 70 mm and 140 mm, respectively. In the ground plane are 7+1 magnetometers, in the middle plane are 1+1 magnetometers and in the upper plane is 1 magnetometer. Magnetometers can be electronically connected so that it is possible to obtain the gradiometer of first order with the base distance 70 mm or 140 mm or the gradiometer of second order. With all 7 modules and with 6 additional magnetometers, positioned between the 7 modules, it can be achieved that 49 dc-SQUID magnetometers plus 14 reference dc-SQUID magnetometers are sensitive for the B_z componenet of measured biomagnetic field, while 14 dc-SQUID magnetometers plus 6 reference dc-SQUID magnetometers are sensitive for the B_x and B_y components of measured biomagnetic field.

b) Bigger magnetically shielded room

Standard magnetically shielded room (Vakuumschmeltze, typ AK 3b) is installed in the laboratory and provides with its dimensions 3m x 4m enough space for the liquid helium dewar with SQUID magnetometers, mounted in a special gantry which enables all necessary kinematic operations, like rotations, the vertical translation and the tilting of the dewar; the patient's bed is also in the shielded room. Within the magnetically shielded room are also all necessary preamplifiers for biomagnetic and bioelectric measurements. All other electronic assemblies are positioned out of the magnetically shielded room. All critical connections are realised via optoliters and the battery operation of critical part of the measuring system is assured for patient's safety. The shielding factor of this magnetically shielded room is smaller, when compared to the one of the BMRS. However, this drawback is compensated with the high quality of dc-SQUID magnetometers.

c) Better liquid helium dewar design

For the clinical use of any diagnostic measuring system it is very important to design it so that it will operate with the optimal technical support, i.e. the utmost care should be taken to avoid the unnecessary technical services. That means in the case of a biomagnetic measuring system the best possible liquid helium dewar design to reduce the intervals between two refillings of liquid helium. We achieved with the new dewar design that the interval between two refillings amounts 6 days.

d) Higher quality of of dc-SQUIDs

The new high quality dc-SQUIDs with ADP (additional positive feedback) achieve average white white noise below 1.4 fT/$\sqrt{Hz}$ [3]. In this case it is reasonably to apply a bias - current - feedback (BCF) in order to optimize the 1/f noise. This has been done in the present biomagnetic system for clinical applications.

e) New concepts in the monitoring part of the measuring system

The multisensor and multichannel measuring system requires a good monitoring system or better to say a visualisation system for the real time visualisation of events in order to facilitate the work of a person who is supervising the measuring system during the biomagnetic measurement and who takes care for the measuring protocole. The principle of parallel processing was applied and realized with transputers. We could achieve this way fast connections without a usual bus system and at the same time it was possible to obtain several connections. In particular, we have achieved a multichannel real-time information on the ongoing measurement (MCG, ECG,...) on the two video displays with different configurations of graphical presentations, further, a different window geometry, choise of active window, online tesing of measured data regarding fundamental errors, ranges, constancy, as well as the permanent information in the separate window on the system status , possible errors.

f) Higher number of magnetic channels

If all SQUID magnetometers are in use, the clinical system works with 83 magnetic channels. The technical data on the system are presented in Table 1.

Table 1: PTB clinical biomagnetic system Technical specifications

- Nr. of magnetic channels: 83
- SQUID average white noise: 1.4 fT/$\sqrt{Hz}$
- Gradiometer aver. white noise: 2.5 ft/$\sqrt{Hz}$
- Magnetometers in the gradiometric configuration: 1st order gradiom. base distance 70 or 140 mm; 2nd order gradiom. base distance: 70 mm
- Vector configuration available
- 15 bit A/D conversion
- Maxim. sampl. frequency: 1.4 kHz/ch
- Analog filters: Bessel 8th order
- Monitoring sys.: 2 displays (parallel processing)
- Liquid He refilling period: 6 days

g) Improved data acquisition and analysis

The data acquisition and analysis software is based on the programmes which have been developed for the Charlottenburg 37 channel system with several improvements. We have to mention a higher user friendliness - an important factor for the system working in the clinical environment where is to expect in the final step less support from reserchears working in informatics or medical physics. We expect to reach in the near future a quasi on-line evaluation of measurements for cardiac and some peripheral nerve measurements. We understand here the quasi on-line evaluation as an evaluation in the clinically accepted time; i.e. as long as the patient stays in the biomagnetic laboratory, for example, for the cardiac WPW biomagnetic evaluation of the onset of accessory pathway about one hour. We would like to underline here the importance of the permant improvement and development of the software for data analysis. It is extremly important to achieve here the best possible results!

3 RESULTS OF SOME TEST MEASUREMENTS

The test measurements started before the magnetically shielded room AK 3b was constructed in order to calculate later the values of shielding properties. It can be said that the shielding property of this room is better than the producer announces in his speciffications. The shielding factor reaches a value of 100 at 0.01 Hz. Later on the properties of sensors were tested in configurations: 1 sensor, 3 sensors, 7 sensors and the whole module of 11 sensors. When the first module was ready, the test biomagnetic measurements were already performed. It became clear that practically all measurements can be carried out with the first order gradiometric configuration of sensors. The results of peripheral nerve measurements were comparable to those, obtained in the BMSR with the SQUID magnetometer [4]. The same conclusion results also from first cardiac measurements.
After all seven modules were assembled and mounted in the dewar, further tests were completed: Instrumentation tests have proved that all modules together work equally well. The scattering of white noise between any two of most distant dc-SQUID magnetometers (the distance is 21 cm) amounts about $\pm$ 20% . A typical test result of an MCG time evolution of unaver-

aged signal is shown on Fig.2 , while the simultaneously taken time evolution of MCG signal over the chest, taken with the multisensor system in 49 points, presents Fig. 3. Further neurological measurements on diffeerent periferal nerves were successful and the results will be published elsewhere.

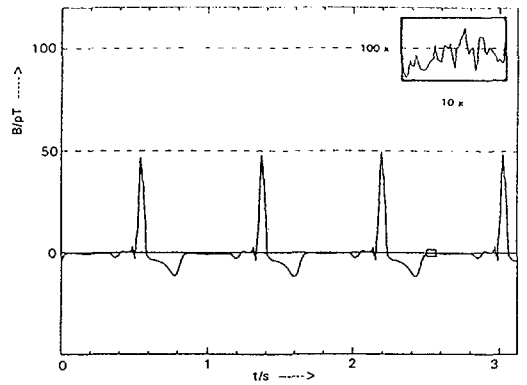

Figure 2: The time evolution of the MCG signal (raw data), detected by one gradiometer of the multisensor system. In the upper right corner an enlarged view of a small rectangular part of the T–P segment is shown

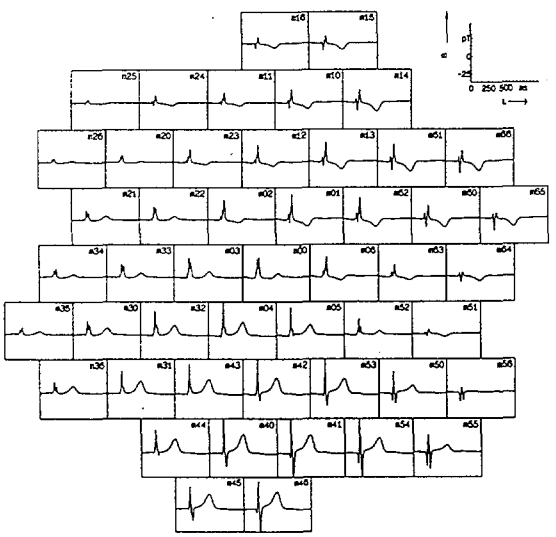

Figure 3: The time evolution of MCG signals simultaneously detected with the multisensor system in 49 points above the chest.

4 CONCLUSIONS

In this evaluation of the new PTB clinical biomagnetic measuring unit, the clinical system was compared with the 37 channel PTB laboratory system installed in the BMSR in Charlottenburg. It can be concluded:

- Measurements which have been carried out in the BMSR can be also repeted within the MSR in the PTB clinical laboratory. This holds for the peripheral nerve system measurements and for the cardiac MCG measurements.
- This clinical biomagnetic measuring system, installed within the moderately shielded room, is due to the very high quality of dc-SQUIDs also suitable for the research work where the biomagnetic signals of about 15 fT (or more) are expected.
- First test results show that such a biomagnetic unit can provide valuable clinical results in the area of functional localization diagnostics in the everyday clinical work, provided that a good coupling to the imaging facilities within the clinic (CT, MRI,PET) exists.

References

[1] H. Koch, R. Cantor, S.N. Erné, K.P. Matthies, M. Peters, T. Ryhänen, H.J. Scheer, H.D. Hahlbohm. A 37 Channel dc SQUID Magnetometer System. *IEEE Trans. on Magn.***27** : 2793–2796, 1991.

[2] S.N. Erné, H.D. Hahlbohm, H. Scheer, Z. Trontelj. The Berlin magnetically shielded room (BMSR). Biomagnetism, 79–87, 1981.

[3] D. Drung. Recent LTS SQUID Developments. Applied Superconductivity, **2**, 1287–1294, 1993. Editor H.C. Freyhardt, DGM, Oberursel.

[4] L. Trahms, S.N. Erné, Z. Trontelj, G. Curio, P. Aust. Biomagnetic Functional Localization of a Peripheral Nerve in Man. *Biophys. J.* **55**, 1145–1153, 1989.

SAMPLING AND IMAGE RECONSTRUCTION OF RIBOSOMAL TETRAMERS

A.Evangelisti, Department of Systems and Informatics, University of Firenze
C.Pallotti, G.Pallotti, Department of Physics, University of Bologna
P.Pettazzoni, Institute of Histology, University of Bologna
Italy

ABSTRACT: Data acquisition often falls into the category of digital sampled data system, in that an initially continuous function is represented by an ordered series of discrete points. Signal recovery, i. e., emulation on those aspects of the original function which are of interest, will depend on the quality and nature of the input, on the sampling interval, and on the effectiveness of the technique used for signal reconstruction. This paper is concerned with the problem of selecting and appraising a sampling interval for digital data collection system in general, moreover the use of Fourier series to solve structural problems of ribosomal tetramers.

1. INTRODUCTION

Chick embryo ribosome, exposed to hypothermia, form plane crystal layers belonging to the P4 symmetry group or superimposed crystal layers of the P422 symmetry group. In previous works the morphology of these crystals in sections and negative staining have been analysed [1-4].Attempts have also been made to purify crystals and to define chemical, physical and functional characters of the tetramers, which are the basic units of the crystals [5-9].

Moreover some attention has paid to the meaning of crystallisation in connection to ribosomal biogenesis an two main contrasting hypotheses have been advanced. The first hypothesis entails that all monomer ribosomes should be able to form crystalline aggregates. The second hypothesis, on the contrary, suggest that only neo-synthesized and not yet programmed ribosomes could be induced to crystallise by hypothermia as well as other agents. This means that the property to crystallise is transient and occurs only when a sufficient length of time elapses between the release of meosynthesized ribosomes and their utilisation in protein synthesis. A final implication of this hypothesis is that the engagement of the ribosomes in protein synthesis induces a permanent differentiation in their structure so that can no longer crystallise [10-11].

The studies carried on till have not yet given crystals large enough for *X*-ray diffraction, and it is important to define the condition of crystal preparation an purification to make progress in this way.

The present work examine the information contain of electron images of regular objects using the basis theory of the image processing in the field of biological structures [12-14].

For a successful application the biological objects must exhibit regularity and the image of the structures are analysed by computer after being digitised.

The aim of the digital analysis is to retrieve the maximum amount of information from the electron image. This paper is concerned with the problem of selecting and appraising a sampling interval for digital data collection systems in general, moreover, the use of Fourier series to solve structural problems is quite common in *X*-ray crystallography, from which many of the methods in this field are derived [15-18].

2. MATERIALS AND METHODS

2.1 General methods

The preparation of embryos and ribosomes and the manipulation of sucrose gradient have been described [19].

2.2. Negative staining

All the pellets are re suspended in few drops of 0 medium and after a gentle stirring the resultant

dense re suspension is dropped on carbon coated Formar covered grids. After a rest of 30 s, the grid is thoroughly washed with several drops of 0 medium; a drop of 2% aqueous glutaraldeyde is then laid on the grid and removed after 1 minute with few drop of distilled water. The damp grid is covered with one drop of 1% aqueous uranyl acetate solution at uncorrected pH and drained with filter paper after 30 s.

To evaluate the influence of pH on staining, a series of grids has been stained with 1% uranyl acetate solution, in which pH has been adjusted at different values from 2.0 to 5.5

2.3. Electron microscopy

The specimens were examined in a Philips EM 300 operating at 100 kV and equipped with anti contamination devices. The grids were inserted in the microscope with the specimen facing the electron beam. The final prints represent the specimens as viewed from the electron source side.

2.4. Hardware architecture

The utilised hardware is given by an image processing system based on a PC IBM AT, and composed by a television camera (Grunding CCD FA 200) to record images, an image analyser (PC vision FG 100) for image digitisation and elaboration, a monitor to visualise the images and graphic tools for interaction with the visualised images. The FG100 is capable of 8 bit (256 levels) grey scale resolution of each digitised image. The spatial resolution is 512x512 pixels and the machine itself may be programmed using C language software. The analogical signal coming from the television camera is sampled and quantified by an analog/digital converter,, whose output is stored in an image memory of adequate characteristics. The data contained in this frame memory are then available for successive processing and/or visualisation: this is achieved by means of look up tables and a successive digital to analog conversion operations, which allow us to obtain a video signal to be sent to the monitor.

2.5. Data Acquisition

In order to be suitable for electron microscopic analysis biological material has to be processed by chemical and physical methods. Generally these combinations of treatments are known al preparation technique. The intention of the particular preparation method is to make the object under study suitable for examination in vacuum uwith electrons, ideally in such a way that the minimum numbers of electrons is required to image the structure. This last requirement is necessary to limit the irreversible changes due to radiation damage, which ultimately effect the biologically relevant information content of the image. As biological material consist of relatively light elements which do not scatter electrons appreciably, procedures have to be carried out in order to enhance the scattering power of the object of parts of it. Heavy metal in solution or as vapour can be used to achieve this.

The vacuum conditions in the microscope require that the specimen be investigated in a dry state. This may prevent a total collapse of the three dimensional structure when the specimen is introduced into the vacuum. The different preparation methods form an integral part of the structural studies by image processing. The development of these preparation methods is among the most important aspects of molecular electron microscopy as the application of image processing methods only serves to obtain an average result or an image which can be interpreted in a strainghforward way.

Data acquisition often falls into the category of digital sampled data system, in that an initially continuous function of one or several independent variables is represented by an ordered series of discrete points. The keystone of such methods is the collection of sufficient information in the samples to permit explicit or implicit emulation of those aspect of the original function which are of interest. The success of this signal recovery will depend on the quality and nature of the imput, on the sampling interval, and finally on the effectiveness of the technique used for signal reconstruction.

Consider a time-varying signal $s(t)$ observed over on interval $[t_0, t+T]$ of duration T. The function $s(t)$ is sampled at $N+1$ successive times $t_0 < t_1 < t_2 \cdots t_{n-1} < t_N = t_0$. These $N+1$ times

$$\{t_k\}_{k=0}^{n}$$

partition the interval $[t_0, t+T]$ into N contiguous subintervals, $[t_0, t_1], [t_1, t_2], \cdots [t_{N-1}, t_N]$,. The mean sampling rate $\overline{f}$ is defined as

$$\overline{f} = \frac{1}{N} \sum_{i=1}^{N} \frac{1}{t_i - t_{i-1}} \qquad (1)$$

when observations are made regularly, $t_i - t_{i-1} = T / N$ for each value of i; hence, the sampling rate $\overline{f}$ is simply N/T. The duration of the longest subinterval between samples is called

the mesh Δ of this particular subdivision of $[t_0, t+T]$ by the sampling times:

$$\Delta = \max_{1 \le i \le N} \{(t_i - t_{i-1})\} \quad (2)$$

For regular sampling, the mesh is simply T/N, the reciprocal of sampling rate.

The use of piece-wise curvilinear approximation based on regular sampling is especially appropriate for signal recovery in digital processing. The $N+1$ sample points

$$\{(t_k, s(t_k))\}_{k=0}^{N}$$

are used to determine the parameters of a sectionally smooth estimating function $\hat{s}(t)$ which consist of adjoining continuous arcs:

$$\hat{s}(t) = f_i\left(t; \{t_k, s(t_k)\}_{k=0}^{N}\right) \quad (3)$$

with $t_{j-1} \le t \le t_j$; $j = 1, 2, \ldots\ldots, N$.

Generally, estimation of signal amplitude at time t will involve antecedent and subsequent measurements of amplitude. By definition, interpolating functions obey the constraints:

$$\hat{s}(t_k) = s(t_k) \quad (4)$$

with $k = 0, 1, 2, \ldots\ldots, N$.

Interpolating line segments, higher order algebraic polynomials and trigonometric series are the most frequently used functions.

Let μ denote the mean imput magnitude over the period of observation:

$$\mu = \frac{1}{T}\int_0^{t_0+T} |s(t)| dt \quad (5)$$

with the estimator $\hat{s}(t)$ of the signal $s(t)$ associate the residual , η^2 the mean residual σ^2 , and the relative residual E, defined respectively as

$$\eta^2 = \int_0^{t_0+T} [s(t) - \hat{s}(t)]^2 dt \quad (6)$$

$$\sigma^2 = \mu^2 / T \quad (7)$$

$$E = \sigma / \mu \quad (\mu \neq 0) \quad (8)$$

The residual η^2 is analogous to the sum of the squares of deviation from a regression curve. The relative residual E is analogous to the coefficient of variation and its reciprocal $1/E$ is reminiscent of measurement signal to noise ratio. E, η^2, and σ^2 measure the error of estimation. There is an implicit relationship between the form of the approximating curve and the sampling rate on the one hand, and the error of estimation on the other for a large class of estimators $\hat{s}(t)$, the following theorem may be proven; as the sampling rate increases, the mesh (maximum interval between samples) diminishes and the fidelity of the approximation improves [20]. Obviously, for complete signal recovery the residual η^2 and the residual E vanish. However, when complete signal recovery is unfeasible or unnecessary, any of the quantities E, η^2 and σ^2, enables a comparison of various data processing algorithms and sampling rates. For example, combinations of data processing techniques and sampling rates may be rank ordered on the basis of the magnitude of the corresponding relative residual. Those combinations which generate values E not exceeding a prescribed tolerance E_0 are equivalently suitable from the point of view of error control.

From amongst these suitable algorithm sampling rate combination, the optimal one is chosen by trying to minimise the sampling rate and the computation time.

2.6. The Fourier Transform of an Electron Micro Graph

The theory of image formation is presented in a form that is applicable to a specimen treated as a continuous two dimensional distribution of mass density, and expression are derived relating the Fourier transform of the image to the Fourier transform of the object density [21-23].

Image formation is frequently explained in terms of production of contrast, which can be attributed to two different mechanisms. Amplitude contrast is traditionally attributed to the removal from the electron beam of electrons that have been scattered outside the objective aperture. Phase contrast is produced by interference between the unscattered electron wave and the electron wave that is coherently scattered within the objective aperture. The contribution to the image from each of these mechanism is yet described, and a number of specific application of the theory to electron microscopy has been given.

The two function that are of central importance in this presentation are the object is assumed to be thin enough so that the variation in focus through the specimen is negligible. The object can than be specified by a two dimensional function, $\sigma(x_0, y_0)$, defined as the projected density, expressed in atom per unit area, and object plane co-ordinates (x_0, y_0). The object transform is

the two dimensional Fourier transform of this function:

$$T_o(\alpha,\phi) = \iint \sigma(x_0,y_0)\ \xi\, dx_0\, dy_0$$

$$\xi = exp\left[\frac{-2\pi i}{\lambda}(x_0 \cos\phi + y_0\, \alpha\ sen\phi)\right]$$

The transform is expressed in circular co-ordinates: α (radial) and ϕ (azimuth). The reciprocal radial co-ordinate is specified in the integral as α / λ , where α is the angle of scattering from the object to the diffraction plane, and λ the electron wavelength. Because $\sigma(x_0, y_0)$ is a real function, the transform obeys to the symmetry relationship

$$T_0(\alpha;\Phi) = T_0^*(\alpha, \Phi+\pi)$$

The first problem in describing the process of image formation is to specify the electron wave in the object in terms of $\sigma(x_0, y_0)$. It is assumed that the object is illuminated by a monochromatic plane wave of electrons.

This incident wave is modulated on passing through the specimen to give the electron wave in the object plane, $\psi_0(x_0,y_0)$. Since actual absorption of electrons in negligible for the thin specimens normally examined in biological and high resolution microscopy, the object is a pure phase object, and modulates the phase but not the amplitude of the incident wave. Assuming the incident wave to be of unit amplitude, the object wave can be written

$$\psi_0(x_0,y_0) = exp[i\,\delta(x_0,y_0)] = exp[i\psi_{ph}(x_0,y_0)]$$

The phase shift, $\delta(x_0,y_0)$, is written here as a wave function, $\psi_{ph}(x_0,y_0)$, because, in the approximation used in the derivations, it is equivalent to the scattered wave in the object plane. This function is closely related to object mass density, $\sigma(x_0, y_0)$. The object wave give rise to a wave in the diffraction or back focal plane of the microscope, $\psi_\alpha(f_\alpha,\phi)$, which is proportional to the Fourier transform of the object wave.

This wave is expressed, for convenience in the derivation, in circular co-ordinates in the diffraction plane: ρ is the radial co-ordinate in the diffraction plane, but is written here as the product $\rho = f\,\alpha$, where f is the focal length of the lens and α is the scattering angle from the object plane; f is the azimuth co-ordinate. The effect of the objective aperture can be accounted for by an aperture function, $A(\alpha)$, which is zero over those parts of the diffraction plane obstructed by the objective aperture and unity otherwise. The modified wave in the diffraction plane is than

$$\psi_d^*(f\alpha,\phi) = \psi_d(f\alpha,\phi)A(\alpha)exp[i\chi(\alpha)]$$

This modified wave in the diffraction plane give rise to the electron wave in the image plane, $\psi_i(x_i,y_i)$, by Fourier transformation. The recorded image is given by the intensity of this wave. With proper photographic processing the optical density of the micro graph is directly proportional to the electron intensity. The transform of the image, which is the central point of this presentation is therefore the transform of this intensity function.

To obtain the Fourier transform of a conventional electron micro graph and reconstruct the image after eliminating all parts of the transform in the reversed contrast zones [24-25]. It can be done by computer processing. This involves scanning the micro graph to convert the image to a two dimensional array of optical densities and calculating the Fourier transform [26-28]. The image is reconstructed by inverse Fourier transformation after setting the Fourier coefficients to zero over the reversed contrast zones.

With this computer processing system, however, one can go much further in reconstructing an improved image. Instead of simply eliminating the reversed contrast zones by setting the transform to zero, these can be corrected to normal contrast merely by changing the sign of the Fourier coefficients. Then the information in these zones would not be lost in the reconstructed image. In addition one can increase the amplitudes of the transform where the transfer function is less than unity, reconstructing an image to which almost the whole transform is contributing with uniform maximum contrast. The only parts of the transform that would be missing from the reconstructed image are those near the zeros of the transfer function, for here the information is actually missing from the original image, not simply modified in amplitude. To obtain this information an additional micro graph at a slightly different defocusing would be needed.

3. RESULTS

Electron micro graphs can be converted to digital form and stored on magnetic tape. The two dimensional Fourier transform can be computed from the stored digital values and output on a

selected grid, Since the micro graph record consist primarily of a periodic array of identical unit cell, the Fourier transform will be discrete rather then continuous, and the non zero intensities will fall on an equivalent reciprocal lattice. Because the process begins with an image, both amplitude and the phases can be directly calculated. The amplitude and phase may than be used in a second Fourier synthesis, or back transform to reimage. The value of such a process lies in the fact that all background and noise components of the micro graph are essentially random and, therefore, contribute nothing to the discrete Fourier transform. Thus, when only the intensities and associated phases found exactly on reciprocal lattice points are included in the back transform, the image so obtained will be filtered free of virtually all noise.

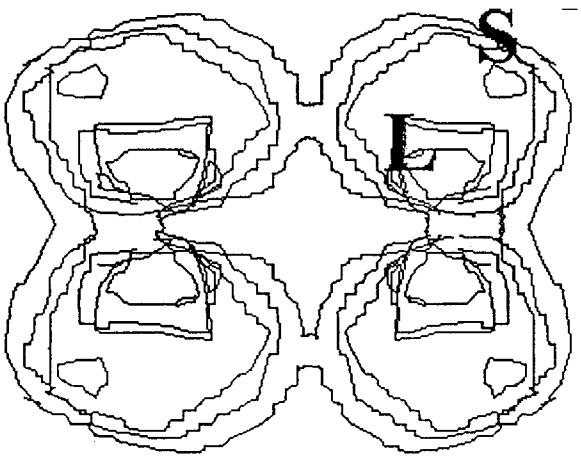

Figure 1. A detail of the projeted layer of crystalline ribosomes obtained after a two dimensional Fourier synthesys. Each ribosome is divided into a large (L) and small (S) subunit as indicated in the figure

From the ultra structural data obtained in this investigation, some hypotheses on the possible arrangement of monomer ribosomes of tetramers and of tetramers in crystals can be advanced.

Fourier synthesis derived from this complete data set gave a projection map. In this map the tetramers are arranged in a right-handed configuration. Tetramers ribosomes seen in the two dimensional projection of negatively stained preparation are elongated bean-shaped particles with diameters 220-280 Ĺ and 195 Ĺ, containing a wedge-like cleft in the outer edge. The cleft frequently continues into a line which extends across the ribosome, apparently dividing it into two unequal parts.

The position of the cleft suggest that almost all tetramers are attached to the electron microscope grid by the same surface. That the cleft of each ribosome is always *clock wise* relative a line, bisecting the ribosome, drawn trough the axis of the tetramer. The smaller part of the particle, as viewed in two dimensions, is thus also on the *clock wise* end of the ribosome the stain distribution associate with the ribosomes correspond to that shown by the images of isolated eukariotic ribosomes, in which the long axis of the small subunit and the line joining the two subunit both lie perpendicular to the viewing direction. Based on this comparison, and the fact that similar features are not evident in other views of isolated ribosomes, we assume that the ribosomal subunits are lying side by side.

It is likely that the small subunit forms dimerization bounds with the small subunit of the monomer of the contiguous tetramer, while the tetrameric arrangement is maintained by the bondings of the large subunits which are in close contract with each other. This configuration is compatible with the available data on different nature of the bondings that are involved in tetramerization, depending on K^+ concentration, and the bondings, that link the tetramer together, which depend on Mg^+ concentration, like the dimerization bounds, between small subunit.

The regular information in the micro crystals is present to a resolution of about 5 nm, as can be derived from the Fourier transform of digitised images. The crystalline sheet are composed of two layers and in each of these ribosomes are organised as tetramers on a P4 type of lattice. The two layers face in opposite directions and tend to be related to one another crystallographically, generating a family of P422 crystals of different unit cell dimension.

The Fourier synthesis permits calculations of electron density at any point in the unit cell. Since the density is a continuous three dimensional function, in order to build up the complete image of the contents the density must be calculated for all points in the unit cell. Figure 1 is one plane of an electron density map. The partition between the subunits cannot be drawn in unambiguously at this resolution-however the assignment S for small and L for large subunit, as indicated would be consistent with the interpretation that is generally given to image of isolated ribosomes.

4. REFERENCES

1. Byers B. Ribosome crystallisation induced in chick embryo tissues by hypothermia. *J.Cell Biol.* **30**: c1; 19663.
2. Nonomura Y., Blobel G., Sabatini D. Structure of liver ribosomes studied by negative staining. *J. Mol. Biol.* 6: 303; 1961.
3. Lake J.A. Reconstruction of three dimensional structures from sectioned helices from escherichia coli. *J. Mol. Biol.* **2**: 10; 1960.

4. Byers B., Structure and formation of ribosome crystals in hypothermic in chick embryo cells. *J. Mol. Biol.* **26**: 155;1967. 5. Byers B. Chick embryo ribosome crystals: analysis of bonding and functional activity in vitro. *Proc. Ntl. Ac. Sci.* **68**: 440; 1971.
6. Carey N.H., Read G.S. The arrangement of ribosome in ribosome tetramers from hypothermic chick embryos. *Biochem. J.* **121**: 511; 1971.
7. Carey N.H., Hobbs J.R., Cook E.A. The structure of ribosome as indicated by studies on tetramers from hypothermic chick embryos. *Biochem. J.* **130**: 871; 1972.
8. Dondi P.G. Analysis by two dimensional gel electrophoresis of ribosome crystal proteins. *Biochem. J.* **149**: 475; 1975.
9. Dondi P.G., Barker D.C. Some properties of ribosome crystals isolated from hypotermically treated chick embryos. *J. Cell Sci.* **14**: 301; 1974.
10. Brunelli M.A., Marini M., Pettazzoni P., Bubola G. Ribosomal crystallisation in hypothermized chicken bone marrow. *J. Ultrastruct. Res.* **60**: 140; 1977.
11. Barbieri M. The primitive Ribosome Model. *J. Theor. Biol.* **47**: 269; 1974.
12. Lipson H., Cochran W.The determination of crystal structures. Bell, London 1966.
13. Crowther R.A., DeRosier D.J., Klug A. The reconstruction of a three-dimensional structure from projection ant its application to electron microscopy. *Pro Roy Soc.* **2**: 10; 1980.
14. Pavlidis T. Structural pattern recognition. Springer Verlag, Berlin, 1977.
15. Brigham E.O. The fast Fourier transform. Prentice-hall, Englewood Cliffs, 1974.
16. Prewitt J.M.S. A New Approach to the selection of Sampling Rate for digital Data IEE *International Conv Rec.* 9:110; 1963.
17. Haine M.E. The Electron Microscope. Interscience Publisher, New York, 1962.
18. Heidenreich R.D. Fundamentals of Transmission Electron Microscopy. Interscience Publisher, New York, 1964.
19. Barbieri M., Pettazzoni P., Bersani F., Maraldi N.M. Isolation of ribosome micro crystals. *J.Mol.Biol.* **54**: 121;1970.
20. Bahr G., Zeitler E. Quantitative Electron Microscopy. Williams and Wilkins Co., Baltimore 1965.
21. Pavlidis T. Filling algorithms for raster graphics. *Comput Graphics Image Process* **10**:126; 1979.
22. Hung T.S. Picture processing and digital filtering. In: Topics in applied physics. Springer Verlag, Berlin, 1975.
23. Bracewell R.N. The Fourier transform and its application. McGraw-Hill, New York, 1965.
24. Lipson H., Cochran W. The determination of Crystal Structures. Bell, London, 1966.
25. Geddes L.A., Baker L.E. Applied biomedical instrumentation. John Wiley & Sons, New York, 1975.
26. Sweets J.A. Signal detection an recognition by human observer. John Wiley & Sons, New York, 1964.
27. De Rosier D.J., Klug A. Reconstruction of three dimensional structure for electron micro graphs. *Nature* **27**: 130; 1968.
28. Merril R.D. Representation of contours and regions for efficient computer search. *A CM Comm.* **16**: 69; 1973.

3D MAPPING OF EEG AND EVOKED POTENTIALS

Damir Danijel Žagar, Mario Cifrek
Faculty of Electrical Engineering
Department of Electronic Measurements and Systems
Unska 3
Zagreb, Croatia

Abstract

3D Graphics used in EEG and evoked potentials data visualization results in their better interpretation and makes them more applicable in clinical neurophysiology for detecting areas with intensive pathological activity. To achieve better quality of represented data without significant loss of information, several spatial and color interpolation methods are considered for brain electrical activity mapping.

TRODIMENZIONALNI PRIKAZ EEG I EVOCIRANIH POTENCIJALA

Sažetak

Upotreba trodimenzionalnih prikaza u analizi EEG-a i evociranih potencijala omogućava njihovo bolje tumačenje te ih čini primjenjivijima u kliničkoj neurofiziologiji za odredivanje područja s izraženom patološkom aktivnošću. U cilju postizanja bolje kvalitete prikazanih podataka bez značajnog gubitka informacija, pri izradi kartografskih prikaza električke aktivnosti mozga razmotreno je više metoda prostorne interpolacije.

1. INTRODUCTION

Since mapping techniques are being used in EEG and evoked potentials analysis as the only way to convey three-dimensional brain electric field data in an immediately understandable form, it has been known that they introduce new possibilities for their misinterpretation. Basic problems are interpolation and projection algorithms as well as head models that are used for the true feature reconstruction on the map.

Conventional brain mapping usually treats orthogonal projection of head region as 64×64 matrix [1], yielding 4096 domains. Each domain's potential is calculated by linear interpolation from the three nearest known points (electrodes) and then presented on the screen or paper as the colored or gray shaded pixel. To avoid map deviation from the original, if linear interpolation is used for data reconstruction, the sampling rate should be at least 5 times higher than the Nyquist frequency [2]. That is not possible with the standard 10-20 system, i.e. more electrodes are required to cover the entire scalp whose limiting factor is its extension size, which is only about 35 cm. Increased number of electrodes or usage of polynomial and other interpolations produces better results, but deformation problem caused by interpolation done in projected three-dimensional space without taking into account the real head shape and conductivity characteristic still remains.

The aim of the present study was to develop a simple spatial mapping technique based on the given geometrical head model with feature to present reconstructed data in projected three-dimensional space.

2. METHODS

Used geometrical model represents the head as a mesh of polygons described in three-dimensional space with their vertices and edges. Simple two-dimensional matrix representation discards the third, volume, component and is therefore insufficient for the spatial interpolation. If the matrix is extended into the third dimension by changing each two dimensional pixel with its spatial equivalent - voxel (volume pixel) and if conductivity properties are known then finite element method can be used for field reconstruction and volume rendering. Because our problem does not include volume characteristics and the computational power that is required for the finite element method is far beyond possibilities of the personal computer we have tried a different approach.

2.1. Spatial interpolation

When more than three values are like to be used for interpolation of an unknown point, simple techniques, such as linear interpolation, are not satisfiable. To avoid this problem the interpolated value (v_i) is calculated as the arithmetical average of known voltage levels (v_k) multiplied with some weighting factor. This method is known as *weighted averaging*. The result depends on the number of electrodes used and on the weighting function. If only nearby, not heavily weighted electrodes are employed, the result is a punctuate display with regions of similar value surrounding each electrode. On the contrary, significant weighting of distant electrodes produces a pleasing display with smoothed and blurred local details. The most commonly used weighting function is the inverse distance between the interpolated and the known point ($1/d_k$) rose to the power n (1).

$$v_i = \frac{\sum_{k=1}^{N} v_k \cdot \left(\frac{1}{d_k}\right)^n}{\sum_{k=1}^{N} \left(\frac{1}{d_k}\right)^n} \qquad (1)$$

Distance based approach can be used without any modification in three-dimensional space, and is very convenient for our problem. The result is even better if used weighting factor is substituted with Parzen probability distribution [3] that is more suitable for natural systems. This substitution results with the following formula (2)

$$v_i = \frac{\sum_{k=1}^{N} v_k \cdot e^{-\frac{d_k^2}{2\sigma^2}}}{\sum_{k=1}^{N} e^{-\frac{d_k^2}{2\sigma^2}}} \qquad (2)$$

Distance d_k between two vectors $\mathbf{X}_i$ and $\mathbf{X}_k$ can be defined as Euclidean distance (3).

$$d_k^2 = (\mathbf{X}_k - \mathbf{X}_i)^T \cdot (\mathbf{X}_k - \mathbf{X}_i) \qquad (3)$$

When the smoothing parameter σ is made large, the estimated distribution is forced to be smooth and becomes Gaussian. On the other hand, a smaller value of σ allows the estimated distribution to assume non-Gaussian shapes, but with the hazard that wild points may have too big effect on the estimate. For intermediate values of σ, all values of v_k are taken into account, but those corresponding to points closer to $\mathbf{X}_i$ are given heavier weight.

Optimal smoothing parameter σ for a given number of observations N can be found by minimizing the mean square error between the real and calculated value of v_i with actual observed value eliminated to avoid artificial minimum error as $\sigma \to 0$.

2.2. Displaying techniques

With the presented procedure potential values for all vertices on the scalp are calculated and one unique color from uniformly distributed range of colors is assigned to each value. Hidden polygons are removed with binary space partition algorithm [4], and then only the visible ones are displayed. To gain finer resolution on the reconstructed map projected polygons are painted on the screen recursively subdivided into triangles in the color that is calculated as the average color of their vertices (Fig. 1).

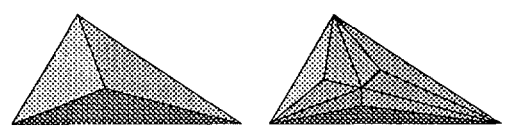

Fig. 1. Triangle subdivision used for color interpolation.

3. RESULTS

The implementation of the described procedure was done on a personal computer using the C programming language. Both, the digitized head model and EEG data collected with BioLogic's EEG equipment, previously preprocessed using "Brain Atlas" software, were imported into the program in the ASCII format. The developed program uses perspective model projection with definable observer position for rendering and is capable to perform analysis in the time and the frequency domain.

Simulated brain electrical activity data are used for testing. Visual comparison between the reconstructed and the original, simulated, data shows little deviation. For this reason we find that used interpolation technique is highly applicable for the brain mapping.

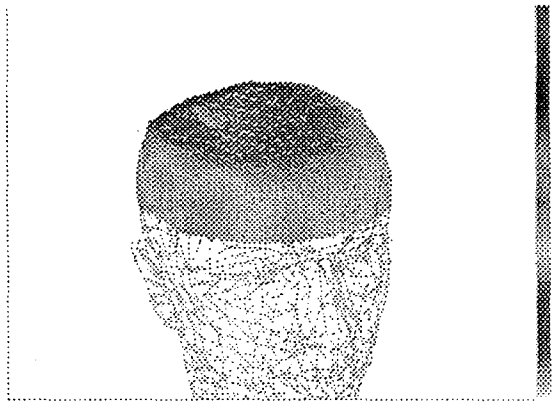

Fig. 2. Analysis of EEG data in the time domain.

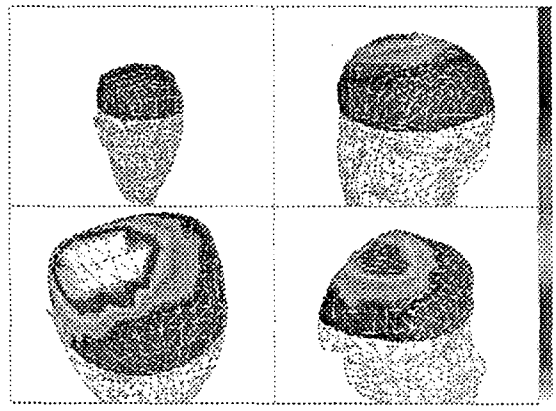

Fig. 3. Analysis of EEG data in the frequency domain. Delta, theta, alpha and beta bands are displayed.

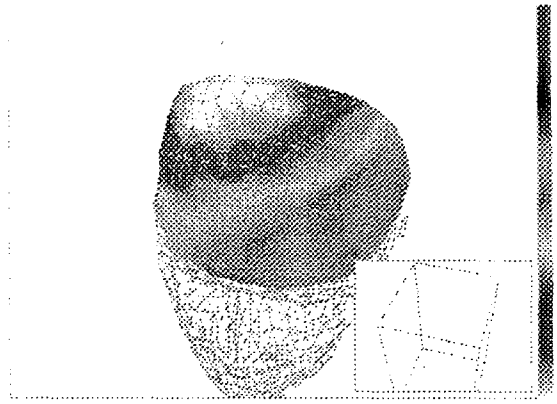

Fig. 4. Defining the observer position.

4. CONCLUSION

Because the developed program is still under the clinical test and complete results are not yet available we are not in the position to make the final judgement. In our opinion, 3D mapping is more applicable and pleasant than ordinary two-dimensional mapping thus yelding with better interpretation of the measured data.

The presented method for the brain mapping can be, without bigger modifications, extended and applied for mapping of any other surface potential.

5. REFERENCES

[1] F. H. Duffy, Topographic Mapping of Brain Electrical Activity: Clinical Applications and Issues, Topographic Brain Mapping of EEG and Evoked Potentials, 19-52, Würzburg, 1989

[2] D. Lehmann, From Mapping to the Analysis and Interpretation of EEG/EP Maps, Topographic Brain Mapping of EEG and Evoked Potentials, 53-75, Würzburg, 1989

[3] D. F. Specht, A General Regression Neural Network, IEEE Transactions on Neural Networks, 2, 568-576, 6, 1991

[4] J. D. Foley, A. van Dam, S. K. Feiner, J. F. Hughes, Computer Graphics: Principles and Practice, Addison-Wesley Publishing Company, New York, 1990

DETERMINATION OF BLOOD FLOW VELOCITY

Gordana Žauhar[1], Branko Breyer[2]
[1]School of Medicine, University of Rijeka
[2]School of Medicine, University of Zagreb

ABSTRACT In order to find a new method for measuring the velocity of the blood flow, the autocorrelations of functions which are the result of reflections of ultrasonic waves on red blood cells have been studied. For simpler cases autocorrelations have been calculated analytically. As real functions are more complex than the functions which have been studied by analytical calculations, the real blood flow has been simulated by computer. The autocorrelation has been calculated from the functions produced in this way. During the generation of the function by computer the form of ultrasonic beam has been taken into consideration, so it is supposed that the beam has the circular form. In all resulting autocorrelation functions one minimum is emphasized. This minimum appears in the period of time which is equal to the period that is necessary for the red blood cells to pass through the ultrasonic beam. As this time is equal to the quotient of the width of the ultrasonic beam and of the horizontal component of the motion velocity of the red blood cells, in this way the velocity of blood flow can also be determined.
Key words: blood flow velocity, autocorrelation, ultrasonic.

ODREĐIVANJE BRZINE PROTOKA KRVI

SAŽETAK S ciljem da se pronađe nova metoda mjerenja brzine protoka krvi proučavane su autokorelacije funkcija koje, po pretpostavci, nastaju uslijed refleksije ultrazvučnih valova na eritrocitima u protoku krvi. Autokorelacije su za jednostavnije slučajeve izračunavane analitički. Budući da stvarne funkcije imaju puno složeniji oblik od oblika koji su razmatrani u analitičkom proračunu, kompjuterski je simuliran stvarni protok krvi i od tako dobivenih funkcija izračunavana je autokorelacija. Kod generiranja funkcije pomoću kompjutera uzet je u obzir i oblik ultrazvučnog snopa, te je pretpostavljeno da snop ima kružni oblik. U svim rezultatima izračunavanja autokorelacijske funkcije jasno se ističe jedan minimum, koji nastaje u vremenu koje odgovara vremenu potrebnom za prolaz eritrocita kroz ultrazvučni snop. Kako je to vrijeme jednako kvocijentu širine ultrazvučnog snopa i horizontalne komponente brzine gibanja eritrocita, na taj se način može odrediti i brzina protoka.
Ključne riječi: brzina protoka krvi, autokorelacija, ultrazvuk.

1. INTRODUCTION

The blood flow velocity can be measured by the Doppler effect. As the ultrasonic waves scatter on erythrocytes, the frequency shift, which is proportional to the velocity of erythrocytes, can be detected. Since the blood flow is usually measured by directed ultrasonic beams, measuring is possible only if the angle between the beam and the flow is not $90^\circ \pm 15^\circ$, because of the unacceptably large measurement error near 90°. The ultrasonic beam is not an ideal plane wave, and therefore measuring might be realized even at right angle [1]. However, in practice it is very hard, because the echoes from the vessel walls are too strong, while the Doppler frequencies are so low that they are hardly measurable [2].

C.Kasai and Namekava showed [3] that measuring of blood flow velocity along the ultrasonic beam can also be done by measuring the value which is equivalent to the Doppler shift, using an autocorrelation technique. This method was used for measuring blood flow volumes [4].

In this paper we shall study the characteristics of the autocorrelation function of reflected waves when the scatterers (erythrocytes) pass transversely to the ultrasonic beam. The preliminary research shows that the autocorrelation function also contains the information about the flow velocity.

The flow velocity which is perpendicular to the ultrasonic beam, could easily be determined if we knew the time required for passing of the particles through the ultrasonic beam (the transit time). In blood flow, erythrocytes are those particles on which ultrasound reflects and scatters. Consequently, the flow velocity should be equivalent to the quotient between the width of the ultrasonic beam (d) and the transit time mentioned above (δ). Since by this method we can measure that component of the velocity which cannot be measured by the Doppler effect, the simultaneous use of both methods would make the measuring of the absolute flow velocity (v) possible, regardless of the angle. The horizontal component of the velocity (v_h) could be determined by measuring of the transit time of particles through the ultrasonic beam. On the other hand, the vertical component of the flow velocity (v_v) could be determined by the well known method of using the Doppler effect. This measuring process is schematically illustrated on figure 1.

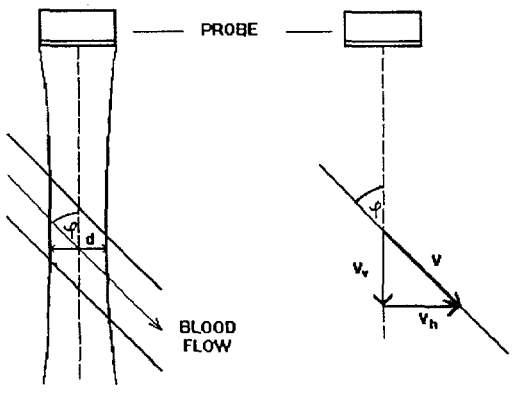

Figure 1. The blood flow through which the ultrasonic beam of the effective width d passes at an angle φ to the flow direction. Accordingly, the flow velocity v can be divided into components v_h and v_v.

The figure shows that the absolute velocity of the blood flow can be obtained from the expression (1)

$$v = \sqrt{v_h^2 + v_v^2} \qquad (1)$$

while the angle (φ) between the ultrasonic beam and the blood flow direction can be calculated from the expression (2)

$$\varphi = \text{arc tg} \left[\frac{v_h}{v_v}\right] \qquad (2)$$

Using the mentioned method we could measure the flow velocity and the angle to the ultrasonic beam . For this reason we have investigated the method of measuring the blood flow in time domain.

2. MATERIALS AND METHODS

Since erythrocytes do not appear in blood in deterministic but in a stochastic sequence in time, it is logical that we used statistical methods to determine the transit time of erythrocytes through the ultrasonic beam. We tried to calculate the autocorrelation function of our stochastic process pre-supposing that by using it we would be able to determine the transit time of erythrocytes through the ultrasonic beam. We solved the simpler cases analytically, while for the more complicated cases we used the computer.

2.1. Analytical calculation for simpler cases

Analytical calculation was done on the assumption that the scattering of ultrasonic waves on erythrocytes is the stochastic process known as shot noise. By shot noise we mean the process

$$s(t) = \sum h(t - t_i) \qquad (3)$$

where t_i are random points in time with average density λ and $h(t)$ a real function. From the definition it follows that $s(t)$ can be represented as the output of a linear system with impulse response $h(t)$ and input the Poisson impulses

$$z(t) = \sum \delta(t - t_i) \qquad (4)$$

According to Papoulis [5], autocorrelation function $R(\tau)$ of such an output signal can be calculated from the expression (5):

$$R(\tau) = \lambda^2 H^2(0) + \lambda \int_{-\infty}^{\infty} h(\tau + t)\, h(t)\, dt \qquad (5)$$

where H denotes the Fourier transform of $h(t)$, while τ is the time shift (delay).

Very similar situation to this is when erythrocytes pass through an ultrasonic beam, because the ultrasonic waves reflect and scatter on

them and in an echo system they generate one signal at a time. In the analytical calculation of the autocorrelation function of the reflected waves we examined two simple impulse responses of the system $(h_1(t)$ and $h_2(t))$ which are shown on figure 2.

a)

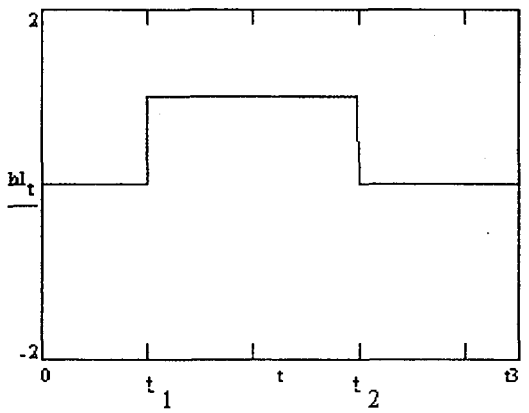

b)

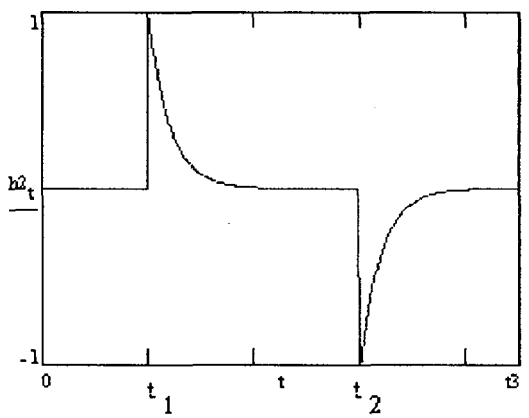

Figure 2. Two simple impulse response of the system. a) impulse response $h_1(t)$; b) impulse response $h_2(t)$.

2.2. The computer simulation of the process

The real functions obtained as a result of the reflection of the ultrasonic waves on erythrocytes in blood have a much more complicated form than are the forms we examined in our analytical calculation. For this reason, by using the computer, we tried to generate the function which would be more similar to the real function and then to calculate the autocorrelation of the function. The program has been written in FORTRAN, and the we used Math-CAD to draw the graphs which show the results.

The real function is the result of the reflection of the ultrasonic waves on erythrocytes the position of which is random. For this reason we used a random number generator for the simulation of the real blood flow. Each random number determines the moment when an erythrocyte meets the ultrasonic beam. We suppose that the reflection of the ultrasonic beam on an erythrocyte causes the emergence of an impulse of a specific form in a resulting function. The duration of an impulse is in the starting hypothesis equal for all impulses and is δ, which corresponds to the transit time of erythrocytes through the ultrasonic beam. During the generation of the function by computer we examined two forms of the impulse. One function was generated by step function as in figure 2.a, while the second was composed of exponential impulses which have the form as in figure 2.b. The total sum of impulses produces the resulting function.

Later we included the form of the ultrasonic beam in our examination supposing that the ultrasonic beam is of circular form. In order to calculate the density function of the duration of impulses $f_y(y)$, we used the formula (6)

$$f_y(y) = \frac{f_x(x_1)}{|g'(x_n)|} + \cdots + \frac{f_x(x_n)}{|g'(x_n)|} + \cdots \qquad (6)$$

where

$$g'(x) = \frac{dg(x)}{dx}$$

In formula (6) $f_X(x)$ denotes the density function for the random variable x, while $x_1, x_2, .., x_n$, are all real roots of equation $y = g(x)$. During the calculation of the probability function of the durations of impulses we started with the following hypotheses: the cross section of the ultrasonic beam is circular and the scatters (erythrocytes) are uniformly distributed widthwise in a vessel. Since x is a random variable and the function of the random variable is given by the equation of a circle , then y will also be the random variable with the density function (7).

$$f_y(y) = \frac{y}{R\sqrt{R^2 - y^2}} \qquad (7)$$

This formula shows that the closer y is to R, the larger is the probability, and this means that the impulses with the longest transit time (δ) will be the most frequent.

The subroutine which generates the function in a case of a circular shape of the

ultrasonic beam, works in the same way as the the function generator mentioned before, but it does not generate n impulses of the same duration. This time the durations of impulses are vary.

The autocorrelation of the stochastic process $x(t)$ which is stationary in wide sense can be calculated from the expression (8)

$$R(\tau) = E\left\{x(t+\tau)\,x^{*}(t)\right\} \qquad (8)$$

where E denotes the expected value and τ is the time shift (delay).

The subroutine 'autocorrelation' calculates the autocorrelation of the stochastic process x(t). From the function treated in this way, the subroutine calculates the autocorrelation by figuring out the mean value of the products $f(t)f(t+\tau)$ for each time shift τ.

3. RESULTS

3.1. Results of analytical calculation

Since in expression (5) the first term is constant we were calculating only the quantity of the second term which presents the auto covariance and is given by (9).

$$C(\tau) = \lambda \int_{-\infty}^{\infty} h(\tau + t)\, h(t)\, dt \qquad (9)$$

Introducing the first shape of impulse response $h_1(t)$ in the expression (9) we obtained the result

$$C(\tau) = \lambda(\delta - \tau) \quad , \quad 0 \le \tau \le \delta$$

$$C(\tau) = 0 \quad , \quad \tau > \delta$$

while for impulse response $h_2(t)$ we obtained the following result

$$C(\tau) = \frac{\lambda}{2\alpha}\left[2e^{-\alpha\tau} - e^{-\alpha(\delta-\tau)} - e^{-\alpha(\delta+\tau)}\right] \quad , \quad 0 \le \tau \le \delta$$

$$C(\tau) = \frac{\lambda}{2\alpha}\left[2e^{-\alpha\tau} - e^{-(\tau-\delta)} - e^{-\alpha(\delta+\tau)}\right] \quad , \quad \tau > \delta$$

These results are shown graphically on the figure 3.

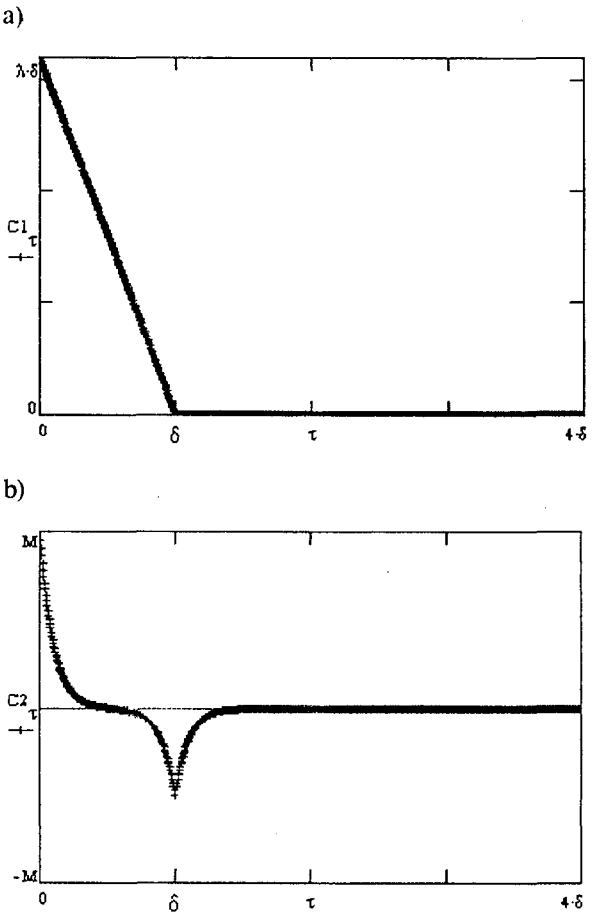

Figure 3. Graphic representation of analytical results of auto covariance calculation. a) for the impulse response of shape $h_1(t)$; b) for the impulse response of shape $h_2(t)$.

The transit time δ is clearly emphasized in the results of analytical calculation of the autocovariance for two shapes of impulse response $h_1(t)$ and $h_2(t)$. The autocovariance (and autocorrelation) has the minimum just when the time delay τ is equal to the transit time δ.

3.2. Results obtained by computer simulation

In order to check the correctness of our program we first calculated autocorrelation for the two well known shapes of functions whose autocorrelations (autocovariances) had been calculated analytically before.

Comparing the results of analytical calculations with the results obtained by computer we learnt that the results correspond. After having checked the program in this way we calculated the autocorrelation of: a) random function which is generated by n step impulses of equal length δ; b) random function which is generated by n

exponential impulses with of equal length δ. The results thus obtained are shown in figures 4. and 5. Each graph of the autocorrelation function (R_τ) is preceded by the graph which shows the function (f_k) from which the autocorrelation has been obtained.

a) n = 500 δ = 200

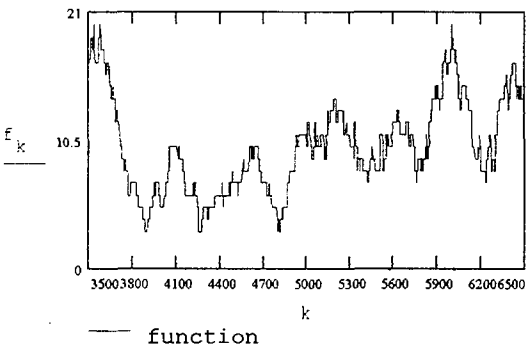

b)

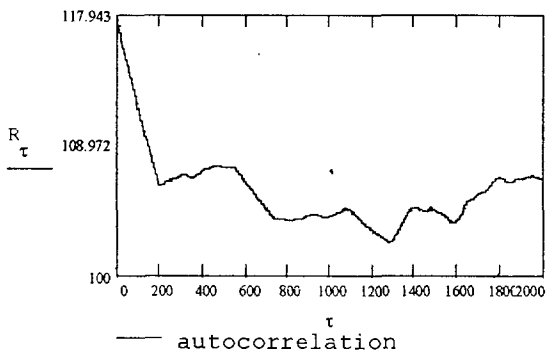

Figure 4. a) A part of the random function which is generated by n step impulses of the same lengt δ .b) Autocorrelation R_τ of the function f_k .

5.a) n = 500 δ = 200

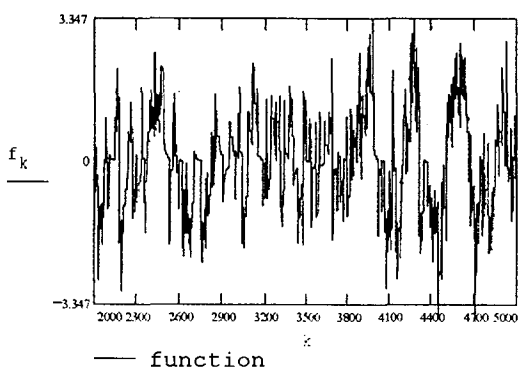

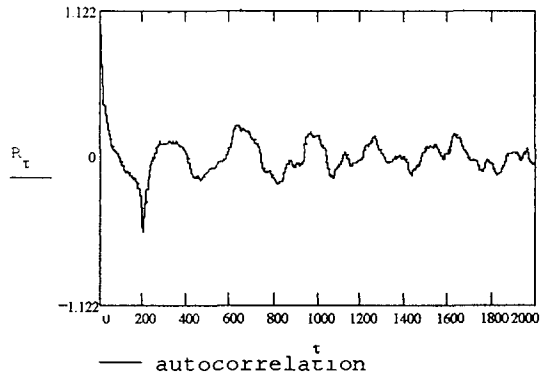

Figure 5. a) A part of the random function which is generated by n exponential impulses of the same length δ. b) Autocorrelation R_τ of the function f_k

On the autocorrelation graphics the first minimum which the autocorrelation has for τ = δ (or when the time delay τ is equal to the duration of the impulse δ) is clearly emphasized.

We also calculated the autocorrelation of the functions which are generated supposing that the ultrasonic beam has got a circular form. The results are shown in the figures 6. and 7.

6.a) n = 500 δ_{max} = 200

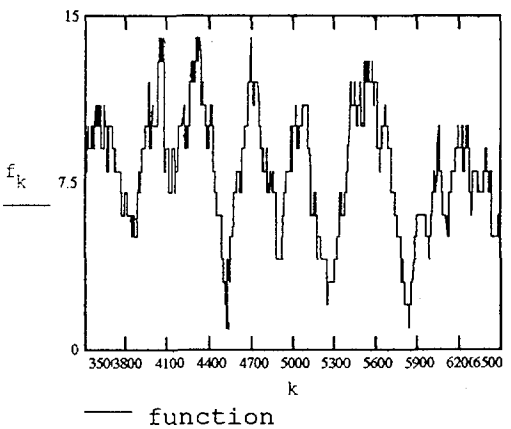

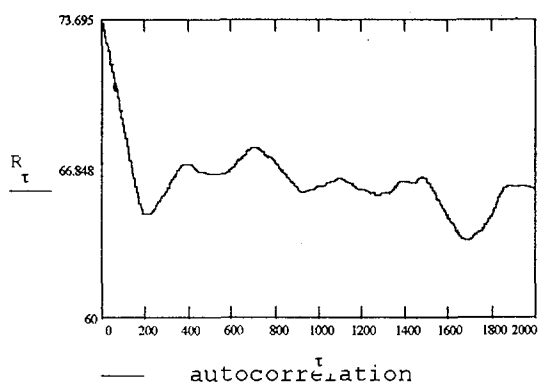

Figure 6. a) A part of the random function f_k which is generated by n step impulses of different lengths (from 0 to δ_{max}). b) Autocorrelation R_τ of the function f_k .

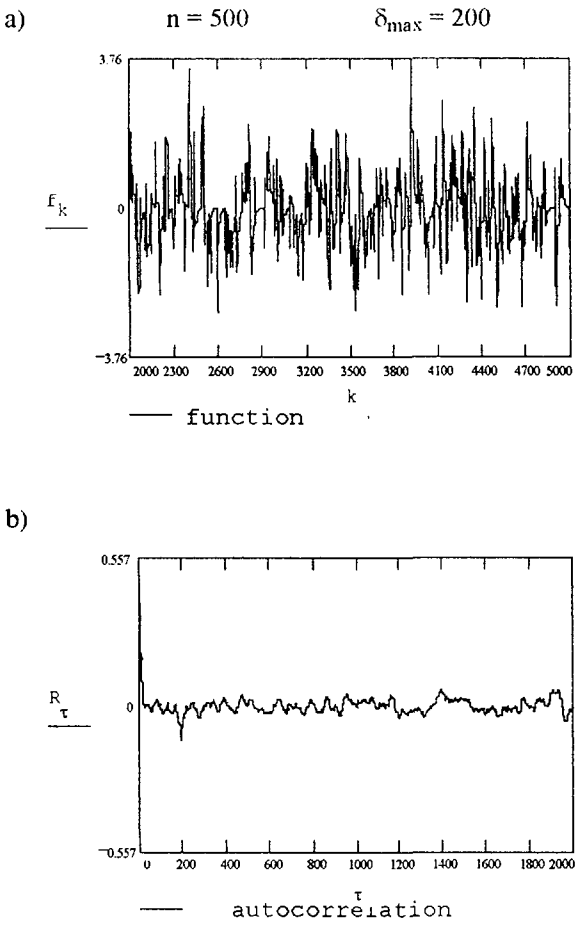

Figure 7. a) A part of the random function f_k which is generated by n exponential impulses with the different lengths (from 0 to δ_{max}). b) Autocorrelation R_τ of the function f_k.

On the graphs of autocorrelation of the above mentioned functions the minimum occurs for the delay time is equal to the maximally possible length of the impulse δ_{max}. The mentioned minimum is less expressed then in a case when the function is generated by impulses which have the same length.

4. DISCUSSION

We have simulated the real blood flow by computer and in this way we obtained a number of random functions very similar to real functions which occur as a consequence of the reflections of ultrasonic waves on red blood cells. From the results it is evident that the autocorrelations of all the functions obtained in this way have an emphasized minimum just when the delay time equals the transit time of erythrocytes through the ultrasonic beam. By the transit time of erythrocytes we can determine the blood flow velocity, which means that blood flow velocity can be determined by autocorrelation calculation. We have shown that it is possible to measure the blood flow velocity in the time domain by the use of autocorrelation technique. This method is particularly suitable for measuring the blood flow velocity in the case when the flow is perpendicular to the ultrasonic beam, which is exactly the most difficult case for measuring the velocity by Doppler effect.

For this reason the combination of these two methods should allow the measuring of blood flow velocity regardless of the angle between the flow and the ultrasonic beam.

5. REFERENCES

[1] D.Censor, W.L.Newhouse, T.Vonz, H.V.Ortega *Theory of Ultrasound Doppler Spectra Velocimetry for Arbitrary Beam and Flow Configurations.* IEEE Trans. Biomed. Eng., 35, 740-751, 1988.

[2] P.Tortoli, G.Guidi, P.Pignoli, *Transverse Doppler spectral analysis for a correct interpretation of flow sonograms,* Ultrasound in Med & Biol., 19(2), 115-121,1993.

[3] C. Kasai, K.Namekawa, *Real-time two-dimmensional blood imaging using an autocorrelation technique,* Proc.IEEE Ultrasonic Symposium, 953-958, 1985.

[4] P.M. Embree, W.D. O'Brien, *The accurate ultrasonic measurement of the volume flow of blood by time domain correlation,* Proc.IEEE Ultrasonic Symposium 1985, 963-966, 1985.

[5] A. Papoulis, *Probability Random Variables and Stochastic Processes,* McGraw Hill Inc., Auckland., 1991.

MODIFIED ID3 ALGORITHM - PREDICTING THE OUTCOMES IN EPIDEMIOLOGY

Zdenko Sonicki, Josipa Kern
Andrija Štampar School of Public Health, Medical School, University of Zagreb
Croatia

ABSTRACT

The epidemiological domain consists of 2684 subjects examined in the period between 1970 and 1971, described by anamnestic and laboratory data, blood pressure and variables presenting living habits. The data on survival in 1990 (living or deceased) were used to make a predictive class. The method based on Quinlan's ID3 algorithm was applied. It uses Shannon's formula on information quantity needed for the subject classification. After 10 runs with different training/testing splits, 70% randomly chosen subjects for training set and 30% for test set, 2 different decision trees with the age as a root were obtained. The absolute predictive accuracy was 65.77% for the first decision tree, and 80.54% for the second one, while relative predictive accuracy was 60.56% for the first decision tree and 67.36% for the second one.

1. INTRODUCTION

Various methodologies can improve prognosis in epidemiological situation. The goal of prognosis is to place a label on a process that manifests itself in an examinee over time [1]. Within the complicated world of epidemiological problem-solving and prognosis, any assistance for the epidemiologist and researcher could be helpful [2].

The aim of this paper is to investigate the possibility of inductive learning method in prediction of outcomes in epidemiology and to evaluate the results.

2. PREDICTION IN EPIDEMIOLOGY

2.1. INDUCTIVE LEARNING METHOD

Original Quinlan's ID3 algorithm was modified by Kononenko and collaborators [3]. The modified ID3 algorithm presumes existence of an appropriate number of learning examples described by set of attributes and by classes representing conditions. It searches for the most informative attribute and constructs decision tree. This method is based on Shannon's expression for information amount necessary to classify an example, E, equals to

$$E=-\Sigma_i\, p_i \log_2(p_i) \qquad (1)$$

where p_i is the a priori probability that the observed example belongs to class i. The informativity of attribute A is defined as

$$Inf(A)=E-I(A) \qquad (2)$$

where

$$I(A)= -\Sigma_v\, p_{vi}\, (p_{vi}/p_v) \log_2(p_{vi}/p_v) \qquad (3)$$

and p_v is the a priori probability that the observed example has the vth value of attribute A, and p_{vi} the probability that the observed example has the vth value of attribute A and belongs to class i. The induction system generates a decision tree automatically by using attribute informativities in decreasing order. Pruning factor ranging from 0 to 9.9 can be used to reduce the decision tree.

2.2. RESULTS EVALUATION

Results are evaluated by calculating absolute accuracy A_a and relative accuracy A_r, as

$$A_a = K/M \quad (4)$$

where K is the number of correctly classified examples, M is the number of testing examples,

$$A_r = (1/M)\ \Sigma_n\ K_n/(R\ P_n) \quad (5)$$

where R is the number of classes, K_n is the number of correctly classified examples from nth class, and P_n is a priori probability of the nth class.

2.3. EPIDEMIOLOGICAL DOMAIN

The epidemiological domain consists of 2684 randomly chosen subjects examined in the epidemiological study "The Study of Fat and Carbohydrate Metabolism Indicators Correlated with the Occurrence of Diabetes in Animal Fat and Oil Consuming Population Groups " in the period between 1970 and 1971 and followed up till 1990. Examinees were described by anamnestic and laboratory data, blood pressure and variables presenting living habits. Data on survival in 1990 (living or deceased) were used to make a predictive class.

According to approximative table of life expectancy for Croatia (1970/71) and data on survival in 1990, the outcome which represents the predictive class was constructed. It was labelled 'bad' for examinees who died without reaching life expectancy period, 'good' for those (living or deceased) who lived longer than expected, and 'unknown' for those alive but below the expected period.

2.4. RESULTS

The decision trees were generated in 10 runs with different, random training/testing splits (training set size of 70% and test set size of 30%) by applying modified ID3 algorithm. They were reduced by pruning factor 4. Out of 10 runs, 7 decision trees were the same, shown in Fig. 1. The outcomes are presented in leaves (final nodes), with related probabilities for each class. Absolute prognostic accuracies were the same, 65.77%, as well as relative prognostic accuracies, 60.56%. The other 3 decision trees, shown in Fig. 2, were somewhat different in structure. Absolute prognostic accuracies were also the same, but much higher than in previous case, 80.54%, with the same relative prognostic accuracies, 67.36%.

3. CONCLUSION

The chosen epidemiological domain, prediction of reaching the life expectancy value is rather fuzzy and hard predictable domain [4,5]. Absolute accuracy of 80.54% and relative accuracy of 67.36% are satisfying. Comparing the results and the outcomes given by random inductive learning method (without any included attributes) showed better prediction. The average of absolute and relative accuracy for "prediction" by random was 42.09% and 33.1% respectively. It means that 38.45% and 34.26% of the extra contribution could be added to given attributes.

4. REFERENCES

[1] RA Miller. Medical Diagnostic Decision Support Systems - Past, Present, and Future: A threaded Bibliography and Brief Commentary. Journal of American Medical Informatics Association 1, 8-27, 1994.

[2] J Ridderikoff. A Diagnostic Decision Support System for Routine Clinical Practice. Journal of Clinical Computing 17, 1-16, 1988.

[3] I Kononenko, I Bratko, E Roškar. A System for Inductive Learning ASSISTANT (in Slovenian). Informatika 10, 43-52, 1986.

[4] E Keeler, R Bell. New DEALEs: other approximations of life expectancy. Medical Decision Making 12, 307-311, 1992.

[5] E Uchida, S Araki, K Murata. Socioeconomic factors affecting the longevity of the Japanese population: a study for 1980 and 1985. Journal of Biosocial Sciences 24, 497-504, 1992.

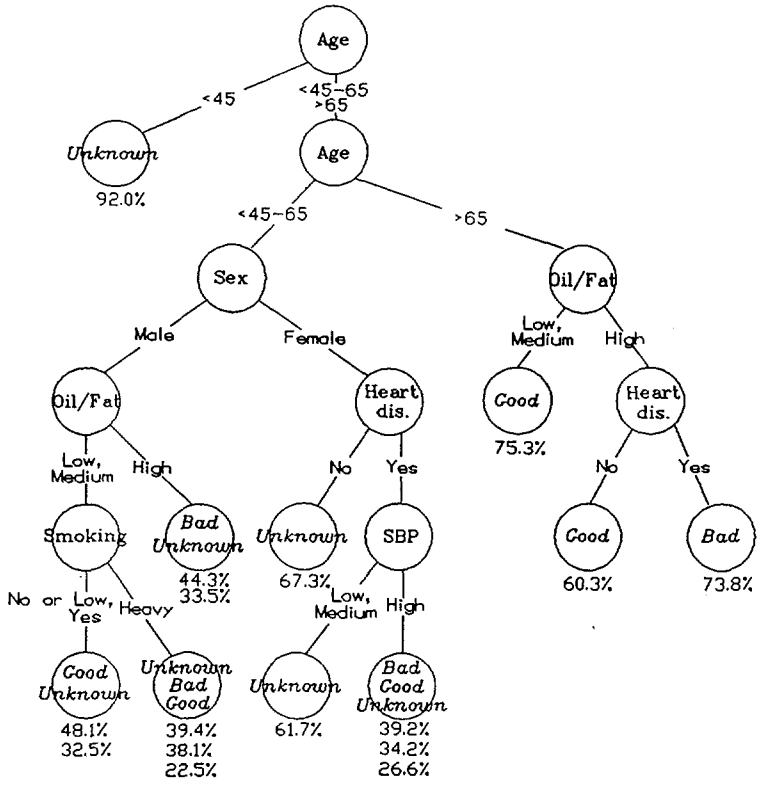

Fig. 1. - First decision tree

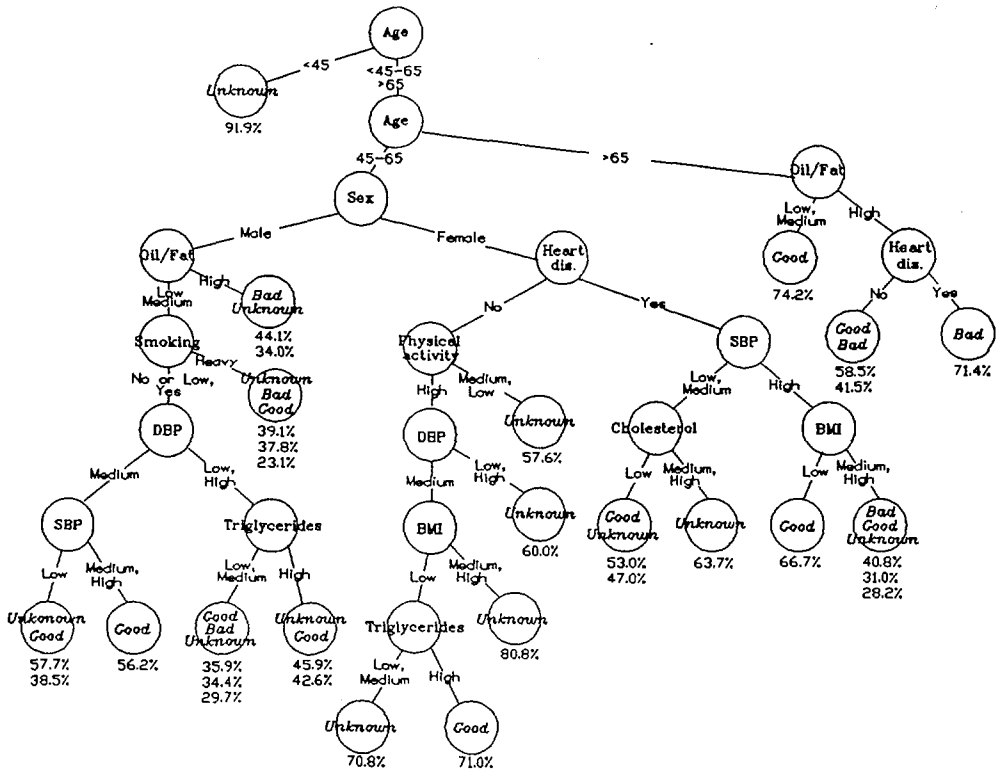

Fig. 2. - Second decision tree

CLASSIFICATIONS, NOMENCLATURES AND STANDARDS IN THE HOSPITAL INFORMATION SYSTEM

Višnja Lovrek
VIP - DATA
Gajeva 12, 41000 ZAGREB

Abstract

This article discusses the indexing and classification of medical terms and describes the most common nomenclatures and classifications in the medicine such as SNOMED, SNOP, ICD, TNM, DRG, ICCS, READ, controlled vocabularies such as MEDLINE with MeSH and UMLS, standards and protocols such as MEDIX and HL7. Special attention to applications within hospital information system is given.

KLASIFIKACIJE, NOMENKLATURE I STANDARDI U BOLNIČKOM INFORMACIJSKOM SUSTAVU

Sažetak

U radu se govori o indeksiranju i klasificiranju medicinskih i ostalih termina, te opisuju najčešće upotrebljavane nomenklature i klasifikacije u medicini kao što su SNOMED, SNOP, ICD, TNM, DRG, ICCS, READ, kontrolirani rječnici kao MEDLINE s MeSHom i UMLS, standardi i protokoli kao MEDIX i HL7. Posebna pozornost dana je korištenju i primjeni unutar bolnijkog informacijskog sustava.

1. INTRODUCTION

The most important precondition for the successful design, production and upgrading of the hospital information system is the determination of the data structure and information to be processed, as well as the selection of the most suitable standards, nomenclatures and classifications for entities and attributes of the system.

The first steps towards a classification of human diseases were taken by John Graunt (1662) in London [1]. Francois Bessier de Lacroix (1706-1777), known as Sauvages was the first who made the systematized classification of diseases: Nosologia Methodica, improved later by British physician William Farr (1807-1883).

It was adopted by the International Statistical Congress in Paris (1855) and became the basic structure for many further classifications. International Statistical Institute adopted a systematic listing of causes of death in 1893 that became the basis for the International Classification of Diseases (ICD). Since 1900 a decennial revision of this listing was undertaken. Beginning with the 6th revision, WHO took over the project in 1946 and added diseases and injuries. Nowadays there are several adaptations of the ICD according to mental disorders (1974), oral and dental medicine (1969), and added diseases and injuries. Nowadays there are several adaptations of the ICD according to mental disorders (1974), oral and dental medicine (1969), oncology (1976), ophthalmology (1977) and neurology (1987). It is interesting to point out that there was known more than 50.000 terms for more than 5000 anatomical structures at the end of the 19th century. These terms were reduced to 5600 Latin words known as nomenclature Basle Nomina Anatomica.

In 1932 the first preliminary edition of the Standardized Nomenclature of diseases and operations was edited by the New York Academy of Sciences. Following editions was prepared by the American Medical Association (1942, 1952 and 1961). In 1965 the College of American Pathologists develops a Systematized Nomenclature of Pathology (SNOP), and in 1975 the same author edits a Systematized Nomenclature of Medicine (SNOMED) according to SNOP.

The 9th revision of the ICD adopted in 1976 by WHO attempted to satisfy the needs by special adaptations: a classification for the oncology was developed (ICD-O).

2. CLASSIFICATIONS AND NOMENCLATURES

Indexing is processing of medical sentences using transformations to the linguistic phrases that results in the structure of methalanguage [2].

Classification is a systematical ordering of all concepts in the field of science. Classification is presented by a list of classification rules or vocabulary of indicated terms. The most important relation for the classification is a hierarchical relation. There are several reasons for indexing or classification:

- standardization of terminology;
- facilitate data archiving;
- presentation of relationships.

Nomenclature is a systematic list of names. Nomenclature must be unambiguous, comprehensive due to the classes and terms and have no redundancy [3].

2.1 International Classification of Diseases, injuries and Causes of Death (ICD)

From its origin, ICD is 1-dimensional classification, the obligatory part of which is coded by 3 digits [4]. Its structural basis does not rest on single semantic dimension, but varies between topography and nosology.

Clinical modification of the ICD (ICD-CM) consists of the origin ICD code followed by two digits. The most recent revision of the ICD is ICD-10, approved by WHO in 1990, that moved from a numeric coding system to an alpha-numeric and comprises about 2000 main categories.

2.2 Systematized NOmenclature of Pathology (SNOP)

SNOP [5] is a nomenclature developed for the needs of pathology and contains essential elements of a classification. It consists of four dimensions: topography (T), morphology (M), etiology (E) and function (F). Each dimension is coded by 4-digit code.

2.3 Systematized NOmenclature of MEDicine (SNOMED)

SNOMED [6], [2] is a systematized multi-axial nomenclature of medically useful terms hierarchically organized where possible and derived from the basic categories of SNOP. The world-wide acceptance and multiple language translations of SNOP support and extend its concept to SNOMED, based on the nature of man as a being to whom health and health care are essential. SNOMED contains more than 45.000 lexemes and became the most comprehensive and voluminous nomenclature in medicine.

SNOMED comprises seven semantic dimensions each with tree structure containing up to five levels. Each code consists of letter (semantic dimension) with up to five characters. Dimensions are topography, morphology, etiology, function, disease, procedure and occupation.

2.4 Tumour-Node-Metastatic tumours (TNM) classification

The TNM classification [1] is a clinical classification of malignant tumours. It resulted from the common observation that the prognosis of a malignant tumour depends on the localization and spread of the tumour. It has three dimensions: tumour size, involvement of regional lymph nodes and metastatic tumours.

2.5 Diagnostic Related Group (DRG) classification

DRG is based upon the Medicare Grouper [7], and is updating according to the Health Systems International edition. Each of the possible DRG groups (about 800) presents the class of patients which can be medically compared and requires the same quantity of health care resources according to the age, sex, diagnosis, procedures, discharge status and mortality. It has been in use in the USA from 1963 and in Europe (GB) from 1988.

2.6 International Classification of Clinical Services (ICCS)

Commission on Professional and Hospital Activities, USA [8] developed the classification system for the clinical services for the inpatient administration data classification. In the USA it is spread in more than 100 hospitals since 1987.

ICCS code consists of 12 or less digits organized in a hierarchical tree, and with four semantic axis: topography, morphology, etiology, and function.

2.7 READ classification

Read clinical classification (named after Dr. Read) [9] covers the field of the entire medicine at the medical record level. It comprises nomenclature including 100.000 terms and the list of synonyms including 150.000 terms. It is hierarchically ordered with 5 digit code and is compatible with other classifications (ICD, ICD-CM).

3. STANDARDS AND CONTROLLED VOCABULARIES

Medicine is becoming increasingly data intensive. In the not too distant past a physician could expected to have store in memory a significant portion of knowledge needed to practice art. Today that model is no longer tenable. The medical database is growing exponentially. The implications of this trend for the teaching and practice of medicine are enormous.

Health professionals attempting to keep a breast of advances in medical knowledge face a formidable task - it was estimated [10] that in 1979 two million articles were published in the biomedical literature annually and that publication growth rate was increasing geometrically. To illustrate the problem: if practicioners attempted to keep up with the literature by reading two articles per day that by the end of one year they would be 55 centuries behind. Clearly there is a serious problem for health professionals to access the medical literature.

3.1 Medical Subjects Heading (MeSH)

The National Library of Medicine's (NLM) MEDLINE database contains over 6.000.000 citations from the biomedical literature published between 1966 and the present. MEDLINE is indexed using Medical Subject Headings (MeSH), a controlled vocabulary of terms derived from the medical literature [11].

MeSH is organized in a linear (alphabetical) form as seen in Index Medicus and also in hierarchical (tree structure) form. The entire list of keywords is organized into seven levels.

3.2 The Unified Medical Language System (UMLS)

The UMLS [12] project is a long-term research and development effort sponsored by the NLM designed to facilitate the retrieval and integration of information from multiple machine-readable biomedical information sources which include biomedical literature, clinical records databanks, knowledge-based systems, and directories of people and organizations. Many terminologies have envolved in many different languages and culture, each with its particular strength. A major disadvantage of this multiplicity is the lack of connections between the concepts in each, so data collected using one terminology cannot be processed directly by the computer with information compiled using a different terminology.

The UMLS is working to overcome this problem in USA. Input into the UMLS may be derived from a variety of existing classifications and nomenclatures such as MeSH, SNOMED, ICD and patient record databanks. The UMLS envisages three knowledge sources to achieve its objectives: The Metathesaurus, The Semantic Network and The Information Sources Map.

3.3 Standard protocols

Interest in standards for electronic medical information exchange between computer systems has been increasing since 1984 and it results in forming at least five standard groups: ASTM E31.11 (American Society for Testing and Materials Committee; HL7 (Health Level Seven); IEEE Medical Information Exchange Committee P1157 (Institute of Electrical and Electronics Engineers); ACR-NEMA (American College of Radiology and Electrical Manufacturers Association); and EFMI WG3 (European Medical Informatics Association Working group 3) /60/.

Additionally HISCC (Health Information Standards Coordinating Committee) has been formed to encourage inter-group communication and sharing of specifications [13].

3.4 MEDIX (IEEE P1157) - Medical Data Interchange Committee

IEEE P1157 MEDIX Committee has been chartered with developing international standards for communication of medical information between heterogeneous healthcare information systems. The IEEE P1157 standards are based upon and will conform to the ISO Reference Model for OSI [14].

To establish a common conceptual model, MEDIX Committee developed the framework model for overall standard into three distinct, but related areas [15]:

- the information model;
- an application level interchange format for message exchange;
- a communication profile.

3.5 Health Level 7 (HL7)

The HL7 Standards Committee [16] is a group of health care institutions, vendors and consultants that have produced standard specification for a number of common interfaces among health care information systems. Level 7 refers to the highest level of ISO communications model for OSI (application level). Since 1987 the HL7 Working Group has developed proposals for the transmission/communications control structure, as well as interface protocol formats for the applications of admission, discharge, transfers, discharge, transfers, orders, entry and query.

4. DISCUSSION

The medical knowledge has grown to the point where the assistance of computers to menage it is necessary. Indexing the content of medical reports requires the data to be organized into appropriate data structures which are capable of recording information at various levels. Classifications and nomenclatures presented are the most spread in the field of medicine, and are suitable for housing medical information and serving as a knowledge base for such information.

The OSI services and protocols have been developed with the goal of meeting the needs of broad class of users. As a result of the differing needs of various applications classes the base standards contain a variety of options. In order to insure interoperability between healthcare institutions and tasks for a particular function it is necessary for all of the participants to select the same set of options.

5. REFERENCES

[1] Wingert F. Medical Informatics. Lecture Notes in Medical Informatics, ed. by DAB Lindberg and PL Reichertz, Springer-Verlag, Berlin, 1981.

[2] Rothwell DJ, Wingert F et al. Indexing Medical Information - The Role of SNOMED. Proceedings of the 13th Annual Symposium on Computer Application in Medical Care, IEEE Computer Society Press, Washington DC, 1989, pp 534-539.

[3] Mađarić M, Lovrek V. Klasifikacija bolesti i šifriranje dijagnoza u bolničkom informacijskom sustavu. 1. Savjetovanje o informatici u zdravstvu, Zdravstvo 3, Zagreb, 1986, pp 330-335.

[4] Međunarodna klasifikacija bolesti, povreda i uzroka smrti (prema 9. reviziji iz 1975.god.), Institut za dokumentaciju zaštite na radu, Niš, 1979.

[5] SNOP - Systematized Nomenclature of Pathology. College of American Pathologist, Chicago, 1969.

[6] Cote AR. SNOMED - Systematized Nomenclature of medicine. College of American Pathologists, Illionis, 1977.

[7] Fleurette F, Fieschi M. The use of Diagnosis Related Groups: Proposition. Medical Informatics Europe '90 Proceed., Glasgow, Lecture Notes in Medical Informatics, ed. Rienhoff O and Lindberg DAB, Springer-Verlag 1990, pp 149-155.

[8] Mendenhall S. The ICCS Code: A New Development for an Old Problem. Proceedings of the 11th Annual Symposium on Computer Application in Medical Care, IEEE Computer Society Press, Washington DC, 1987, pp 703-709.

[9] Read JD. The Read Clinical Classification (Read Codes). Proceedings of Medical Informatics Europe '90, Glasgow, ed. by Rienhoff O and Lindberg DAB, Springer-Verlag, Berlin, 1990, pp 645-649.

[10] Lowe HJ, Barnett GO. MicroMesh: A Microcomputer System for Searching and Exploring the National Library of Medicine's medical Subject Headings (MeSH) Vocabulary. Proceedings of the 11th Annual Symposium on Computer Application in Medical Care, IEEE Computer Society Press, Washington DC, 1987, pp 717-720.

[11] Dimse SS, O'Connell MT. Cataloging a medical Curriculum Using MeSH Keywords. Proceedings of the 12th Annual Symposium on Computer Application in Medical Care, IEEE Computer Society Press, Washington DC, 1988, pp 332-336.

[12] Cimino JJ. Representation of Clinical Laboratory Terminology in the Unified Medical Language System. Proceedings of the 15th Annual Symposium on Computer Application in Medical Care, IEEE Computer Society Press, Washington DC, 1991, pp 199-203.

[13] Huff SM, Evans RS, Gandhi S. An LIS to HIS Interface Using CCITT Standard Protocol. Proceedings of the 13th Annual Symposium on Computer Application in Medical Care, IEEE Computer Society Press, Washington DC, 1989, pp 692-695.

[14] Harrigton JJ, Benson TJR, Spector AL. IEEE P1157 Medical Data Interchange (MEDIX) COMMITTEE Overview and Status Report. Proceedings of the 14th Annual Symposium on Computer Application in Medical Care, IEEE Computer Society Press, Washington DC, 1990, pp 230-234.

[15] Ostler DV, Harrington JJ, Hannemyr G. A Common Reference Model for Healthcare Data Exchange - P1157 MEDIX System Architecture. Proceedings of the 14th Annual Symposium on Computer Application in Medical Care, IEEE Computer Society Press, Washington DC, 1990, pp 235-239.

[16] Rishel W. Pragmatic Considerations in the Design of the HL7 Protocol. Proceedings of the 13th Annual Symposium on Computer Application in Medical Care, IEEE Computer Society Press, Washington DC, 1989, pp 687-690.

CHARACTERISTICS OF SOFTWARE ENGINEERING IN MEDICAL INFORMATICS

Miroslav Mađarić

Department of Medical Informatics,
Graz University Hospital,
Auenbruggerplatz 9/III, A-8036 Austria

Summary

In the paper the author is presenting his experiences over a period of 20-years in hospital departmental applications in the form of hints for software engineering professionals in the field. Three areas of interest are described: hospital data, medical user characteristics and integration issues. A short review of software engineering (SE) characteristcs in medical informatics is presented, with emphasis on the rapid application development techniques. The issues of functionality, development efficiency, application maintenance and development interface are discussed.

1. INTRODUCTION

The author of this paper has experience in developing medical information systems (MIS) with both SE knowledge and the overview of medical theory and everyday operation. These facts are prerequisites for realizing the characteristics of the application area (medicine) and related challenges to the information technology (IT) tools.

Pitfalls in the area of medical informatics (MI) are not rare. When we exclude severe "human errors", such as the lack of concept, so called "objective circumstances" are always related to the peculiarity of the application area (medicine) and IT tool (SW, HW) imperfection.

Medicine is a very complex discipline in each of its characteristics. This relates to medical data, end users and organisation of everyday operation of medical institutions. The IT tools of yesterday were not able to meet justified information processing needs in medicine: too slow, too small and too expensive computers with no real solution for the integration needs in MIS.

It seems that we now stand at the eve of solving all of the problems mentioned:

- powerful and affordable workstations
- local distribution, however coupled
- possibility of integrating a number of different applications or subsystems (e.g. local subsystem for CT control and HIS will be integrated on the same PC under the Windows user interface, although running on different computers).

During the dawn of advanced MI, a few "teething troubles" of the new IT generation remain: The operating stability of PC, network and distributed DB in the large scale systems, plus one not yet solved problem: Efficient development of medical applications, which is the topic of this paper.

In the development and maintenance of MIS almost all characteristics of the application field are present [1,2]:

- medical data are very complex and subject to frequent structural changes
- medical endusers are not prepared to deal extensively with the MIS development
- organizational procedures within the medical institutions are often not well defined or are subject to arbitrary implementation or changing
- EDP professionals are rarely suitably trained for the medical environment
- medical users are not prepared to change their habits to adapt to standardized EDP solutions

All these problems reflect severely on development and maintenance of MIS: classical SE methods failed to be as successful in the medical environment as they were in other fields. Thus, the question: "Is SE in MI becoming a science (instead to be only a craft)?" obviously requires a positive answer [3]. So, as the newest IT advances bring the solution to an operational level of MIS, so the new SE technologies give hope for a solution in the development and maintenance of MIS.

2. WHAT IS RAPID APPLICATION DEVELOPMENT (RAD)?

As the dream of middle-age alchemists was converting base materials into gold and precious stones, the ultimate wish for strategic developments in the IT field is application development without EDP-trained professionals. So, trends in programing language improvement were aimed at obtaining better SW-products from broadly trained EDP-experts within less time. The next logical advance from 3GL and 4GL development was a 5GL programing language that understood restricted natural language, and was aimed at development through the endusers [4].

Unfortunately, this prospect is, in the mid-90es, not likely to be achieved soon. Instead of 5GL, high productivity application generators, based on graphic user interfaces, entered the SW-development market, mainly due to the major improvement of PC performance. This technological progress brought two main advantages to the endusers: Those with some EDP-skills acquired the tool for individual development of local applications. The others could interactively assist the SE-experts in the process of SW-development and develop parts of the application themselves (usually ad-hoc reports).

Predecessor to the term of "Rapid Application Development" was the term "Rapid Prototyping". Prototyping is the process of producing prototypes for showing the layout and functionality of parts of the system developed. When these prototypes are not disposed of, but the same code (modified to some extent) is used for obtaining the end product, we are refer to versioning or evolutionary prototyping [4]. When this prototyping is fast enough for the enduser to take an active part in it ("userside SE"), we are dealing with the RAD. The prerequisites for the successful RAD are [5]:

- High productivity SE-tool (data modelling, layout and functions generation)
- running on efficient development HW (integrated for corporate development when used for complex systems development)
- used by highly trained SE-experts (with emphasis on interactive communication with the enduser).

3. HOW COULD RAD BRING MAJOR IMPROVEMENTS IN MIS DEVELOPMENT AND MAINTENANCE ?

RAD brings following solutions for the MIS development problems mentioned in the introduction:

- complexity of medical data causes the main problems within the specification phase: these are to be solved interactively with the enduser during the prototyping procedure
- medical endusers will be motivated to deal intensively with the MIS development (within a few hours or days, seeing how their system grows)
- RAD supports the changes in organizational procedures and solves the problem of medical data dynamics on enduser site or even through the enduser itself
- the decreasing complexity of programing language and other SE development tools, facilitates the EDP training for medical environment

The advantage of RAD within the medical environment is the possibility of developing the application without the classical model of "specification - development - testing", where the first and third step usually require major involvement of the enduser.

4. EXPERIENCES

Experiences in the Department of Medical Informatics (Graz University Hospital, Austria) with some types of RAD are very positive. On-site creation of ad-hoc reports is an example of rapid development, where an enduser sits near the programmer, obtaining his/her report in a few minutes. Of course, new IT solutions are able to offer to skilled endusers their own development

environment for presentation and statistical applications.

Another of our experiences is the usage of our own programing system SYGMA (SYstem for General Medical Applications) for prototyping purposes [6]. With this parameter driven system, based on DEC FMS (Forms Management System) screen layout editor, our programmers are able to develop a functioning prototype within a few hours or days, depending on its complexity. These prototypes are presented to the endusers and their remarks are used as specification for further refinement or for including new functionalities. Some of the final refinements are made on-site during the beta-test procedure. Using this procedure, departmental application of moderate complexity (5 screens, 50 data fields) can be developed within 3 iterations in one week.

5. "3-DAY-CYCLE" FOR MEDICAL APPLICATION DEVELOPMENT

System described does not represent any kind of competition for new graphical SE tools used for RAD. New SE tools will bring substantial improvement in the field of medical applications development. This improvement should touch three important issues of application development:

- sufficient functionality
- ease and speed of application development
- flexibility and consistence of maintenance

We consider that simple medical applications (e.g. local medical documentation system, patient archives etc.) should be developed within three days (5-10 screens or 30-50 data fields). This "3-day-cycle" should encompass following steps of SE (schematically presented in Figure 1):

1. **day**: Studying the data and procedures description, data and functions modelling, layout design.
2. **day**: Presenting early prototype to the enduser, correcting and improving it in several iterations in enduser's presence.
3. **day**: Presenting mature prototype to the enduser on location, correcting when necessary, releasing beta version for testing.

6. DISCUSSION

The approach proposed is to be tested in the Department for Medical Informatics in Graz, Austria, using the SE tool for development of medical documentation system in the teaching hospital in Graz. This SE tool is produced by the Austrian company SYSTEMA which also produced the application SW for the HIS in Styrian hospitals. Functionality and efficiency of this SE-tool will be compared to our existing system SYGMA, as well as to the new PC-based graphical SE-tools (MS-ACCESS and GUPTA-SQLbase).

7. REFERENCES

[1] Madjaric M, Gell G. Hints for applications development in hospital departmental systems: 20 years of experience. In: MIE 93. Reichert A, Sadan BA, Bengtsson S, Bryant J (eds). London: Freund Publishing House, Ltd, 1993: 231-234.

[2] Slack W V. Assessing the clinician's use of computers (Editorial), *M.D. Computing*1993, 10:357-360.

[3] Blum BI, Timmers T. Software Engineering in Medical Informatics. In: Software Engineering in Medical Informatics. Timmers T, Blum BI (eds). Amsterdam: North-Holland, 1991:xi-xvi.

[4] Sommerville I. *Software Engineering*. Wokingham, England: Addison-Wesley Publishing Co., 1991.

[5] -. Prototyping and RAD. In:*CASE 93*. ADV-Arbeitsgemeinschaft für Datenverarbeitung, Vienna, 1993:6-121.

[6] Madjaric M, Gell G. SYGMA: An Object-oriented Medical Data Processing System. In: MIE 91. Adlassnig KP, Grabner G (eds). Vienna: Springer-Verlag, 1991: 127-131.

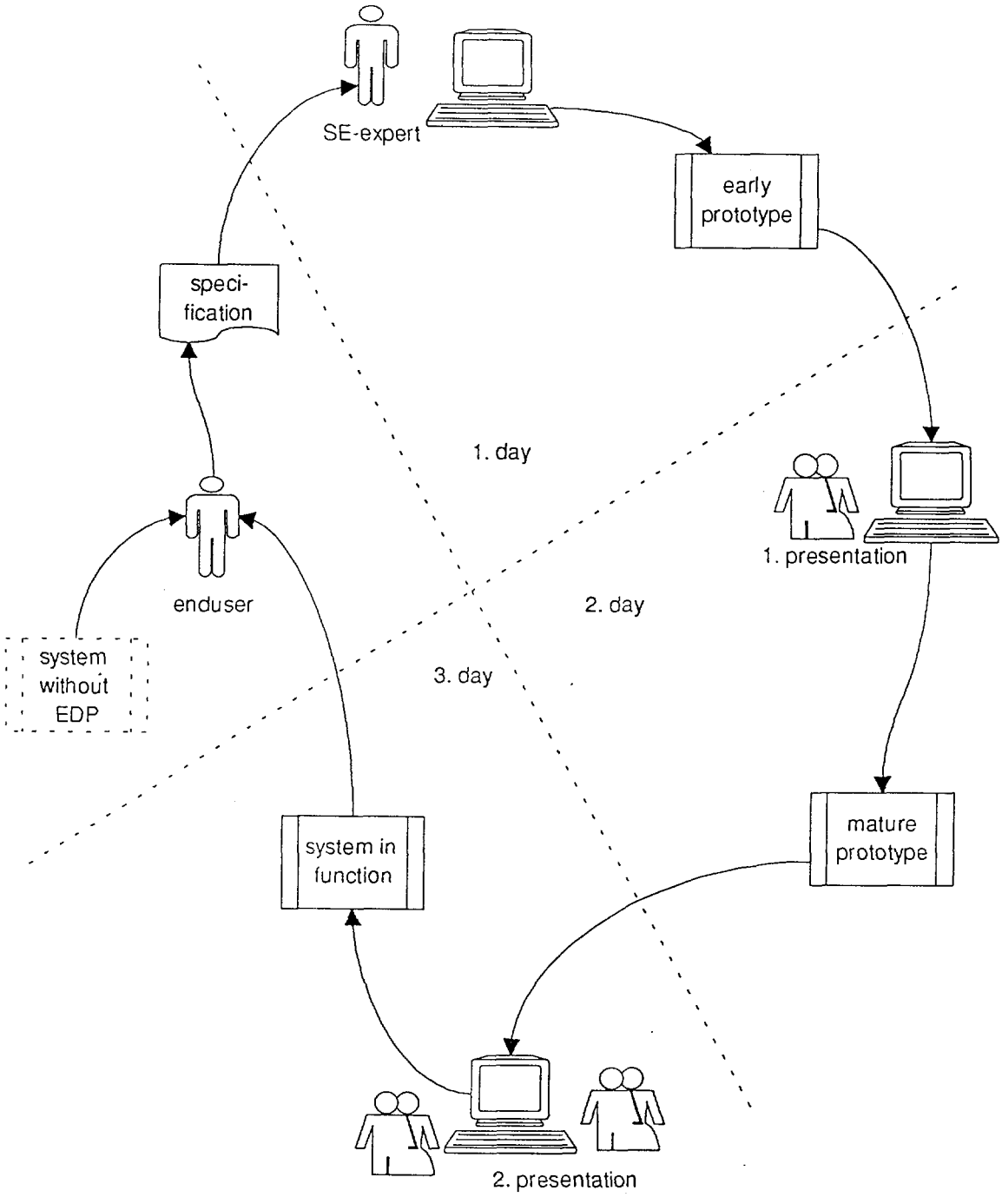

Fig. 1: "3-day-development" using RAD tools

EPIDEMIOLOGICAL INFORMATION SYSTEM BASED ON SMALL AREA ANALYSIS

1 Marijan Erceg, 2 Gjuro Deželić
1 Dom Zdravlja Split, Starčevićeva 1, Split
2 Škola narodnog zdravlja "Andrija Štampar" Medicinskog fakulteta u Zagrebu, Rockefellerova 4, Zagreb

Abstract

A model of information system for epidemiologic research based on method of small area analysis is developed and implemented on a personal computer. As an example morbidity analysis of chronic obstructive pulmonary disease is presented. The possibilities of using the model in epidemiologic research, in evaluation and planning of health care are discused.

EPIDEMIOLOŠKI INFORMACIJSKI SUSTAV ZASNOVAN NA ANALIZI MALIH PODRUČJA

Sažetak

Model informacijskoga sustava za kontinuirano epidemiološko istraživanje zasnovan na metodi analize malih područja, kreiran je i implementiran na mikroračunalu. Kao primjer primjene prikazana je analiza morbiditeta od kronične opstruktivne bolesti pluća. Razmatrane su mogućnosti primjene modela u epidemiološkim istraživanjima te evaluiranju i planiranju zdravstvene zaštite.

1.INTRODUCTION

Development and use of health information systems must enable feasible generation of population health status information which can, as on global so on local level, differentiate environmental influence on the population health. Development of the epidemiological information systems based on small area analysis enables researching populations which are dispersed in less clusters which are more homogeneous in their health caracteristics and thus more sensitive on the environment and socioeconomic factors influence (1,2).

Small area analysis is being used increasingly for research in community medicine, but there are no numerouse examples, and this may be explained in part by the practical difficulties which are encountered in carying these out (2). In ideal circumstances epidemiological information system based on small area approach must have full access of quality health data for entire population (with verified diagnoses) which was being collected continuously, and they must have accurate demografic data for small area. This circumstances can hardly be met in common practice. Difficulties appear when cases can not be allocated in the small area weather for lack of data weather for migration of population. Low number of cases can constrain analysis wich can be overcome by aggregation of data (for example over a group of diseases, over number of years, over number of small areas). These results must be interpreted cautiously (3,4,5). Analysing the results it is necessary to be careful not to attribute statistical importance just to chance variation. One of the possible approauches is to describe the distribution of a phenomenon with three

indicators: one showing the absolute counts of the phenomenon; second showing rates; and the third showing which rates are statistically high and which are statistically low (6). The probability value itself,calculated on the assumption that the true geographic distribution is uniform. , may be a form of measure to distinguish merely random departure from the norm on one hand, and on the other hand, a degree of departure which is substantial enough to be considered non-random. A non-random departure in either direction implies an underlying cause that explanation be demanded (7).

Even if there is statistically significant variation, the size or importance of the differences among the small areas remains in question, since with populations large enough even tiny differences will produce statistically significant result (8).

The aim of this research is to establish a model of epidemiological information system based on the method of small area analysis.

2. METHODS

Methodological principles of this study is to applay methods of descriptive epidemiology, statistics and informatics.

Standard information system development methodology will be applied, which includes conceptual, logical and phisical modelling of the information system, which includes data modeling, processes modelling, database modelling, programs modelling and implementation (9,10).

Data base has been designed and implemented by using standard microcomputer database software FOXPRO-LN running under MS-DOS on IBM - 286 microcomputer.

Possibility of the model implementation has been tested on routinely collected data as a half year sample (year 1991) of everyday primary health care practice in Medical Centers in the city of Split. Small areas have been defined by the local community areas according to the city organization in 1991. Number of inhabitants has been taken from 1991 Census data (11). Group of diseases has been classified under ICD (IX-th revision) (12).

Statistical method has been used wich for low observed counts ($x < 40$) assumed the Poisson probability which was calculated from the recursion formula (13,14):

$$Pr(0)=Exp(-Lambda) \quad (1)$$

$$Pr(k+1)=Pr(k)* Lambda/(k+1)$$

$$PoisProb(x)=Sum(Pr(k)) \text{ for } k=0,1...x \text{ for } x <= Lambda$$

$$PoisProb(x)= 1-Sum(Pr(k)) \text{ for } k=0,1....x-1 \text{ for } x > Lambda$$

For high observed counts ($x > 40$) approximation to the normal distribution is assumed and probability values are calculated from the Z scores by looking up in a table . Z score is calculated from (14):

$$Z=(x-Lambda)/Sqrt(Lambda) \quad (2)$$

3. RESULTS

Database model is created according to the data model. Entities are shown with series of interacted normalized relations.

Database model is determined by theese relations:

1.SEX (Sex code, Sex name)
2.AGE (Age group, Inferior limit, Superior limit)
3.STATE (State cod, State name)
4.PRIMARY HEALTH TEAM (Primary health team code, Name)
5.ADRESSES (Adress code, House number, Name)
6.SMALL AREA (Small area cod, Small area name)
7.ADRESSES-SMALL AREA (Adresses code ,House number, Small area code)
8.DIAGNOSES (Diagnosis code according to ICD, Diagnosis name, Type of disease)
9.GROUPES OF DISEASES (Group of disease code, Group name)
10.DIAGNOSES-GROUPES (Diagnosis code according to ICD, Group of disease code)
11.NUMBER OF INHABITANTS (Small area code, Sex code, Age group, Number of inhabitants)
12.PATIENT (Unique inhabitants code, Second name, First name, Sex code, Primary health team code, Adress code, House number, State code, First date of registration, Last date of registration)

13.PATIENTS-DIAGNOSES (Unique inhabitants code, Diagnosis code according to ICD, Date of diagnose)
14.NUMBER OF PATIENTS (Small area cod, Group of disease code, Sex code, Age group, Number of patient)
15.NUMBER OF NEWPATIENT (Small area cod, Group of disease code, Sex code, Age group, Year, Number of new patient
(NNP) for January, NNP for February, NNP for March, NNP for April, NNP for May, NNP for June, NNP for July, NNP for August, NNP for September, NNP for October, NNP for November, NNP for December)

In tables 1 and 2 are presentated results of the model implementation, which are reffered to cronic obstructive pulmonary disease.

4. DISCUSION

Morbidity data of cronic obstructive pulmonary disease (COPD) will serve as an example of possible implementation of the model based on small area approach.

COPD is defined as a condition in which there is chronic obstruction to airflow due to chronic bronchitis and/or emphysema. Exept smoking as one of the main risk factors, air polution is another contributory factor. Exacerbation of COPD are clearly related to periods of heavy pollution with sulphur dioxide and particulate matter (15).

Results presented in tables 1 and 2 show that COPD is an important medical problem, especially in older age. Proportion is greatest for under the age of sixty, 0,09 for men and 0,04 for women. According to all surveys approximately 10 - 25 percent of adult population have COPD, and men are more often affected then women (15). Observed results are lower then expected, and more men are found affected.

Analaysing the results for those above the age of sixty (table 2) differences in distribution of disease among small areas are observed. Signifficantly higher number of cases appears in areas Grad, Kman, Lovret, Lučac-Manoš, for both sexes, and in Spinut for men. Results for areas Žnjan for women and Stomorske for men should be interpreted cautiously due to the low number of observed cases.

Whether these differences are conditioned by environmental factors or

GROUP OF DISEASE. CHRONIC OBSTRUCTIVE PULMONARY DISEASE

SEX	WOMEN				MEN			
AGE	40 - 59		> 60		40 - 59		> 60	
SMALL AREA	Xo	p	Xo	p	Xo	p	Xo	p
BAČVICE	16	0.02	22	0.04	5	0.00	20	0.10
BLATINE-ŠKRAPE	3	0.00	3	0.01	4	0.00	4	0.02
BOL	18	0.01	32	0.04	24	0.01	31	0.10
BRDA	15	0.02	6	0.01	20	0.02	11	0.06
DONJE SITNO	.		.		1	0.02	2	0.20
GORNJE SITNO	2	0.05	1	0.05	.		1	0.14
GRAD	17	0.02	32	0.08	11	0.01	32	0.19
GRIPE	8	0.01	25	0.04	8	0.01	28	0.12
GROHOTE	.		3	0.05	.		3	0.12
KAMEN	.		.		.		2	0.08
KMAN	29	0.03	41	0.10	20	0.02	45	0.26
KOCUNAR	11	0.02	8	0.03	12	0.02	16	0.13
LOKVE	13	0.01	15	0.03	9	0.01	19	0.10
LOVRET	33	0.02	83	0.09	16	0.01	102	0.16
LUČAC MANOŠ	15	0.01	31	0.06	5	0.00	28	0.13
MEJAŠI	1	0.00	1	0.00	9	0.02	7	0.08
MEJE	5	0.01	6	0.02	3	0.00	13	0.13
MERTOJAK	19	0.02	17	0.03	19	0.01	22	0.10
NESLANOVAC	5	0.01	11	0.04	6	0.01	2	0.02
PLOKITE	23	0.02	22	0.04	16	0.01	26	0.13
PODSTRANA	3	0.01	3	0.01	6	0.01	4	0.03
PUJANKE	10	0.01	7	0.01	12	0.01	7	0.01
RAVNE NJIVE	10	0.01	7	0.02	15	0.02	10	0.06
SIROBUJA	.		1	0.01	2	0.01	1	0.02
SLATINE	2	0.02	1	0.02	.		1	0.05
SPINUT	27	0.02	20	0.03	14	0.01	39	0.15
SPLIT 3	15	0.01	9	0.01	17	0.01	12	0.04
SRINJINE	1	0.01	2	0.03	.		3	0.09
STOBREČ	1	0.00	4	0.03	1	0.00	.	
STOMORSKA	2	0.05	2	0.10	1	0.02	4	0.40
SUČIDAR	15	0.01	10	0.01	16	0.01	15	0.05
ŠINE	2	0.01	1	0.01	2	0.01	2	0.06
TRSTENIK	21	0.02	7	0.02	10	0.01	11	0.06
VAROŠ	7	0.01	13	0.03	14	0.01	13	0.08
VISOKA	6	0.01	4	0.01	8	0.01	5	0.05
ŽNJAN	.		6	0.11	1	0.04	1	0.01
ŽRNOVNICA	2	0.01	1	0.01	3	0.01	7	0.10
UKUPNO	357	0.01	457	0.04	312	0.01	549	0.09

LEGEND: Xo = observed frequencies p = proportion

Table 1. A report from the database containing data about chronic obstructive pulmonary disease in local community units in the city of Split

by different health standards is to be researched in addition. Fact that areas with a signifficant number of disease are close to the industrial zone should be considered.

It has to point out that output information, which can be obtained from the data which system contained in this moment, can not explain observed differencies and can serve as a preliminary information for cause - effectivnes analysis which can be done after further investigations about characteristics of the population and environment. Population and environmental data must be structured and linked by unique key that represents small area organisation (16).

Relational database model showed good characteristics during implementation of the system. Data structure enables various ways of data analaysis by changing the values of atributes in the relations. For example, changing the age limits in relation age we can change age groups; changing the atributes in relation diagnoses - group of diseases we can change sorting principle.

5. CONCLUSION

Epidemiological information system based on small area analysis has been developed and implemented on the microcomputer and has proved to bee a good tool for continuous epidemiological research.

Output information showed that it is possible to produce easy understandable and comparable data about population health status. Differencies in distribution of diseases among the small areas predicts the differences in population, environment and health standard characteristics which can influence population healt status.

In order to explain differencies in characteristics of small areas by output information and to make epidemiological conclusions, further research is needed. The system can not be based only on data produced in everyday health service practise. It is necessary to define which extra data needs to be collected and to consider mechanism of their processing.

GROUP OF DIAGNOSES: CHRONIC OBSTRUCTIVE PULMONARY DISEASE

AGE: > 60

SEX	WOMEN				MEN			
SMALL AREA	Xo	Xe	P(x)	I	Xo	Xe	P(x)	I
BAČVICE	22	17.69	0.1802	2	20	18.28	0.3741	2
BLATINE-ŠKRAPE	3	15.18	0.0002	1	4	15.80	0.0005	1
BOL	32	27.83	0.2382	2	31	28.84	0.3680	2
BRDA	6	15.63	0.0051	1	11	16.06	0.1240	2
DONJE SITNO	-				2	0,53	0.0994	2
GORNJE SITNO	1	0.66	0.4831	2	1	0.62	0.4621	2
GRAD	32	14.58	0.0001	3	32	15.09	0.0001	3
GRIPE	25	19.76	0.1437	2	28	20.50	0.0663	2
GROHOTE	3	2.27	0.3960	2	3	2.22	0.3826	2
KAMEN	-				2	2.31	0.5934	2
KMAN	41	15.00	0.0000	3	45	15.44	0.0000	3
KOCUNAR	8	10.56	0.2734	2	16	10.92	0.0884	2
LOKVE	15	16.96	0.3751	2	19	17.57	0.3976	2
LOVRET	83	30.81	0.0000	3	102	56.53	0.0001	3
LUČAC-MANUŠ	31	18.67	0.0055	3	28	19.35	0.0378	3
MEJAŠI	1	7.38	0.0052	1	7	7.72	0.4927	2
MEJE	6	9.76	0.1460	2	13	9.05	0.1279	2
MERTOJAK	17	19.62	0.3267	2	22	20.23	0.3759	2
NESLANOVAC	11	10.49	0.4780	2	2	10.47	0.0019	1
PLOKITE	22	17.27	0.1541	2	26	17.93	0.0430	3
PODSTRANA	3	10.14	0.0093	1	4	10.47	0.0215	1
PUJANKE	7	22.13	0.0002	1	7	67.27	0.0001	1
RAVNE NJIVE	7	14.51	0.0238	1	10	15.09	0.1142	2
SIROBUJA	1	3.53	0.1328	2	1	3.73	0.1135	2
SLATINE	1	1.71	0.4901	2	1	1.86	0.4452	2
SPINUT	20	22.13	0.3765	2	39	22.99	0.0014	3
SPLIT 3	9	26.02	0.0001	1	12	26.89	0.0011	1
SRINJINE	2	2.73	0.4863	2	3	2.84	0.5400	2
STOBREČ	4	4.58	0.5170	2	-			
STOMORSKA	2	0.73	0.1663	2	4	0.89	0.0130	3
SUČIDAR	10	25.49	0.0004	1	15	26.36	0.0120	1
ŠINE	1	3.11	0.1833	2	2	3.11	0.3	2
TRSTENIK	7	14.65	0.0220	1	11	15.18	0.1731	2
VAROŠ	13	14.79	0.3836	2	13	15.18	0.3462	2
VISOKA	4	9.44	0.0418	1	5	9.76	0.0767	2
ŽNJAN	6	1.92	0.0138	3	1	10.83	0.0002	1
ŽRNOVNICA	1	6.22	0.0144	1	7	6.48	0.4703	2
UKUPNO	457	453.95			549	544.39		

LEGEND: Xo = observed frequecies
Xe = exppected frequences
P(x) = probabilities
I = level of signifficans indikator: 1 - lower then expected
2 - no signifficant differences
3 - higher then expected

Table 2. A report from the database containing data of chronic obstructive pulmonary disease

6. REFERENCES

1. Deželić GJ, Deželić N, Hrastić-Novak L, and Kopjar B. A Space Oriented Approach in the Analysis of the Health Status of the Population, In: Proceedings 9th International Congress Medical Informatics Europe'90. Glasgow, August 20-23,1990.Berlin-Heidelrberg-New York-London -Paris - Tokyo-Hong Kong-Barcelona: Springer-Verlag 1990: 592-596.
2. Carstairs V. Small Area Analysis and Health Service Research. Community Medicine 1981;3: 131-139.
3. Eliott P. Data requirements and methods for analysing spatial patterns of diseas in small areas. In: Data requirements and methods for analysing spatial patterns of disease in small areas, Extended summaries from a WHO Consultation. Rome, 22-24 October 1990. Copenhagen: WHO Regional office for Europe 1991: 20-24.
4. Johnson Z, Johnson H, McNee N andLacey G. The Epidemiological Information System. In: Proceedings 7th International Congress Medical Informatics Europe'87. Rome, September 21-25. 1987: 113-120.
5. Thomsen I. Population data for small area studies. In: Data requirements and methods for analysing spatial patterns of disease in small areas, Extended summaries from a WHO Consultation. Rome, 22-24 October, 1990. Copenhagen: WHO Regional office for Europe 1991: 20-24.
6. Choynowski M. Maps based on probabilities. Journal of the American Statistical Association 1959; 54:385-388.
7. McGlashan N. Uses of the Poisson probability model with human populations. Pacific Viewpoint 1976;17:167-174.
8. Dierh P. Small Area Statistics:Large Statistical Problems. AJPH 1984; 74: 313-314.
9. Strahonja V, Varga M i Pavlić M. Projektiranje informacijskih sustava. Zagreb: Zavod za informatičku djelatnost Hrvatske i INA-INFO, 1992.
10. IBM CORPORATION. TEHNICAL PUBLICATIONS / SYSTEMS INSTALLATION MANAGEMENT. Systems development method (SDM). New York: IBM Corporation, 1986.
11. Popis stanovništva 1991.godine. Prvi rezultati po mjesnim zajednicama. U: Dokumentacija 811. Zagreb: Zavod za statistiku Republike Hrvatske, 1991.
12.International classification of impairements, disabilities and hendicaps. Geneva: World Health Organization, 1980.
13. Power M, Thompson M, Heese H, Louw H, Khan M. Priorities for provision of health care services for children in the Cape Province. SAMJ 1991;80:481-486.
14. Rosner B. Fundamentals of biostatistics. Boston: Duxbury Press,1982.
15. William G, Braunwald E. Chronic bronchitis, emphysema, and airways obstruction In: Harrison's ed: Principles of Internal Medicine. 9 edition. New York: Mc Graw-Hill book company, 1987: 1024-1026.
16. Pukkala E. Record linkage. In: Data requirements and methods for analysing spatial patterns of disease in small areas, Extended summaries from a WHO Consultation. Rome, 22-24 October, 1990. Copenhagen: WHO Regional office for Europe 1991: 59-60.

THE HEALTH ECOLOGICAL BASE V O D E

Berezina Matoković
Nives Štambuk-Giljanović
Zorana Klišmanić

Abstract

The ecological approach to the disease facilitates the understanding of the reasons for the multiplity of causal factors and the finding of those on which the preventive measures will be easily and successfully directed. That is the reason why data integration of the individual and the space for getting insight into the existing condition from medical and health ecological point of view is necessary. The ecological need to sum up the work of the water research and to estimate the future water quality trends by observing the relevant parameters as influental ecological factors for the health of the population resulted in relation data base VODE. Besides waters data it also integrates the data group of patients and from the medical-ecological standpoint is situable for the several years study of trends of existing water supply system condition with special survey of the results of the water quality analyses in view of the recognition of the actual pollutions that are significant for the health problems of population, group and individuals. Health worker gets his informations by putting questions and brings them into correlation with health condition of patient and then solves health problems and plans necessary interventions.

ZDRAVSTVENO-EKOLOŠKA BAZA V O D E

Sažetak

Ekološki pristup bolesti olakšava razumijevanje uzroka multipnosti uzročnih faktora i pronalaženje onih na koje će se lako i uspješno usmjeriti preventivne mjere. Stoga je nužna integracija podataka o pojedincu i prostoru za dobivanje uvida u postojeće stanje s medicinskog i zdravstveno-ekološkog stanovišta. Ekološka potreba da se sumira rad na ispitivanju voda i procijene buduća kretanja kvalitete voda putem praćenja relevantnih parametara, kao utjecajnih ekoloških faktora na zdravlje stanovništva, rezultirala je relacijskom bazom podataka VODE. Ona integrira uz podatke o vodama i skup podataka o bolesnicima i prikladna je s medicinsko-ekološkog stanovišta za proučavanje višegodišnjih trendova o postojećem vodoopskrbnom stanju, s posebnim pregledima rezultata analiza kvalitete voda u smislu prepoznavanja aktualnih zagađenja bitnih za zdravstvene probleme populacije, grupa u njoj i pojedinaca. Zdravstveni radnik upitima dolazi do informacija koje povezuje s zdravstvenim stanjem bolesnika te rješava zdravstvene probleme i planira nužne intervencije.

FOREWORD

It is well known that the health is influenced by hereditary factors on the one hand and environmental factors on the other hand [1-3]. In regard of that the ecological approach to the disease facilitates the multiplity understanding of causal factors in the pathogenesis and finding those factors on which preventive measures will be easily and successfully directed. That is why the space data integration is suitable for getting insight into existing ecological situation.

In this papaer the special attention is paid to the data volume of Dalmatian (Southern Croatian) aquatory, i.e. to the environmental factor which significantly influences the quality of population living.

Ecological need to sum up the work on water quality examination and to estimate future water quality trends brought us to the environmental monitoring. It is necessary to notice that in present conditions of manual data processing the large number of analytical data practically prevents faster interpretation of the results of examination so that manu attempts were made to present data in understandable and acceptable way using water quality index [4].

However, for systematic (more comprising) presentation of the results and execution of the water sources protection measures it is necessary to have at disposal not annual but continuing (for longer time periods) statistical informations about waters. That is the reason why it is clever to collect and in adequate way process data relevant for "description" of waters in order to carry out successful protection coordinated with development plans, environment protection plans and basic postulates of water resources management.

Since it is rational from informatical aspect to organize health databases, the goal of this work is to define relational database for gathering and studying the correlation of Dalamtian aquatory data and individual patient data.

RESEARCH METHODS

For working out informatical solution of code system and relational database **V O D E** (WATERS) the following informatical methods are applied: ecological documentation, code system - system analysis procedures [4-7]; relational database - data modeling [4,7,8]. Basic parameters are determined by analysis of regulations, standards and methods [9-13] as well as by analysis of so far performed health-ecological researches [3-5,13-18].

New documents of sampling are defined (for surface waters, waste waters and seas-pools-beaches) which are tested in the line of variants on original data (cca 50 samples) in Water and Air Examination Section of the Public Health Institute of Split what is estimated as adequate sample of examination.

Data used for prototype implementation of relational database **VODE** are based on research results of Water and Air Examination section for period 1989-1993 [15] and epidemiological data of ecological accidents [5]. Over 5000 data are included what is sufficient sample of research.

Prototype of relational database **VODE** is implemented on PC 386, 2 MB RAM, floppy 1,2 MB, hard disk 170 MB, printer. Used SW relates to PARADOX 3.5 & 4.0.

RESULTS AND DISCUSSION

Ecological relational database **VODE** (**Figure 1**) presents logical data integration of the Health Information System (segments: REGION, LEGENDS, STANDARDS, SAMPLING including SURFACE WATERS, WASTE WATERS, WATERPOOLS, SEA AND RESEARCHES subsegments) and the Health-ecological information System (segment PATIENT including DIAGNOSES, RESEARCHES subsegments). During the formation of new model as starting point the records (segments) were taken, the stocks were removed i.e. redundancy of dara was diminished by normalization procedure.

Figure 1
RELATIONAL DATABASE VODE
(Structure and relations)

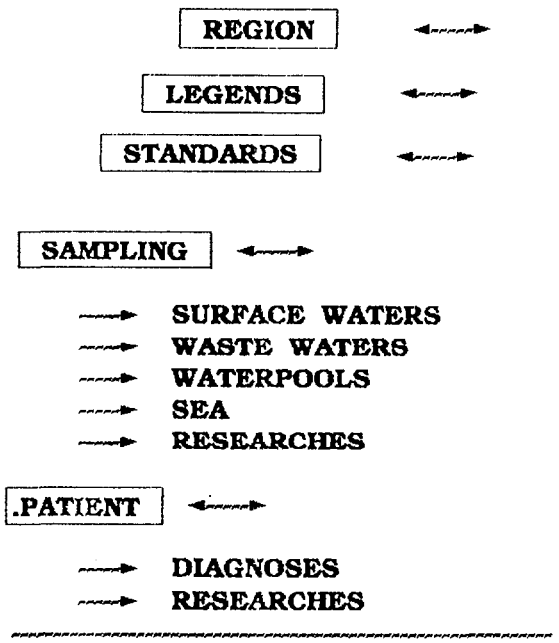

Logical structure satisfied the following requests:

- ensures the approach to all data;
- enables dynamic rearranging and searching of parameters (netting) in regard to ecological problem which is to be studied;
- gives fast "ad hoc" answers;
- gives statistical periodical reports by general and special request of users.

Within data processing all possible relations are not presented (namely, relational database enables netting of all relevant parameters by user's choice) but only few example reviews important for further particular or cummulative continuing researches. Examinations of this type are not so far investigated nor presented. the data were analyzed using multiple-correlation and cross correlation.

It is necessary to notice that manual regular monitoring of waters (frequency depends of economic power of the region) is accessible in annual reports of Public Health Institute of Split [15], but it does not contain continuing monitoring after every sampling what computer data processing enables (**Figure 2**); it is not posssible to define statistical processing or to get several years long comparable data as well as to connect them with individual disease data what data processing(enables easily (**Figure 3**).

In future directed research the whole array of relevant reviews is presumed because applications of relational database anable simple addition of attributes as well as realization of new correlations and addition/realization of new correlations in accordance with rules of relational algebra. In addition, the analysis of ecological burdening (today not yet sufficiently discovered) with intensity and duration of exposure as well as possible reversibility of effects will be included in ecological registries of geographically observed region. By data integration with methodologically prepared database **VODE** the meaning of age in the beginning of exposure could be established what would be of grat interest for primary prevention.

Shown database **VODE** by which ecological factors are monitored enables systematization and quality processing of large data quantity necessary for epidemiological research. Such models are suitable for directed researching of different types (variations in volume of parameters).

CONCLUSIONS

1. New ecological database **VODE** (new logical system) is developed and is suitable for:
   - automatization of water quality index calculation;
   - continuing monitoring of water quality index by momentary number of samples;
   - continuing monitoring of index dynamics in given period;
   - continuig monitoring of index trends by comparing several years long results of examination etc.

2. Data included in this model are standardized in accordance with accessible domestic or international classifications what improves the quality of accumulated data and enabled their comparability on national and international level. In this way the prercquisites for linkage with some

Figure 2: Trend of index – Kosinac

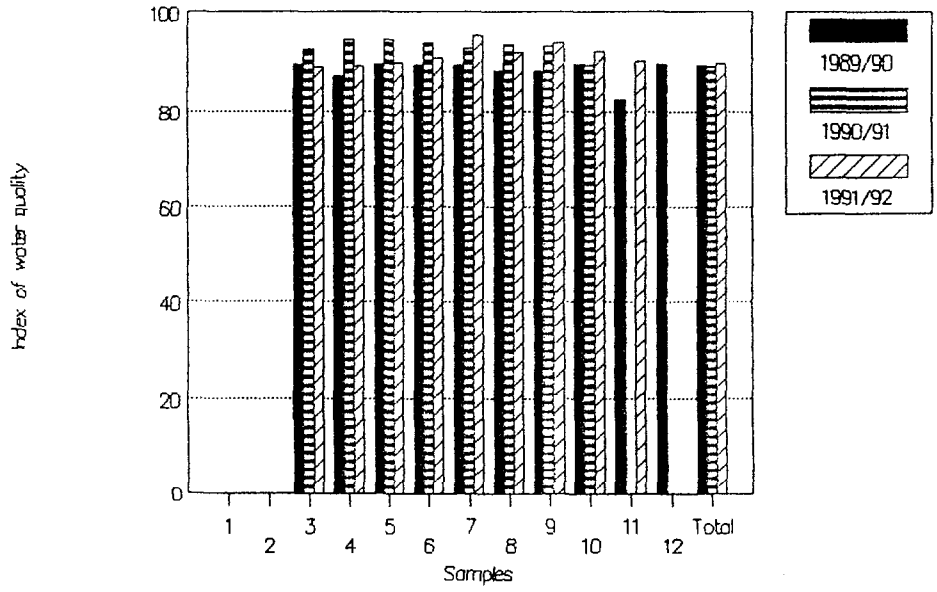

Figure 3: Accidents – Sinj

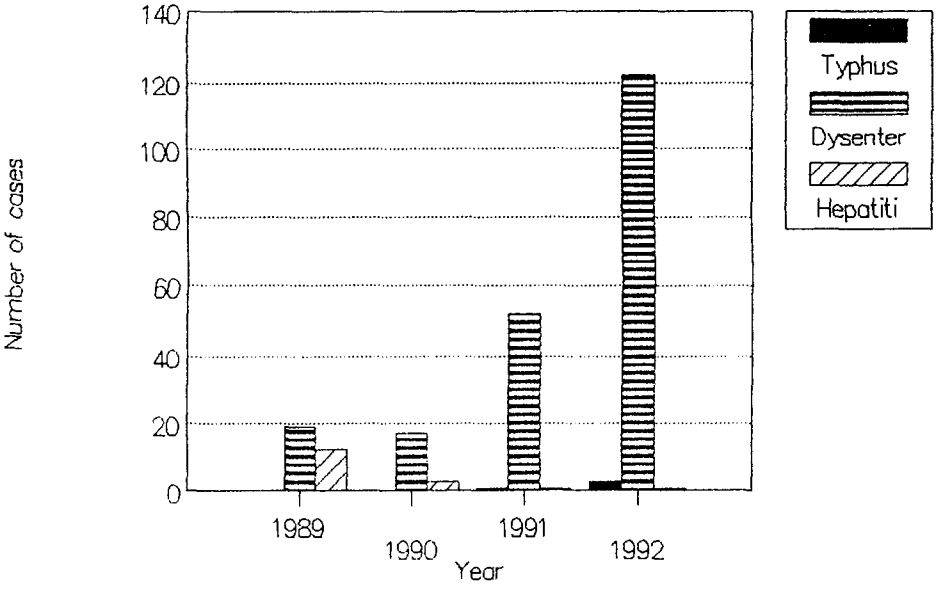

developed international informatical systems and databases are created (for instance INFOTERRA - information system of human environment developed by UN organization - UNEP).

3. Model creates new possibilities for:

- quick insight into existing condition of population from ecological and health-ecological standpoint;
- improvement of daily work organization but also scientific research work because it allows the possibility of own information parameters selection and directs the researches at one's own discretion;
- extension of code system content and database by adding new parameters in certain phases and final integration of human environment data with other information systems data.

REFERENCES

[1] F.Valić et al. Health Ecology. University of Zagreb. Zagreb, 1990.

[2] M.Primic-Žakelj, B.Ravnihar, V.Pompe-Kirn. Carcinogenes in Professional Environment . Zdrav.vestn, 53: 125-28, 1984.

[3] N.Štambuk-Giljanović. Kaštela Bay Polluters. Public Health Institute of Split. Split, 1989.

[4] N.Štambuk-Giljanović. Parameters and Indexes of Surface and Underground Waters Quality in Dalmatia. University of Zagreb. University of Technology (Dissertation). Zagreb, 1980.

[5] Z.Klišmanić. Preliminary Report of Dysenteria Epidemical Accident in Metković. Public Health Institute of Split, Split, 1983.

[6] IBM Corporation. Data Processing Division. Bussiness Systems Planning. Information Systems Planning Guide. New York, 1981.

[7] B.Matoković. Making of Models of Informatical Methods for Malignant Diseases Data Linking With Ecological Data. Univeristy of Zagreb (Dissertation). Zagreb, 1989.

[8] S.Tkalac. Relational Model of Data. Informator. Zagreb, 1988.

[9] V.Štrcaj. Proposal of Rules for Performing Sea Water Quality Control for Bathing and Recreation. In: Cummulative reports of Conference about actuel problems of sea protection (Protection'83). Opatija, 1983.

[10] Library of Jugosalv Public Health Institute. Standard Methods for Physical, Chemical and Bacteriological Water Examination. Beograd,1961.

[11] Hydrometeorological Institute of Croatia. Hydrometeorological Bulletin, 4. Zagreb, 1989.

[12] Jugoslav Public Health Institute. Drinking Water, Standard Methods for Hygienical Propriety Examination. Beograd, 1990.

[13] N.Pavišić. Water Supply Conditions Survey in Dalmatian Settlements - 11 Municipalities. Public Health Institute of Split- Hygienic Section -Sanitary technics (archives). Split,1976.

[14] University of Split. Jugoslav Academy of Science and Art. Project Economic Management with Kaštela Bay Area. Split, 1988.

[15] Public Health Institute of Split. Analysis of the Health Situation, the Health-ecological Condiditions, Organization and work of the Health System in Split Municipality Area. Split, 1980 -1984

[16] V.Smolčić, N. Štambuk-Giljanović. Our Experiences with Evaluation of Pool Water Quality. In: Cummulative reports of XVI Meeting of nutritiony-sanitary chemists. Supetar, 1987..

[17] Z.Klišmanić, N.Štambuk-Giljanović, V.Smolčić. Water Quality in Cisterns in the Area of Split Municipality. In: Marine medicine III (Scientific discussions). Marine library,sv 33. Mornarički glasnik: 127-134, 1983.

[18] N.Štambuk-Giljanović, V.Smolčić Characteristics of Source Waters in Dalmatia. In: Cummulative reports of Conference about actuel problems of water protection (Water protection'87). Jugoslav Society for Water Protection: 371 -382, Kranjska Gora, 1987.

INVESTIGATION ON pH AND IMPEDANCE MODULE OF BROILER'S BREAST MUSCLES AT THE SLAUGHTERY LINE

Gordana Kralik[1], Stanko Tonković[2], Uroš Bego[3], Antun Petričević[1]

[1]Faculty of Agriculture, Kardinala F. Šepera 6, 54000 Osijek
[2]Faculty of Electrical Engineering, Unska 3, 41000 Zagreb
[3]Center for Biomedical Research, Šalata 2, 41000 Zagreb

Abstract

A research of pH and impedance module of breast muscles was carried out on carcasses of Ross-208 broilers 15' p.m. The fattening was going on for 42 days and the average slaughtery mass of carcasses was 1481 ± 206,89 gr. The CARNETEST III device, which works on frequency of 15 kHz, was used to measure the impedance module. The pH was measured in the same picked spot. Researching the conection between the pH and impedance module the following correlation coefficients at vertical and cross measurements, respectively, regarding direction of muscle fibers, were found out: linear 0,446 and 0,405, exponential 0,440 and 0,409, logarithmic 0,459 and 0,409, potential 0,445 and 0,414, square 0,473 and 0,438. The regression analyse showed that data best conform to equation $y' = 11306,51 + 3541,74x - 267,37x^2$ by vertical measurement and $y' = 12279,58 + 3872,23x - 294,57x^2$ by cross measurement, respectively.

ISTRAŽIVANJE pH I MODULA IMPEDANCIJE PRSNIH MIŠIĆA PILIĆA NA LINIJI KLANJA

Sažetak

Istraživanje pH i modula impedancije prsnih mišića obavljeno je na trupovima pilića Ros-208 15' p.m. Tov pilića trajao je 42 dana, a prosječna klaonička masa trupova bila je 1481 ± 206,89 g. Za mjerenje modula impedancije upotrebljen je uređaj CARNETEST III koji radi na frekvenciji od 15 kHz. U istom ubodnom mjestu mjeren je pH. Istraživanjem korelacije pH i modula impedancije ustanovljeni su slijedeći korelacijski koeficijenti kod uzdužnog, odnosno poprečnog mjerenja s obzirom na smjer mišićnih vlakana: linearni 0,446 i 0,405, eksponencijalni 0,440 i 0,409, logaritamski 0,459 i 0,409, potencijski 0,445 i 0,414 te kvadratni 0,473 i 0,438. Regresijska je analiza pokazala da se podaci najbolje prilagođavaju jednadžbi $y' = 11306,51 + 3541,74x - 267,37x^2$ prilikom uzdužnog, odnosno $y' = 12279,58 + 3872,23x - 294,57x^2$ prilikom poprečnog mjerenja.

1. INTRODUCTION

Considering nutritive composition, breast muscle is a category of high quality chicken meat especially convenient for dietetic food either fresh or processed. Relative share of breast as one of the main parts of the broiler's body depends on genotype and sex as well as on the level of the feeding substances in the ration [5,8]. Researches showed undesired occurrences expressed on meaty genotypes, identical to ones occurred on pork, known as PSE and DFD type of meat [2,9]. Intensive gain of body weight, related to large formation of muscle tissue is in negative genetic relation with the meat quality. Longterm selection on enhanced meatiness, hypodinamic of the poultry in the presence of the stressors during intensive breeding, handling the broilers before and after slaughter are basic factors which influence the meat quality. Meat quality is a wide term, so it could be defined from biologically nutritional, psychologically commercial, and technological aspect and it is usual to compare different markers that point to particularity of muscles and tissues during the researches, keeping in mind that complex postmortal biological processes are in question. In that sense, the relation of the glycolysis rhythm with the technological quality of the meat was researched[3,9]. Faster glycolysis p.m. has, as a consequence, high frequention of PSE meat occurrence. By measuring the pH_{15} values, determined normal flow of glycolysis for 27,7% of the samples, while for 69,6% of the samples faster glycolysis was determined and they classified into PSE meat. Water holding capacity was in relation to the concentration of the hidrogen ions in the meat, and the most convenient values were determined in the samples with normal flow of glycolysis. PSE type of meat occurred more often in male chicken than in female. Our researches intend to find the flow of the glycolysis by measuring the pH value 15' p.m. and possible relation of this occurrence to the bioelectric characteristics of the meat. So far, results of the researches about impendance module and phase angle show that significant differences between white (breast) and red (drumstick and thighs)meat of broilers exist [1,4,6,7,11].

2. MATERIAL AND METHODS

Research on the pH values and the impendance module of the breast muscle was performed on the bodies of Ross-206 15' p.m. at the age of 42 days. Temperature of the muscles at the time of measuring was ranged from 39,5 to 40,5°C. CARNETEST III device has been used for measuring the impendance module. This device, which works on the frequency of 15 kHZ, was constructed at the Electrotechnical faculty of Zagreb. Measurements were performed on the breast muscles (n=500) on the middle part of the left side of the thorax, a bit dorsal from the christa sterni. Impendance measurements were performed by two electroplates with 1,5 cm space between them and 0,6 cm puncture depth, along and across the direction of the muscle fibers. Hydrogen ions concentration, as the glycolysis flow indicator, was measured at the same spot by the pH-meter MA 5122 "Iskra". The results of the measurements were processed by the PC computer using the standard statistical methods.

3. THE RESULTS OF THE RESEARCH

Value of pH, measured 15' p.m. on 500 samples, shows that the glycolysis rhythm in the breast muscles of the broilers had mainly normal flow, although there are certain inaccuracies in the sense of accelerated or decelerated rhythm (tab. 1.). Normal processes of glycolysis (pH>5,8>6,39)were denoted for 81,8% of the meat samples. Low pH values of the meat (pH<5,79), as a consequence of the accelerated flow of glycolysis, were denoted only for 1,4%, while high pH values (pH>6,4), which imply decelerated glycolysis, occurred in 16,8% of the samples. According to the researches white meat of the broilers with low pH_1 values (<5,8) or high pH_1 values (>6,5)is characterized by poorer technological quality, which was confirmed by examination of the additional parameters[2,9]. On the contrary, some researchers found no relation between pH_1 values and additional quality parameters[10]. It is relevant to emphasize that low frequency of untypical glycolitic processes (0,4% accelerated : 3,3% decelerated flow) was also denoted [7]. On the other side, other researches showed accelerated rhythm of glycolysis in 69,6% of the samples [2].

Mean value of the pH_{15} (6,19±0,01) and the variability (3,34%) could be evaluated as

satisfactory, keeping in mind that broilers breast muscles are in the question. As our research so far, as well as the research of other authors, showed that low or high pH_1 value does not necessary have to give rise to PSE or DFD type of meat, we presume approvable to research this problem more detailed.

Table 1.Frequency of pH-values and impedance module

pH_{15}-values			Impedance module Ω					
	Number	%	Along	Number	%	Across	Number	%
5.6-5.79	7	1.4	100-176	34	6.8	105-189	31	6.2
5.8-5.99	62	12.4	177-253	51	10.2	190-274	53	10.6
6.0-6.19	187	37.4	254-330	80	16.0	275-359	66	13.2
6.2-6.39	160	32.0	331-407	126	25.6	360-444	171	34.2
6.4-6.59	68	13.6	408-484	179	35.8	445-529	153	30.6
6.6-6.79	15	3.0	485-561	25	5.0	530-614	24	4.8
6.8-6.99	1	0.2	562-639	3	0.6	615-699	2	0.4
Total	500	100.0		500	100.0		500	100.0

The results of the impedance module measurements show that relatively high variability of the impedance module (tab 2.) is present in analyzed samples of the breast muscles. Significant difference ($P<0,05$) between impedance module measured along and across the direction of the muscle fibers have been determined, which points to conclusion that it should be stated how the measurements were conducted when showing the results of the impedance module. Mean values of the impedance module measured along and across the direction of the muscle fiber were 316,82±4,52 Ω and 391±4,80 Ω respectively.

Table 2.Mean value, variability and connection between pH-value and impedance module.

Parameter	X_{AVG}	s	s_x	V	X_{min}	X_{max}
Carcass mass, g	1481.81	206.89	9.25	13.97	900	2180
pH_{15}-value	6.19	0.21	0.01	3.34	5.56	6.85
Impedance,Ω						
- along	361.82	101.12	4.52	27.95	101	638
- across	391.05	107.31	4.80	27.44	109	699
Coefficients of correlation (r)						
	pH_{15}:impedance(along)			pH_{15}:impedance(across)		
Linear	r=0.446**			r=0.405**		
Exponential	r=0.440**			r=0.409**		
Logarithmic	r=0.450**			r=0.409**		
Potential	r=0.445**			r=0.414**		
Square	r=0.473**			r=0.438**		
Regression equations						
y'=impedance(along), x=pH_{15},				y'=impedance(across)		
$y'=-989.74+218.19x$				$y'=-913.18+210.55x$		
$y'=3.75*e^{0.73x}$				$y'=5.90*e^{0.67}$		
$y'=-2126.34+1364*\ln x$				$y'=-2012.78+1318.5*\ln x$		
$y'=0.082*x^{4.57}$				$y'=0.18*x^{4.50}$		
$y'=-11306.51+3541.74x-267.37x^2$				$y'=-12279.56+3872.23x-294.57x^2$		

Measurements of the pH values and impedance module taken at the same time on 500 samples of breast muscles showed that there is medium strong, positive and highly significant relation (r=0,440** exponential to 0,473** square) for along, as well as for across impedance (r=0,406** linear ;0,438** square). Other researches confirmed existence of medium strong and positive relation between pH_1 value and impedance in the breast muscle, but not in the drumstick meat . Measuring the breast muscle by the MC device that was working on the lower frequency, 80' p.m. Our reeseach identified stronger relation between pH and impedance (r=0,648** potential) [7].

During the researches of relation between pH_{15} and impedance modul in the broilers' breast muscles, linear, exponential, logarhytmic, potential and square relationship have been analyzed (tab 2.). Analysis shows that the biggest correlation ceficient exists in the square relationship ($r=0,473^{**}$; $r=0,438^{**}$ respectively). Because of that, square regression is suggested as optimal curve for identification of the examined occurrence in the meat.

Regression curve of impedance, measured along, on pH_{15} value, has equotation $y'=-11306,51+3541,74x-276,37x^2$ and $y'=-12279,58+3872,23x-294,57x^2$ for impedance measured across. These results show that impedance modul can be used as a parameter enough good for researching meat characteristics beside pH value of the meat. For white meat of the Ross-208 chickens measured along and across values from 238 to 408 Ω and 312 to 436 Ω respectively can be considered normal.

4. CONCLUSION

Characteristics of the 49 days old Ross-208 hybrids breast muscles have been researched in this work. Average body weight of the slaughtered chickens was 1481±9,25 g. Results of the researches of the breast meat characteristics (n=500) on the basis of pH value and impedance modul showed as follows:

- Mean value of the pH_{15} for breast muscles was 6,19±0,001 and variability 3,34%.
- Mean value of the impedance modul was 361,82±4,52 Ω measured along the direction of the muscle fibers and 391,05±4,80 Ω for one measured across. Variability of the impedance modul was 27,95% and 27,44% respectively.
- Relationship between pH_{15} value and impedance modul is medium strong and positive ($r=437^{**}$ and $0,438^{**}$ respectively for along and across measuring).Regression curve matches equation $y'=-11306,51+3541,74x-276,37x^2$ for impedance measured along and $y'=-12279,58+3872,23x-294,57x^2$ measured across.
- Carnetest III showed as good for researching of the broiler's breast muscles characteristics at the slaughter line. Tolerancy margins for the impedance modul measured along are 283 to 408 Ω and 312 to 436 Ω for one measured across.

5. REFERENCES

[1] U. Bego, S. Tonković, Gordana Kralik, Karmen Petrak : Bioelectric and chemical properties of white and red muscles in chickens of different weight. Periodicum Biologorum, vol. 95, 1, 93-96, 1993.

[2] R. Gilewski, J. Nemec, M. Trojan : Quality characteristics of meat Biale Brunrinowskie chicken strain. Annuals of Warsaw Agriculture University, Animal Science, 19, 53-57, 1985.

[3] D. Klosowska, A. Niewiarowicz, B. Klosowski, M. Trojan : Histochemishe und histologische Untersuchungen am M. pectoralis superficialis mit beschleniger, normal und verzorgerter Glykolysenrate in broilern. Fleischwirtschaft, 59, 1004-1008, 1979.

[4] G.Kralik, S. Tonković, U. Bego, D. Ratkaj : Bioelectrical and physico-chemical properties of white and red muscles in chickens. Zbornik radova Veterinarskog fakulteta Univerziteta Ljubljana, 29,2,179-185, 1992.

[5] G. Kralik, A. Petričević, Z. Maltar, Đ. Senčić : Utjecaj genotipa i spola pilića na prinos i kavoću mesa. Stočarstvo, 47, 1-2, 39-47, 1993.

[6] G. Kralik, A. Petričević : The influence of initial pH value in broiler breast on other meat characteristics. 11th European Syimposium on the Quality of Poultry meat. 1-5, Tours, France, 1993.

[7] G. Kralik, S. Jovanovac, K. Soos, I. Takasci : Impedance module and pH value in the quality evaluation of breast muscles of broilers. Scientific Days in Kaposvar, 146-151, 1993.

[8] A.A. Mendes, E.A. Garcia, A.B. Gonzales, P. Silva : Effect of nutritional level of diet and sex on broiler carcass yield. XIX World's Poultry Congress, p. 246, Amsterdam, 1992.

[9] A. Niewiarowicz : Meat anomalies in broilers. Poultry International, 17, 1, 50-51, 1978.

[10] G. Seeman : Beziehungen zwischen der pH Wert Anderungen nach dem Schlachten und anderen Fleischqualitatsparametern bei Hanchen. Fleischwirtschaft, 4, 604-606, 1986.

[11] S. Tonković, U. Bego, G. Kralik : Bioelectrical, biochemical and morphohistochemical pecularities of chicken's muscles. 5. spominski sastanak prof.dr. Frana Zavrnika, Gozd Martuljak, Zbornik prozvetkov, 26, 1992.

SOME DIAGNOSTIC FEATURES OF BIOELECTRIC IMPEDANCE MEASUREMENTS

Stanko Tonković*, Mladen Petrunić, Igor Kršić*, Uroš Bego*, Ivana Tonković****
***-Faculty of Electrical Engineering, 3 Unska, 41000 ZAGREB, Croatia**
****- Department of Surgery, KBC Rebro, Kišpatićeva 12, 41000 Zagreb, Croatia**

Summary

The physical bases and assumptions, theoretical and practical limitations, applications and different features of the bioelectric impedance measurements reveals an important interest since electronic instrumentation has been involved in biomedical applications. We have explored diagnostic possibilities and comparison of "static" bioelectric impedance properties in estimation of determining human body composition considering especially "compartmental syndrome" detection possibilities. Influence of measuring parameters (frequency and current) is also investigated in order to improve the reliability of measuring results.

1. INTRODUCTION

The electrical characteristics of biological systems have intrigued scientific investigators for many years. The measurements of bioelectric impedance, "static" and "dynamic" or "in vivo" and "post mortem" revealed a special point of investigators interest [1-5]. Current researches focuses not only on checking the link between physiological states and/or muscle composition and bioelectrical parameters at various frequencies, but also on the improved interpretation of the measurement results that have been used to this point, the concept of "sample" impedance characteristics in particular. In fact, for a general two-port with presumably unknown characteristics inside (considering an examined sample between two electrodes) one can only conclude that an important frequency dependence exists. Hence only the multi-frequency method can make possible to determine the behaviour of the two-port characteristics as a function of frequency and to compare it to the expected model. An important number of investigators have explored this problem proposing different electrical models [6] some of them are shown in Fig. 1. We have concentrated our

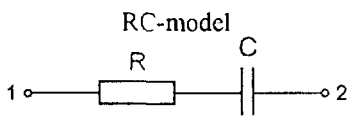

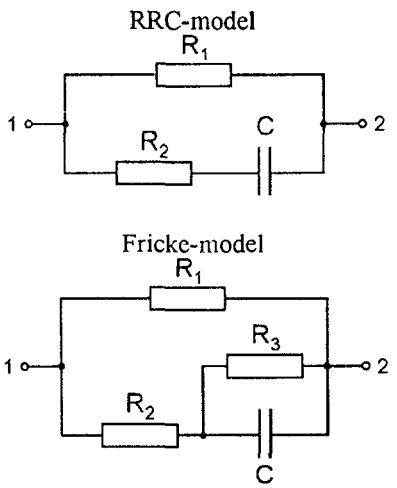

Fig. 1: Some models of bioelectrical impedance Z_B

interest investigating the possibility of early noninvasive detection of compartmental syndrome of lower-extremity muscles using bioelectric impedance measurement with surface electrodes [7,8,9]. The measurements were performed in the frequency range from 10 kHz to 1 MHz in order to avoid the electrode impedance problems. Compartmental syndrome measurement results as well as measurements of skeletal muscles properties show that a good correlation exists between bioelectric impedance and the illness severity. The investigation of correlation with the water volume or electrolyte composition in explored subjects in also underway.

2. MATERIAL AND METHODS

The hypothesis that body impedance can be used to measure a sample characteristic is based on the principle that the impedance of simple geometric system is a function of the interelectrode length and cross-sectional area, sample specific resistivity and relative permittivity and frequency. Perhaps it is important to underline that the often stated relations (2) such as

$$Z_B = \rho\frac{l}{S} \quad \text{or} \quad V = \rho\frac{l^2}{Z_B} \tag{1}$$

does not hold, because they neglect capacitive (or frequency depending) component of measured impedance. For any of models in Fig. 1. it can be shown that the following relation holds:

$$Z_B = (\rho, \varepsilon_r, l, S, \omega) = k(l,S)\cdot F[\rho(\omega), \varepsilon_r(\omega), \omega] \tag{2}$$

where

Z_B = biological impedance (Ω)
V = volume (cm^3)
l = distance between electrodes (cm)
S = cross-sectional area (cm^2)
ρ = specific resistivity (Ωcm)
ε_r= relative permittivity
ω = radian frequency (s^{-1})

During these studies we measured the impedance magnitude and phase angle using HP RLC-Meter 4284A with two electrodes technique and constant current source of 0.1 mA (the testing has shown that the current magnitude does not significantly affect the measurement results if it is maintained under 1 mA). The measurements on the examined lower-extremity muscle groups were performed by use of self-adhesive cutaneous electrodes on the three groups of patients: first with "severe" clinically manifesting, second with "medium" clinically manifesting and the third one with the "very low signs" of compartmental syndrome. All the patients were carefully selected, having one leg healthy and the other one with the manifesting "severe", "medium" or "very low" compartmental syndrome. The position of electrodes was determinated by the palpation of the major muscle bulge strictly controlling the distance of 12 cm between electrodes. Simultaneously, the tissue pressure, being the primary pathophysiological factor in compartmental syndromes, was measured by catheter using Wick technique [4].

3. RESULTS

After selection of the patients using above mentioned classification, the results of measurements were statistically analyzed in order to find frequency and current giving the most reliable results. At the same time, the correlation between impedance and pressure measurement results was explored as well as the difference between, by the clinical symptoms, separated groups. The results show that a significant difference in impedance magnitude exist between these three groups whereas there is no significant difference in phase angle. Table I. (a-c) shows the averaged results of impedance magnitude measurement, as well as the results with most aberrant values rejected following Chauvenet criterion. The existing difference between results can be easily shown up. It is interesting to note that the phase angle does not shows significant differences. Further investigations of phase angle measurement results are underway.

The averaged differences in the tissue pressure between ill and healthy legs in the three mentioned groups were as follows, respectively:

- p_1=19.67 mmHg (2.62 kPa)
- p_2=7.75 mmHg (1.03 kPa)
- p_3=0.2 mmHg (26.6 Pa)

Comparison between the results of impedance and pressure measurements in these three groups give very significant high correlation (indices indicates the measuring frequency in kHz).

- r_{10}= 0.9774
- r_{20}= 0.9909
- r_{50}= 0.9846
- r_{100}= 0.9725

This leads to the conclusion that the optimal frequency measuring range is between 15 to 50 kHz.

4. CONCLUSION

Considering and comparing the results obtained in patients taking into account the patient's different status we should maintain that all the results show significant differences between groups especially when impedance magnitude is considered. Very high correlation between impedance and pressure measurements results justify the expectancy that the compartmental syndrome could be noninvasively detected by using the proposed impedance measurement technique.

a)

Healthy leg	Frequency [kHz]	10	20	50	100	200	500	1000
	Mean [Ω]	1905.2	1227.7	805.2	653.2	572.7	523.6	498.2
	St. dev. [Ω]	355.0	251.5	265.1	279.9	289.1	285.3	295.0
	Var. [%]	18.6	20.5	32.9	42.9	50.5	54.5	59.2
	$Mean_{Ch}$ [Ω]	1832.5	1190.3	735.0	569.3	480.5	432.2	398.0
	$St.\ dev._{Ch}$ [Ω]	203.3	202.1	63.0	39.2	48.4	64.6	51.8
	$Var._{Ch}$ [%]	11.1	17.0	8.6	6.9	10.1	15.0	13.0

a)

Ill leg	Frequency [kHz]	10	20	50	100	200	500	1000
	Mean [Ω]	1226.2	752.7	459.2	358.5	306.2	271.0	257.3
	St. dev. [Ω]	155.4	106.2	90.9	80.2	72.0	68.6	70.3
	Var. [%]	12.7	14.1	19.8	22.4	23.5	25.3	27.3
	$Mean_{Ch}$ [Ω]	1243.5	758.8	454.0	347.5	292.5	255.0	239.5
	$St.\ dev._{Ch}$ [Ω]	65.2	52.4	77.2	65.5	48.1	34.3	28.5
	$Var._{Ch}$ [%]	5.2	6.9	17.0	18.9	16.4	13.5	11.9

b)

Healthy leg	Frequency [kHz]	10	20	50	100	200	500	1000
	Mean [Ω]	1479.9	885.9	521.9	398.8	336.9	297.4	281.4
	St. dev. [Ω]	669.1	347.0	144.2	80.3	53.1	39.2	34.7
	Var. [%]	45.2	39.2	27.6	20.1	15.8	13.2	12.3
	$Mean_{Ch}$ [Ω]	1398.8	840.5	503.7	394.2	338.8	301.7	283.7
	$St.\ dev._{Ch}$ [Ω]	521.6	265.9	108.4	58.3	39.5	28.9	21.7
	$Var._{Ch}$ [%]	37.3	31.6	21.5	14.8	11.7	9.6	7.7

b)

Ill leg	Frequency [kHz]	10	20	50	100	200	500	1000
	Mean [Ω]	1071.8	633.1	351.5	255.0	206.5	176.6	165.3
	St. dev. [Ω]	469.5	226.2	81.4	37.6	21.5	15.7	15.3
	Var. [%]	43.8	35.7	23.1	14.7	10.4	8.9	9.3
	$Mean_{Ch}$ [Ω]	1005.7	599.2	337.0	248.8	205.7	178.8	167.3
	$St.\ dev._{Ch}$ [Ω]	368.5	167.7	51.8	19.5	11.3	11.3	10.7
	$Var._{Ch}$ [%]	36.6	28.0	15.4	7.8	5.5	6.3	6.4

c)

Healthy leg	Frequency [kHz]	10	20	50	100	200	500	1000
	Mean [Ω]	1337.9	824.2	500.5	387.7	329.4	291.3	276.1
	St. dev. [Ω]	631.6	320.6	143.2	107.2	101.7	100.0	97.5
	Var. [%]	47.2	38.9	28.6	27.6	30.9	34.3	35.3
	$Mean_{Ch}$ [Ω]	1270.3	798.3	496.6	376.5	314.3	280.5	267.5
	$St.\ dev._{Ch}$ [Ω]	489.8	268.3	137.4	83.4	70.4	59.9	54.8
	$Var._{Ch}$ [%]	38.6	33.6	27.7	22.2	22.4	21.4	20.5

c)

Ill leg	Frequency [kHz]	10	20	50	100	200	500	1000
	Mean [Ω]	1348.4	811.9	470.6	352.4	289.4	250.1	232.0
	St. dev. [Ω]	631.6	322.1	145.4	107.1	103.0	101.6	100.4
	Var. [%]	46.8	39.7	30.9	30.4	35.6	40.6	43.3
	$Mean_{Ch}$ [Ω]	1278.8	786.0	469.6	343.0	275.1	233.4	215.3
	$St.\ dev._{Ch}$ [Ω]	477.4	257.5	139.1	81.6	66.8	63.1	60.6
	$Var._{Ch}$ [%]	37.3	32.8	29.6	23.8	24.3	27.1	28.2

Table I:

Tables (a-c) show averaged results of impedance magnitude measurements on healthy and ill legs for patients groups with severe (a), medium (b) and very low (c) manifested compartmental syndrome.
(Ch-means values calculated after rejection of aberrant values following Chauvenet criterion)

5. REFERENCES

[1] H.P. Schwan, Determination of biological impedances, In.: A. Nastuk: Physical techniques in biological research, Part B/6, Academy Press, 1966

[2] E.C. Hoffer, C.K. Meador, D.C. Simpson, Correlation of whole-body impedance with total body water volume, J. of Appl. Physiol., 27, No.4, 531, 1969

[3] H.C. Lukaski, Methods for the assessment of human body composition: traditional and new, Am.J.Clin.Nutr., 46, 537, 1987

[4] F.A. Matsen, Compartmental syndromes, Grune&Stratton, N.Y., 1980

[5] B.J. Thomas, B.H. Chornish, L.C. Ward, Bioelectric impedance analysis for measurement of body fluid volumes: A review, J. of Clin.Eng., 17, No.6, 505, 1992

[6] Dietosystem Scientific Monographs, Bioelectric impedance and body composition, Milano, 1991

[7] S. Tonković, U. Bego, V. Gjurčević, Neka svojstva skeletnih mišića, In. U. Bego (Ed.): Biodinamika mišića, Veterinarski fakultet, Zagreb, 1987

[8] S. Tonković, U. Bego, D. Ratkaj, Determining the criterion of normality for some bioelectric characteristic of skeletal muscles in animals, Period. Biolog., 95, No.1, 89, 1993

[9] I. Tonković, D. Ratkaj, S. Tonković, M. Petrunić, A nonivasive method for tissue pressure evaluation of lower-extremity muscles, Period. Biolog., 95, No.1, 97, 1993

INFLUENCES OF SPEECH AND BITE ON EMG AND MORPHOHISTOCHEMICAL CHARACTERISTICS OF MASSETER MUSCLE

Melita Valentić-Peruzović[1], Uroš Bego[2], Dragica Bobinac[3]

1. Dental School, University of Zagreb, Croatia
2. Faculty of Electrical Engineering, University of Zagreb, Croatia
3. Faculty of Medicine, University of Rijeka, Croatia

ABSTRACT: *Electromyographic recordings were made in 5 subjects bilaterally on m.masseter by surface electromyography in different functional movements, i.e., in maximal voluntary clenching (MVC) and in speech (SPC). The range of the EMG activity during SPC was 1.27% minimal to 19.29% maximal in percentages of MVC. A new approach in categorization of muscle fibres by using distribution frequency technique of muscle fibre diameters showed significant proportion of II fibres with small diameter 15-27μm in masseter specimens. These small fibres are relatively weak and it is justified to relate them with the special activity in humans as it is moving the mandible during the speech. The results of present EMG-study are in good agreement with the new functional categorization of the morphofunctional units (MFU) by using distribution frequency technique of muscle fibre diameters.*
Key words: *EMG, speech, bitting, m.masseter, motor units, distribution frequency technique of muscle fibre diameters.*

UTJECAJ GOVORA I ŽVAKANJA NA ELEKTROMIOGRAFSKE I MORFOHISTOKEMIJSKE KARAKTERISTIKE M. MASETERA

SAŽETAK: *Izvršeno je registriranje aktivnosti m.masetera površinskom elektromiografijom u pet ispitanika, pri različitim funkcijskim kretnjama, kao što su maksimalni voljni stisak zuba (MVC) i govor (SPC). Aktivnost pri govoru (SPC) iznosi minimalno 1.27% do maksimalno 19.29% EMG aktivnosti pri maksimalnom voljnom zagrizu (MVC). Novi pristup kategorizaciji mišićnih vlakana upotrebom frekvencije distribucije pokazao je značajnu prisutnost vlakana sa malim promjerom od 15-27μm u uzorcima humanog masetera. Ta mala relativno slaba vlakna tipa-II, povezuju se sa specifičnom aktivnošću u čovjeka, kao što su npr. kretnje mandibule za vrijeme govora. Rezultati ovog EMG istraživanja su u skladu sa rezultatima nove funkcijske klasifikacije tipova morfofunkcionalnih jedinica (MFU) pomoću tehnike difrakcione frekvencije promjera mišićnih vlakana*
Ključne riječi: *EMG, govor, žvakanje,m.maseter, motorne jedinice, tehnika difrakcione frekvencije promjera mišićnih vlakana*

INTRODUCTION

Human masseter muscle has a very complex internal anatomical architecture. It is composed of three to five tendon plates running in parallel alternatively from the zygomatic arch to the mandibular ramus. They are interconnected with multiple tendon-stripes between which are numerous short muscle fibres multipenatelly directed (1-5). Such a complex macroscopic structure suggests that masseter muscle is organized in functionally separate compartments with possible regional specialization inside the muscle. This was confirmed by electrophysiological examinations by Stålberg and Eriksson (6), who found that most motor units have territories less than 5 mm. These separated areas or compartments within the masseter muscle with small and localized territories of the motor

units suggest about their different control. Namely, during mastication and especially during speech, precise jaw movements are performed and selective recruitment of motor units from relevant compartments occurs with little impulse variability, as well as recruitment of some adjacent compartments with balanced tension.

Precisely, fine mandibular movements are involved within a space around the mandibular postural position during speech (7). There are generally no heavy forces involved and no extensive lateral or protrusive movements, with action mainly directed vertically. Some long muscle fibres are also involved during short muscle fibre activity, as they extend over a few different compartments. These long fibres are recruited during force production in a static contraction at the occlusal bite. They are also important to maintain the mandible in a stable position against the gravitational forces during walking or running.

It is obvious from the above mentioned that anatomical and electrophysiological characteristics of the masseter muscle are very complex, which arises from its adaptation to a special role during functional movements such as speech and mastication. This complexity of structure and function is not adequately presented through the simplified histochemical description of the muscle fibre properties.

There are a large number of classification systems for describing muscle fibre types. Much of the recent work on mammalian jaw muscles has however been realized using two systems which correlate with muscle and motor unit physiological properties. These two systems, the I/IIA/IIB/IIC system proposed by Brooke and Kaiser (8) and the SO/FOG/FG system proposed by Peter et al. (9), are interchangeable when applied to most limb muscles but are not equivalent when applied to jaw-closer muscles (10). Muscle fibre type compositions give a guide to the overall contractile properties of the muscle in which they occur. A major determinant of contraction speed of muscle fibres is their myosin ATPase activity (11), and this varies according to myosin type. Using different methodology (12-16) two main muscle fibre type are described based primarily on diameter and histochemical characteristics of masseter muscle: type I (slow) and type II (fast). Conventional ATPase and NADH-TR histochemistry (17) also distinguished their subtypes as IM (intermediate-) and IIA, IIB, and IIC .

Such histochemical classification of fibre-types is partly dependent on subjective estimation and limited by the resolution of the method applied. Only a certain number of main fibre types is due to this clearly recognizable by qualitative histochemical methods (18).

Considering all of the above, data obtained by different histochemical methods incompletely describes characteristics of the masseter muscle, especially fibre type II. It fails to show the functional complexity and heterogeneity of the task of individual morphofunctional muscle fibre groups.

The fibre's heterogeneity implies functional specialization and economical energy usage by contraction. Functional specialization is suggested also by single-fibre EMG studies in the human masseter and temporal muscles, which have revealed significant changes in the firing pattern of motor units correlated with the type of activation and the location in the muscle (19). In a previous study (20) a new categorization of the muscle fibres was used, i.e., the frequency distribution of the muscle fibre diameters introduced by Bego,1994 (21).

The aim of this study was to confirm the proposed new functional morphohistochemical classification of muscle fibres by electromyographic study in the human masseter muscle during different functional movements, especially in maximal clenching effort and during speech sequences.

MATERIALS AND METHODS

EMG Instrumentation

Five young adults, age ranged 19-23 years, participated in the electromyographic part of this study. The electromyographic registrations were made by means of surface bipolar electrodes, 10 mm in diameter, positioned over the right and left masseter muscles. Electrodes were separated by a distance of 25 mm centre to centre and positioned parallel to the main direction of the muscle fibres. The ground electrode was attached to a wrist of the examinee. The skin was thoroughly cleaned with alcohol prior to the application of the electrodes and conductive jelly was applied on the inner surface of the electrodes.

The bioactivity from both masseter muscles was recorded on an eight channel instrument, EMGA-1 system (22,23) working under Medwin-1 software, which was specially designed for electrophysiological investigations in dentistry, and capable of simultaneous registration of up to six electromyographic and two acoustic signals. Data was displayed in graphic windows on the PC monitor and recorded on magnetic media for later analysis.

EMG activity was recorded during maximal voluntary clenching (MVC) of the teeth in centric occlusion. The subject was asked to clench maximally for a period of 3 seconds. Periods of rest were provided between the

clenching tasks. The second sequence was EMG recording of the masseter muscle activity during speech over a period of 3 seconds, with periods of relaxation between each recording sequence. During the experiment the subject was seated upright in a dental chair.

Morphohistochemical categorization

Examinations were carried out on 5 masseter muscles (distal-superficial part) in human specimens (25-45 years) with normal dentition. Muscle samples were stained with alkaline ATP-ase (pH-9.4) and distribution of light (type I) and dark (type II) muscle fibres was studied. A classification of muscle fibres was made on microphotographs of the muscle cross sections from the masseter muscles by determining the frequency distribution of their diameters with step of 3 μm and tonality of their colours .The frequency distribution of muscle fibre diameters was made by scanning microphotographs and using developed software based on colour classification and muscle fibres diameter as described in a previous report by Bego and Bobinac (20).

RESULTS

Table I reports the mean values and the relevant standard deviations of biopotentials recorded over the right and the left masseter muscles in maximal voluntary clenching (MVC) in the position of maximal intercuspation of teeth, as well as during speech sequence SPC).

The registrations are expressed in microvolts (μV). The results of SPC are also expressed as percentages of MVC to compare their relationship.

Table 1. EMG registrations of the right and left masseter muscles (RM,LM) during maximal voluntary clenching (MVC) and during speech (SPC) expressed in microvolts (μV), and as a percentage of MVC.

	EMG-MVC (μV)		EMG-SPC (μV)		SPC(%)	
SUBJECT	RM μV	LM μV	RM μV	%	LM μV	%
A.S.	57	109	11	19.29	13.6	12.47
I.T.	391	200	5	1.27	5.5	2.75
A.B.	70.3	97.3	12.3	17.49	8.6	8.84
M.M.	164	160	8.3	5.06	7.3	4.56
S.L.	194	184	5.5	2.83	6	3.26
X	175.26	150.06	8.42	9.18	8.2	6.38
SD	134.18	45.31	3.23	8.53	3.2	4.16

X : mean value; SD : standard deviation

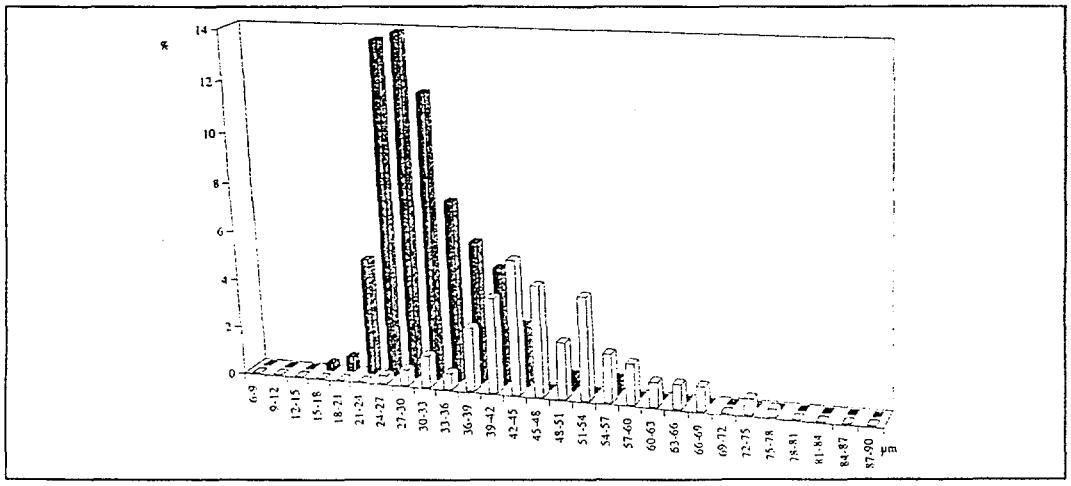

Fig.1. The graphic presentation of frequency distribution of muscle fibre diameters in the human masseter. Dark columns represent dark alkaline (pH 9.4) ATP-ase stained fibres and light columns-represent light alkaline (Ph 9.4) ATP-ase stained fibres. The frequencies are determined with step of 3μm.

Table 2. Frequency distribution of muscle fibre diameters and colour diffraction between ATP-ase stained masseter muscle fibres.

M.MASSETER					
LIGHT FIBRE			DARK FIBRE		
µm	MFU	%	µm	MFU	%
24-42	6	9.32	15-27	4	19.33
42-57	5	17.48	27-42	5	43.58
57-78	7	7.43	42-57	3	3.86
total	18	33.23	total	12	66.77

DISCUSSION

The investigation enabled the evaluation of the variability range of EMG activity of masticatory muscles and the relative contribution of masseter muscles in different functional movements. Muscular effort in MVC (maximal voluntary clench) was directed to achieve a very strong bite, as in masticatory cycle during biting and food crushing or in performing heavy work (i.e., sports, etc.) when jaw elevator muscles contribute to the overall muscular effort.

Both masseter muscles (RM, LM) participated in guiding the mandible in various non occlusal positions according to the opposing maxilla during speech pattern (SPC). The range of the EMG activity in these functional movements was calculated from 1.27 % minimal to 19.29 % maximal in relation to MVC. Mean SPC value for the right masseter is 9.18 % of MVC activity, and for the left masseter 6.38 %, which is less than 10% of the EMG activity in maximal clenching effort. These results prove to what extent the muscle is adapted to efficient use in a wide variety of situations and suggested that small motor unit territories may indicate local specialization and a potential for selective recruitment of separate motor regions, which would favour fine adjustment of jaw movements. In contrast, large territories may reflect widespread motor-unit actions, which is advantageous in force development where fine movement control is less important, as in biting in the intercuspal position or opposing gravity.

According to the categorization results of the morphofunctional units (MFU), by using distribution frequency technique of masseter muscle fibre (Table 2.), the fibre diameter range was 15-78 µm, of which 33.23% were ATP-ase light (distributed in 18 morphofunctional units-MFU) and 66.77% were dark fibres (distributed in 12 MFU). 19.33% of dark fibres were distributed in the range of 15-27 µm. It can be concluded that numerous dark muscle fibres represented in the studied distal part of the masseter muscle with small motor unit territories may indicate local specialization and a potential for selective recruitment of separate motor regions, providing fine adjustment of jaw movements. This is most likely due to adaptation capabilities of human jaw muscles that are caused by unique feeding and speech habits, thus a part of an intricate, evolutionary advanced motor system.

As mentioned above, recent histochemical data is not sufficient to completely disclose the role of a certain muscle type population in the masseter muscle in man. This is especially evident with the fibre type IIB, with its small diameter, which were considered as the result of inactivity or a form of 'disuse' (24) since mastication of modern civilization diet requires only small forces, resulting in infrequent recruitment of type II fibres, which therefore atrophy.

It is known that the masticatory cycle lasts only a limited time during the day and the other activities of the masticatory apparatus in modern man are more differentiated, such as speech, singing, whistling, wind instrument playing, than in other species. Therefore this special type of activity should not be taken as inactivity but as an evolutionary advancement. A new approach in categorization of the morphofunctional units (MFU) by using distribution frequency technique of muscle fibres (21) showed significant proportion of II fibres with the diameter 15-27 µm, (table II). These small fibres are relatively weak and it is justified to relate them with special activity in humans such as mandibular movements during speech.

It is obvious that the results of this EMG-study are in good agreement with new approach in categorization of the morphofunctional units (MFU) by using distribution frequency technique of muscle fibres.

REFERENCES

1.Ebert H. Morphologische und Funktionelle analyse des Musculus masseter. Z.snst. EntwGesch. 1938/39; 109:790-802.

2.Schumacher G H. Funktionsbedingter Strukturwandel des M.masseter. Morph Jb.1961; 102:150-169.

3.Sicher H, DuBrul E L. Oral Anatomy, 1970; 5th edn.Mosby, St Louis, Miss.

4.Gaspard M. Les Muscles Masticateur Superficiels des Signes a l' Homme.Libraire Maloine, 1972;S.A. Editeur, Paris.

5.Mosolov N N. On the anatomy of human masticatory musculature. In : Morphology of the Maxillo-Mandibular Apparatus. (Ed by Schumacher G H.). 1972; pp. 65-69.VEB G.Thieme, Leipzig.

6.Stålberg E, Eriksson P O. A Scanning electromyographic study of the topography of human masseter single motor units. Arch oral Biol. 1987; 11: 793-794.

7.Gibbs C H, Messerman T. Jaw motion during speech. American Speech and Hearing Association. Reports/ASHA, Report No.7,pp. 104-112. 1972).

8.Brooke M H, Kaiser K K.. Muscle fiber types: how many and what kind? Archs Neurol,1970;23: 369-373.
9.Peter J B, Barnard R J, Edgerton V R, Gillespie C A, Stempel K E. Metabolic profiles of three fiber types of skeletal muscle in guinea pigs and rabbits. Biochemistry 1972; 11: 2627-2623.
10.Rowlerson A M. Specialization of Mammalian Jaw Muscles: Fibre type composition and the distribution on male spindles. In: Neurophysiology of the Jaws and Teeth.1990; pp 1-48. (Ed. by A.Taylor) MacMillan Press ltd.
11.Barany M. ATP-ase activity of myosin correlated with speed of muscle shortening. JGen Physiol.1967; 50: 197-216.
12.Ringqvist M. Fibre types in human masticatory muscles. Relation to function. Scand J dent Res. 1971; 82: 333-335.
13.Serratrice G, Pellissier J F, Vignon C, Baret J. The histochemical profile of the human masseter. An autopsy and biopsy study. J neurol Sci. 1976; 30: 189-200.
14.Taylor A. Fibre Types in the Muscles of Mastication. In: Mastication.1976; (Ed.by Anderson D. and Matthews B) Wright Bristol. pp. 16-24.
15.Vignon C, Pellissier J F, Serratrice G. Further histochemical studies on masticatory muscles. J neurol Sci. 1980; 45: 157-176.
16.Eriksson P O, Thornell L E. Histochemical and morphological muscle fibre characteristics of the human masseter, the medial pterygoid and the temporal muscles. Arch oral Biol. 1983; 28: 781-795.
17.Dubowitz V, Brooke M H. Muscle Biopsy - A Modern Approach.1973; Sounders, London.
18.Pette D, Starron R S. Cellular and molecular diversities of mammalian skeletal muscle fibres. Rev Physiol Biochem Pharmacol 1990; 116: 1-76.
19.Eriksson P O, Ståhberg E, Antoni L.Flexibility in motor-unit firing pattern in human temporal and masseter muscles related to type of activation and location. Archs oral Biol. 1984; 29: 709-712.
20.Bego U, Bobinac D.The functional classification of the human masseter and temporal muscles. 1994, (in press)
21.Bego U. Frequency distribution of muscle fibre diameters in the pigeon's pectoral muscle and a new fibre classification. Period biol; 1994; 96:53-56.
22.Valentić-Peruzović, M., Magjarević R. Sustav za mjerenje i analizu mišićne aktivnosti i zvukova u stomatologiji. Zbornik radova JUREMA, ZAGREB, 1990, 43-46.
23.Valentić-Peruzović M., Magjarević R , Stipetić, D., Cifrek, M., Žuljević, Ž. The recordings of the occlusal sounds and bioelectrical activity of the masticatory muscles by the new designed configuration EMGA-1. Proceedings of 7th.International Conference on echanics in Medicine and Biology, ,1991; 57-58.
24. Ringqvist M. Size and distribution of histochemical fiber types in masseter muscle of adults with different states of occlusion. J Neurol Sci 1974; 22: 429-438.

ANALYSIS OF THE ELECTRICAL AND ELECTROCHEMICAL EFFECTS BY STABLE COMPRESSIVE OSTEOSYNTHESIS

Vedran Batoš
Pomorski fakultet Dubrovnik
Ćira Carića 4

Abstract

The usual way of treatment the fracture by fixing with the metal plates,screws and wedges (stable compressive osteosynthesis) is often unsuccessful because of the reaction of the tisssue on the brought in metal. Examining the larger number of samples of various characteristics (concerning the section and the way of treatment of the surface) conclusions about the factors influencing the quality of implant have been adopted concerning its electrochemical properties. The dimensions proportional to the determined damages are defined by statistical treatment of results and the characteristics that could be the base of the classification of negative phenomena are pointed out.

Comparing conventional methods of measuring the method that leads practically most to the corresponding conclusions is chosen.The possibilities of the use of these results in clinical purposes are pointed out.

ANALIZA ELEKTRIČKIH I ELEKTROKEMIJSKIH UTJECAJA KOD STABILNE KOMPRESIVNE OSTEOSINTEZE

Sažetak

Uobičajeni način obrade prijeloma fiksacijom pomoću metalnih pločica, vijaka i klinova (stabilna kompresivna osteosinteza) često u praksi doživljava neuspjeh zbog reakcije tkiva na uneseni metal. Ispitivanjem većeg broja uzoraka različitih karakteristika (s obzirom na presjek i način obrade površine) doneseni su zaključci o faktorima koji utječu na kvalitet implanta s obzirom na njegova elektrokemijska svojstva. Statističkom obradom rezultata definirane su veličine proporcionalne određenim oštećenjima i podvučene su karakteristike koje bi mogle biti temelj klasifikaciji negativnih pojava. Uspoređivanjem konvencionalnih metoda mjerenja, izabrana je ona koja najpraktičnije dovodi do odgovarajućih zaključaka.

Istaknute su mogućnosti primjene ovih rezultata u kliničku svrhu.

1. INTRODUCTION

The processes of crystallization and healing of a fracture are directly related to the piezoelectric effects, whereas bone compression induces a negative potential on the compressed side and positive potential elsewhere in the bone. It has however, been observed, as shown in [1], [2], [3] and [4], that small amounts of charge passing through the bone cause osteoblastic activity at the negative end of the current flow, which partly accounts for the increased bone deposition in the area exposed to compression. On the other hand , bone resorption occurs where bone tissue is impaired, this being attributed to osteoclastic activity. The periosteal and intraosteal osteoblasts are maximally activated at the fracture surface. Bone loading is a method applied in the process of speeding up the healing of fractures, and is carried out with special devices for mechanical fixture.

Such devices hold fractured bones together, which enables the patient to use them immediately to a certain degree. Surgical treatment of fractures by fixture with metal plates, screws and special wedges is known as stable compressive osteosynthesis.
Although the objective value of such treatment has been proved, the therapy of applying internal metal bone fixtures has yielded partly or completely unsuccessful results. The reaction of the surrounding tissue and the bone to the implanted metal is negative, thus leading either to rather slow healing of fracture or to its failure.
If thermic, infectious or physical damage, which is considered inherent in surgery, is ruled out, attentio should focus on the electrochemical reaction of the metal implant to the surrounding tissue, when the organism rejects metal osteosynthetic endoprostheses, which causes undesirable effects. The intensity of this phenomenon depends on the kind of metal implanted as well as on the surrounding tissue, into which the endoprosthesis has been implanted. Electrochemical processes cause direct dependence of electrode potential on the density of the current flowing through the electrical double layer of metal and tissue. The well-known measuring methods are devided into the following groups:

- stationary
  (the speed of the respective processes does not change with time);
- transitional
  (a change of one electrical dimension with time is noted, the other dimension being kept constant or changing controllably).

However, if we intend to observe temporal changes of electrical potentials occuring in contacts of metal with electrolytes, measuring can be done in a more acceptable way, i.e., by applying the method described below. This provides both a quantitative and a qualitative picture of the changes in the potential of the implant, depending on its electrochemical properties.

2. THE METHOD OF MEASURING IMPLANT QUALITY

2.1. DESCRIPTION

The method is based on the fact that the input of the measuring instrument is higher than the internal resistance of the electrochemical sample, which practically does not affect the change in electrical potential of the double layer observed. Figure 1. clearly suggests that a voltmeter with lower input would, if used, induces an electrical discharge through the instrument itself, in which case we would not get an exact picture of the transient being studied.
Measuring is done in the following way. One end of a high input measuring instrument (over 100 GΩ) of the desired resolution (MU) is connected to the metal sample (M) which is loose, while the other end is connected to the reference electrode (Re) already dipped into electrolyte (E).

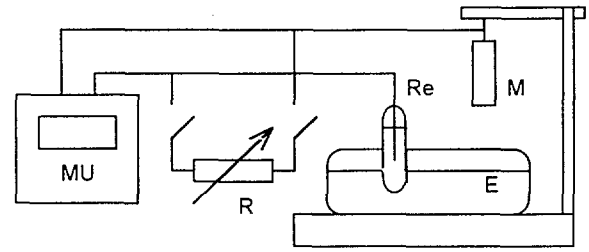

Figure 1. Measuring of sample quality

Dipping the sample induces a rapid increase in the potential , followed by its temporal change, which is recorded by the measuring instrument. Once the stationary condition has been reached, the variable resistor (R) is connected in order to decrease the resistance to half its value. The interior resistance of the sample is thus equalized with the exterior resistor, giving us its exact value. The surface of the dipped samples can be exactly determined, which is necessary for reducing electrical dimensions to the surface unit. Kalomel's saturated electrode , e.g., K401, whose potential depends on temperature, is used as shown in table 1.

T [°C]	0	10	20	30	40
U [mV]	260,2	254,1	247,7	241,1	243,3

Table 1. Kalomel's saturated electrode potential

Ringer's solution is used as an electrolyte, its composition being very similar to the physiological solution of the surrounding cells in human organisms.

2.2. PHYSICAL REPRESENTATION OF MEASUREMENTS

In physical terms, the transient is supposed to follow the exponential law as well as the majority of natural falling and rising functions. If this phenomenon is accounted for by introducing the probable structure of double layer represented by the corresponding combination of capacitor and resistor,

it is likely that the exponential fall will most closely approximate the indicated changes as in equation (1).

$$U(t) = Um\ e^{(-b\ t)} + Uo \qquad (1)$$

2.3. MATHEMATICAL APPROXIMATION

In mathematical terms, function

$$y(x) = a\ e^{(-b\ x)} + c \qquad (2)$$

will be a good approximation of the measured value of function f(xi), if the minimum sum of square errors is

$$s = \sum_{i=0}^{n} [\ f(xi) - y(xi)\ ]^2 \qquad (3)$$

Partial derivation of equation (3) and application of the conditions for the function's minimum result in

$$\delta s/\delta a = 0 \qquad (4)$$
$$\delta s/\delta b = 0 \qquad (5)$$
$$\delta s/\delta c = 0 \qquad (6)$$

Substitution of

$$z(x) = \ln(\ y(x) - c\ ) \qquad (7)$$
$$ao = \ln(a) \qquad (8)$$
$$w(xi) = \ln(\ f(xi) - c\ ) = wi \qquad (9)$$

results in

$$z(x) = ao - bx \qquad (10)$$

Introduction of (8), (9) i (10) into the equations (4),(5) and (6) results in linear system

$$\sum_{i=0}^{n} [\ wi - ao + b\ xi\ ] = 0 \qquad (11)$$

$$\sum_{i=0}^{n} [\ wi\ xi - ao\ xi + b\ xi^2\ ] = 0 \qquad (12)$$

Equation (1) then gives

$$a = Um\ [mV] \qquad (13)$$
$$b = 1/RC\ [1/ms] \qquad (14)$$
$$c = Uo\ [mV] \qquad (15)$$

The average square error will be

$$s = \left(1/(n-2) \sum_{i=0}^{n} [\ U - Ui\ ]^2 \right)^{1/2} \qquad (16)$$

where Ui is a calculated and U a measured value at the same moment t.

2.4. TYPES OF SAMPLES

Measurements have been taken of several types of samples grouped according to their respective section and the method of treating the implant surface: - mechanically treated and
- electrically polished samples.

For practical reasons, we give below a graphic representation of the results of several typical implants, namely three mechanically treated samples (M) and three electrically polished ones (E).

2.5. MEASURING RESULTS

All voltage values (U) are in [mV], and time (t) is expressed in [s].

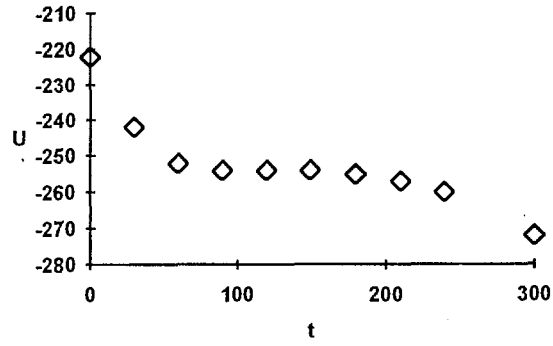

Figure 2. Rectangular sample, type (17 x 4 M)

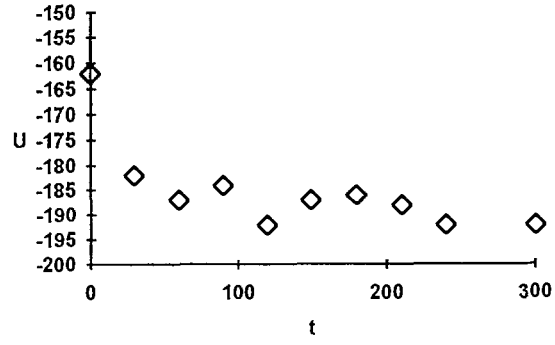

Figure 3. Rectangular sample, type (15 x 5 M)

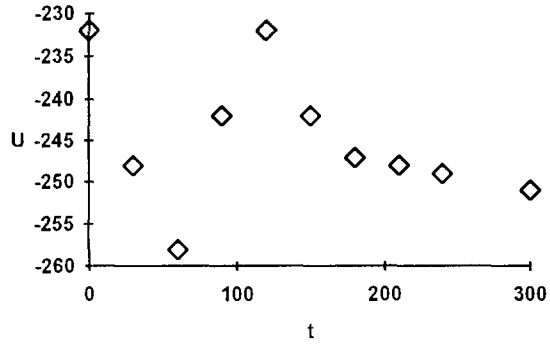

Figure 4. Kuentscher's sample, type (7 x 1,5 M)

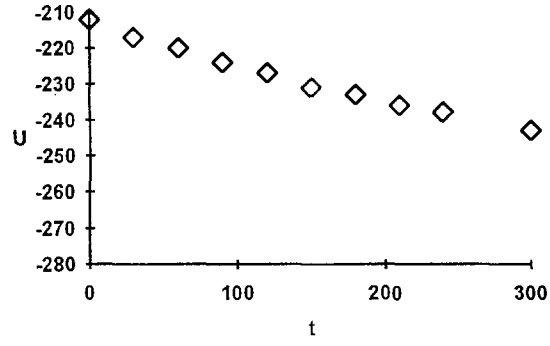

Figure 5. Rectangular sample, type (15 x 4 E)

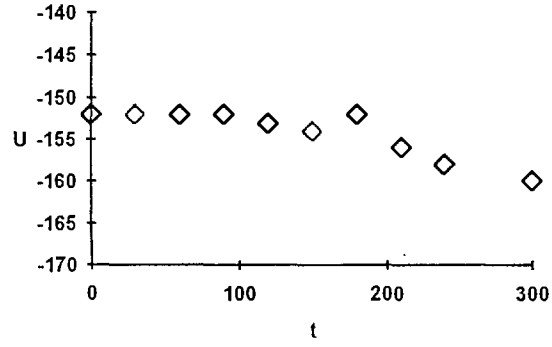

Figure 6. Rectangular sample, type (11 x 4 E)

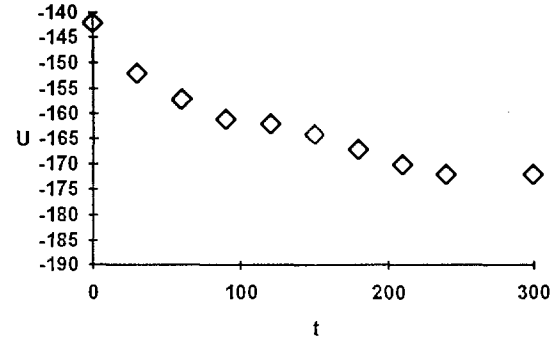

Figure 7. Cylindrical sample type (8 E)

2.6. PROCESSING OF RESULTS

A considerable number of samples have been measured. The following table shows the average value of the parameters, depending on the surface treatment of the samples.

	Mech. tr.	Electrically pol.
Um [mV]	60	53
Uo [mV]	-190	3
b [1/ms]	31	26
Ru [kΩ]	140	311
s	4,5	1,5

Table 2. Average values of measuring parameters

3. CONCLUSION

The results obtaind suggest that consideration should be given to the siye of the average square error of the measurements and to the internal resistance, which should be high, this being characteristic of electrically polished samples. Mechanically treated implants, whose test results were poores, should be avoided. Particularly undesired are those samples whose voltage changes unpredictably and whose average measuring error is so great as not to allow any conclusions. Such changes in potential will probably affect the healing process of the bone tissue and lead to the organism's rejection of the implant. These phenomena very often result from damage or inadequate treatment of samples prior to surgery.

4. REFERENCES

[1] E. FUKADA, Piezoelectric Properties of Biological Macromolecules, Adv. Biophys. Vol. 6, 121, 1974.

[2] P.B. MARTIN, Theoretical Analysis of the Pizoelectric Effect in Bone, J. Biomech., Vol. 12, 55-63, 1979.

[3] M.W. JOHNSON, D.A. CHAKKALAKAL, A. HARPER, J.L. KATZ, Compression of the Electromechanical Effects in Wet and Dry Bone, J. Biomech., Vol. 13, 437-442,1982.

[4] J.W. SPARADO, Electrically Enhanced Osteogenesis at Various Metal Cathodes J. Biomed. Mater. Res., Vol. 16, 861-873, 1982.

MATERIALS FOR BIOMEDICAL APPLICATIONS

Zdravko Schauperl
Franjo Kovačiček
Faculty of mechanical engineering and naval architecture
Đ. Salaja 1, Zagreb

Abstract
Materials for biomedical application (for instruments, implants and other equipment production) have to satisfy the most rigorous demands on their properties.
This paper presents a review of four basic groups of material (metals, plastics, ceramics and composites) used in medicine, with their properties (characteristics) and specific applications. New materials and new technologies directed to improvement of material properties (such as surface engineering) are especially described. The paper also describes a database called "MEDMat" with materials for orthopaedic implants and instrument, created at Department of Materials, Faculty of Mechanical Engineering and Naval Architecture University of Zagreb. At this moment 91 different metallic materials (stainless steel, Ti, Ti- and Co-alloys) defined by ISO and DIN standard are in MEDMat. MedMat is adequate for medical equipment producers as well as for the users.

1. INTRODUCTION

One of the most propulsive science disciplines of today is undoubtedly the science of material. Improvement of the properties of existing and the development of completely new materials occurs as a result of markedly interdisciplinary research in which scientists and experts of various profiles take part.
Development of medicine, particulary modern surgery with the use of orthopaedic implants and protheses, is to a large extent dependent of this research, because the materials used in this field have to satisfy special rigorous demands.
Among others, three basic conditions for every material in this field can be isolated:
1. corrosion resistance,
2. biocompatibility,
3. adequate mechanical properties.

Besides those mentioned, there are numerous additional demands on material which depends on the site of application, such as: anticoagualatory properties for materials in cardiovascular application, good tribological properties (wear resistance) for artificial joints, ductility for implants (to adjust shape to bones), and last but not least economical acceptability (cost analysis) for each material. A large number of new materials and also current materials treated by new high technologies and techniques, satisfy the above demands and can be used in medicine.
Their complete examination and also development tendencies is almost impossible to carry out, because each characteristic group of design materials and each new manufacturing technology should requires a separate study. Hence, this survey will give a brief review of some major properties of basic material groups and technologies, with examples of their medical application.

2. MATERIAL GROUPS

The foundation for the manufacture of instruments, implants and protheses, consists of four basic material groups: metals, plastics, composites and ceramics.

2.1 Metals

Metals have the widest and oldest application in medicine. They are used in the manufacture of all kinds of medical equipment (instruments, implants, protheses). For such a wide application area we use a large number of different metals and their alloys. Their usage in the manufacture of orthopaedic implants is significant. The history of metal

implantation in the human body, and therefore the exclusive usage of metal in medicine began with Petronius, who implanted a gold plate in the oral cavity in 1565. However the first written evidence of metal implant applications date from the year 1775. when the Frenchman Lapeyode u. Sicre used metal wire for bone binding [1].

Today it is known that it is extremely important for metals for orthopaedic implant manufacturing to satisfy the above demands. To ensure this, in 1975. the International Standard Organization formed a Committee for standardization of material for orthopaedic implants (Norm-Komitee fur chirurgische Implantate). The function of this Committee is to standardize implant material, and also coordination of those standards with the standards of various countries. According to the ISO standard the following groups of materials for orthopaedic implants manufacturing have been defined:

a) Fe based alloys (ISO 5832/I)
b) Ti based alloys (ISO 5832/II, III)
c) Co based alloys (ISO 5832/IV, V, VI)

These standards define the chemical composition of metal for manufacture of implants, which defines chemical-physical and mechanical properties.

Also, all medical instruments should be made according to standards (ISO or national), which besides the material also regulate treatment technique and testing (ISO 7153; DIN 58298/1...18). For medical instrument productions today Fe based alloys - various types of stainless steel, which besides highly satisfying properties are cheapest, are used almost exclusively.

A part from the mentioned standardised materials, several other materials are used but because of their high price, only for special purposes (pure Ta and Nb, various precious metals and alloys) [1].

Also use of hard metals should be mentioned. It is an artificial material, produced by special technological processes, and its basic characteristic is extreme hardness, but also extreme brittleness. Therefore such hard metal plates are used only for the parts exposed to intense wear - cutting edges of scissors, forceps... The use of hard metal significantly increased duration (3-5 times), and also work safety has been improved.

Trends in the application of metal in medicine: In metallurgy efforts have been made to produce alloys with an increased share of alloying elements which improve corrosion resistance (Cr, Mo, Ni). At the same time the aim is substitute of expensive alloying elements by cheaper ones (Mn, N), but without decreasing mechanical properties and corrosion resistance.

A completely new type of material is also being developed - Memory effect alloys on Ni-Ti or Cu bases, the main characteristic of which is, after deformation, small changes in temperature can be used to regain the previous shape of the material. Stainless Cr-Ni-Mn-Si steel has been developed in Japan with mentioned memory effect, the use of which is predicted for parts of medical equipment and also in orthopaedic implant manufacturing [2].

2.2 Plastics

Compared to metals, the main advantages of plastics are solid corrosive and chemical stability, low density, easy shaping and good sliding properties. Today there are over ten thousand commercial types of plastics present on the market. Among them there are many materials used in medicine, and the number is increasing. Disregarding their current most extensive application in the production of different bags, gloves, instruments and the other equipment for one-shut use (injections, scalpels, tweezers), use of these materials for producing implants with additional parts and substitutes for soft tissue body parts, has proved to be successful. For example, polyethylene-high density (PE-HD)is a standardized material (ISO, DIN standard) used in the production of cups for artificial joints. Several new plastics have been developed and applied in the manufacture of cardiovascular protheses (foamy poly(thetraflourethylen)-PTFE or polyurethane-PUR). For these materials it is very important that, beside the above mentioned request concerning biocompatibility, they have low trombogenic effect and do not cause hemolyze of the red blood cells. Mechanical properties of these materials are also significant criterium for the choice and application of these materials. For example, the company SULZERMedica is developing artificial ligament for a damaged knee, using poly(ethylene-terephthalat)-PET, made from directed fibers which have been found to be good bearers of loads over a longer period [3].

The problem with regard to the application of plastics is that there is relatively small quantity produced especially for use in medicine, so it is hard to get good insight of their composition, structure and characteristics. In spite of this, the use of plastics in current medicine is unavoidable, and their role will become more and more widespread.

2.3 Composite materials

According to the definition, composites are homogeneous materials made as a result of artificial linking of two or more different materials (matrix and fibers), in order to obtain a new material with specific, improved characteristics [4].

It is a relatively new group of materials, which became well known among other construction materials, due to its specific properties. These materials are also used in medicine, especially those composites with polymer matrix, so called polymer composites. Due to their specific weight (1/3 compared to steel), and also high stiffness, polymer composites are almost ideal materials for making orthopaedic prostheses, wheelchairs and crutches. Other products can also be made from these materials, i.e. Swiss cooperation AKZO has made a complete endoprothesis using fiber reinforced polymer composites [5].
Since these materials are relatively new, it is understandable that much additional research has to be done, not only in the field of materials, but also defining possibilities for their application in medicine. In order to obtain the necessary information, cooperation between physicians and engineers is essential.

2.4 Ceramics

Although ceramics is one of the oldest materials known to people, and ceramic materials have been used in medicine as a substitute for bones since 1890. [6], there are several serious problems at present which obstruct wider use of these materials in medicine, as well as other construction purposes. Primarily these are insufficient toughness-high rigidity, low tensile strength and the wide dispersion of the measured results for different properties. Therefore, ceramics is often used in medicine only partially, for parts where there is no marked impact and dynamic loads. These materials are often used as a part of a friction pair of artificial joints (the other part PE-HD) and for making cutting surfaces and in dentistry for artificial teeth.
Inertness to aggressive surroundings, a modulus of elasticity similar to the modulus of elasticity of bones and excellent wear resistance are reasons why ceramic materials are potentially attractive materials in medicine. Intensive study of composition, structure and technology of modelling are some of the methods for improving the disadvantageous properties of classic ceramic. In the next few years significant development in this field is expected.

3. TECHNOLOGIES OF SURFACE MODIFICATION

Surface engineering, a relatively new field of functional surface improvement, refers to a number of processes which have been transferred from laboratory conditions to commercial technologies. Within those processes metal or non-metal materials are inflicted to the surface of basic material. The result is a "surface composite material", with a specific combination of properties, based on demands of application [2].
In medicine these technologies have really proved their usefulness, because expensive materials can be replaced with cheaper ones - modified by new technologies. A characteristic example of application is the spreading of a layer of TiN (by Physical vapour deposition-PVD or Ion Beam Assisted Deposition-IBAD procedure) on the head of the endoprothesis (to part of a friction pair of artificial joints). TiN layer has excellent tribological properties and corrosion resistance. By using this layer durability of the protheses is prolonged, and the basic material can be of inferior quality, which makes the whole product much cheaper. Spraying in plasma is also a customary procedure, e.g. depositing a bioactive layer (Hydroxylapatit or pure Ti) on Ti alloys (TiAl6V4) in the case of artificial hips, knees and teeth. This layer enables the creation of a natural chemical link between bones and implants, thus avoiding the use of cement.
These are just some of the surface modifying procedures used in medicine, while a number of others have to be discovered in that field.

4. CALCULATION METHODS

Recently, in medical procedures examples have occurred of calculation of stress and deformation of bones, various plates, bolts, fixators under load, as well as simulations of their reaction once they are built into the body. These simulations, i.e. anticipation the reactions of certain elements in the human body, are facilitated by a special numeric method - Finite Elements Method (FEM), and by special computer software designed for that method.
The software enables anticipation of element deformation and stress based on information of shape and dimension of the element, material and expected load during exploitation. Thus critical points can be located, breakage foreseen and insight into its behaviour (deformation) obtained under load. Using FEM this can be done without even experiment or significantly reduce their number.
This method and its application in medicine, regardless of the fact that many institutions have adequate software at their disposal, is not used enough, probably because of insufficient knowledge of the method and its possibilities.

5. SELECTION OF MATERIALS

Examination and systematization of materials used in the production of medical instruments and implants has been made in the Department of materials, Faculty of mechanical engineering and naval architecture, Zagreb. Database "MEDMat" has been created, containing information on 91 metallic materials (stainless steel, Ti and Ti- and Co-alloys) defined by ISO and DIN standard. "MEDMat" includes designation of these materials according to various standards (ISO, DIN, W.Nr., EUS, SNV), application sites, chemical composition (in limits min-max), mechanical properties, wear resistance index, corrosion resistance, biocompatibility and information about producers (name, address, telephone, telefax, price index).

Although all information available in literature have been included, there is a lack of data in the database. To fill "MEDMat" with more data, it is necessary to collect information through cooperation with the manufactures of medical equipment as well as the their users.

It is also necessary to enlarge the database by including non-metallic materials, although their properties significantly differ from metal properties. Obtaining relevant information on these materials used in medicine is difficulty, due to the fact that very few non-metallic materials are standardized.

Because of lack of data on materials in medicine in this country, such a base with adequate software is the best way for systematizing this data.

Therefore, depending on the quantity of data in the database, "MEDMat" gives users the opportunity of obtaining easily and quickly information on materials, medical equipment and producers, as well as help in selection of the optimal material for a defined purpose. "MEDMat" is intended primarily for producers of medical equipment but also for physicians actively on the development of new medical instruments and equipment.

6. CONCLUSION

Detailed analysis of just one segment of the above field requires a great deal more space and time then available at present. The materials and technologies listed here are only one part of the technical achievements or methods used in medicine. There is, however, a large number which are suitable and the application of which in medicine has still to be discovered. Large manufactures have teams of experts from various field of medicine and techniques working on this problem. In this country, where there is a lack of finance for such groups of experts, close cooperation is needed in the field of development between physicians, manufacturers and university personnel. Consequently, the need arises to unite such experts in projects which would be useful for all.

This work should be an incentive for contemplation and initiation of work on systematization of material for the production of instruments and implants, with the aim of establishing a Croatian standard, hopefully in the near future. Particulary since the manufacture of medical instruments in Croatia is a very old tradition; one of the oldest in Europe.

7. LITERATURE

[1]. M. Ungethum, W. Winkler-Gniewek, Metallische Werkstoffe in der Orthopadie und Unfallchirurgie, Georg Thieme Verlag, Stuttgart, 1984.

[2]. T. Filetin, Stanje razvoja i primjene tehničkih materijala, CIM 93, B1-B17, Zagreb, 1993.

[3]. S. Freudiger, Anforderungen an kunstliche Kreuzbander, Technical review Sulzer, 2/1993, 13-17, February, 1993.

[4]. J. Indof, Razvoj i primjena kompozitnih materijala, Materijali u strojarstvu, 90-101, Zagreb, 1992.

[5]. AKZO, prospects

[6]. J. Pirš, O primjeni materijala u biomedicini, Strojarstvo, 20(1978)2, 93-99, February, 1978.

EFFECT OF GRADUAL ISOMETRIC BITE FORCE ON ELECTROMYOGRAM OF HUMAN JAW MUSCLES

Valentić-Peruzović M,[1] Čelebić A,[1] Magjarević R[2], Cifrek M[2], Prpić-Mehičić G[1], Varga S[1]

[1] Dental School, University of Zagreb, Croatia
[2] Faculty of Electrical Engineering, University of Zagreb, Croatia

ABSTRACT: The aim of this study was to evaluate the effect of gradual isometric bite force on electromyogram of the temporal and masseter muscles during determined functional movements, such as biting at different clenching levels i.e. maximal (EMG-1), middle (EMG-2) and minimal (EMG-3), and during speech movements such as reading aloud an unfamiliar text (EMG-4).

Symmetry was examined, as it is generally accepted that in a functionally normal and balanced occlusion bilaterally symmetrical EMG activity should occur. Very high values of asimmetry indices were obtained in this study (-65.04% to +67.72%), which was associated to the very strong influence of visual feedback except in the EMG-4, where asimmetry indices were lower than 20%.

INTRODUCTION

Maximal voluntary contraction of jaw closing muscles in the centric occlusal position was used for many years as a representative for the steady condition of isometric muscle tension (1,2). The activity index (3) was used to quantify the participation of different jaw elevator muscles (masseter and temporalis anterior) to the clenching force in order to calculate the physiological range of muscle contribution.

The aim of this study was to evaluate the contribution of the right and left masseter and right and left anterior temporalis muscles in certain functional movements, such as maximal clenching, submaximal clenching and non-contact activity (speech), and also to evaluate to which extent symmetry is present in certain muscle activities.

MATERIALS AND METHOD

Five dental students participated in this study (2 males and 3 females), age ranged from 18 to 24 years. The method of surface electromyography was used employing the bipolar technique of electrode placement. Electrical activity from the left and right anterior temporal muscles and the left and the right masseter muscles was recorded. The 8-channel PC based EMGA-1 apparatus, which was specially designed and developed (4-6) for the purpose of the electro-kinesyological examinations of the stomatognathic system, was used for recording and processing of the signals, presentation on the monitor as well as their storage on magnetic media for subsequent mathematical or statistical analysis. The recording system was connected to the clenching level indicator which was used for visual feedback information about the clenching level. The clenching level indicator is an additional unit which rectifies and smooths the amplified myoelectric signal obtained from one of the amplifiers of EMGA-1 apparatus and visualises the average myoelectrical activity (voltage) through switching of a correspondent number of light emiting diodes (LED) on. The active rectifier in the clenching level indikator has continous setting of amplification so that during maximal clenching level, the number of LEDs switched on is 10. In submaximal clenching, the number of LEDs switched on is smaller, but proportional to the clenching level. The right temporal muscle was used as a control and its maximal contraction was taken as referent for maximal muscle activity, half of this activity as middle and again half as minimal level of muscle activity. The corresponding number of LEDs switched on at the clenching level indicator was 10, 5 or 2, respectively.

The investigation was made with continuous biting in the centric occlusal position (CO) with maximum voluntary contraction of elevator muscles (EMG-1), then with half of that activity (EMG-2) and after that with only minimal activity (EMG-3) of elevator muscles. The second part of the examination was the functionally dynamical phase as reading aloud an unfamiliar text (EMG-4).

In order to compare the activity on the right and the left side, asymmetry index by Naeije et al.,(3) was applied for statistical evaluation.

$$ASSYMETRY\ INDEX = \frac{RM - LM}{RM + LM} \cdot 100\%$$

A positive index indicates a right side dominance and a negative index a left side dominance. The index ranges from -100% to +100%. The asymmetries of the masseter and the anterior temporalis muscles were investigated.

The relation of the right and left sided muscle was also compared at different clenching levels and during reading, as a non-forced excursions of the mandible.

$$ACTIVITY\ INDEX = \frac{RMS_A - RMS_B}{RMS_A + RMS_B} \cdot 100\%$$

The Activity Index (3) was used to compare the quantitative contributions of EMG activities of muscles A (masseter) and B (temporalis) to the clenching effort. The higher the index, the greater the contribution of muscle A compared with that of B. The index ranges from -100% to +100%, with -100% indicating exclusively muscle B activity and +100% exclusively muscle A activity.

RESULTS

Table 1 reports mean values and relevant standard deviations of electric potentials recorded from the right and left maseter and temporal muscles, at three different clenching levels (EMG-1, EMG-2, EMG-3) controlled by visual feedback method and the fourth EMG sequence that was recorded during reading aloud an unfamiliar text (EMG-4).

TABLE 1 The results of EMG recordings at different clenching levels (EMG-1 to EMG-3) and during speech activity (EMG-4) for the group of five subjects for the masseter and temporal muscles.

	RM		LM		RT		LT	
	X (μV)	SD	X (μV)	SD	X (μV)	SD	X (μV)	SD
EMG-1	175.26	134.18	150.16	45.41	193.03	141.63	166.59	122.57
EMG-2	46.12	27.70	69.78	51.52	73.37	43.18	60.6	59.62
EMG-3	17.96	13.20	25.56	14.68	28.10	20.82	18.20	14.02
EMG-4	8.42	3.24	8.2	3.25	7.82	3.26	7.52	4.58

EMG-1 maximal vountary clench, EMG-2- moderate clench (about 50%) and EMG-3 -very low clenching level (about 25%). EMG-4 the activity of the muscles during speech.
RM - right masseter muscle, LM - left masseter muscle, RT - right temporal muscle, LT - left temporal muscle, X - arithmetic mean in microvolts, SD - standard deviation.

The asimmetry indices were calculated individually for each subject for masseter (Table 2) and for temporal muscles (Table 3)

TABLE 2 Asimmetry index (As-I) for the right and left masseter muscles at 3 different clenching levels, and during the speech activity.

As-I (%) for RM and LM				
	EMG-1	EMG-2	EMG-3	EMG-4
1.	2.51	-0.36	15.38	-4.35
2.	-31.32	-42.99	-32.43	-10.56
3.	32.32	9.26	11.28	-4.76
4.	-16.11	-13.37	-35.85	17.70
5.	1.23	-24.01	-65.04	6.41

EMG-1 maximal vountary clench, EMG-2- moderate clench (about 50%) and EMG-3 -very low clenching level (about 25%). EMG-4 the activity of the masseter muscles during speech.

TABLE 3 Asimmetry index (As-I) for the right and left temporal muscles in 3 different clenching levels, and during the speech activity.

As-I (%) for RT and LT				
	EMG-1	EMG-2	EMG-3	EMG-4
1.	4.35	54.98	25.00	4.76
2.	-0.78	-4.96	4.35	0.
3.	8.11	0.80	23.08	33.33
4.	30.18	67.72	52.94	-8.13
5.	1.15	7.46	15.00	5.02

EMG-1 maximal vountary clench, EMG-2- moderate clench (about 50%) and EMG-3 -very low clenching level (about 25%). EMG-4 the activity of the masseter muscles during speech.

The activity index (AI) was also calculated to obtain the relation of the activities in percentages of the masseter and temporal muscles in different dynamic and static activities.

TABLE 4 Activity index for masseter and temporal muscles

A-I (%) for M and T				
	EMG-1	EMG-2	EMG-3	EMG-4
1.	11.67	31.50	23.80	4.54
2.	-13.75	-4.53	23.33	5.58
3.	-4.25	-22.81	-21.99	27.27
4.	-10.77	-6.17	1.92	-8.13
5.	2.69	12.08	-23.84	6.85

Activity index between masseter and temporal muscles expressed in percentages

DISCUSSSION

In order to determine the relative contribution of the masseter and temporalis muscles to global isometric bite force, activity indices were constructed and applied (3,7). Contrary to the findings of Naeije (3) who stated as the bite force increases, so does the myoelectrical activity of the masseter muscle, and positive index values appear to increase as a logarithmic function of bite force, we found masseter predominance only in the speech registrations, while in different isometric clenching efforts no such regularity was observed.

Asimmetry indices for temporal muscles had higher values for submaximall clenching levels (EMG-2, EMG-3), while low values were given for maximal clenching level (EMG-1) and speech sequence (EMG-4). Asimmetry indices for masseter muscles were higher and in the 12 of 20 cases had negative sign, while temporal asimmetry indices were negative only in three occasions. Asimmetry indices were also variously ranged for both muscles (-65.04%, +67.72%) and interesting observation was made about combination of the masseter and -temporalis cross-sided dominance. According to this finding predominance of masseter muscle on left side in some cases is connected with right side temporalis dominance and vice versa (Tab.2,3). Only in EMG-4 sequence the asimmetry indices were lower than 20%, which was considered normal (8,9).

The results obtained in this study were strongly under influence of visual feedback except in the EMG-4, where subjects were reading an unfamiliar text and concentrated on it. In all other sequences (EMG-1, EMG-2, EMG-3) the visual feedback was obtained by monitoring the activity of the right temporal muscle connected with the diodes-lightening-set, and it seems that subjects were not

retained the same occlusal position throughout the procedure, specially during submaximall clench. Some more research should be done to improove the applicability of the feedback control.

REFERENCES

1. Moller E. (1970), "Computer analysis of electromyographic data in clinical studies of oral function", Scand J Dent Res, Vol.78. pp. 411-416.

2. *Michler L, Moller E, Bakke M, Andreassen S and Henningsen E.* (1988), "On-line Analysis of Natural Activity in Muscles of Mastication", J Craniomandib Disord, Vol.2, pp. 65-82.

3. Naeije M, McCarroll RS and Weijs WA. (1989), "Electromyographic activity of the human masticatory muscles during submaximall clenching in the inter-cuspal position", J Oral Rehabilitation, Vol. 16, pp.63-70.

4. *Valentić-Peruzović M and Magjarević* R. (1990), "System for data acquisition and analysis of muscular activity and sounds in dentistry", 8th Symp edicine and Engineering", JUREMA Proc 35, Zagreb, pp.43-46.

5. *Valentić-Peruzović M, Magjarević R, Stipetić D, Cifrek M and Žuljević Ž.* (1991), "The recording of the occlusal sounds and bioelectrical activity of masticatory muscles by the new designed configuration EMGA-1". 7th ICMMB Proceedings: pp. 57-58.

6. *Cifrek M, Magjarević R, Valentić M, Stipetić D and Žuljević Ž.* (1991), "PC based system for simultaneous recording of myoelectric activity and occlusal sounds." Proc. of IV Int. Symp. on Biomedical Engineering, Peniscola, Spain, pp.120-121.

7. *Christensen LV, and Kundinger KK.* (1991) "Activity index and isometric contraction velocity of human jaw muscles", J Oral Rehabilitation, Vol. 18, pp. 555-561.

8. *Ferrario VF, Sforza C, Miani A Jr , and D'Addona A..*(1993) Electromyographic activity of human masticatory muscles in normal young people. Statistical evaluation of reference values for clinical application", J Oral Rehabilitation, Vol. 20, pp. 271-280.

9. *Valentić M, čelebić A, Prpić G, Magjarević R, Cifrek M.* (1994) "The evaluation of the functional symmetry with a new PC-based system for simultaneous electromyographic and gnathosonic registrations of mandibular kinetics" Proc. of 16th International Conference on Information Technology Interfaces, Pula, pp. 453-458.

ISOTONIC AND ISOMETRIC MUSCLE ACTIVITY IN AN OPEN-CLOSE-CLENCH CYCLE IN INDIVIDUALS WITH NORMAL OCCLUSION AND ARTIFICIAL OCCLUSAL INTERFERENCE

Asja Čelebić[1], Melita Valentić-Peruzović[1], Mario Cifrek[2], Ratko Magjarević[2], Josipa Kern[3], Denis Vojvodić[1]

[1] - School of Dentistry, Univ. of Zagreb, Gundulićeva 5, 41000 Zagreb, Croatia

[2] - Faculty of Electrical Engineering, University of Zagreb, Croatia

[3] - School of Health, University of Zagreb, Croatia

ABSTRACT: The purpose of this study was to compare the isotonic (UIT) to isometric (UIM) muscle activity in an open-close-clench cycle (OCC cycle) in individuals with normal occlusion and to compare the isometric muscle activity in an OCC cycle to the isometric activity of the maximum voluntary clenching, as well as to find out the influence of an artificial occlusal interference on the UIT and UIM in an OCC cycle. EMG signals were recorded from 4 masticatory elevator muscles: anterior right and left temporal (RAT, LAT) and right and left masseter muscle (RM, LM) simultaneously with the signals of the occlusal sound in 10 OCC cycles on the EMGA-1 apparatus for each of 62 individuals with healthy occlusion. In 35 individuals an artificial occlusal interference of a self-curing acrylic resin was applied to the right lower premolar and ten EMG registrations of an OCC cycle for each participant were again recorded. There was no significant difference between UIT and UIM in an OCC cycle ($p > 0.05$), while UIM was significantly greater in the maximum voluntary clenching than in the OCC cycle ($p < 0.01$), proving an increased spatial and temporal summation of motoneuron drive under central voluntary command during maximum voluntary clenching. When the artificial occlusal interference was applied, the UIT was significantly reduced only for the RAT and LAT ($p < 0.01$), while UIM was significantly reduced for RTA, LTA, RM and LM ($p < 0.01$). This results confirm the existence of the reflex arch with positive feed back, which reduces the harmful influence an artificial occlusal interference on the periodontal ligament and also prove that the temporal muscle is more responsible for the spatial controll of the lower jaw than the masseter muscle, which is more responsible for the powerful contraction. Key words: Isotonic and isometric muscle activity, open-close-clench cycle

IZOTONIČNA I IZOMETRIČNA MIŠIĆNA AKTIVNOST U OPEN-CLOSE-CLENCH CIKLUSU U ISPITANIKA S NORMALNOM OKLUZIJOM I UMJETNOM OKLUZIJSKOM INTERFERENCOM

SAŽETAK: Cilj ovog rada bio je usporediti izotoničnu (UIT) i izometričnu (UIM) mišićnu aktivnost u open-close-clench (OCC) ciklusu i UIM u OCC sa izometričnom aktivnošću prilikom maksimalne voljne kontrakcije (Umax) u ispitanika s normalnom okluzijom, kao i ustvrditi utjecaj umjetne okluzijske interference na UIT i UIM u OCC ciklusu. EMG signali registrirani su iz lijevog i desnog m. temporalisa (LTA,DTA), i lijevog i desnog m. massetera (LM,DM) metodom površinske elektromiografije simultano sa zvukom okluzije u 10 OCC ciklusa kod svakog od 62 ispitanika s normalnom okluzijom. U 35 ispitanika napravljena je umjetna okluzijska interferenca na donjem desnom premolaru od autoolimerizirajućeg akrilata i 10 EMG registracija OCC ciklusa ponovo je zabilježeno kod svakog ispitanika. Nije bilo statistički značajne razlike između UIT i UIM u OCC ciklusu ($p > 0.05$), dok je Umax bio veći od UIM, što dokazuje veće prostorno i vremensko uključenje motornih jedinica pod voljnom centralnom kontrolom za vrijeme maksimalne interkuspidacije. Nakon aplikacije umjetne okluzijske interference, UIT se značajno smanjio ($p < 0.01$) za LTA i DTA, dok se UIM značajno smanjio za sva 4 mišića (DTA,LTA,DM,LM). Ovi rezultati dokazuju postojanje refleksnog luka pozitivne povratne veze uslijed čega se smanjuje mišićna kontrakcija kako bi se smanjio štetni utjecaj okluzijske interference na parodoncij zuba, a također se potvrđuje da je m. temporalis odgovorniji za položaj donje čeljusti od m. massetera, koji je odgovorniji za snažnu

izometričnu kontrakciju. Ključne riječi: izotonička i izometrična mišićna aktivnost, open-close-clench ciklus

INTRODUCTION

Many studies have analyzed the mandible elevator muscles isometric activity at various lower jaw occlusal positions, as well as their activity during mastication. The isotonic elevator muscle activity, however, has not been studied and compared to the isometric activity. Duration of the isotonic muscle activity was measured in only a few studies, but the mean voltage was not (1,3). The isotonic activity in the lower jaw elevators spans from the beginning of the elevator contraction until the occlusal contact of the teeth, after which muscle activity becomes isometric; i.e. the length of the muscle fibres no longer changes, but it is the tension that becomes greater.

The isometric muscle activity of the mandibular elevator muscles can be studied during chewing or in an open-close-clench cycle (OCCC). OCCC is a cycle when an individual opens and then firmly closes the mouth. When the teeth come into occlusal contact, after a latency of approximately 10-15 ms, a silent period of approximately 15-27 ms can be observed on an electromyogram of jaw elevator muscles, after which the isotonic muscle activity continues (1,3).

The purpose of this study was to compare the isotonic (UIT) and the isometric (UIM) muscle activity in an OCC cycle in individuals with normal occlusion, as well as to compare the isometric muscle activity in an OCC cycle to the isometric activity during maximum voluntary clenching. The aim of this study was also to examine the influence if an artificial occlusal interference on the isotonic or isometric muscle activity in an OCC cycle.

MATERIALS AND METHODS

EMG registrations were taken on the EMGA-1 apparatus, a new configuration of a PC controlled multichannel system for electromyographic and audio-signal registrations, recently developed in collaboration between the Faculty of Electrical Engineering and the School of Dentistry, University of Zagreb, Croatia (4,5). EMG signals were recorded in 62 individuals with full dentitions and normal occlusion and were stored on a floppy disk for subsequent analysis. The signals were recorded by methods of surface electromyography from 4 elevator masticatory muscles: right and left anterior temporal (RAT, LAT) and right and left masseter muscles (RM, LM) during ten subsequent OCC cycles (6) in each individual (time base 240-300 ms). An artificial occlusal interference (0.2-0.5 mm thickness) of a self-curing acrylic resin was fabricated and applied to the lower first premolar in 35 individuals. Again, EMG activity was recorded during ten OCC cycles. EMG activity was also recorded in all the individuals during the maximum voluntary clenching (time base 2,4 s).

All measurements were made directly on the screen by using the Medwin software package which enables the use of tracers and directly calculates the mean muscle activity between the tracers. UIT (mean isotonic muscle activity) was measured from the muscle activity commencement, which triggers the registration to the occlusal sound trace (Figure 1) and isometric muscle activity (UIM) was measured from the end of a silent period to the EMG trace completion on the screen. Umax (mean muscle activity during maximum voluntary clenching) was measured during the recorded 2,4 s, 3 time intervals for each individual.

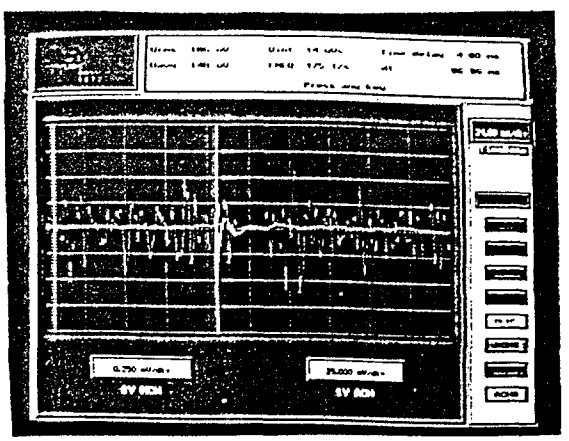

Figure 1. Measurement of the mean voltages of UIT directly on the screen by using tracers (software Medwin)

From the obtained data a statistical analysis was made by using the SPSS software (descriptive statistics, t test, analysis of variance).

RESULTS AND DISCUSSION

From the 10 OCC cycles registered for each individual, the mean values of UIT and UIM were calculated and used for subsequent statistical analysis. The mean values of Umax were also

INDIVIDUALS WITH NORMAL OCCLUSION (n=62)			
variable	x (μV)	sd	min-max
UIT-RAT	112.71	47.97	51.1-322.5
UIT-RM	133.76	76.88	26.1-334.7
UIT-LAT	116.05	59.19	34.7-366.8
UIT-LM	155.25	97.98	15.4-523.3
UIM-RAT	113.74	51.67	39.7-346.6
UIM-DM	140.39	80.25	20.7-331.8
UIM-LAT	118.64	66.35	29.0-410.5
UIM-LM	150.54	94.55	9.2-494.1
UMAX-RAT	160.54	77.17	72.0-526.0
UMAX-RM	221.92	114.04	32.0-687.0
UMAX-LAT	167.64	81.37	56.0-421.0
UMAX-LM	218.84	104.03	30.0-579.0
INDIVIDUALS WITH ARTIFICIAL OCCLUSAL INTERFERENCE (n=35)			
variable	x (μV)	sd	min-max
UIT-RAT	81.81	30.53	25.4-187.5
UIT-DM	111.42	46.07	26.0-231.9
UIT-LAT	74.21	31.38	15.3-132.0
UIT-LM	112.09	47.99	24.0-208.9
UIM-RAT	74.70	35.79	16.4-208.7
UIM-DM	97.45	56.38	15.7-310.6
UIM-LAT	61.20	32.79	14.5-129.3
UIM-LM	91.11	48.44	14.5-239.6

Table 1. descriptive statistics of UIT and UIM obtained from the mean values of 10 subsequent OCC cycles for each individual and Umax obtained from the mean values of 3 maximum voluntary clenches during 2.4 s; UIT=mean isotonic activity; UIM=mean isometric activity; RAT,LAT=right and left temporal muscles; RM,LM=right and left masseter muscle

SIGNIFICANCE OF THE DIFFERENCE OF MEAN VOLTAGES OF UIT AND UIM BEFORE AND AFTER APPLICATION OF ARTIFICIAL OCCLUSAL INTERFERENCE			
UIT	DF	T	p
UIT-RAT : UIT-RAT-EXP	34	4.70	<0.0001 **
UIT-RM : UIT-RM-EXP	34	2.01	= 0,053 ns
UIT-LAT : UIT-LAT-EXP	34	4.78	<0.0001 **
UIT-LM : UIT-LM-EXP	34	2,54	= 0.016 *
UIM	DF	T	p
UIM-RAT : UIM-RAT-EXP	34	5.14	< 0,0001 **
UIM-RM : UIM-RM -EXP	34	3.74	< 0,001 **
UIM-LAT : UIM-LAT-EXP	34	5.44	< 0,0001 **
UIM-LM : UIM-LM -EXP	34	4.78	< 0,0001 **

Table 2. significance of the differences for UIT and UIM in OCC cycle before and after application of an artificial occlusal interference; DF=degree of freedom, **-significant at 99%probability; *-significant at 95% probability; ns=not significant; UIT=mean isotonic activity; UIM=mean isometric activity; RAT,LAT=right and left temporal muscles; RM,LM=right and left masseter muscle

calculated from the 3 registered maximum voluntary clenches for each participant. The UIT and UIM mean values were also calculated from the 10 OCC cycles of 35 individuals who participated in an experimental study, i.e. after the application of artificial occlusal interference. The values obtained in this way were used to calculate descriptive statistics (mean, sd, minimum and maximum values) and are shown in the Table 1.

Statistical significance of the mean voltages of UIM, UIT and Umax in individuals with normal occlusion was tested by using the multivariant analysis. There was no significant difference between the UIT and UIM in OCC cycle ($p>0.05$) for all the muscles tested (RAT, LAT, RM, DM). Significance was established between the UIM in OCC cycle and Umax during the maximum voluntary clenching for all the examined muscles ($p<0.01$), at greater mean voltages during Umax.

It may thus be concluded that the mean voltages of the UIT and UIM do not differ during the OCC cycle ($p>0.05$). The mean voltages of Umax are greater during the maximum voluntary clenching than those in the OCC cycle ($p<0.01$), suggesting that more motoneurons are activated under the voluntary central command.

In order to test the influence of the artificial occlusal interference on the UIT and UIM in OCC cycle, Student's t test for the dependent samples was used. Results of the test are shown in the Table 2. When an artificial occlusal interference is applied, the UIT is significantly reduced for both of the temporal muscles ($p<0.01$), but not for the masseter muscles. The isotonic temporal muscle activity reduction confirms the existence of a reflex arch with a positive feed back for the temporal muscle, which is generally considered to be responsible for the lower jaw spatial control. Meanwhile, the masseter muscle is supposed to be responsible for the amount of isometric contraction. The reduction of UIM for both muscles ($p<0.01$) confirms the existence of a reflex arch with positive feed back, which diminishes the harmful influences on the periodontal ligament by reducing the level of muscle activity.

CONCLUSIONS

1. UIT and UIM do not differ significantly for RAT,LAT,RM and LM in an OCC cycle in individuals with normal occlusion ($p>0.05$). Umax is significantly greater than UIM ($p<0.01$) which proves the spatial and temporal summation of an increased motoneuron drive under the central voluntary command.
2. After the application of artificial occlusal interference on the lower first premolar, UIT is significantly reduced for the both of the temporal muscles ($p<0.01$), while UIM is significantly reduced for both temporal and masseter muscle. The results confirm the existence of a reflex arch with positive feed back, which reduces the harmful influence of an artificial occlusal interference on the periodontal ligament and proves that the temporal muscle is more responsible for the spatial relationship of the lower jaw than the masseter muscle, which, again is more responsible for the powerful contraction.

LITERATURE:

1. GRIFFIN CJ,MUNRO RR. EMG of the jaw closing muscles in the open-close-clench cycles in man.Arch Oral Biol 1969;14:141-149
2. CHONG-SHAN S,HUI-YUN W.Value of EMG analysis of mandibular elevators in open-close-clench cycle to diagnosing TMJ disturbance syndrome.J Oral Rehabilitation 1989;16:101-107
3. FREESMEYER WB. Funktionelle Befunde im orofazialen System und deren Wechselwirkung. Carl Hanser Verlag, Munchen Wien, 1987, pp 1-154
4. VALENTIĆ-PERUZOVIĆ M, MAGJAREVIĆ R, CIFREK M, ČELEBIĆ A, STIPETIĆ D. Tooth contacts and electromyographic characteristics of craniomandibular muscles. Periodicum biologorum 1993;95:43-46
5. VALENTIĆ-PERUZOVIĆ M, MAGJAREVIĆ R. Sustav za mjerenje i analizu mišićne aktivnosti i zvukova u stomatologiji. Zbornik radova JUREMA, Zagreb 1990, 43-46
6. ČELEBIĆ A, VALENTIĆ-PERUZOVIĆ M, KERN J, MAGJAREVIĆ R, VOJVODIĆ D, KATUNARIĆ M. Evaluation of the number of measurement necessary to represent the mean value for silent period latency and duration on non-rectified EMG signals. Proceedings of the 16th International Conference on Information Technology Interfaces, Pula, Croatia, June 14-17, 1994, pp 411-416.

THE SPEED ANALYSIS OF JAW OPENING AND CLOSING IN PATIENTS WITH UNILATERAL CROSS-BITE

Renata Gržić
Stanko Vukovojac
Ivonne Uhač

Medicinski fakultet Rijeka
Stomatološki studij-Sudska medicina
Braće Branchetta 20
51000 Rijeka

Summary

Considering the fact that the occurrance of occlusal interferences and damages to mandible muscle elevator is directly related to posterior cross-bite,we chose an objective method for quantitative analysis. Two groups of patients were selected 10 individuals with unilateral cross-bite and 10 students without temporomandibular disorders(TMD)symptoms. By means of the Robert Jenkelson K5A kinesiograph we measured maximal opening velocity of the mandible(mm/s),maximal opening velocity(mm/s),and first tooth contact velocity. The following values were obtained:maximal opening velocity in the study group was 349 mm/s and 380 mm/s in the control group. This difference was incidental. The maximal closing velocity in the study group was incidental. The maximal closing velocity in the study group was 204.9 and 345.2 in the control group with p<0.05. The first tooth contact velocity in the study group was 75.93 and 325 in the control group with p<0.01.

1. INTRODUCTION

Kinesiology describes mandible movements on the basis of anatomic, fisiological and mechanical principles. The movements of the mandible are primarily determined by the position of the cusps because the condyles have to move according to a certain trajectory whereas the mandible is moved by the muscles (5). The teeth make posible the guidance of mandibular movements in several ways: the posterior teeth maintain vertical support during closing and guide into the position of maximal intercuspation(11), the anterior teeth participate in protruding movements, while the canines and premolars participate in lateral movements. We decided to study a group of patients with cross-bite, being a specific occlusal disorder usually occuring in primary and mixed dentitions. According to Kutin and Hawers(1969), this disorder accounts for 7.7% of cases, whereas Helm ascertained this occurrance in 17% of cases(1). The causes of this disorder may be skeletal and dental origin, and they give rise to a change in mandible position and sometimes to the deviation of the centar of the jaw. It has been generally adopted that the construction of the maxillary arc causes premature contacts giving rise to occlusal interferences. In order to avoid these obstructions, the mandible has to make a lateral movement resulting in functional posterior cross-byte. The electromyograph(EMG) research revealed also an asymmetric activity of m.temporalis during chewing and maximal intercuspation. Occlusal interferences are considered to be greatly responsible for the occurance of the TMD(10,7). For this reason we wanted to measure by an objective and noninvasive method the maximal velocity at opening, closing and first contact, which velocity is indicative of the presence

of occlusal interference. The introduction of eletronic tehnology more than three decades ago has facilitated advanced analysis of mandible kinetics. With his kinesiograph, designed to measure mandible movements, Jenkelson contributed greatly to special development of these analyses. There are two such instruments in comercial practice: syrognatograph, constructed by Lewin, and mandible kinesiograph(MKG), constructed by R.Jenkelson.

2. THE BASIC PART OF THE REVIEW

2.1. The Study Group

The measuring of the movementes of the mandible symphysis point was conducted in two groups of 10 selected individuals each. The study group consisted of young patients with unilateral cross-bite. In cooperation with orthodontists of the Dom zrdavlja Rijeka we selected from their files a specimen of 30 pacients already treated. At our written request 10 patients consented to examination.
The control group of 10 individuals was selected among the students of the school of Dental Medicine of Rijeka. Their medical history data revealed no orthodontic therapy, and clinical-functional analysis revealed no sign of any disfunction of the temporomandibular system(TMD). Records of anamnesis, condition and functional analysis, according to the original diagnostic form of Myotronic Research Inc. 6/77, were taken.

2.2. K5A Robert Jenkelson Kinesiograph general information

The MKG is an integrated electronic system designed for the specific purpose of monitoring the position of an incisal point on the mandible in three dimensions within the range of functional and diagnostic movements. An array of sensors suspended on a lightweight headgear is sensitive to alterations in the magnetic field of a permanent magnet which is affixed to the mandibular incisor with a quick curing acrylic. Data generated by the Kinesiograph represents the spatial position of the mandibular incisal point relative to skull. The sensor array is maintained in a constant relationship to the skull,by the aluminium tubing supports and the eye glass frames. The spatial position of the magnet relative to the incisal edge is a constant. Note that condylar position in the glenoid fossa is not obtainable with this system.A pure rotation about the incisal point would not involve a displacement of the magnet,thus,no output signal will result. The MKG readout consists of one or two simultaneous planes of movement (sagittal, frontal, or horisontal) or a simultaneus sweep of two, three, or four channels, selected from the three mutually perpendicular axial components of mandible position and the vertical component of mandible velocity.
The kinesiograph consists of three parts (6,2):
1. a magnet which should be affixed with selfcuring acrylic to the vestibular plate of the lower incisors taking care that the magnet gets not contact with the upper teeth. Its weight is 21.6 mN and dimensions are 12x6x3 mm.
2. magnetic sensors - there are three pairs of sensors mounted on an alluminium frame. One pair of sensors register the changes of the magnetic field in the saggital, the second in the frontal and the third in horizontal plane. The sensors weight 912.3 mN, alluminium frame weights 1255.7 mN, being altogether affixed to eyeglasses.
3. osciloscope - transformer of the magnetic field into electric signal. The osciloscope is Tektronix 5110 Model modified for the purpose of the Myotronic Research. For movement registration the Tektronix C-5C camera adapted to the osciloscope screen is used.

2.3. Standardized Method Of Recording MKG Robert Jenkelson K5A

The screen simultaneously displays the velocity (vertical projection) and lateral projection of the frontal plane in x-y system. Dual Display Selector is set on vert./vel. position. Lateral gain control 10mm/div. Leave vertical gain control 10mm/div. Vertical velocity gain control 100mm/s/div. Thus prepared the MKG records movements in xy coordinate system. The velocity is displayed in the left and frontal projection in the right part of osciloscope. Each division represents 10 mm. The patient keeps his mouth closed, he is instructed how to open and close quickly his mouth and the MKG is turned on. The tracing is correct when upon respected movements of the traces are identical.

2.4. The Results

2.4.1. Maximal Opening Velocity(mm/s)

Table 1.

STUDY GROUP	CONTROL GROUP
390	409
518	354
212	309
450	512
162	287
512	400
275	250
300	312
312	512
359	462

x=349 x=380.7

Sx=38.02 Sx=29.57

There was no significant statistical difference.

2.4.2. Maximal Closing Velocity (mm/s)

Table 2.

STUDY GROUP	CONTROL GROUP
227	345
247	354
125	281
275	462
125	312
262	325
187	237
215	237
180	462
206	437

x=204.9 x=345.2

Sx=16.41 Sx=26.84

There was significant difference with p<0 05.

2.4.3. Velocity At The First Tooth Contact (mm/s)

Table 3.

STUDY GROUP	CONTROL GROUP
45.4	327
72.7	318
50	245
156	462
50	300
62.5	362
112	237
62.3	200
70.1	437
78.3	362

x=75.93 x=325

Sx=10.75 Sx=26.77

There was significant difference with p<0.01.

2.5. Discussion

2.5.1. Maximal Opening Velocity

On the basis of an analysis in which one of the quadratus of the coordinate system measures 10 mm/s, we assessed that the maximal opening velocity in the study group was 349 ± 38.02 and 380 ± 30 in the control group. There was no significant statistical difference, it was only incidental. In the

respective literature we have come accross some data of maximal velocity reading 253±48.7(13), 250-350 (9), 221.7-263.4 mm/s (12). Such results show that the mandible
opening muscles, not participating in avoiding occlusal interferences, are preserved.

2.5.2. Maximal Closing Velocity mm/s

Maximal closing velocity in the study group was 204.9±16.6 and 345.2±26.84 in the control group with $p<0.05$. While measuring the maximal closing velocity we arrived to an interesting discovery which confirmed Moyers - Schreder's observations regarding the presence of prematur contacts due to which the patients with cross-bite have habitual occlusion with forced lateral movement of the mandible in its terminal phase of closing (8,1). As a consequence the patient had traumatic occlusion with damaged closing muscles. An average closing velocity was 10.6±1.93% and it was slower that the average closing velocity in the control group whereas in the study group this velocity was 39.07±2.85. According to Tsolka (12) the maximal closing velocity ranged from 267.5 to 299.9 and according to Tsukiyama it was 311.9±48 (13). On the osciloscope screen the traces of the incisal point during such movement is very specific. An eliptic tracing, usual in the central subjects, changes into an irregular circle with deep depression in the fourth quadrant, namely the terminal phase of the closing trajectory.

2.5.3. Velocity At The First Tooth Contact mm/s

The highest rate of the slowdown was observed at the first tooth contact. In the study group this rate was 75.93±10.75 whereas in the control group it was 325±26.77 with $p<0.01$, namely the velocity at the first contact in the control group was by 76.64% higher than such velocity measured at the first tooth contact in the study group. By recalling sensor and motoric paths which control occlusal relationships of the teeth and their changes we can see the reason why the act of closing slowed down at such a great rate, and why in four patients m.temporalis was so sensitive. This was the consequence of occlusal precontacts. The patients with miofacial pain moved their mandible at a lower speed than those without such pain, which corresponds to the well known fact that a painful muscle can perform quick movements with great difficulty (4).

3. CONCLUSION

Kinesiography as an objective method makes possible the analysis of the mandible movements, as well as accurate quantitative diagnosis. We have confirmed the findings of the authors who closely rate the cross-bite to numerous occlusal interferences and closing muscle alterations. Orthodontic therapy is therefore required to prevent the TMD in advanced age population. Clinical researches revealed that the subjects undergoing orthodontic therapy experienced far fewer disturbances in their temporomandibular system (3). The advantage of the described method was in its reproductibility, objective presentation of the relationship between the two jaws without producing occlusal interferences. The main fault was nonlinearity (4). Hannah observed that in spite of the producer's instructions the occurance of error increases with the mandible departing from its position of maximal intercuspidation. This error could be avoided by constructing a new linearizing K6MKG.

4. LITERATURE

(1) Y. Ben-Bassat, A. Yaffe, I. Brin, J. Freeman, Y. Ehrlich, Functional and morphological occlusal aspects in children treated for unilateral posterior cross-bite,Europ-J-Of-Orthod, 15, 57-63,1993.
(2) J.C. Combadazou, Apport de la kinesiographie et de l'electromyographie dans le syndrome olgodyfunctionnel de l'articulation temporomandibulaire, Actualites odonto-stomatologiques, 163, 627-652, 1988.
(3) I. Egermark, B. Thilander, Craniomandibular disorders with special reference to orthodontic treatment: an evaluation from chilhood to adulthood, Am-J-Orthod-Dentofacial-Orthop, 101(1), 28-34, Jan. 1992.
(4) J.S. Feine, M.O. Hutchins, J.P. Lund, An evaluation of the criteria used to diagnose mandibular dysfunction with the mandibular kinesiograph, J-Prosthet-Dent, 60(3), 374-380, Sept. 1988.
(5) S. Fushimi, The relationship between the position of upper and lower cusps and the path of condyles and cusps in lateral move-

ment - studies with three dimensional measuring system, Nippon Dental University, vol 21, 60, Nippon, 1987.
(6) R. Jenkelson, Instruction manual - Model K5 Mandibular Kinesiograph, Myotronic Research Inc. Seattle, March 1977.
(7) P. Kirveskari, P. Alanen, T. Jamsa, Association between craniomandibular disorders and occlusal interferences in children, J-Prosthet-Dent, 67(5), 692-697, May 1992.
(8) M. Marković, Ortodoncija, drugo izdanje, Medicinska knjiga, Beograd-Zagreb, 1988.
(9) T. Okamura, N. Asanuma, M. Ueki, T. Sato, K. Koide, S. Hatate, Clinical studies on evaluation of condylar movement in TMJ derangements (part 7), Advanced Prosthodontics, Worldwide editors, Locedings of The World Congress Prosthodontics, 338-339, Hiroshima, Sept. 1991.
(10) P.R. Pocock, A.H. Mamandras, N. Bellamy, Evaluation of an anamnestic questionaire as an instrument for investigating potential relationships between orthodontic therapy and temporomandibular disorders, Am-J-Orthod-Dentofacial-Orthop, 102(3), 239-243, Sept 1992.
(11) Ramfjord - Ash, Occlusion third edition, W.B. Saunders Company, Philadelphia 1983.
(12) P. Tsolka, H.W. Preiskel, Kinesiographic and electromyographic assessment of the effects of occlusal adjustment therapy of craniomandibular disorders by a double blind method, J-Prosthet-Dent, 69(1), 85-92, Jan. 1993.
(13) Y. Tsukiyama, K. Koyano, T. Suetsugu, The speed analysis of jaw opening and closing movements, Advanced Prosthodontic, Worldwide editors, Locedings of The World Congress Prosthodontic, 380-381, Hiroshima, Sept. 1991.

DURATION AND TYPES OF INHIBITORY REFLEXES IN INDIVIDUALS WITH HEALTHY OCCLUSION AND IN INDIVIDUALS WITH OCCLUSAL INTERFERENCES

Asja Čelebić[1], Melita Valentić-Peruzović[1], Ratko Magjarević[2], Mario Cifrek[2], Hrvoje Brkić[1], Denis Vojvodić[1]

[1] - School of Dentistry, University of Zagreb, Gundulićeva 5, 41000 Zagreb, Croatia
[2] - Faculty of Electrical Engineering, University of Zagreb, Croatia

ABSTRACT: Evaluation of the duration and the type of the silent periods (SP) in individuals with normal occlusion and occlusal interference was made. EMG signals were recorded from 4 masticatory elevator muscles: anterior right and left temporal (RTA, LTA) and right and left masseter muscle (RM, LM) simultaneously with the signals of the occlusal sound on the EMGA-1 apparatus. Ten subsequent registrations of open-close-clench (OCC) cycle were made for each of 62 individuals with healthy occlusion. In 35 individuals artificial occlusal interference of was applied to the right lower premolar and ten OCC cycles for each participant were registered. A conclusion can be arrived at that the method of SP recordings is sensitive enough to produce a proper diagnosis of an occlusal interference. If a type of prolonged SP (> 31 ms) appears in any single record of the ten registrations of an OCC cycle, or SP with 2, 3 or 4 inhibitory pauses, or a period of depressed muscle activity after the inhibitory pause, or if SP is absent, the clinical diagnosis of occlusal interference should be established. KEY WORDS: silent periods, normal occlusion, artificial occlusal interference, OCC cycle

TRAJANJE I OBLICI INHIBICIJSKIH PAUZA U ISPITANIKA S NORMALNOM OKLUZIJOM I UMJETNOM OKLUZIJSKOM INTERFERENCOM

SAŽETAK: Napravljena je evaluacija trajanja i tipa perioda tišine (SP) u ispitanika s normalnom okluzijom i umjetnom okluzijskom interferencom. EMG signali registrirani su iz 4 mišića elevatora mandibule (desni i lijevi m. temporalis, desni i lijevi m. masseter) simultano sa zvukom okluzije na novoj EMGA-1 aparaturi. Napravljeno je po 10 registracija open-close-clench (OCC) ciklusa u 62 ispitanika sa zdravom okluzijom. U 35 ispitanika aplicirana je umjetna okluzijska interferenca na desni donji premolar i registrirano po 10 OCC ciklusa. Zaključeno je da je metoda registracije perioda tišine na ovaj način dovoljno precizna za postavljanje dijagnoze okluzijske interference. Ako se u bilo kojoj registraciji OCC ciklusa pojavi produženi SP (p>31 ms), ili SP s 2, 3 ili 4 inhibitorne pauze, ili period smanjene mišićne aktivnosti nakon inhibitorne pauze, ili ako se SP uopće ne pojavi, može se postaviti klinička dijagnoza okluzijske interference.
KLJUČNE RIJEČI: Period tišine, normalna okluzija, umjetna okluzijska interferenca, OCC ciklus

INTRODUCTION

The silent period (SP), defined as the cessation of motoneuron activity following a stimulus in a contracting muscle (1) has been known for more than 20 years in jaw elevator muscles. Still, the real importance of this inhibitory reflex has not yet been elucidated. Various stimulti elicit silent periods, by e.g. occlusal contacts, tap to the menton, direct mechanical or electrical stimulations of the oral and perioral region, the only condition is that the muscle is contracted before the stimulus is applied (2).

The SP received a lot of interest since it had been claimed that it has a longer duration in patients with craniomandibular dysfunction (CMD) than in healthy individuals and that it may be a tool of diagnostic interest (3,4). On the contrary, some

other studies could not prove the prolongation of SP in CMD and even claimed that the duration of SP is even shorter in CMD patients (5). The upper limits of a prolonged SP also vary from study to study.

However, there have been some questions raised on the possible effects of testing methods on the duration and thus the reliability of the SP data and it has been established that SP varies, depending on the method, the force of the stimulus, the reticular formation excitement and the level of previous muscle activity.

The aims of this study were: 1. to establish normal values of SP latency and duration in individuals having all the teeth and normal occlusion in an open-close-clench cycle (OCC); 2. to find out if artificial occlusal interference changes the SP latency and duration; 3. to find out if the method is applicable in clinical practice

MATERIALS AND METHODS

EMG and audio registrations were made in 62 individuals having all the teeth in the jaws and normal occlusion on the EMGA-1 apparatus by means of surface electromyography. EMG signals were recorded and stored on a floppy disk for subsequent analysis from 4 elevator masticatory muscles: right and left anterior temporal muscles (RAT;LAT) and right and left masseter muscles (RM,LM). Silent periods were elicited in an OCC cycle. OCC cycle is a cycle when the mouth is closed firmly from the position of opened mouth. Following a certain latency after the occlusal contact, the silent period commences in the electromyogram of jaw elevators. The silent period latency was measured from the commencement of an occlusal sound trace to the peak of the last significant spike preceeding the inhibition. The duration was measured from the peak of the last significant spike preceeding the inhibition to the peak of the first significant spike being a part of the ongoing muscle activity. Ten subsequent OCC cycles were registered for each individual (6). All the measurements were made on the screen by using the Medwin software which enables the use of the zoom-in technique on a graphical window and the tracers for determining the peak of an amplitude. The program directly calculates the duration of an inhibition in milliseconds (ms) depending on the distance between the tracers.

In an experimental part of this study an artificial occlusal interference of selfcuring acrylic resin was applied to the first lower premolar in 35 individuals and 10 OCC cycles were registered again.

From the obtained data a statistical analysis was made on an IBM compatibile computer by using the SPSS software (descriptive statistics, t test, analysis of variance and MANOVA).

RESULTS AND DISCUSSION

In all EMG registrations of the OCC clench cycles in 62 individuals with full dentition and normal occlusion, only one complete inhibition of motoneuron activity could be recognized as a silent period. Mean values for latency and duration are shown in the Table 1. These mean values should be considered as normal values for individuals with healthy occlusion. Multiple analysis of variance (repeated measurements) showed that the mean values for the latency and duration between the muscles examined (RAT,LAT,RM,DM) do not differ significantly ($p>0.05$).

62 INDIVIDUALS WITH NORMAL OCCLUSION			
VARIABLE	x(milis)	sd	%
L-RAT	12.96	1.20	100
L-RM	12.56	1.21	100
L-LAT	12.94	1.26	100
L-LM	12.53	1.29	100
D-RAT	20.16	3.29	100
D-RM	20.61	3.19	100
D-LAT	20.80	3.14	100
D-LM	21.55	3.07	100

Table 1. L=latency; D=duration
RAT,LAT=right and left temporal muscle;
RM,LM=right and left masseter muscle
%=percent of SP commencement in all OCC cycles observed for any individual

In 35 individuals, various types of SPs emerged when the artificial occlusal interference was applied: single prolonged (long duration) SPs (D1), double SPs (D2), SPs with three (D3) or even four (D4) inhibitory pauses, periods of the depressed muscle (DA) activity following the first, the second or the third inhibitory pause, SPs of relative inhibition or, in a low percentage (0.5-2%) SP was missing (Table 2). The number of inhibitory pauses varied in each OCC cycle; sometimes single prolonged SP emerged, sometimes double, triple etc. Latencies of the second and the third SP also varied in each OCC cycle. The described parameters also varied between the muscles; e.g. sometimes a single SP emerged in one muscle and the double or the triple

	RAT		RM		LAT		LM	
	x	%	x	%	x	%	x	%
L1	13.17	98.0	12.76	100.0	13.20	99.3	12.94	98.69
L2	66.22	48.2	60.83	45.2	61.42	48.2	60.99	43.32
L3	109.95	10.1	107.87	8.7	107.45	9.7	112.74	12.05
L4	*	0	132.40	1.3	151.77	1.3	136.83	0.98
D1	32.19	98.0	31.29	100.0	33.31	99.3	33.98	98.69
D1DA	50.86	13.6	52.01	14.6	51.89	14.3	57.70	19.54
D2	72.26	48.2	68.66	45.2	69.94	48.2	68.55	43.32
D2DA	64.32	1.3	80.96	2.2	81.44	3.2	64.47	1.95
D3	118.59	10.1	114.37	8.7	118.00	9.7	119.03	12.05
D3DA	*	0	*	0	65.40	0.3	156.00	0.32
D4	*	0	137.50	1.3	155.55	1.3	143.00	0.98
D4DA	*	0	*	0	*	0	*	0.98
CDSP	64.38	98.0	61.55	100.0	64.38	99.3	66.48	98.69

TABLE 2. L1,2,3,4=latency of the first, the second, the third and the fourth SP; D1,2,3,4= duration of the first, the second, the third and the fourth SP; D1DA,D2DA,D3DA=duration of the SP together with the depressed muscle activity following the SP; CDSP=complete duration of SP complex - this was measured in the cases of more than one SP; *= parameter was missing; x=arithmetic mean; %= percent of the commencement of the observed parameter in all the registrations of OCC cycles in all examined individuals

one in the other. Sometimes an assimetrical duration of the SP complex (SPC) appeared in the examined muscles. In the case of the double or the triple SPs the complete duration (CDSP) was measured, as well as the duration of each SP.

FREQUENCY OF SP TYPES				
No. of SP	MUSC.	CI	RI	MISS.
FIRST SILENT PERIOD	DTA	95.4%	2.6%	2.0%
	DM	95.1%	4.9%	1.3%
	LTA	94.5%	4.9%	0.7%
	LM	93.2%	5.5%	1.3%
SECOND SILENT PERIOD	DTA	36.5%	11.4%	51.8%
	DM	34.5%	10.7%	54.7%
	LTA	39.1%	9.1%	51.1%
	LM	30.0%	13.4%	57.1%
THIRD SILENT PERIOD	DTA	4.6%	5.5%	89.6%
	DM	3.9%	8.5%	87.9%
	LTA	4.9%	4.9%	90.2%
	LM	3.6%	8.5%	87.9%
FOURTH SILENT PERIOD	DTA	0 %	0.0%	100%
	DM	0.3%	1.0%	98.7%
	LTA	0.7%	0.7%	98.7%
	LM	0 %	1.0%	99.0%

Table 3. CI=complete inhibition; RI=relative inhibition; RAT,LAT,RM,LM=right and left temporal muscle, right and left masseter muscle; MUSC.=muscle; MISS.= missing

In some registrations of the OCC cycle with occlusal interference, the inhibition of motoneuron activity was not complete, but partial. In a low percentage (0.5-2%) of registrations SP was missing. Relative inhibition was more frequent in late inhibitory pauses. Percentages of the first, second, third or fourth SP with complete and relative inhibition of motoneurons and the percentages of missing SPs are shown in the Table 3.

Duration of all inhibitory pauses was considered as the silent period complex duration (CDSP) and was significantly longer ($p<0.01$) than that without the occlusal interference ($p<0.01$),(table 4). The latency of the silent period was not changed by an artificial occlusal interference ($p>0.05$) (Table 4).

CONCLUSIONS

Based on the results obtained a conclusion can be arrived at that the method of silent period recordings is sensitive enough to make a proper diagnosis of an occlusal interference. If a type of the prolonged SP (>31 ms) appears in any single record of the ten registrations of an open-close-clench cycle, or SP with 2, 3 or 4 inhibitory pauses, or a period of the depressed muscle activity after the inhibitory pause, or if SP is absent, the clinical diagnosis of the occlusal interference should be established. In order to obtain an accurate diagnosis it is necessary to

THE SIGNIFICANCE OF THE DIFFERENCE FOR SP LATENCY AND DURATION BEFORE AND AFTER INSERTION OF AN ARTIFICIAL OCCLUSAL INTERFERENCE			
SP LATENCY	**DF**	**T**	**p**
L1-RAT : L1-RAT-EXP	34	- 2,01	= 0,053 ns
L1-RM : L1-RM -EXP	34	- 2,02	= 0,052 ns
L1-LAT : L1-LAT-EXP	34	- 1,98	= 0,059 ns
L1-LM : L1-LM -EXP	34	- 2,03	= 0,051 ns
SP DURATION			
D1R-AT : CDSP-RAT-EXP	34	- 13,46	< 0,0001**
D1-RM : CDSP-RM -EXP	34	- 13,07	< 0,0001**
D1-LAT : CDSP-LAT-EXP	34	- 15,08	< 0,0001**
D1-DM : CDSP-LM -EXP	34	- 16,42	< 0,0001**

Table 4. L1=latency of SP or SP complex; D1=duration of SP in the case of only one SP that always emerged without an interference; CDSP= in case of more than one SP complete duration of SPs was measured; RAT,LAT,RM,LM=right and left temporal muscle, right and left masseter muscle; EXP=after insertion of an occlusal interference; DF=degree of freedom; T=t value; p=level of significance; ns=not significant; **=significant at 99% probability

obtain registrations from all the four elevator muscles as SPs are necessarily not equal in all muscles.

LITERATURE

1. ALGHREN J. The silent period of the EMG of the jaw muscles during mastication and its relationship to tooth contact. Acta Odont Scand 1969;27:219-227

2. OWAL B, ELMQUIST D. Motor pauses in EMG activity during chewing and biting. Odont Revy 1975;26:17-38

3. BESSETE R, BISHOP B, MOHL ND. Duration of masseteric silent period in patients with TMJ syndrome. J Applied Physiol 1971;30:864-872

4. WIDMALM SE, HEDEGARD B. Reflex activity in the masseter muscle of patients with TMJ disfunction. J Oral Rehab 1976;3:41-55

5. De LAAT A.A longitudinal study on masseteric PSEC morphology during treatment of TMJ dysfunction. J Dent Res 1986;65:754 (257)

6. ČELEBIĆ A, VALENTIĆ-PERUZOVIĆ M, KERN J, MAGJAREVIĆ R, VOJVODIĆ D, KATUNARIĆ M. Evaluation of the number of measurement necessary to represent the mean value for silent period latency and duration on non-rectified EMG signals. Proceedings of the 16th International Conference on Information Technology Interfaces, Pula, Croatia, June 14-17, 1994, pp 411-416.

INFLUENCE OF THE AGEING TREATMENTS ON THE BOND STRENGTH BETWEEN ALLOYS AND POLYMER VENEERING MATERIALS

Denis Vojvodić, Hanzi Predanić-Gašparac, Asja Čelebić
School of Dentistry, University of Zagreb, Gundulićeva 5, 41000 Zagreb, Croatia

*Abstract: **One of the biggest problems in oral rehabilitation is the reduction of bond strength values between the veneering material and dental alloy after the placement in oral cavity, causing detachment of the veneer, thus discrediting the aesthetic appearance. The aim of this study was to investigate how the ageing treatments (simulating conditions in the oral cavity) influenced the bond strength values obtained after polymerisation. 60 specimens made from the most commonly used materials were tested by using the Smitz-Schulmeyer shear test. The data were statisticaly analysed using descriptive methods,factorial analysis of variance and Tukey test. From the results obtained it could be concluded that ageing treatments reduced bond strength values which were not sufficient for a safe attachment of the veneers in the conditions within the oral cavity.***
Key words:ageing treatment, bond strength

UTJECAJ POSTUPAKA UMJETNOG OSTARIVANJA NA ČVRSTOĆU VEZE IZMEĐU LEGURA I POLIMERNIH MATERIJALA ZA FASETIRANJE

*Sažetak: **Jedan of najvećih problema oralne rehabilitacije je smanjenje vezne čvrstoće između materijala za fasetiranje i dentalne legure koje se zbiva nakon postave zubnog nadomjestka u usta, uzrokujući odvajanje fasete i tako upropaštavajući njegov estetski izgled. Svrha ovog rada bila je istražiti kako postupci umjetnog starenja (simulirajući uvjete u usnoj šupljini) utječu na vrijednosti vezne čvrstoće postignute odmah nakon polimerizacije. 60 uzoraka napravljeno je iz najčešće uporabljivanih materijala i testirano Smitz-Schulmeyerovim smičnim testom. Podaci su statistički analizirani uporabom deskriptivnih metoda, faktorskom analizom varijanci i Tukeyevim testom. Iz dobivenih rezultata može se zaključiti da su postupci umjetnog starenja smanjivali vezne čvrstoće koje tada nisu bile dovoljne za čvrst pripoj fasete u uvjetima usne šupljine.***
Ključne riječi: postupci umjetnog starenja, vezna čvrstoća

1. INTRODUCTION

The production of prosthetic appliances in oral rehabilitation today includes their aesthetic appearance which is often more important to the patients than their function. The aesthetic appearance of the fixed prosthetic appliances can be achieved by covering the metal framework with polymer veneering materials, such as dental resins. According to their physical properties, these materials must resist the chewing and biting forces without any damages which would influence the aesthetic appearance or function.

One of the greatest objections to the veneers is the rise of the marginal gap (which is about 10 micrometers wide) between the resin and the metal surface of the framework because of the polymerising contraction (even to 7%), different coefficients of the volume expansion in the water, especially at different temperatures (1).

So reduced, the bond strength values between veneering material and the metal base could cause detachment of the veneer subsequently discrediting the aesthetic appearance (2).

Dental manufacturers usually give information about the bond strengths between veneering materials and metal bases obtained just a short time after the polymerisation. But that values are not equal to those obtained after the placement of a prosthetic appliance in to the mouth for a certain period of time, because of water absorption and thermal stress which happenes after the ingestion of hot and cold food or drinks.

For that reason, ageing treatments should be used to investigate the bond strength values and to provide results comparable with those obtained in the biological enviroment like human mouth. Usual ageing treatments are those imitating the absorption of water (immersion in distillated water at 37°C for

three weeks) and thermal stress (thermocycling - periodical changes of the temperature).
Musil and Tiller 1984 (3) stated that the bond strength values of 10N/mm^2 give the security for the veneer attachment on metal framework within the oral cavity. Kappert's research (4) revealed that bond strength values after the polymerisation were not sufficient, and after the thermocycling, were not even close to the recommanded values. The bond strength values obtained on Pd-Ag alloys after the polymerisation were 6.3-6.4 N/mm^2 and reduced by 39-50%.
The purpose of this investigation was to find out to what extent different ageing treatments reduce the bond strength values obtained after the polymerisation on the specimens made of the most commonly used dental materials.

2. MATERIALS AND METHODS

The mechanical part of the research was performed in the Department for Materials, Faculty of Machine and Naval Constructions and the Laboratory of Fixed Prosthodontics, School of Dentistry, both at the University of Zagreb. The metal bases used were two Ag-Pd alloys (Auropal-Zlatarne Celje, Slovenia; Palador-Rafinerija plemenitih kovina Zagreb, Croatia) in combination with two different resins (Ivocron PE and Isosit N-Ivoclar, Schaan, Liechenstein).
Rivet-shaped alloy patterns were produced in common casting procedure, with the dimensions: disk 2 mm thick and 7 mm in diameter, pedicle 12 mm long, 2.5 mm in diameter and with beads (200 micrometers in diametar) on a metal surface anticipated for veneering.
In that way 30 auropal and 30 Palador alloy patterns were produced. These patterns were sandblasted in the blasting apparatus with the micropencil (BasicDuo-Renfert, Hilzingen, Germany) using the sand grain size of 250 micrometers. The distance between the micropencil and the patterns was 5 mm, the blast pressure was 4 bars and the time of sandblasting was 15 seconds per surface. After sandblasting all specimens were cleaned with ethylacetate.
The patterns made of both alloys were divided in two groups depending on the veneering material. Half of the specimens were veneered with Ivocron PE and another half with Isosit N acording to the manufacturer's instructions. Each combination of alloy and resin (four of them) was divided in three subgroups with 5 specimens each. The first subgroup of the specimens was tested 24 hours after the polymerisation (TR.1), the second subgroup, after a three-weeks immersion in distilled water at a constant temperature of 37^{0}C (thermostat BTUJ, Poznan,Poland) (TR.2), and the third after the cyclic changes of the temperature the so-called thermocyclic procedure described by Hansson (TR.3)(5).
The specimens were tested according to the Smitz-Schulmeyer shear test (4) in a universal testing machine for polymer materials - WPM (Tueringen, Germany). The blade of the breaking device was placed on the polymer material 1mm from the bond with the metal surface (Fig. 1).

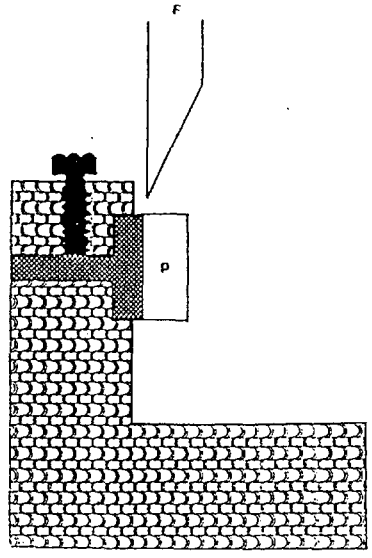

Fig. 1. The sheme of the breaking device placed on the specimen mounted in the holder of the testing machine.

The blade was moving at a constant speed of 7mm per minute and the values of the force detaching the polymer were recorded.
The data obtained were statistically assessed on the IBM compatible 386 computer, by using the SPSS software. Normality of the distribution was tested by Kolmogorov-Smirnov's test. As the distribution was normal, descriptive statistics (mean and SD) and 3-factor analysis of variance were done and in the cases where significant differences were observed, Tukey test was performed.

3. RESULTS AND DISCUSSION

This study was performed in order to reveal to what extent different ageing treatments reduce the bond strength values between different dental materials (alloys and veneering materials) though simulating the enviromental conditions within the oral cavity. The shear test was chosen because fixed prosthetic appiances are mostly subjected to the shear forces in the mouth (6), and also because this test has a smaller dispersion of the results compared to the tensile tests (7).
Descriptive statistics is shown in Table 1.

TREAT-MENT	AUROPAL				PALADOR			
	IVOCRON		ISOSIT		IVOCRON		ISOSIT	
	x	sd	x	sd	x	sd	x	sd
1.	9.53	1.09	9.78	0.71	9.83	0.88	9.61	0.74
2.	7.68	0.65	8.83	1.66	7.89	0.69	7.57	0.96
3.	7.04	0.64	6.10	0.73	6.31	0.46	7.33	0.73

TABLE 1. Descriptive statistics of share boud strength between the alloy and the vencering material. Treatment: 1.- 24 hrs. after polymerisation, 2.- after 21 days in waterbath of 37° C, 3.- after thermocycling procedure;
x = mean values of shear bond strength (in N/mm^2);
sd = standard deviation

Source of Variation	Sum of Squares	DF	Mean Square	F	Signif of F
Main Effects	119111.533	4	29777.883	29.208	.000
TREAT.	118536.700	2	59268.350	58.134	.000
RESIN	476.017	1	476.017	.467	.498
ALLOY	98.817	1	98.817	.097	.757
2-way Interactions	2797.817	5	559.563	.549	.738
TREAT. RESIN	660.033	2	330.017	.324	.725
TREAT. ALLOY	2137.633	2	1068.817	1.048	.358
RESIN ALLOY	.150	1	.150	.000	.990
3-way Interactions	10164.700	2	5082.350	4.985	.011
TREAT. RESIN ALLOY	10164.700	2	5082.350	4.985	.011
Explained	132074.050	11	12006.732	11.777	.000
Residual	48936.800	48	1019.517		
Total	181010.850	59	67.981		

TABLE 2. Analysis of variance of shear test after ageing treatments on 2 resins combined with 2 alloys

3-factor ANOVA for the shear test was performed and the results are shown in Table 2.
The main effect that produced significant difference between the specimens examined was the treatment applied to the specimen (TR.1, TR.2, TR.3) (Table 2). Therefore a one-way analysis and Tukey test (Table 3) were performed in each group of the examined alloys and resins in order to assess the significance of the difference between the treatments (TR.1, TR.2, TR.3).

In combination, Palador-Ivocron PE F test showed that the difference for the values of the shear test between the 3 treatments was significant and Tukey test revealed that the difference was significant between all the 3 examined treatments.

In combination Auropal-Ivocron P and Palador-Isosit N the difference was also significant and Tukey test revealed that the specimens tested, after immersion in water at 37°C (TR.2) and the thermocycling (TR.3) had significantly lower bond strength values than the specimens tested 24 hours after the polymerisation (TR.1).

COMBINATION OF ALLOYS AND RESINS	F RATIO AND F SIGNIFICANCE	TUKEY TEST
PALADOR-IVOCRON PE	F=31.0533; p<0.01	TR.1: TR.2: TR.3
PALADOR-ISOSIT N	F=11.7762; p<0.01	TR.2, TR.3: TR.1
AUROPAL-IVOCRON PE	F=12.4494; p<0.01	TR.2, TR.3: TR.1
AUROPAL-ISOSIT N	F=14.4621; p<0.01	TR.3: TR.1, TR.2

TABLE 3. Oneway analysis of variance between various treatments after polymerisation of the specimens and Tukey test

In combination Auropal-Isosit N the difference between the means of the shear test was significant too, and according to the Tukey test this difference was due to the termocycling procedure (TR.3), which was significantly different from the bond strength values obtained 24 hrs. after the polymerisation and after the immersion in water at 37° C (TR.3 differs from TR.1 and TR.2).

4. CONCLUSION

From the results of the statistical analysis it could be concluded that ageing treatments significantly reduce shear bond strength values. Although they are not, in all segments, equal to the conditons in the oral cavity, these tratments are good enough to reveal the reduction of the initially obtained bond strenght values.

In order to obtain bond strength values, which should be constant, regardless to the enviromental conditions (providing constant and secure aesthetic appearance) chemical bonding systems between dental alloys and resins have been developed, but they are still not widely used and more research is required.

5. LITERATURE

1. J Skowron, JB Moser, EH Greener, L Jemeson. Bond Strength of Ceramics and Resin using Silane Coupling on Dental Alloys. Northwestern Dental Research, Fall, 22-3, 1989.

2. M Hofmann. Aestetische Langzeit von kunststoffverblendetem Zahnersatz. Dtsch Zahnaerztl Z, 29, 455-8, 1980.

3. H Tiller, R Musil, A Garschke, B Magnus, R Goebel, R Sachse. Eine neue Technologie zur Herstellung des Verbundes Kunststoff-Metal in der Zahntechnik. ZWR, 93, 768-73 & 918-22,1984.

4. HF Kappert. Der Einfluss zweier Haftvermittler-Systeme auf den Kunstoff-Metal-Verbund. ZWR, 98, 129-30, 1989.

5. O Hansson. Strength of bond with Comspan Opaque to three silicoated alloys and titanium. Scand J Dent Res, 98, 248-56, 1990.

6. BZ Laufer, JI Nicholls, JD Townsend. SiOx-C Coating: A composite-to-metal bonding mechanism. J Prosthet Dent, 60, 27-32, 1988.

7. Y Mathey, P Dubied, AH Geering. Vergleich der haftfestigkeiten von ungealterten und gealterten Metal-Kunststoff-Verbundsystemen. Schweiz Monatsschr Zahnmed, 100, 401-7, 1990.

THE INFLUENCE OF POLISHING ON THE ELECTRIC POTENTIAL OF AMALGAM FILLINGS

Nada Galić, Goranka Prpić-Mehičić, Ivica Anić, Dora Najžar Fleger, Dunja Buntak-Kobler

School of Dentistry, University of Zagreb, Gundulićeva 5, 41000 Zagreb, Croatia

SUMMARY. *- For the purpose of this study we used Electronic-endodent instrument EED-11 to measure the height of electric potential of gingive of fresh amalgam fillings, fillings older than seven days, before and after polishing. 400 fillings in 187 patients were examined.*

We wanted to find out the quality of subjective and objective discomforts as well as the influence of prothetic metals (gold, palador) in the oral cavity on the height of electric potential and occurrence of discomforts.

The differences in potential between fresh, polished and non-polished fillings are statisticaly significand in all kinds of tested amalgams. Subjective discomforts occurred in 1,2 % of total number of cases and in 6,7 % of tested patients who had prothetic metals in their mouths.

Electric potential of amalgam fillings lowers due to aging and polishing.

INTRODUCTION

Dental amalgam (DA), which has been widely used as material for fillings of back teeth, has some negative characteristics besides its numerous positive ones. Here we are concerned with its electric potential (EP), which occurs in electric occurrences in oral cavity, what makes amalgam liable to corrosion. this process lowers its hardness and allows mercury and other elements to be discharged (10,15).

We started this study with the assumption that every difference in EP that is higher than 200 mV can cause some subjective and objective discomforts. It is also presumed that bigger differences in the potential lead to higher corrosion in oral cavity, which can also lead to some biological reactions as the time passes. Intra-oral occurrences can be attributed to electric stimulation of excitered cells (muscular, nerve or gland cells) or to the concentration of ions in the tissue with the accompanying chemical reaction (1). It is considered that density of electricity higher than 1.3 $\mu A/mm^2$ is needed to stimulate hard nerve fibers (12).

Some authors (Lacazedieu (8), Tamarut (14)) point out the fact that it is possible to lower EP and the degree of corrosion by polishing the amalgam fillings (AF). Basic purpose of polishing is to get smooth surface of AF by which it is possible to stop the retention of plaque. On the part of the filling where there is no plaque there is a high partial pressure of oxygen while this pressure is low on the part of the filling coated with plaque. Therefore, the polished part of the filling plays the part of cathode opposite the part coated with plaque on which anode corrosion takes place (5,6,2).

The objective of this study has been to examine the following:

- EP level of different kinds of commercial DA
- Influence of polishing the filling on the value of its EP
- Presence of the differences in EP higher than 200 mV
- Presence of subjective and objective discomforts due to high EP in oral cavity

MATERIALS AND PROCEEDINGS

1. AMALGAM ALLOYS

1. Lekalloy-HR, non-gama-2 DA (LEHR)
   Produced by : Lek Ljubljana i cooperation with Vivadent, Schann, Liechtenstein.
   Total examined : 130 fillings

2. Amalcap-SAS, non-gama-2 DA (AMAL)
   Produced by : Vivadent, Schann, Liechtenstein.
   Total examined : 130 fillings

3. DNG-2 and MEDI-KAP, non-gama-2 DA (DNG and Medi)
   Produced by : DMG Hamburg
   Total examined : 140 fillings (DNG: 81 fillings, MEDI: 59 fillings).

2. MEASURING INSTRUMENT

Measuring instrument EED -11 is a multi-purposed device, battery charged, which is used in dental clinic examination of qualitative changes on soft and hard tissue. This instrument has three modes of work : V, G and STIM. While the instrument is in mode V it is possible to measure bioelectric potential of the tissue between the examined tissue (active electrode) and surface of the skin in the patient's hand (passive electrode).

3. PROCEEDING

Amalgam fillings were applied according to requirements of proffession. Passive electrode was put into the patient's hand and instrument was turned to the mode V. First, measuring of the value of EP of gingives had been done three times, by using the active electrode with the silver wire ending and then the value of freshly aplied AF was measured. Average value of EP has been accepted. Seven days after the fillings had been done measuring of EP of gingives and AF was performed in the same manner. The filling was polished during the same visit according to the requirements of the profession, and then measuring of polished fillings and gingives was performed in a previously staded manner. Measuring values of EP for the groups of fillings were mutually compared by using the statistic test of T distribution.

RESULTS AND DISCUSSION

Literature reports on different attitudes toward the measurability of EP of filling. Schriever and Diamond (11) claim that it is impossible to measure EP in vivo, while Lukas (9), Nomoto (13) and Yontchew (16) describe different measuring possibilities. But, all of them agree that is absolutely necessary to have EP voltmeter with high impedancy as well as to use referential electrode if we want to get exact measuring. EP of amalgam fillings that were measured for the purpose of this study have pointed out to the fact that AF takes part in electric occurrences in oral cavity (Fig. 1, 2, 3, 4). Electric current flows from gingive to the filling through saliva which plays part of the electrolyte. When there is a big difference in EP between gingive and filling, it can cause dissociation of saliva and tissue liquid and accordingly cause depolarizattion of nerve fibers (14).

The span of measured values of EP of gingive ranged from 20 to 180 mV, and the average value was about 100 mV. Electric potentials were highest in fresh AF. The highest was in Amalcap, then in Medi-kap, Lekalloy-HR and then in DNG-2. As Almacap contains more Hg compared with powder, we could assume that longer time is needed for a bigger quantity of mercury to unite with elements of powder. Frykholm and Boyer (3) have reported that fresh AF releases Hg into saliva, and that its share lowers with hardening of DA. Fresh AF has a high density of electricity, which can be seen on its polarization curve, which reveals higher charge (7). Accordingly, we could assume that fresh AF has a high EP due to larger quantity of free electric charge (4).

Values measured seven days later, but still before polishing, have shown that EP lowers for about 75 mV in all kinds of DA, which could be the result of partial stabilization of chemical processes of hardening of amalgam alloy. Measuring after polishing have shown that EP lowered in the range of 40 to 180 mV.

Results of this study show that all differences in EP between gingive and AF are higher than 200 mV and that we didn't lower the value of EP under 200 mV by polishing. Besides, among 187 tested patients with 400 fillings only 5 of them reported subjective discomforts. It is 1.2 % of the total number, or 6.7 %of the patients who have prothetic precious metals (gold, palador) in their mouths. Subjective discomforts correspond to Farell's findings, who thinks that periodical contact between two different metals can bring about strong electricity, which can provoke acute pain and weaker electricity, which can stir a kind of metal taste, prickling end feeling of broiling in the mouth (1).

CONCLUSION

Examined amalgam alloys (Lekalloy-HR, Amalcap-SAS, Medi-kap and DNG-2) cause approximately the same electrical potential in the oral cavity. Polishing lowers potential in the span from 40 to 180 mV (on average 130 mV). The presence of prothetic metals in the oral cavity (gold, paldor) hasn't had any influence on the electrical potential during the examined time.

Differences in electrical potential higher than 200 mV are present in all examined amalgam fillings. Temporary discomforts appeared in 1.2 % of the tested patients, which confirms the assumption that patient's sensitivity depends a great deal on his biological stimulation threshold as well as his psycho-somatic tolerance.

According to the reports of the American Dental Association (ADA) measuring of EP with open and closed mouth didn't yield the same results. Therefore, with presently available devices for measuring EP it is only possible to determine relative values. Basic reason for that is only vaguely known way of expanding of the electric current through hard and soft tissues of the oral cavity, which causes difficulties in constructing appropriate devices for recording these currents (1).

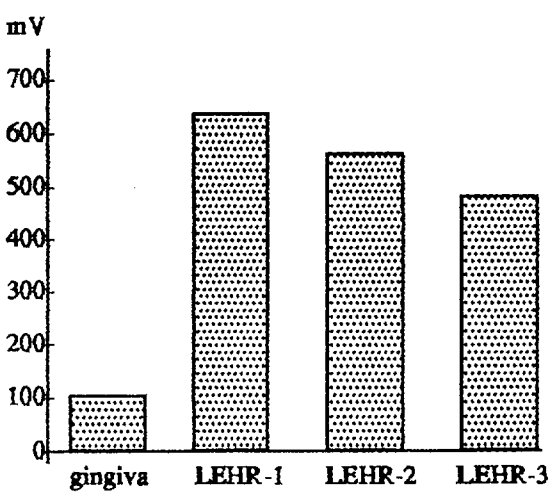

FIGURE 1.
Electrical potential of gingive, EP of fresh dental amalgam (LEHR-1), EP of dental amalgam seven days old before polishing (LEHR-2) and EP of the same dental amalgam after polishing (LEHR-3).

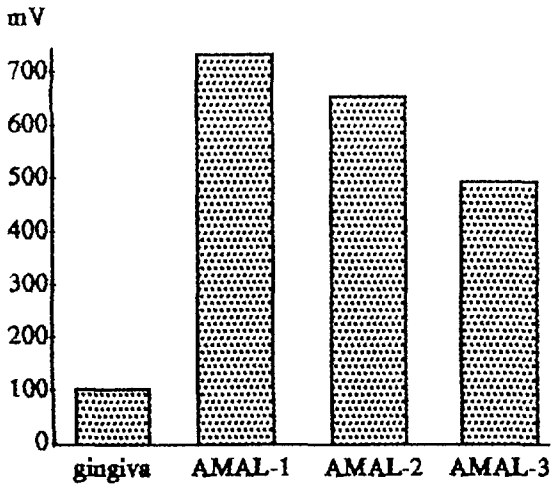

FIGURE 2.
Electrical potential of gingive, EP of fresh dental amalgam (AMAL-1), EP of dental amalgam seven days old before polishing (AMAL-2) and EP of the same dental amalgam after polishing (AMAL-3).

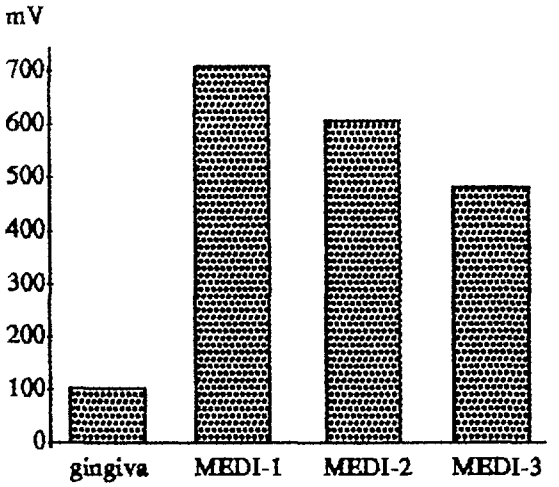

FIGURE 4.
Electrical potential of gingive, EP of fresh dental amalgam (MEDI-1), EP of dental amalgam seven days old before polishing (MEDI-2) and EP of the same dental amalgam after polishing (MEDI-3).

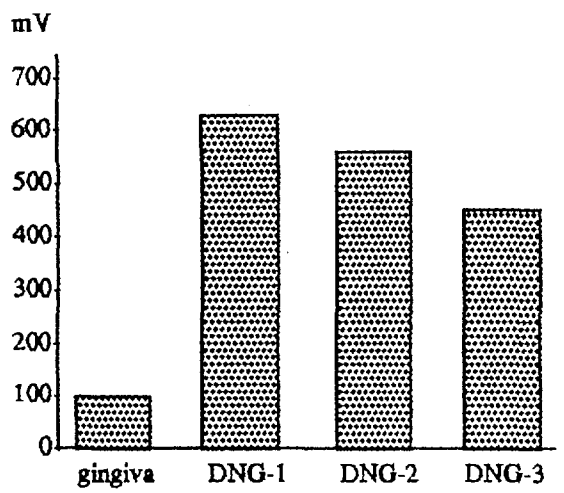

FIGURE 3.
Electrical potential of gingive, EP of fresh dental amalgam (DNG-1), EP of dental amalgam seven days old before polishing (DNG-2) and EP of the same dental amalgam after polishing (DNG-3).

REFERENCES

1. ADA report on the occurence of galvanic corrosion in the mouth and its potential effects, JADA, 115, 783-787,1987.

2. J P AMERONGEN, C PENNING, Temperature changes during the finishing of amalgam restorations, J Prosthet Dent, 64, 455-458, 1990.

3. B D BOYER, Mercury vaporization from corroded dental amalgam, Dent mater, 4, 89-93, 1988.

4. J FILIPOVIĆ, S LIPANOVIĆ, Opća i anorganska kemija, Zagreb, Školska knjiga, 1987, 1091-5.

5. J A VON FRAUNHOFER, P J STAHELI, Corrosion of amalgam restorations, Br dent J, 131, 522-4, 1971.

6. F GEIGER, et al., Burnishing, finishing and polishing amalgam restorations: a quantitative scanning electron microscopic study, Quintessence Int, 20, 461-468, 1989.

7. E H GREENER, Anodic polarization of New Dental Amalgam, J Dent Res, 55, 1142, 1976.

8. M LACAZEDIEU, et al., Finition des oburations d'amalgame, Odont Conservatrice, 2, 69-84, 1975.

9. D G LUKAS, Uber die Messung von Spannungen und Kurzschlusstromen an Zahnartztlichen Metallen, Dtsch Zahnartzl Z, 28, 394, 1973.

10. M MAREK, interactions between Dental Amalgams and the Oral Environment, Advances in dental Research, Volume 6, 100-110, September, 1992.

11. A W J Muller, A J DE GROOT, C L DAVIDSON, The determination of the electrical potential of a metallic restoration in the oral cavity, J Oral Rehabil, 16, 271-77, 1989.

12. J M MUMFORD, Pain due to Galvanism, British Dental J, 19, 299-301, 1960.

13. S NOMOTO, M ANO, ONOSE, Micro-probe for mesaurement of corrosion potential of metallic restorations in mouth, J Dent Res, 58, 1688, 1979.

14. T TAMARUT, L GENC, Elektronicko-endodontski uredaj, Zagreb, 1984.

15. J WIRZ, TH LEUPIN, F SCHMIDLI, Modeme Amalgam-Politur und Korosionsverhalten in In vitro-Veruch, Quintessenz, 7, 1219-1226,1990.

16. E YONTCHEW, et al., An examination of the surface corrosion state of dental fillings and constructions, II A chemical study on patients with orofacial complaints, J Oral Rehabil, 13, 365, 1986.

EVALUATION OF ENDOMETER ES-2 ACCURACY THROUGH CONTROL MEASUREMENTS OF EXTRACTED TEETH

Zoran Stare[1], Nada Galić[2], Jozo Šutalo[2], Sanja Šegović[2], Katica Prskalo[2]
[1]Faculty of Electrical Engineering, University of Zagreb
[2]School of Dentistry, University of Zagreb

Summary

This study was conducted in order to establish the precision of the Endometer ES-2 device in the assessment of the apical foramen position. The control method was the teeth extraction with the apical foramen position previously measured with the mentioned device. The study comprises 30 root canals of one- and multi-rooted teeth previously determined for the extraction.

With 0.5 - 1.0 mm tolerance, the precision of the Endometer ES-2 was 96.6%, and with 2.0 mm tolerance, it was 100%.

The results show that the Endometer ES-2 device is sufficiently reliable for the clinical use.

1. INTRODUCTION

One of the basic prerequisites for a successful endodontic treatment is correct assessment of the length of the root canal (RC) or the location of the apical foramen (AF). All studies agree that the cementodentinal junction (CDJ) is the ideal place to finish instrumentation and endodontic obturation. Some authors (1,2) believe that the endodontic treatment should end 0.5 to 0.7 mm before the actual CDJ. Dental literature mentions three different apical foramina: anatomical, physiological and radiographic. The anatomical foramen is usually above the physiological, which is actually the apical construction, or CD junction. There are inherent problems associated with the use of radiographs, including image distortions, interference of anatomical structures and radiographic interpretation of the clinician. Several researches have shown that the location of the apical construction varies in relation to the anatomic apex, usually within the range of 0.5 to 3.0 mm from the radiographic apex (3). It is very difficult to be precise in the procedure without a control radiograph of the tooth with the control endodontic needle or gutta-percha point in the root canal. A great variety of apex locators that determine the position of the apical construction are on the market (4,5,6,7). Clinical measurements, done by such equipment, were controlled either by X-raying (4,5) or by an analysis of the extracted tooth (6,8,9). In our earlier studies (10) the accuracy of the Endometer ES-1 was controlled by radiographs, having 97.1% precision. The reliability of the precise determination of the AF with Rtg is known to be very questionable (11). For that reason in our previous studies we have augmented the need for the control of this device by extracting the teeth with previously measured AF with Endometer ES-1. In this study we controlled Endometer ES-2 device improved, (market advanced version of the laboratory Endometer ES-1) by extracting the teeth on which the length of the root canal was previously measured by the same device.

2. MATERIAL AND METHODS

This study comprised 30 root canals on single- and be- and trirooted teeth, that had been scheduled for extraction because of periodontal, prothetic or other reasons.

Measurement was done by the Endometer ES-2 device, used for measurement of the AF position. The Endometer ES-1 works by measuring the impedance at high frequencies. The device has two connected pieces, one joined to the metal clip used as an electrode, and the other containing the adequate needle. It also contains the scale with the sign AF, which represents the average AF obtained by examining the corresponding working model (12).

The previous number of teeth included 8 single-rooted, 5 bi-rooted and 4 tri-rooted teeth. Local anaesthesia was routinely given before tooth extraction. All of the teeth were X-rayed and then endodontic cavity preparation was done according to standard requirements. After extirpation of the root-

canals content by endodontic reamer, the root canal was rinsed with the 2% NaOHCl solution, dried by the Miller-Donalds needles wrapped in cotton wool, and the procedure preceded by measuring the root canals with the Endometer ES-2. The metal clip, functioning as an electrode, was connected to one of the joined pieces. It was placed on the corner of the mouth in order to make contact with the mucosa. The other joined piece was connected to the endodontic reamer adequately sized which was then applied into one root-canal. The reamer was drawn into the root canal until the indicator on the Endometer ES-2 scale showed the AF value. This length was registered on the reamer and on the teeth by a water-proof pen in order to mark the exact position of the reamer in relation to the tooth. Special care was given to the tooth in the process of extraction, as this part of the tooth could not be fractured. If this was the case, the whole crown was cut and measurements done on the rest of the root. After the extraction, the teeth were washed, dried and cut with diamond turbine cutters. The marked reamer was then placed on the root, so that the marks on the reamer and the tooth concur, after which, the length between the apical construction and the point of the reamer was measured.

3. RESULTS AND DISCUSSION

From 30 root-canals measured (Table 1), 24 had the reamers point directly in the apical constriction (± 0.5 mm), 3 RC had the point over the apical constriction by 0.5 - 1.0 mm, 1 RC had over the apical constriction by 1.5 mm, and in 2 cases the point was short of the apical constriction by 0.5 - 1.0 mm, with 80% precise measurements, and 6,6% shorter measurements, and 13,3% longer measurements (Fig. 1). With ± 1.0 mm tolerance, the precision of the measurements was 96,6%. With these results it can be said that Endometer ES-2 is sufficient to meet the clinical requirements.

Precise endometric instrument would be of great value in the endodontic treatment, as the need for the control radiograph would be eliminated. Practitioners would need only two radiographs the first one for the orientation about the anatomical configuration of the root and the existence of possible pathological changes of the root, and the second one after the definite obturation of the root canal following the endodontic treatment (RC is filled with Apexit paste and gutta-percha points) in other to control the dental work.

As the Rtg-technique is very unreliable in the assessment of the AF position, so it is also unreliable in the precise assessment of the endodontic devices. However, this study shows great concurrence in the Rtg-control of the Endometer ES-2 and the extraction method, with a ± 1.0 mm tolerance. With Rtg-control of Endometer ES-2 the precision of the device was 97.1 %, and with the method of extraction it was 96.6 %. With the clinically acceptable tolerance of ± 2.0 mm, precision of the device would be 100%.

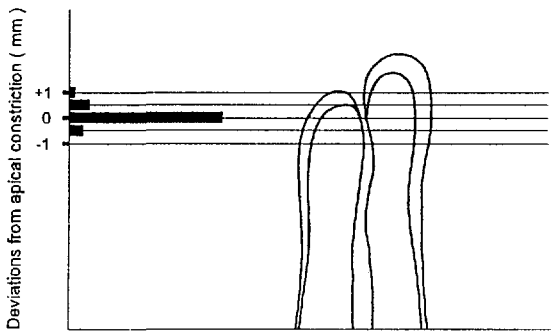

Fig. 1. Apical constriction located by Endometer ES-2

Our results are similar or even better compared to the precision of other endometric devices, controlled by the extraction method. Wu et al. (6), find the precision 77,5 % with tolerance of 0.5 mm, and the 100% precision with a ± 2.0 mm tolerance, which is also clinically acceptable. Berman and Fleischman (8), find the precision of the endometric device to be between 83% and 94%. O'Neill (9) and Ricard (13) had a 86% precision in the extracted teeth controlled by them.

Huang (14), Fouad et al. (7), Wu and al. (6) augment the size of the apical foramen and its importance for the precision of the endometric devices they used. Those endometric instruments measured AF with smaller diameters (as they are in elder) with more precision, than the AF with greater diameters.

In this study of Endometer ES-2, no difference was noticed between the diameter of the AF and the precision of the device used. In the work with Endometer ES-2, it is of greatest importance to use the endodontic reamer of the sufficient diameter, as to completely obturate the apical constriction. So, for the larger root canal, the bigger diameter of the

	The reamers point directly in the A.F. ± 0.5 mm	The reamers point over the A.F. 0.5-1 mm	The reamers point over the A.F. 1-1.5 mm	The reamers point short of the A.F. 0.5-1 mm
Single-rooted	6	2	0	0
Bi-rooted	8	1	0	1
Tri-rooted	10	0	1	1
Total	24	3	1	2

Table 1. Results of the measurement of apical constriction by Endometer ES-2

reamer would be used. It was noticed that the Endometer ES-2 was sensitive to the EDTA (Calcinase) and blood. However, in both cases, it was sufficient to rinse both root canals with 2% NaOHCl and dry it with Miller-Donalds s needles wrapped with cotton. The device was not moisture-sensitive, so there was no need to obtain the absolutely dry conditions.

4. CONCLUSION

In this study, previously devitalised teeth were studied. In order to complete the clinical tests of the Endometer ES-2, more teeth scheduled for extraction should be measured, which should include the teeth that need vital extirpation, mortal extirpation and necrosis.

With the great number of Rtg-controlled teeth in years long studies of the Endometer ES-1, and Endometer ES-2, and with the results of this study, it can be concluded that the Endometer ES-2 satisfies the clinical demands.

5. REFERENCES

1. Kuttler Y. Microscopic investigation of root apexes. J Am Dent Assoc 1955; 50: 544-552
2. Green D. Stereomicroscopic study of 700 root apices of maxillary and mandibular teeth. Oral Surg 1960; 13: 728-733
3. Burch JG. The relationship of the apical foramen to the anatomic apex of the tooth root. Oral Surg 1972: 34: 262-268
4. Keller et al. A clinical evaluation of the Endocater - an electronic apex locator. J Endodon 1991; 17: 271-274
5. Himel Van T, Cain Ch. An evaluation of two electronic apex locators in a dental student clinic. Quintessence International 1993; 24: 803-806
6. Wu, et al. Variables affecting electronic root canal measurement. In End J 1992; 25: 88-92
7. Fouad AF et al. A clinical evaluation of five electronic root cannel length measuring instruments. J Endodon 1990; 16: 446-449
8. Berman LH, Fleischman SB. Evaluation of the accuracy of the Neosono-D electronic apex locator. J Endodon 1985; 10: 164-167
9. O'Neill Lj. A clinical evaluation of electronic root canal measurement. 1974; Oral surg 1974; 38: 469-473
10. Galić N., Stare Z., Šutalo J. Clinical evaluation of the accuracy of the endometer ES-1 in locating the apical foramen. Period biol 1993; 95: 153-155
11. Chunn, et al. In vivo root canal length determination using the Forametar. 1981; J Endodon 1981; 7: 515-520
12. Stare Z., Šutalo J. On electronic measurement accuracy of a root canal length. Jurema Proceedings 1986; 31: 55-59.
13. Richard, et al. Clinical evaluation of the accuracy of the Evident RCM Mark II apex locator. J Endodon 1991; 17: 576-569
14. Huang L. An experimental study of the principle of electronic root canal measurement. J Endodon 1987; 13: 60-64

Biological Cell in an External Electric Field: Mathematical Model of Induced Transmembrane Potential and Ca^{2+} Influx

Fedja Bobanović, Dejan Šemrov, Tomaž Jarm, and Lojze Vodovnik

Faculty of Electrical and Computer Engineering, University of Ljubljana,
Tržaška 25, 61000 Ljubljana, SLOVENIA

ABSTRACT *- In order to understand the global effects that electric fields have on biological systems, it is necessary to analyse the changes on a cellular level. Past research has demonstrated that the application of a local electric field causes an imbalance in the transmembrane potential of the cell, with one side becoming hyperpolarized and the other depolarized. Since these perturbations in transmembrane potential directly influence voltage gated ion channels, the permeability of the membrane to specific ions differs in various regions of the membrane. This study focused on mathematical modelling of the transmembrane potential and of the Ca^{2+} influx as they are altered by an external electric field. In the study, computation of transmembrane potential changes was performed using proffesional system BEASY which implements boundary element method. Distribution of transmembrane current density was calculated using Pascal program which was basad on experimental data, rules of electrodifusion and probability that channels are open. The strong corelation between results of the mathematical model and the experimental results has been found.*

1. INTRODUCTION

An external electric field can produce a variety of biochemical or physiological changes in biological systems. Global effect may be the result of local electric field stimulation at the cellular level, in which one end of cell is depolarized while the other end is hyperpolarized [1,2,3]. Therefore, it is important to be able to calculate and measure perturbations in membrane potentials and intracellular ion concentrations induced by electric field if it is attempted to understand the cell biological responses which follow (muscle contraction, exocytosis, etc.

The spatial complexity of induced transmembrane potential and ion currents along the cell membrane preclude successful use of traditional microelectrode technique for monitoring these parameters during electric field exposure. Optical methods based on voltage- and ion-sensitive dyes have advantage of providing both high temporal and high spatial resolution because the effect is instantaneous and is localised to the level of individual indicator molecules. Electrical stimulation represents a particular problem where such methodology have significant advantages over microelectrode techniques, because fast changes in transmembrane potential and ion concentration induced by an external electric field can be monitored simultaneously over many different regions of the cell [4].

In order to better understand phenomenon of electrical stimulation and to correlate our experimental results obtained by optical recording of intracellular ionised calcium (Ca^{2+}), we have modelled two steps in the cascade of cellular signal transduction, for which we believe that are

crucial in excitation by an external electric field. The first is spatial distribution of transmembrane potential changes induced by external electric field and the second is distribution of transmembrane current density of calcium (Ca^{2+}).

The spatial distribution of transmembrane potential changes induced by external electric field can be calculated by solving Laplace's equation. This could be done by using either analytical or numerical methods. Simple analytic solutions are easily attained only when the geometry is describable in the chosen co-ordinate system, otherwise numerical methods should be used. In our study, the computation was performed using a professional system BEASY (Computational Mechanics Ltd., Southampton, UK) [5]. which is based on boundary element method (BEM).

Ca^{2+}, the known second messenger, is involved in triggering many cellular responses in various cells. During the excitation of electrically excitable cells like neurones, muscle fibres or neuroendocrine cells, Ca^{2+} enters the cell through voltage-gated channels in plasma membrane. Permeability of voltage-gated channels is dependent on transmembrane potential of the cell. Since perturbations in transmembrane potential induced by an external electric field are position dependent, the permeability of the membrane in the cell exposed to electric field should differ in various regions of the membrane. The mathematical model programmed in Pascal was based on experimental data obtained by patch clamp technique, rules of ion electrodifusion and probability that channels are open.

2. MATHEMATICAL MODELLING

2.1 Induced transmembrane potential

The external electric field induces a position-dependent modulation of membrane potential difference which is superimposed on resting potential. Equation (1) represents analytical solution for spherical cell in an homogenous electric field. V is transmembrane potential, V_0 is resting potential, E is electric field, r is radius of the cell and q is angle between vector of electric field and radius vector of the point where membrane potential is calculated.

$$V = V_0 + 1.5Er\cos\varphi \qquad (1)$$

In our model, induced transmembrane potential was calculated using boundary element method (BEM). The theoretical basis for the method has been understood for quite a long time and can be found in numerous references [6]. The fundamental advantage of BEM over domain methods like finite differences (FD) or finite element method (FEM) is that the discretization and computation is made only on the boundary of the domain. The modelling time is reduced since the user is required to model only the boundary. The number of elements is smaller than in the FEM. The number of equations is reduced compared to FD and FEM. The result of all these is a reduction of a computation time.

In the first step, 2D model of a round shape cell in the external homogenous electric field was evaluated. This model corresponds to a 3D infinite cylinder model, where the situation is the same along the z-axis. The conductivity of the region inside and outside the cell was 0.2 S/m, while the conductivity of the membrane was 0.2 mS/m. In addition the 3D model of a spherical cell in homogenous electric field was constructed.

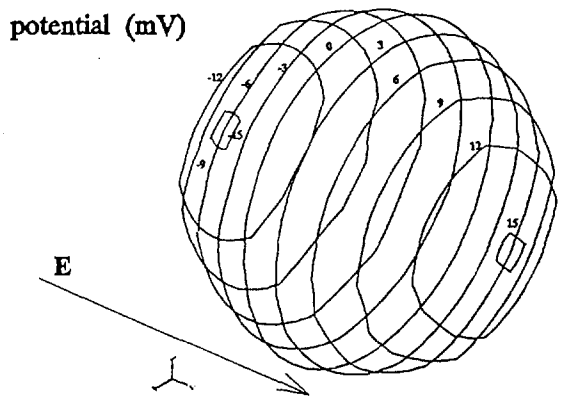

Fig. 1. The 3D model of spherical cell

The typical sinusoidal shape of the induced membrane potential reached by numerical computation was in good agreement with distributions obtained analytically and experimentally using voltage-sensitive dye. Since the electric field inside the cell is relatively small, the isolated structures were modelled at all subsequent evaluations.

2.2 Calcium current density

Experimental data was used in combination with the Goldman-Hodgkin-Katz (GHK) equation to create a graph of membrane permeability versus transmembrane potential. The GHK equation (2) describes transmembrane current density due to electrodiffusion gradient if all channels are open [7].

$$I = \frac{4PsVF^2}{RT} \cdot \frac{[Ca^{++}]_{inside} - [Ca^{++}]_{outside} \times e^{\frac{-2FV}{RT}}}{1 - e^{\frac{-2FV}{RT}}} \quad (2)$$

The product of the permeability and the current density that would occur because of electrical and diffusion gradients yields the actual current density. Thus, by dividing the experimental data on current density by the GHK equation the permeability curve was obtained. The resulting curve was modelled by optimisation of Boltzman's equation which represents proportion of open channels using software package Simcos (B-open channels, A-closed channels).

$$\frac{B}{A + B} = \frac{1}{1 + e^{w - zeE/kT}} \quad (3)$$

Once the permeability curve was modelled, all the necessary information was available for predicting the calcium ion flux across the membrane of a cell in fields of different intensities. A computer program was written in Pascal which utilizes Boltzman's equation, the GHK equation, and the solution to Laplace's equation for spherical cells. Results of calculation predict the resulting calcium flux in each equipotential region by taking the average value of angle φ equation (1) to calculate the transmembrane potential for that slice. The program requires the following parameters: electric field intensity, initial transmembrane potential, initial internal ion concentration, initial external ion concentration, cell radius, and number of slices. The higher the number of slices or regions the cell is divided into, the greater the accuracy of the calculation. Once these parameters are given, the program is able to produce a color-coded graphical representation of the current densities on all regions of the cell membrane. An output file can also be created, containing the angle from y-axis, membrane permeability, transmembrane potential, current, and current density for each slice.

The data files with results were used to create a number of graphs for theoretical cells of varying size and in varying fields. These graphs show the same patterns as those that have been observed experimentally.

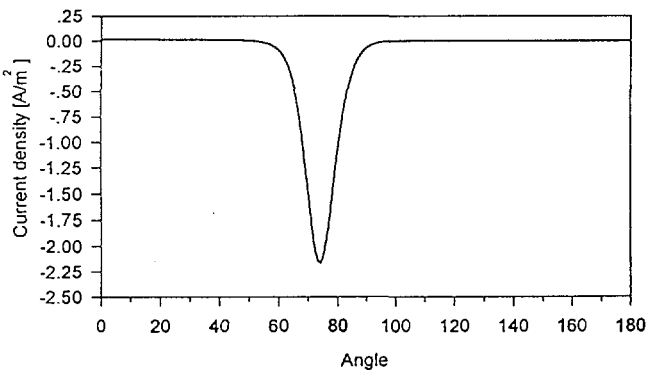

Fig 2. Calculated density of transmembrane Ca currents induced by 40 V/cm. The radius of the cell is 20 μm.

An increase in magnitude of current density as well as a shifting of the angle at which the maximum flux occurs are characteristic patterns that are related to raising the electric field intensity. Also, the graphical output of the Pascal program is similar to experimental pictures obtained by using calcium sensitive dyes. In addition the program calculates the net current for the entire cell. Cells of different radii show a shift in the field strength which results in

the maximum calcium influx. In this way it can be seen how in a biological system where there are cells of many different sizes, certain ones can be affected greatly by a certain electric field, while others experience little or no changes.

4. CONCLUSIONS

The strong correlation between results of the mathematical model and the experimental results on Ca^{2+} intracellular distribution in electrically stimulated cell has been found.

These theoretical results, obtained by mathematical modelling, may be used to predict the induced transmembrane potential and change in Ca^{2+} concentration. In this way the effects of the field for all cases are known without performing a separate experiment for each one. Knowledge of the changing calcium concentration is extremely important in understanding how the activities of a cell will be altered since Ca^{2+} is pivotal for many cellular functions, which in turn change the condition of the global biological system.

In conclusion, we can say that mathematical modelling in combination with optical techniques based on indicator dyes may provide valuable information for elucidation of biological responses to electric field

5. REFERENCES

[1] K.R. Robinson. The Responses of Cells to Electrical Fields: A Review. *The Journal of Cell Biology*, 101:2023-2027, 1985.

[2] M. Klee, R. Plonsey. Stimulation of Spheroidal Cells - The Role of Cell Shape. *IEEE Transactions on Biomedical Engineering*, Vol. BME-23, No. 4, 347-354, 1976.

[3] L. Vodovnik, D. Miklavčič, G. Serša. Modified cell proliferation due to electrical currents. *Medical & Biological Engineering & Computing*, 30:21-28, 1992.

[4] L.M. Loew. Voltag-sensitive dyes: Measurement of membrane potential induced by DC and AC electric fields. *Bioelectromagnetics Supplement*, 1:179-189, 1992.

[5] D.J. Danson. BEASY A Boundary Element Analysis System. In C.A. Brebbia, editor, *Boundary Element Methods in Engineering, Proceedings of the Fourth International Seminar*, pages 557-575, Southampton, England, 1982.

[6] C.A. Brebbia. *The boundary element method for engineers*. Pentech Press, London: Plymouth, 1978.

[7] B. Hille. Ionic Channels of Excitable Membranes, Sinauer Associates Inc., Sunderland, MA, 1984.

IMPROVED TORSO MODELLING AND ITS INFLUENCE ON THE LOCALIZATION OF ARHYTHMOGENIC CENTER(S) IN HEART

Vojko Jazbinšek[1,2], Martin Burghoff[2], Michael Oeff[3], Roger Zimmermann[2] and Zvonko Trontelj[1]
[1]Oddelek za fiziko in Inštitut za matematiko, fiziko in mehaniko, Univerza v Ljubljani, Jadranska 19, 61111 Ljubljana, Slovenija
[2]PTB Institut Berlin, Abbestr. 2-12, D-10587 Berlin, Germany
[3]Klinikum Steglitz der FU Berlin, Hindenburgdamm 30, D-12203 Berlin

Summary

It is desirable to get noninvasively the information on the spatial position of anomalies in the cardiac conduction system. Body surface potential map and/or magnetic field distribution in the vicinity of a human chest are obtained from cardiographic measurements. With this information we start the necessary forward and inverse calculations. In this work several types of torso models (realistic torso with the NMR support, elliptic cylinder) have been used to analyse 7 patients with WPW syndrome. The spatial coordinates of the tip of ablation catheter, obtained by the X-ray system, have been used as a reference in the evaluation procedure of current source coordinates (the onset of the accessory pathway), calculated from the noninvasive magnetic measurements.

1 INTRODUCTION

A well known problem in bioelectric modelling is the estimation of the electrical source inside a volume conductor from potential measurements at the outer surface. The biomagnetic equivalence of this problem is the estimation of an electric source from squid measurements outside the volume conductor. This deduction of electrical information from measured data is called the inverse problem. In the contrast to the forward problem, which can be solved uniquely, the inverse problem does not have a mathematically unique solution. In order to localize electrical current sources one has to introduce some models and constraints. Here modelling includes models of current sources as well as models of volume conductors where this sources are situated.

In this contribution we have studied a group of 7 patients suffering from Wolf-Parkinson-White syndrome. For these patients an additional accessory conduction pathway between the atria and ventricules occurs which leads to a preexitation of ventricules and can cause heart arhythmias which in turn can produce sudden cardiac death. We have used moving current dipole as a model of current source. This point-like model is justified by the fact that the accessorry pathway is limited to a small region. We have tested several volume conductor models like half-space model, elliptic cylinder and three different realistic torso models. The catheter ablation was performed in all studied patients. Before the ablation the location of accessory pathway was determined by the invasive electrophysiological technique. The spatial coordinates of the tip of ablation catheter obtained by the X-ray system have been used as a reference in the evaluation procedure of current source coordinates (the onset of the accessory pathway) calculated from the noninvasive magnetic measurements.

2 METHOD

In order to find successful solution to the inverse problem one has to solve first the forward problem for the chosen current source and volume

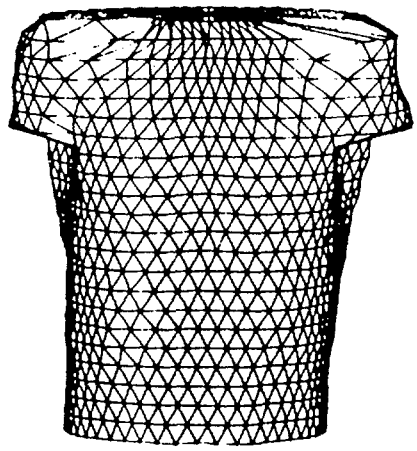

Figure 1: Tringulated human torso constructed from MR images.

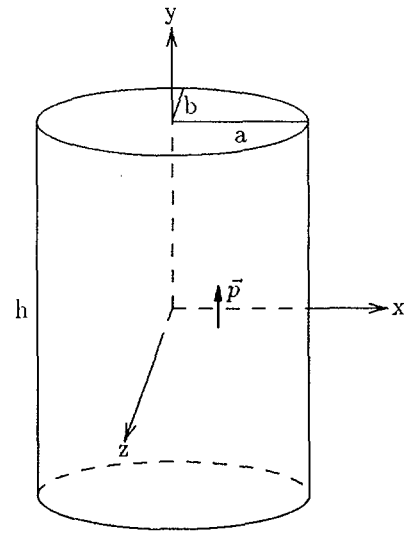

Figure 2: Elliptic cylinder

conductor model, i.e. the mathematical relation between the source model and corresponding magnetic field should be known in terms of finite number of parameters. The inverse problem is then solved by the parameter estimation procedure.

The simplest and the most widely used volume conductor model in magnetocardiographic studies is so called half-space model where the border of human chest is approximated by the infinite plane separating space into two parts, one with uniform conductivity representing the human body and the other with conductivity zero coresponding to the air. This is very rough model. The step further is a realistically shaped human torso. We have constructed such a model from the patient's tomographic images obtained by magnetic resonace (MR) images (see Fig. 1). Studies in electrocardiography have shown that the individual realistic torso, including inner volumes (lungs, heart), gives the best results in the localization of current sources [6]. However, it is not so easy to quickly accommodate the patients' geometric dimensions to obtain the individual torso for each patient. In order to evaluate possible simplification we have studied the elliptic cylinder as a model for the individual patient torso. This model is defined by only three parameters: height h and two axes of elliptic base a and b (see Fig. 2).

Magnetic field generated by current sources within an arbitrary shaped volume conductor is defined by [4]

$$\vec{B}(\vec{r}) = \vec{B}_\infty - \frac{\mu_0}{4\pi}\int_S \phi(\vec{r}\,')\frac{\vec{n}(\vec{r}\,')\times(\vec{r}-\vec{r}\,')}{|\vec{r}-\vec{r}\,'|^3}\,dS'\,, \tag{1}$$

where $\vec{B}_\infty$ denotes the solution in infinite homogeneous space. The integration in the second term of equation (1) is performed around volume conductor border, where $\vec{n}$ and ϕ represent a normal and an electric potential in a point $\vec{r}\,'$ on the border surface, respectively. The electric potential on the surface is determined by the following integral equation [3]

$$\phi(\vec{r}\in S) = 2\phi_\infty(\vec{r}) + \frac{1}{2\pi}\int_S' \phi(\vec{r}\,')\,d\Omega_{\vec{r}}(\vec{r}\,'\in S)\,, \tag{2}$$

where $d\Omega_{\vec{r}}(\vec{r}\,')$ is a solid angle of a surface element dS in the point $\vec{r}\,'$ observed from the point $\vec{r}$. $2\phi_\infty(\vec{r}\in S)$ corresponds to an electric potential for the case of infinite homogeneous conductor. Equation (2) has analytical solution only for some special cases. For an arbitrary shaped volume cunductor it has to be solved numerically by means of boundary element method (BEM) [1, 5]. The border surface is tesselated with flat triangles (see Fig. 1). Equation (2) becomes a system of N linear equations

$$\mathbf{A}\,\mathbf{\Phi} = \mathbf{a}\,, \tag{3}$$

where $\mathbf{\Phi}$ and $\mathbf{a}$ represent N–dimensional vectors containing the electric potential $\phi(\vec{r}\in S)$ and $[2\phi_\infty(\vec{r}\in S)]$ in the N border points, respectively. In our calculations the node based BEM were used. In this approach the electric potentials on triangle nodes (vertices) are calculated. The matrix element A_{ij} in this case corresponds to an average solid angle of the sorounding of point j observed from point i. These matrix elements can be calculated analytically [2]. Electric potential is defined uniquely only to within a

constant for the zero of potencial. This property results in the singularity of matrix **A** which can be overcome by so called deflation technique [8].

Electric potential of an arbitrary point on the border triangle is assumed to be a linear combination of electric potentials on triangle nodes. The surface integral over the particular triangle in the equation (1) has in this approxamation analytical solulution [7]. The magnetic field in magnetocardiography is measured in a grid of N_{grid} points on a plane near the human chest. Each sensor detects only one component of magnetic field, which is usually perpendicular to the body surface. This enables to write the equation (1) in the matrix form

$$\mathbf{b} = \mathbf{b}_\infty + \mathbf{b}_S = \mathbf{b}_\infty + \mathbf{C}\Phi \ , \qquad (4)$$

where $\mathbf{b}$, $\mathbf{b}_\infty$ and $\mathbf{b}_S$ are N_{grid}–dimensional vectors contaning magnetic fields in grid points, magnetic fields in infinite space and magnetic fields due to the border surface, respectively. Φ is the solution of (3). Elements of matrix $\mathbf{C}$, which has dimension $N_{grid} \times N$, contain a geometrical part of the surface integral in the equation (1). Final solution for the magnetic field in measured grid points is

$$\mathbf{b} = \mathbf{b}_\infty + \mathbf{C}\mathbf{A}^{-1}\mathbf{a} \qquad (5)$$

It should be emphasized that matrices $\mathbf{A}$ and $\mathbf{C}$ depend only on the geometry of volume conductor border and on the position of measured grid. The product of $\mathbf{C}$ in $\mathbf{A}^{-1}$ for the chosen volume conductor model and particular positioning of measured grid has to be calculated only once. The forward problem can be solved very fast for any choice of the current source model, once the inverse $\mathbf{A}^{-1}$ has been obtained for a certain volume conductor model [9]. Only magnetic fields $\vec{B}_\infty$ and electric potentials ϕ_∞ in the infinite homogeneous space have to be determined for each configuration of current sources within the chosen volume conductor model. These quantities for the current dipole model $\vec{p}$ located in $\vec{r}_p$ are defined by the following relatively simple formulas

$$B_\infty(\vec{r}) = \frac{\mu_0}{4\pi}\frac{\vec{p}\times(\vec{r}-\vec{r}_p)}{|\vec{r}-\vec{r}_p|} \ , \qquad (6)$$

$$\phi_\infty(\vec{r}) = \frac{\mu_0}{4\pi\sigma}\frac{\vec{p}\cdot(\vec{r}-\vec{r}_p)}{|\vec{r}-\vec{r}_p|} \ . \qquad (7)$$

In this case the current source model is determined by six parameters, 3 for the spatial coordinates plus 3 for the dipole strength and orientation.

Table 1: Localization errors averaged over 40 samples for elliptic cylinder model ($h = 50\,cm, a = 18\,cm, b = 12\,cm$) and half–space approximation. E_x,E_y,E_z are average errors of source coordinates (x, y, z) and E is the average localization error. All results are in cm.

dipole direction	ELLIPTIC CYLINDER			
	E_x	E_y	E_z	E
p_x	0.25	0.52	0.43	0.82
p_y	0.21	0.44	0.65	0.91
dipole direction	HALF–SPACE			
	E_x	E_y	E_z	E
p_x	0.60	0.71	2.08	2.44
p_y	1.48	0.53	1.20	2.40

The magnetic field component perpendicular to the border in the special case of half–space volume conductor model is determined only by $B_{\infty,\perp}$ which is the reason why this simplified model is one of the most frequently used in magnetocardiographic studies.

3 RESULTS AND CONCLUSIONS

We have performed at first some simulations studies. The magnetic isofield maps of unit current dipoles in x and y direction (p_x, p_y) in 40 different locations within van Oosterom standard torso were generated. The locations were then reconstructed by the half–space model and several elliptic cylinders models with different parameters (a, b, h). It has been found that the height h of the elliptic cylinder does not influence much the generated magnetic field if height is not too small. For heights between 40 and 60 cm the average localization errors change less than 2 mm. The ratio of ellipse's axes is more sensitive. We kept b constant (12 cm) and varied a. The change of a by 2 cm altered the average localization error by approximately 5 mm. Errors are here defined as differences between the real source location used for generating isofield maps and source location obtained by inverse solution. The best results were obtained for $a = 18\,cm$ and $h = 50\,cm$. Parameters $(a, b) = (18, 12)\,cm$ determine the ellipse which corresponds approximately to the cross section of van Oosterom torso in the heart region. The average localization errors for the elliptic cylinder model and the half–space model are shown on Table 1. Results show an improvement of about 1.5 cm on average localization error when the elliptic cylinder model is used instead of the half–space model.

Table 2: Localization results for two patients (P_1 and P_2) obtained by the following volume conductor models: half–space, elliptic cylinder and three different realistically shaped torsos. Two torso models were originally developed by van Oosterom (TORSO I)[10] and Horaček (TORSO II)[5], respectively. The third torso model (TORSO III) was constructed from MR images (see Fig. 1). For comparison the invasive localizations obtained with X–rays during the cathether ablation are shown. All results are in cm.

		X RAYS	HALF SPACE	ELLIPTIC CYLINDER	REALISTIC TORSO I	REALISTIC TORSO II	REALISTIC TORSO III
P_1	x	2.0	0.5	2.2	1.3	2.4	1.7
	y	-11.6	-11.7	-11.4	-10.5	-11.4	-11.4
	z	-6.7	-4.2	-7.1	-8.1	-7.0	-8.8
P_2	x	2.5	0.8	2.5	3.4	2.9	4.2
	y	-10.5	-25.8	-12.6	-6.8	-6.7	-7.8
	z	-8.2	-16.8	-12.1	-9.4	-12.3	-8.3

We have tried to determine the onset of accessory cunduction pathway in the group of 7 patients with WPW syndrome by using current dipole source model situated in different volume conductor models. For all patients the actual locations were known, obtained by means of X–rays during the invasive catheter ablation procedure. Results for two cases, denoted by P_1 and P_2, are shown on table 2. The first one is the patient with the best matching between results obtained invasively by catheter and noninvasively by magnetocardiographic technique. The diference was around $3\,cm$ for the half–space model and between 1 and $1.6\,cm$ for other models. For the other example senseless result was obtained by the half–space model. For other models differences between 3.5 and $6.5\,cm$ were found.

Our group of patients was not big enough to make some general quantitative conclusion. Qualitatively we can say that for noninvasive magnetocardigraphic localization of preexitation onset at least the homogeneous torso model has to be considered. Our simulation study showed that the elliptic cylinder is a good approximation of realistic torso which has been also confirmed by using that model with patient data.

References

[1] A.C. Barnard, I.M. Duck, M.S. Lynn, W.P. Timlake. The application of electromagnetic theory to electrocardiography II: The numerical solution to the integral equation. *Biophys. J.* **7** : 463–491, 1967.

[2] J.C. de Munck. A Linear Discretization of the Volume Conductor Boundary Integral Equation Using Analytically Integrated Elements. *IEEE Trans. Biomed. Eng.***BME–39** : 986–990, 1992.

[3] D.B. Geselowitz. On Bioelectric Potentials in an Inhomogeneous Volume Conductor. *Biophys. J.* **7** : 1–11, 1967.

[4] D. B. Geselowitz. On the Magnetic Field Generated Outside an Inhomogeneous Volume Conductor by Internal Current Sources. *IEEE Trans. Magn.* **MAG–6** : 346–347, 1970.

[5] B.M. Horaček. Digital model for studies in magnetocardiography. *IEEE Trans. Magn.* **MAG–9** : 440–444, 1973.

[6] G. Huiskamp, and A. van Oosterom. Tailored versus realistic geometry in the inverse problem of electrocardiography. *IEEE Trans. Biomed. Eng.* **36** : 827-835, 1989.

[7] V. Jazbinšek. *Modeliranje tokovnih izvorov magnetnega polja srca ob upoštevanju realnih robnih pogojev.* Doktorska disertacija, Univerza v Ljubljani, Oddelek za fiziko FNT, Ljubljana, 1994.

[8] M.S. Lynn and W.P. Timlake. The use of multiple deflations in the numerical solution of singular system equations, with applications to potential theory. *SIAM J.Numer.Anal.* **5** : 303–322, 1968.

[9] J. Nenonen, C.J. Purcell, B. M. Horaček, G. Stroink and T. Katila. Magnetocardiographic Functional Localization Using a Current Dipole in a Realistic Torso. *IEEE Trans. Biomed. Eng.***BME-38** : 658–664, 1991.

[10] A van Oosterom. Triangulating the human torso. *Comput. J.* **21** : 253-258, 1978.

HR9600006

SCATTER TO PRIMARY RATIO IN BROAD BEAM GAMMA IRRADIATION OF ANTHROPOMORPHIC PHANTOMS

Mladen Vrtar
Clinic of Oncology and Radiotherapy, Clinical Hospital Center Rebro
Kišpatićeva 12, 41000 Zagreb, Croatia

Abstract
The concept of Scatter-to-Primary Ratio (SPR) was applied to the broad beam 60-Co gamma Total Body Irradiation (TBI). First, the absorbed dose measurements in anthropomorphic water phantom were verified (up to 2.1%) through a reference theoretical model formed of 20 cylindrical ellipsoids. Further, an extrapolation to the proportional sized phantoms of different lengths (1.0-2.0 m) and weights (19-150 kg) was performed. It was found : 1.) r/d had almost the constant value i.e. 2.5, 2.) the geometrical parameter z=rd/(r+d) (where r is radius of the beam's cross section at depth d=AP/2 in abdomen midplane) was included into the interval 4<z<10 , according to the various dimensions of the single phantom and 3.) SPR appeared linearly dependent on z (in 1. approx.). The deviation from linearity was expressed by SPR = 0.083z + 0.000687z^2, with errors 0.5% and 3.0% respectively, concerning the coefficients. The method facilitates the dose calculations in TBI.

1. INTRODUCTION

The separation of absorbed dose D(d,r) of a high energy beam into primary Dp(d) and scatter Ds(d,r) component is the basis for the calculation of dose in an irregular field or a field with inhomogeneity in tissue. Here r is radius of the beam's cross section at depth d. Until now, many approaches have been established to define the mentioned separation in an absorbing medium, but introduction of a concept of Scatter-to-Primary Ratio (SPR) [1,2,3,4,5] in the last years made the method more suitable for application. In general, the primary dose is also a function of r, but under the condition of lateral electronic equilibrium (r>λ, where λ is a lateral electron mean free path in a phantom) it depends only on d. Therefore, the quantities needed to define Dp(d) remained the narrow beam attenuation coefficient μ and the normalisation factor. The latter determines the value of the primary relative to the total dose. As is known SPR is defined by SPR(d,r)= Ds(d,r)/Dp(d). It was found [2] that in the case of small r and d and for fixed values of the ratio r/d, SPR is (in the first approximation) linearly dependent on a geometrical parameter z = rd/(r+d). The deviation from linearity was found to be pronounced specially in the case as the field size or the depth increases and was expressed by SPR = az+bz^2, where a and b varied with r/d and were proportional to μ and μ^3 respectively [2].

2. EXTRAPOLATION TO THE BROAD BEAM CONDITIONS

In all cited calculations (mainly using the Monte Carlo method) the primary photons were considered to incident perpendicular to the surface of an "infinite" water phantom (radius 50 cm and depth 50 cm), and the SPR was restricted to small fields and depths. Let us extrapolate it now to broad beam conditions. Instead of the "infinite" phantom (with dimensions larger than the field) and variable (small) field size, we can apply the large field which exceeds the ("finite") variable sized anthropomorphic phantom limits, as in determination of the Total Body Irradiation (TBI) dose of the important locations (such as for example: abdomen mid plane dose. r can be assigned now to the range of scattered irradiation, i.e. to the equivalent radius of effective

field size. The conditions of the lateral electronic equilibrium are also released in this case.

2.1. Experimental method

The basic measurements of the total absorbed dose D(d,r) and the primary dose Dp(d) were performed in an anthropomorphic water phantom (made by a sculptor) [6], situated in a broad horizontal 60-Co beam in TBI conditions. We used the semiconductor detector with increased sensitivity (1200 nC/cGy), constructed specially for the measurements in low dose rate γ field and connected to the dosimetry equipment consisting from Direct Patient Dose (DPD-5) monitor and Radiation Field Analyser (RFA-3) (all Scanditronix, Uppsala). Empty RFA-3 served the purpose of precise positioning of the detector so that the coordinates could be transferred automatically to water filled anthropomorphic phantom. Determination of the primary dose was performed by the "small absorber method" [3], which was adjusted to TBI (Fig. 1). The SPR values, as dependent on depth along AP-PA central ray of the beam (passing the abdomen location in the hight of umbilicus), were available from these measurements.

2.2. Theoretical model

The theoretical model of the anthropomorphic phantom consisted of 20 cylindrical ellipsoids, in an arrangement which reflected the experimental situation (in position and shape) as close as possible. The computer program allowed that the dimensions of the constituent parts could be selected very carefully and could be changed in their sizes. We were able to define, in a mathematical form, a number of proportionally sized phantoms, which looked like as having been puffed up to an arbitrary dimension from the referential one (which closely coincided with the experimental phantom). So, the whole practical range of real situations (phantoms in length 1.0-2.0 m and weight 19-150 kg) was covered. The analytical form of the primary was used from literature ([5], eq. (10a)), and the calculations of scatter were performed by a sector integration method, adjusted to broad beam conditions [7].

3. RESULTS

A comparison of experiment and theory in the referential case, i.e. at phantom's length 1.5 m and volume Vo = 0.06318 m^3 (weight 63.18 kg) resulted in close agreement (2.1% on average) in SPR as function of depth along central ray direction. The result encouraged the extrapolation of the theory to 11 phantoms of proportional sizes defined by the proportionality coefficient $\alpha = \sqrt[3]{V/Vo}$, which covered the interval from 0.667 to 1.333. The next step was the calculation of equivalent radius r of the effective field, at depth AP/2 (AP=20xα) in the theoretical phantoms. It was performed in 3 positions (Fig. 2) of the absorbed dose determination point for each AP, along the phantom's mid line, i.e. 0, -L, +L, where L=10xα., in order to investigate the behaviour along this direction in abdomen region. If we analyse the r/d behaviour at d=AP/2 either as function of AP or α, an interesting result appears; in all practical cases the value was 2.5 ($\pm$ 5.5%). It means that r/d is almost a constant. Now, introducing a geometrical parameter z = rd/(r+d) [2] applied to our conditions, it was found that in the first approximation SPR has a linear dependence on z, though a certain spread is visible due to position of the point along abdomen mid plane line and due to the particular α, which relates to certain z region. It was demonstrated by a parallelogram attributed to the abdomen part of a single phantom (Fig. 3). The deviation of SPR from linearity was investigated by expressing SPR/z = a + bz. The least square fit method gave: a = 0.083 ($\pm$0.5%), b = 0.000687 ($\pm$ 3%) (Fig. 4). A similar investigation can be applied to obtain the mid plane SPR in other regions in the body, such as head, thorax etc.

4. DISCUSSION AND CONCLUSIONS

In Fig. 3 and Fig. 4, also a comparison with the known literature data [2] was presented. The straight lines which represented kerma SPR and SPR/z as functions of z, fitted the Monte Carlo calculated values for a given r/d = 0.25, 1.0 and 2.0 up to the fields of 15x15 cm^2. As concluded in [2], there is no significant difference between kerma SPR and absorbed dose SPR for z > 0.25 cm. So, the results representing SPR in our broad beam conditions, where 4 < z < 10, can be understood as an extrapolation. The coefficients a and b also vary with r/d. To find this behaviour, it seemed worth to present a/μ and b/μ^3 as function of r/d in our case and to compare it with the known results of the smaller fields [2]. The mean TBI values were 1.277 and 2.502, respectively. Also, it was found that the contribution of the second term in SPR/z, i.e. bz is only about 3%, so with good accuracy we can accept that a semiempiric relation describing the scatter component Ds(d,r) = Dp(d)az is rather similar to the scatter - radius function, but it is linear. The method is applicable for the purpose of absorbed dose calculations in dose planning systems based on the concept of separating absorbed dose into primary and scatter parts in irregular fields, or "irregular" (anthropomorphic) phantoms in broad beams.

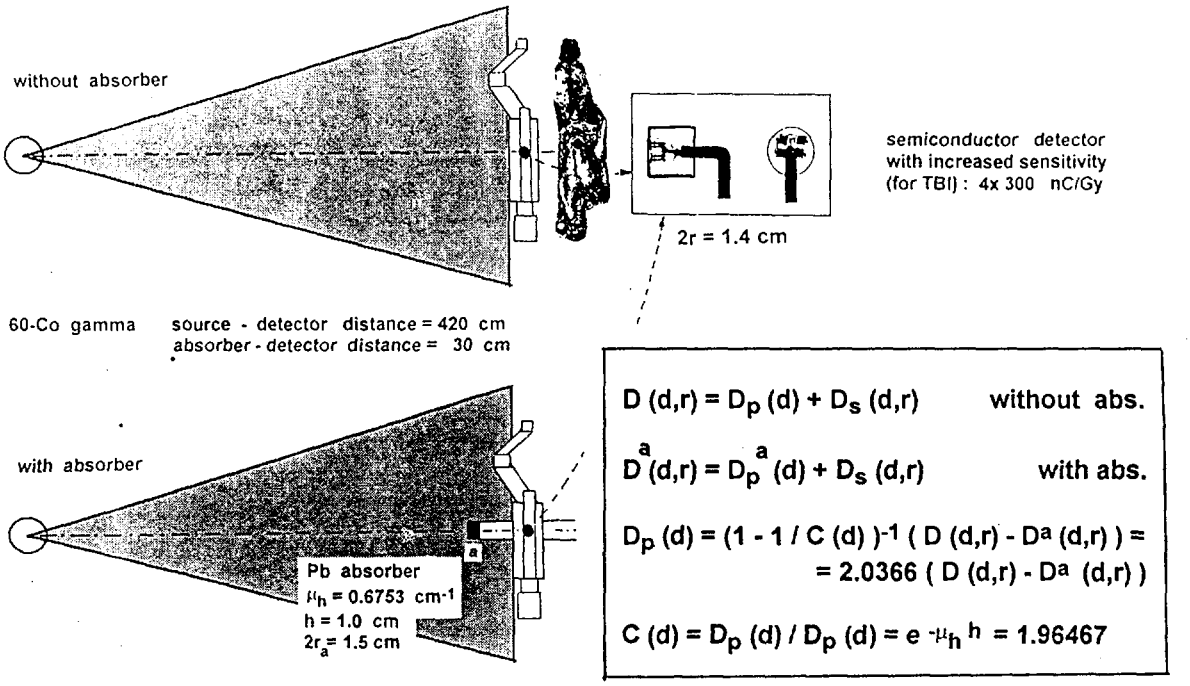

EXPERIMENTAL SETUP FOR DETERMINATION OF SPR IN 60-Co BROAD BEAM (TBI)

Fig.1

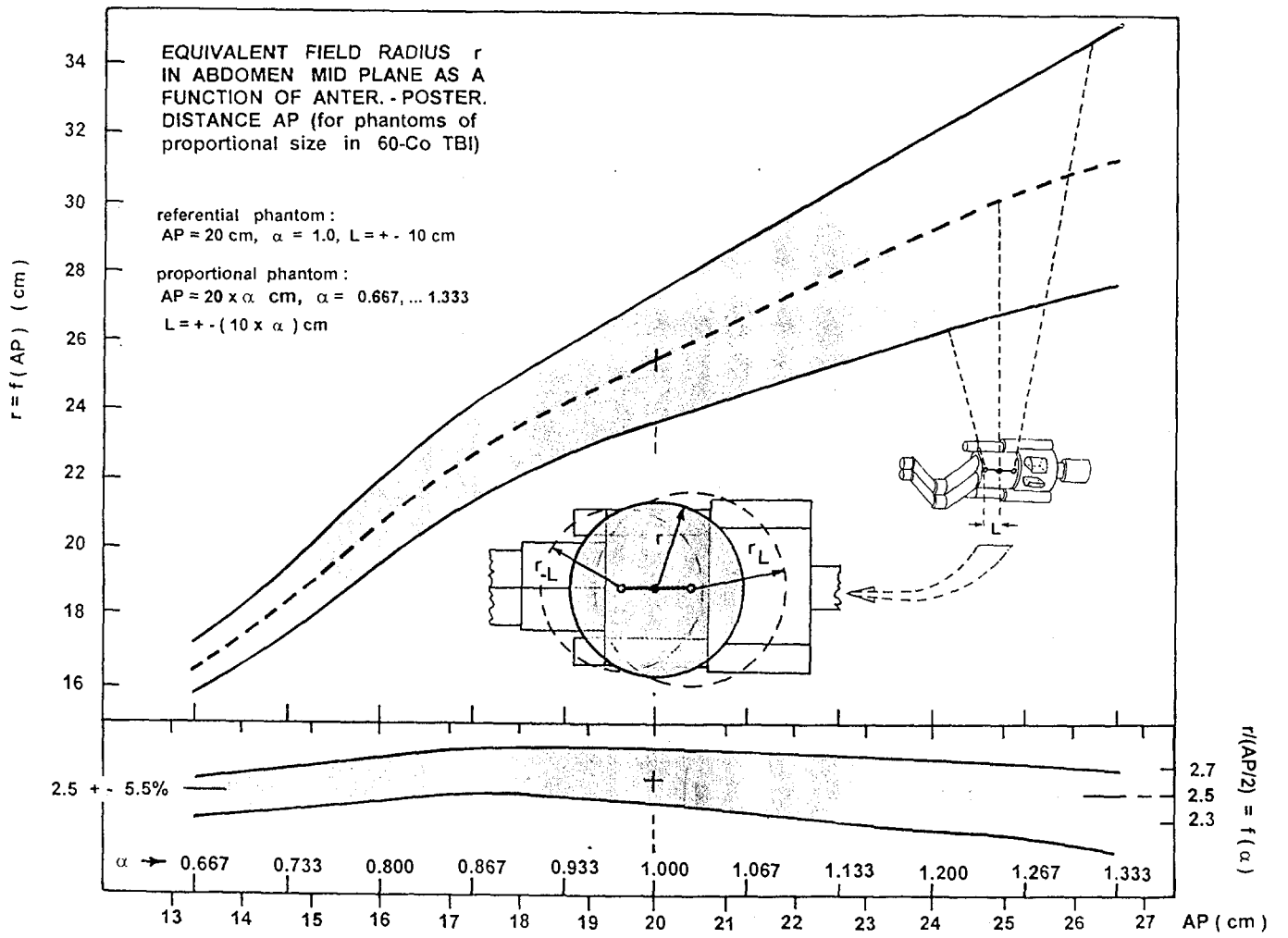

Fig. 2

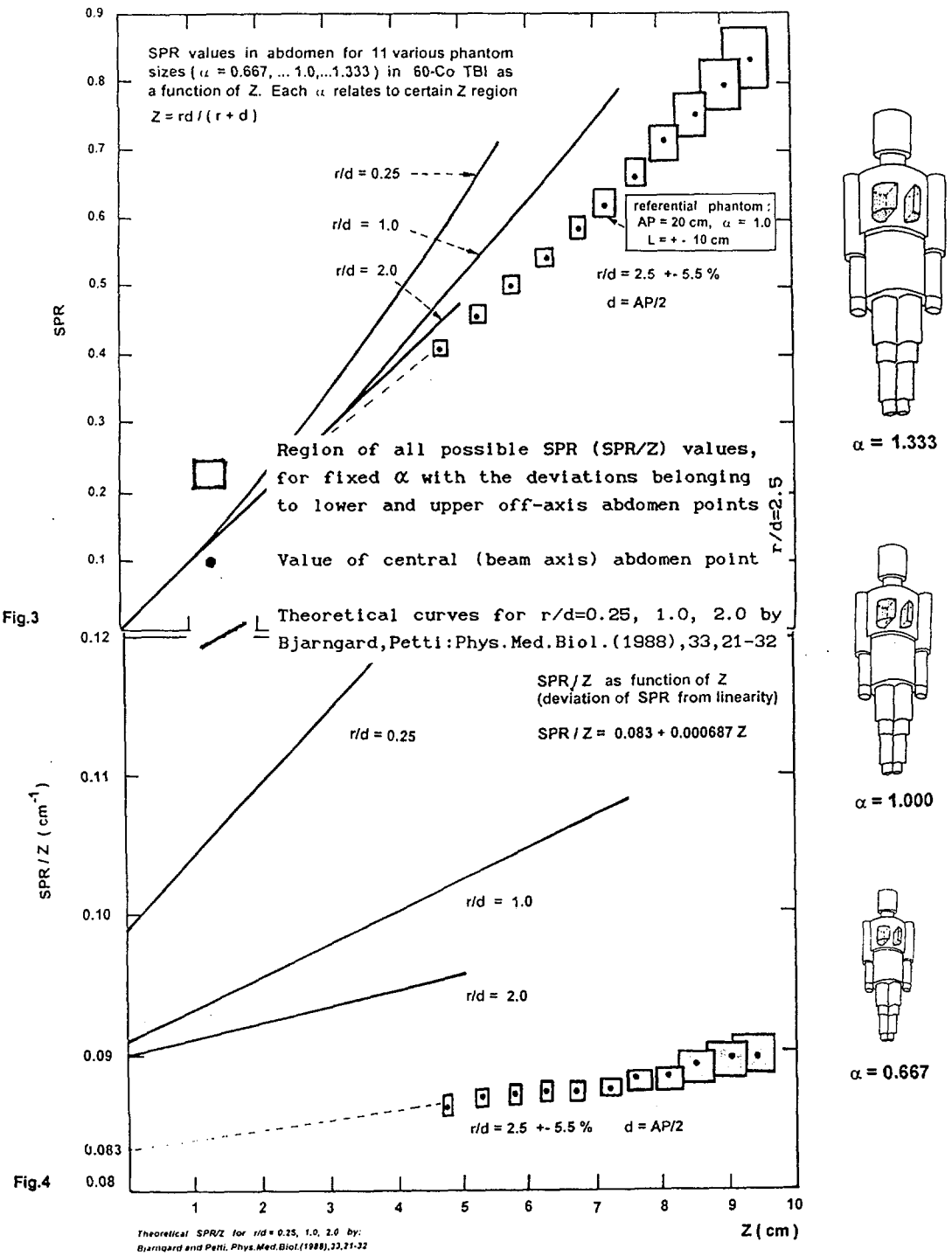

Fig.3

Fig.4 Theoretical SPR/Z for r/d = 0.25, 1.0, 2.0 by: Bjarngard and Petti, Phys.Med.Biol.(1988),33,21-32

5. REFERENCES

[1] P.K. Kijewski, B.E. Bjarngard, P.L. Petti, Monte Carlo calculations of scatter dose for small field sizes in 60-Co beam. Med. Phys. 13, 74-77, 1986.

[2] B.E. Bjarngard, P.L. Petti, Description of the scatter component in photon beam data. Phys. Med. Biol. 33, 21-32, 1988.

[3] P.S. Nizin, Determination of the primary dose in 60-Co gamma beam using a small attenuator. Med. Phys. 17,92-94, 1990.

[4] R.K. Rice, L.M. Chin, Monte Carlo calculation of scatter to primary ratios for normalisation of primary and scatter. Phys. Med. Biol. 35, 333-338, 1990.

[5] P.S. Nizin, Geometrical aspects of scatter to primary ratio. Med. Phys. 18, 153-160, 1991.

[6] M. Vrtar, A. Purišić, Local tissue air ratio in an anatomic phantom for 60-Co total body irradiation. Radiother. Oncol. 21, 157-162, 1991.

[7] M. Vrtar, W. Schmidt, Lung Correction and Mid Plane Irradiation Dose Factors in Anatomic Phantoms of Proportionl Sizes; Acta med. Croat. 48, 21-26, 1994.

FLOW STUDIES OF NON-NEWTONIAN FLUID THROUGH MODEL CAROTID ARTERY

Budimir Mijović
Faculty of Technology
University of Zagreb

Abstract

Arteriosclerosis is one of the most frequent disease of blood vessels. The most outstanding consequences of the disease are a narrowing of blood vessels at branching points and bifurcations. To determine the causes of arteriosclerosis, it is necessary to be acquainted with hemodynamic parameters of blood flow. These hemodynamic parameters play an important role in formation of arteriosclerotic layers, especially at branching points and bifurcations. The most important hemodynamic factors are: blood vessels geometry, pulsatile blood flow, blood vessel wall elasticity and non-Newtonian flow behaviour. An elastic silicone model of carotid artery, unclear cut from the body of a person killed in an accident, has been used in the analysis of these parameters. Carotid model is characterised by the elasticity similar to that of blood vessel wall and 80% stenosis on internal and external carotid. The flow in internal carotid branches (ica) and external carotid branches (eca) has been set to 70:30 relation, using DMSO-Separan mixture. This mixture behaves like a non-Newtonian fluid. After areas of disturbed flow were detected and localised, using photoelasticity apparatus and birefrigent solution, velocities have been measured at characteristic cross-sections, employing LDA. Component velocities have been measured using a single-component laser-Doppler-anemometer.

Introduction

Arteriosclerotic layers can most frequently be found inside large arteries, around bends and bifurcations (Liepsch et al., 1992; Caro et. al., 1992; Ku et al., 1985). Flow disturbances at these anatomically important points play an important part in arterogenesis. Local hemodynamic conditions at bifurcations and bends are principal factors in localising arteriosclerotic layers (Nerem, 1992; Caro et. al., 1992). Laser-Doppler-anemometer is used to determine qualitative parameters of flow velocity and pressure in the carotid model, in the case of pulsating flow of a non-Newtonian fluid. The model analyzed by LDA is transparent, so laser can penetrate it. As the velocity measurements of fluid flow have been performed at a contactless measuring point, they do not depend upon density, temperature and pressure. Blood can not be used in LDA experiments, as red blood cells absorb the laser light. DMSO-Separan mixture has been used to simulate human blood behaviour in blood vessel models. This mixture behaves as a non-Newtonian fluid. Our previous investigations proved than a non-Newtonian fluid exhibits radically different behaviour in flow from a Newtonian one (Mijovic et al., 1994.). These investigation of the flow are significant for understanding the causes of arteriosclerosis, its diagnosing and treatments.

Experimental Methods

Elastic silicone carotid model has been used, Figure 1. It was prepared in the likeness of an in vivo model. Entrance tube diameter of carotid model (eca) was 7.5 mm, internal carotid diameter was 5.8 mm, and external carotid diameter was 4.5 mm. Eighty percents stenosis was present at the point 2.5 mm inside both branches, so inside branch diameter (ica) was 0.46 mm, and inside branch (eca) 1.42 mm.
Visualisation of the flow in the carotid model and localisation of the area of disturbed flow have been done by use of a photoelastic device. After the areas of disturbed flow were detected and localised, velocity in characteristic cross-sections has been measured using LDA. The velocity has been measured by moving the model situated on a movable table. As seen in the Figure 1, a cross section has been taken on the straight part of the model of carotid artery (eca), 15 mm upstream from bifurcation. Then cross-sections have been taken on (ica) and (eca) branches at the point of

bifurcation (0.0 mm), at 2.5 mm, 5.0 mm, 10.0 mm and 15.0 mm downstream of the bifurcation. One cross-section has been divided into 9 diameters designated (-4,-3,-2,-1,0,1,2,3,4). At pulsating flow, velocities have been measured in 9 measuring points, step by step, at the diameters (-2,-1,0,1,2), or in 7 measuring points, at the diameters (-3,3) and 5 measuring points at the diameters (-4,4), Aqueous solution (51,7%) of dimethilsulfoxid, mixed with 1:1 mixture of 0.005% AP45 and 0.007% AP302 of polyacrylamide aqueous solution, have been used as the model fluid, imitating a non-Newtonian flow in the carotid model.

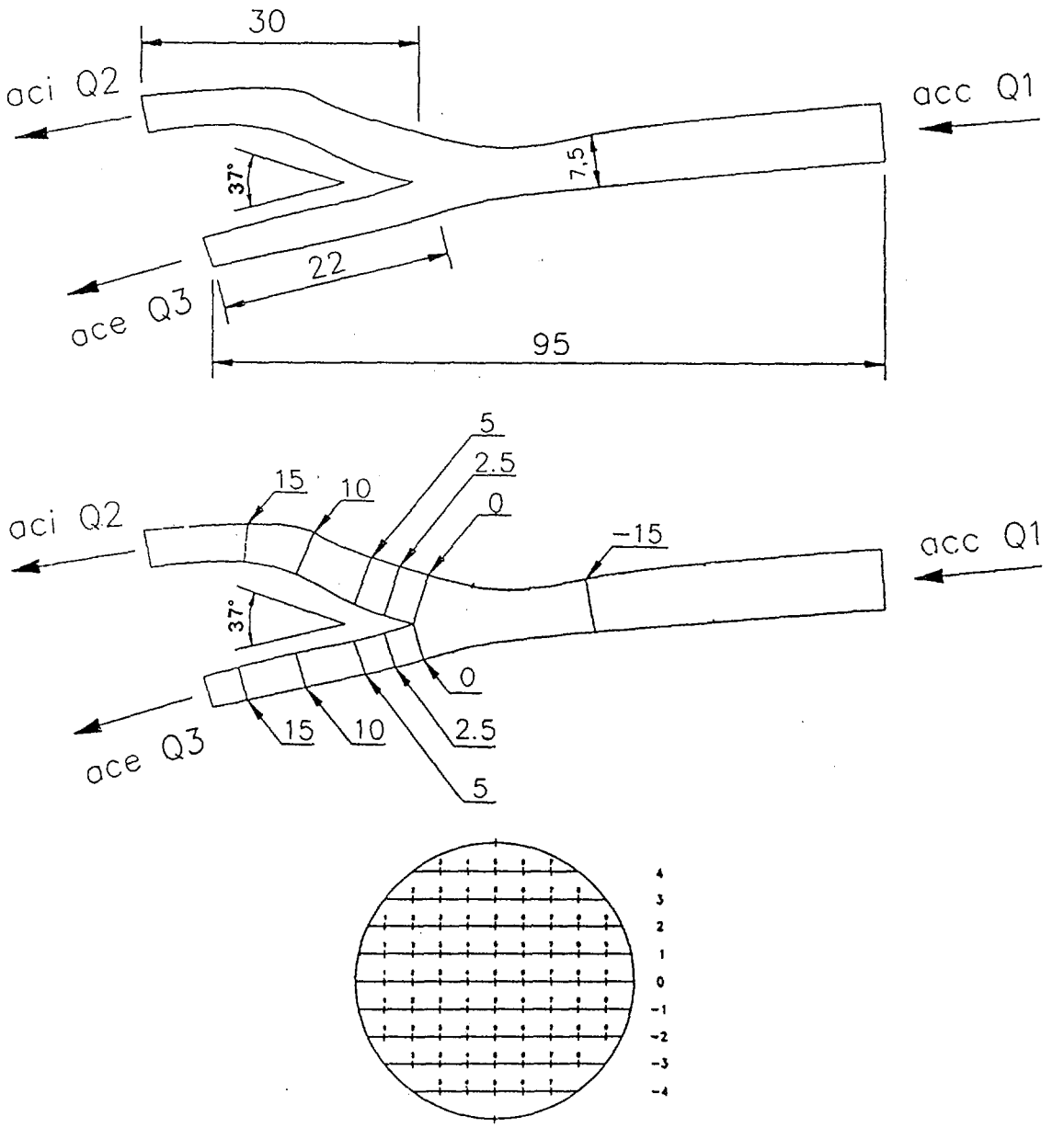

Figure 1. Silicon rubber carotid artery model.
Position of measurement cross section

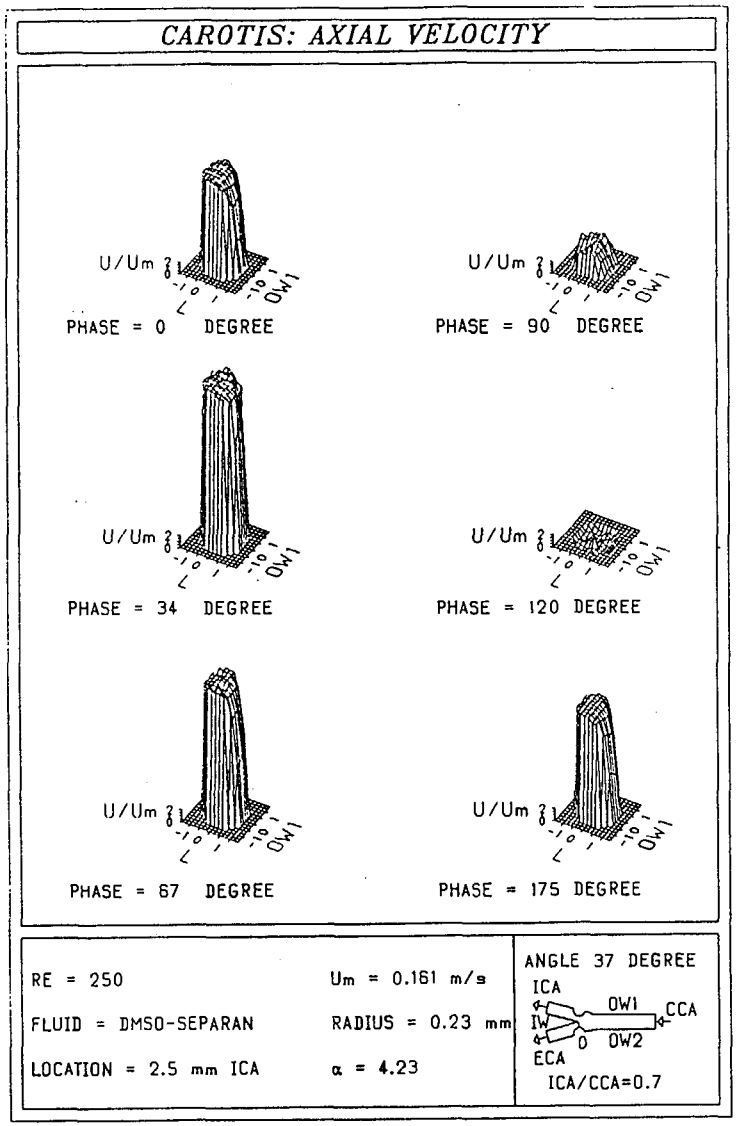

Figure 2. Velocity distribution over the cross section 2.5 mm downstream of the bifurcation in the internal carotid artery with a 80% stenosis at the sinus

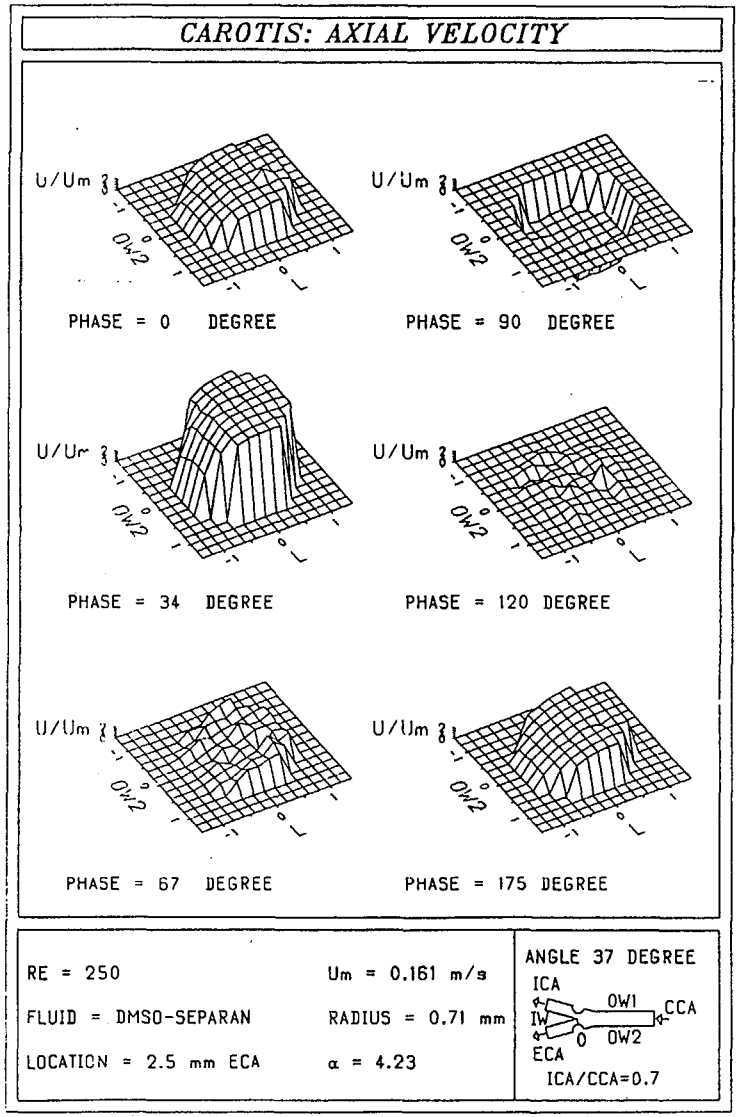

Figure 3. The same as Fig. 2 but in the external carotid artery

Representative dynamic viscosity η_{rep} = 6.162 mPas at the density of ρ = 1050 kg/m^3 and temperature t = 21 °C has been determined through viscosity measurements. It can be said that the representative dynamic viscosity of the model fluid is approximately the same as for human blood at a shear rate of 8 to 200 s^{-1}, according to Liepsch et al. /3/. Model fluid refractive index is n = 1.41, identical to the refractive index of silicone rubber, the walls of the model are composed of. Entire model has been submerged in a glycerine-water solution, with refractive index n = 1.41, to enable the laser beam to pass through the model without any refraction.

The measurements have been done for the value of Reynolds number Re = 250 and for the relation of the flow in the branches $Q_2 : Q_3$ (70 : 30), with the entrance tube of the carotid model diameter being d = 7.5 mm. Pulsating fluid flow is achieved with the help of a membrane pump. Five periods of velocity and pressure profiles for one measuring point have been analyzed.

Results and Discussion

Measurements of a non-Newtonian fluid pulsating flow through an elastic carotid model has been done. Reynolds' number (Re = 250) is taken, and average velocity calculated using a continuity equation. Pulsating wave used for phase angle for 0° to 360° has been divided into 100 measuring units, or measuring points. Phases of 0, 34, 67, 90, 120 and 175 degrees have been chosen. Model fluid DMSO-Separan is taken, with a know representative dynamic viscosity η_{rep} = 6.612 mPas and density ρ = 1050 kg/m^3, while pulsating wave frequency is f = 1.045 Hz and entrance carotid tube radius (cca) 7.5 mm. The result is Womersley parameter α = 4.32. Figure 2. gives velocity profiles at various phase angles at the point 2.5 mm downstream from the bifurcation in the branch (ica), where 70% of the fluid goes (ow1 denoting the outer wall and L the left side). High flow velocities have been recorded in the systole area of the phase ωt = 34° and 67°, due to maximum stenosis at that point. Further on, significant velocity fluctuation have been recorded in the diastole area for phase angle ωt = 120°, indicating reverse flow. Broader areas of reverse flow have been detected behind stenosis, some 5 mm downstream of the bifurcation. Figure 3. shows velocity profiles at the point 2.5 mm downstream of bifurcation at the part of the branch (eca) where 30% of the flow goes (ow2 denoting outer wall and L left side). Analysis of six velocity profiles in Figure 3. shows also a high velocity in the branch (ica) in the systole area for the phase ωt=34°. Reverse flow has been recorded in the diastole area for the phase ωt = 90° and 120°. Different velocity profiles in the branch (ica) and the branch (eca), for phase angle ωt=90°, can be related to the quantity of the flow through the branches and to the elasticity of the model walls. Significant velocity change has been determined on stenosis in both carotid branches, external and internal. Broad areas of reverse flow have been recorded behind stenosis on the outer sides of the model ow1 and ow2. These areas of flow separation are smaller for the elastic wall of the model (Liepsch et al. 1992). Elasticity of the model wall influences the behaviour of the flow, especially in the areas where the flow is separated from the wall. Measurement also show that a non-Newtonian fluid exhibits different velocity distribution from a Newtonian flow, especially in the area of separation. It can be concluded that the geometry, wall elasticity, fluid characteristics, velocity and pulsation form, all influence the phenomenon of the flow. Analysis of the model shows that not a single of these hemodynamic parameters can be neglected.

References

1. Caro, C.G., Dumonlin, C.L., Graham, J.M.R., Parker, K.H., Souza, S.P.: Secondary Flow of the Human Common Carotid Artery Imaged by MR Angiography, J. Biomech. Eng. 111:147-149,1992
2. Ku, D.N., Giddens, D.P., Zarins,C.K.,Glagov, S.:Pulsatile Flow and Arteroscleroses in the Human Carotid Bifurcation, Arteriosclerosis 5:293-302,1985
3. Liepsch,D.,Poll,A.,Mijovic,B.,Pflugbail,G:Flow Studies in Rigid and Elastic Y-junction Models Using Newtonian and non-Newtonian Fluids, ASME Adv. Bioeng. BED 22, 277-280,1992
4. Mijovic, B., Liepsch, D.: Pulsatile Flow Studies of Newtonian and non-Newtonian Fluids Through Elastic Y-models, Editor D. Liepsch, VDI Verlag, Reihe 17, Nr 107, 255-260, Düsseldorf, 1994.
5. Nerem, R.M.: Vascular Fluid Mechanics, the Arterial Wall, and Atherosclerosis, J. Biomech. Eng. 114, 274-282, 1992.

PLIVA'S LONG-TERM RESEARCH PROJECTS, SUPPORTED BY NATIONAL SCIENTIFIC FUND, REPUBLIC OF CROATIA:

- *Structure, Complexity and Stability of the Streptomycetes Genom;*
- *Gene Expression in Micellar Microorganisms;*
- *Organisms Used in the Conversion of Glucose into Ketoacids: Studies, Constructions and Cloning;*
- *Biosynthesis and the Properties of Microbial Hydrolytic Enzymes;*
- *The Waste Water Treatment Process through Anaerobic Microbial Consortium;*
- *The Optimization of Chemical and Biotechnical Processes;*
- *The Chemistry and Biochemistry of Antimicrobial Agents;*
- *Immunomodulators - Biosynthesis, Transformations, Effects;*
- *The Preparation of Medical Suspensions, Pharmacology and Clinic;*
- *Immune Response to Virus Antigen in Immunocomplex;*
- *An Information System for the Natural and technical Sciences (ISPTZ)*

PLIVA

Pliva d.d Zagreb

41000 Zagreb, Croatia, Ulica grada Vukovara 49

Phone +385 41/62 09 99, Fax +385 41/62 10 11